DISSERTATION

UNDERSTANDING AND MITIGATING TSUNAMI RISK FOR COASTAL STRUCTURES AND COMMUNITIES

Submitted by

Park, Sangki

Department of Civil and Environmental Engineering

In partial fulfillment of the requirements

For the Degree of Doctor of Philosophy

Colorado State University

Fort Collins, Colorado

Fall 2011

Doctoral Committee:

Advisor: Rebecca A. Atadero
Co-Advisor: John W. van de Lindt

Paul R. Heyliger
Bolivar A. Senior

ABSTRACT

UNDERSTANDING AND MITIGATING TSUNAMI RISK FOR COASTAL STRUCTURES AND COMMUNITIES

Tsunamis have attracted the world's attention over the last decade due to their destructive power and the vast areas they can affect. The 2004 Indian Ocean Tsunami, killed more than 200,000 people, and the 2011 Great Tohoku Japan Earthquake and Tsunami, resulted in 15,000 deaths and an estimated US $300B in damage, are recent examples. An improved understanding of tsunamis and their interactive effects on the built environment will significantly reduce loss of life in tsunamis. In addition, it is important to consider both the effect of the earthquake ground motion and the tsunami it creates for certain coastal regions.

A numerical model to predict structural behavior of buildings subjected to successive earthquakes and the tsunamis was developed. Collapse fragilities for structures were obtained by subjecting a structure to a suite of earthquake ground motions. After each motion, the numerically damaged structural model was subjected to tsunami wave loading as defined by FEMA P646. This approach was then extended to the community level; a methodology to determine the probability of fatalities for a community as a function of the number of vertical evacuation shelters was computed.

Such an approach also considered the location and number of vertical evacuation sites as an optimization problem. Both the single structure cases and the community analyses were presented in terms of fragilities as a function of the earthquake intensity level and evacuation time available. It is envisioned that the approach may be extended to any type of structure as they are typically modeled nonlinearly with strength and stiffness degradation.

A logical fragility-based, or performance-based, procedure for vertical evacuation for coastal buildings and for whole communities was developed. A mechanism to obtain a reduction in the collapse risk of structure and more critically maximize the survival rate for a community was a major outcome of this dissertation.

The proposed tsunami vertical evacuation methodology was intended to provide key information to better understand and mitigate risk caused by earthquakes and tsunamis, thus it is possible to mitigate hazard for a community with only several large vertical evacuation shelters. It is able to provide a framework for a vertical evacuation plan and for the mitigation of collapse risk and fatalities of structures and a community based on a limited amount of information.

ACKNOWLEDGEMENTS

First of all, I would like to thank Dr. John van de Lindt, my former advisor and currently co-advisor, for all the time he spent helping and guiding me and financial support that he has given to me through my graduate study in United States. Words cannot express my appreciation enough.

I would like to thank especially Dr. Rebecca A. Atadero for accepting to serve as my advisor and Dr. Paul Heyliger and Dr. Bolivar A. Senior for being part of my graduate committee. My gratitude is extended to Dr. Daniel Cox and Dr. Rakesh Gupta at Oregon State University for providing me with their valuable comments.

Colorado State University and the Department of Civil and Environmental Engineering have been very thankful for the help that they provided in getting me prepared for this dissertation.

I also would like to thank to my friends at Colorado State University, Fort Collins and University of Alabama, Tuscaloosa for their friendship, support, and help during my study in U.S. I must appreciate my family and family-in-law for their love and support during my graduate study.

Finally, but certainly not least, I would like to appreciate my wife, HyunJung Lee and my son, Aiden Yongwon Park. Their endless love, friendship, and devotion have sustained me through the peaks and valleys I have experienced. With their love, I have truly been blessed.

The material presented in this dissertation is based on upon work supported by the National Science Foundation under Grant No. CMMI-0830378 (NEES Research) and CMMI-0402490 (NEES Operations). This support is greatly appreciated.

DEDICATION

To my wife, Hyunjung Lee, my son, Aiden Yongwon Park, my parents, my parents-in-law, my sister, and my brothers-in-law who have raised and guided me with a love and faith stronger than any I could hope to deserve. Thank you so much.

San, my lovely dog, rest in peace.

TABLE OF CONTENTS

LIST OF TABLES

LIST OF FIGURES

CHAPTER 1

INTRODUCTION AND LITERATURE REVIEW

1.1 BACKGROUND

Evidence of natural disasters and the human attempts to overcome and mitigate them has been evident and becoming common since the beginning of time. In 2011, the National Oceanic and Atmospheric Administration (NOAA) reported that over 50 percent of the U.S. population lives in coastal areas. Moreover, almost 60 percent of the U.S.'s gross domestic product (GDP) is generated in coastal regions (NOAA 2011). This concentration of economic production, population, and infrastructure in and around coastal communities is the motivation for this dissertation work.

Tsunami is the Japanese word meaning "harbor wave" or "seismic sea waves", and has been given worldwide attention over the last decade because of the hydraulic power associated with the water flow and the fact that they affect long shorelines. They can occur for several reasons which include an earthquake-initiated seabed displacement, a volcanic eruption, landslides including underwater landslides, or the impact of large objects into the open ocean, i.e. a meteor. Such impulsive disturbances create water-wave motions where the entire water column from the bottom to the free surface is set in motion. Typically, tsunami hazards can be categorized into far, mid, and near-source-

generated tsunamis. Infrastructure at risk from near-source-generated tsunamis will generally feel the effects of the triggering event, e.g. shaking caused by the near-source earthquake. Every year, on average, there are 20 tsunami-generating earthquake events, with five of these large enough to generate tsunami waves capable of causing economic damage and loss of human life.

Throughout history, there is evidence showing the relationship between earthquakes and tsunamis. In 426 B.C., the Greek historian Thucydides described the correlation between tsunamis and earthquakes for the first time in recorded history. On March 27 1964, after the magnitude 9.2 Good Friday Earthquake, tsunamis hit Alaska, British Columbia, California, and coastal Pacific Northwest towns, leading to waves up to 30 meters (100 feet) tall and over 100 fatalities in Alaska. The 1993 tsunami that hit the small island of Okushiri, off the west coast of Hokkaido, Japan arrived at the shoreline just five minutes after the earthquake. It led to 240 fatalities as victims were trapped by debris from the tsunamis.

The 2004 Indian Ocean tsunami, triggered by a 9.2 magnitude undersea earthquake (the third largest earthquake on record), killed over 200,000 people in 11 countries. Coastal communities were inundated with waves up to 33 meters (108 feet) high, devastating entire coastal regions. This tsunami has been characterized as one of the worst natural disasters in human history. After the disaster, the United Nations Educational, Scientific and Cultural Organization (UNESCO) and other world bodies called for an international tsunami monitoring and warming system.

In 2010, a large offshore earthquake, ranked as the sixth largest earthquake on record, rocked Chile. It led to 562 fatalities and seriously affected many cities including Talca, Linares, Chillán, and Concepción by the earthquakes. After the earthquake, tsunami surges reaching heights from 1.29 meters (4.23 feet) to 2.34 meters (7.68 feet) hit coastal regions. The surges caused serious damage to port facilities and lifted boats out of the water in Talcahuano and the Juan Fernandez Islands were struck by a large wave that killed four hundred people and left eleven missing. After several hours, a series of 1 meter (3 feet) tsunamis hit the Big Island of Hawaii, Hawaii's largest island, but caused no apparent damage.

Recently, the Great Tohoku Japan Earthquake and tsunami occurred off the east coast of Japan on March 11, 2011. The 9.0 magnitude undersea earthquake was recorded as one of the five most powerful earthquakes in the world and the largest ever recorded in Japan. A tsunami triggered by the earthquake produced waves of up to 23.6 meters high (77 feet) and struck Japan minutes after the earthquake. The waves traveled as much as 10 kilometers (6 miles) inland due to the flat land near the coast. Officially, there were 15,093 deaths, 5,301 injured, and 9,093 people missing, as well as over 125,000 buildings damaged or destroyed. The earthquake and tsunami caused extensive and severe structural damages in Japan, including heavy damages to roads and railways as well as fires in many areas, and a dam collapse (Japanese National Police Agency 2011).

The study of tsunami engineering in the United States and elsewhere have improved significantly over the last 40 to 50 years, especially the hydraulics and seismology aspect, but there has been less progress on the interaction between tsunamis and structures. Scientists and engineers have developed methods to better understand the basis and mechanisms of tsunamis and help mitigate losses and fatalities caused by tsunami disasters. Casualties are often extremely high for this particular hazard because there is little warning and the waves move rapidly, making escape to higher ground difficult. It is clear that the earthquake ground motion reaches a target structure before the tsunami wave that was generated by the earthquake because of the high shear wave velocity in soil and rock versus the wave velocity in water. Thus, the better understanding of earthquakes and tsunamis, and their interactive effects on the built environment can significantly reduce loss of life in tsunamis.

These tsunami disasters highlight the need for tsunami monitoring and evacuation plans, as well as resistant construction around the world. Recently, as a result of many of these early design codes for tsunami design and analysis, the overall system including warning, monitoring, and evacuation for tsunamis were introduced in many countries around the world.

1.2 OBJECTIVES AND SCOPE

Estimates of the Great Tohoku Earthquake and Tsunami of 2011 are at 300 billion dollars, making it the world's most costly natural disaster. Both earthquakes and their resulting

tsunamis caused loss of numerous lives and tremendous loss of property, often devastating an entire region.

To reduce the damages from these disasters, one must be able to predict the structural behavior and its response, including collapse probability, accurately when they are exposed to these disasters. To do this, an understanding of the hydraulic loading and the influence on wave forces is needed. The wave forces, i.e. tsunami wave forces, can be computed based on mathematical formulations or by using numerical simulations directly. Wave forces are a function of numerous variables including wave height, wave speed, bathymetric configurations, etc. Thus, the first objective of this study focuses on applying a numerical method to calculate tsunami wave loading on a coastal structure.

In the United States, light-frame wood construction represents the vast majority of the building stock. In fact, 90 percent of residential structures in the U.S. are woodframe structures. These structures are built using a combination of engineered wood products such as plywood or oriented strand board (OSB), laminated lumber, and dimension lumber. As their name implies, these buildings are light-weight and are therefore susceptible to high wave forces such as tsunamis. When a wave impacts a woodframe structure, it typically results in separation from the foundations due to insufficient anchorage, collapse of entire wall sections, and excessive structural damage. Shearwalls and diaphragms are one of the major components of a woodframe structure and play an important role in lateral force resistance to wave, earthquake, and wind loads.

FEMA P646 (2008) recommends the consideration of both the earthquake demand from shaking and the tsunami demand for the design of structures in certain coastal regions such as the U.S. Pacific Northwest. While this may not be current practice in most areas, it is important to develop a better understanding of how one hazard affects the other since they may occur rapidly in succession, i.e. without the ability to repair between the loadings. Building design codes are based on load occurrence probability and resistance statistics of the components comprising a building system, however tsunamis are typically not considered in design except in very rare circumstances. The second objective of this study is to predict the structural behavior, especially wood construction, under these natural disasters, and provide methods of mitigation in the form of vertical evacuation. To accomplish this requires the investigation of structure behavior to successive earthquakes and tsunamis due to their correlation.

Due to other natural disasters, such as tornadoes, the U.S. Federal Emergency Management Agency (FEMA) strongly encourages homeowners and communities to build safe rooms (FEMA-320 2008). FEMA indicates that having a safe room at home or in a small business can help provide "near-absolute protection" for the family or employees from injury or death caused by the dangerous forces of extreme winds. Near-absolute protection can be defined as, based on our current knowledge of tornadoes, a very high probability that the occupants of a safe room built according to this guidance will avoid injury or death (FEMA-320 2008). This situation can be similarly applied to tsunami hazard, but rather than staying low or underground, the safe room must be located in the highest part of the structure with sufficient lateral capacity under the safe

room. Such logic can provide a way to retrofit an existing structure for tsunami loading. When a tsunami wave load hits a structure in a coastal community, occupants must evacuate to higher ground which is not always possible because of local topography, short warming times, etc. In this case, sheltering-in-place or “shelter-near-place” may be an alternative way to evacuate from the tsunami hazard. Thus, the last and most important objective of this dissertation study is to make an evacuation plan for existing structures and for the entire community by considering risk as a whole to the community.

In summary, the objectives of this study can be outlined as: (1) investigation of tsunami wave forces on coastal structures, particular buildings; 2) the correlation between the generating earthquakes and their tsunamis and their influence on structures; 3) extension of current state-of-the-art models to predict the structural behavior and responses under successive earthquake and tsunami loads; and 4) providing a better evacuation planning methodology, through optimization community vertical evacuation plans.

1.3 LITERATURE REVIEW

1.3.1 TSUNAMIS

1.3.1.1 WAVE HEIGHTS

Tsunamis generate waves with large heights as they approach the coast with very high speed. Scientists have found that wave heights play an important role in computing wave forces, as one would expect. Two distinct methods have been broadly accepted to identify

wave heights and their relationship with wave forces: the first is by using empirical formulas based on conducting experiments using scale models or field observations and the second is to apply analytical and numerical techniques and solve the fluid dynamics equations of motion.

A laboratory study by Hunt (1959) focused on examining run-up and proposed a non-dimensional equation for run-up as a function of beach slope, wave height, and wave period. Battjes (1974) proposed that the non-dimensional grouping be named the Iribarren Number, also known as the surf similarity parameter. Holman (1986) calculated numerous runs using data from a natural beach for different experiment conditions. Synolakis (1987) proposed an approximate linear and nonlinear theory to derive the maximum run-up of solitary waves and conducted a series of laboratory experiments to support the proposed theory. Kobayashi and Karjadi (1994) studied the relationship of solitary wave run-up to coastal flooding and damage caused by tsunamis and proposed a separate empirical and numerical approach to predict solitary wave run-up height.

Somewhat recently, Hughes (2004) re-examined existing wave run-up data with various wave and slope conditions and derived a new wave run-up equation in terms of a dimensionless wave parameter representing the maximum, depth-integrated momentum flux. Madsen and Fuhrman (2008) reviewed and re-examined the classical analytical solutions for run-up of periodic long waves on an infinitely long slope, as well as on a finite slope attached to a flat bottom. They proposed an empirical formula for the maximum run-up height as a function of surf similarity through numerical simulations.

The work of Baldock et al (2009) used a set of laboratory data for tsunami wave kinematics on an impermeable slope and showed that a simple empirical formula, expressed as the function of tsunami wave height, is a better predictor of the maximum run-up height in comparison to Hunt's formula.

Since the study was done by Hunt, many scientists have been involved in this particular problem. Nonetheless, it has been concluded that one equation is not enough to express the wave height or the wave run-up height for all cases and more research is needed to find the solution for this particular problem.

Several recent numerical models capable of simulating tsunami run-up height for complex, three-dimensional shoreline topography have been developed (e.g. Liu 2009; Kirby 2009). Since the 2004 tsunami, there has been significant work on tsunami models, particularly at the ocean-basin scale. Fewer models are capable of handling complex overland flows (Lynett 2007), and the flow around individual and groups of buildings is an area of investigation (e.g.Tomita et al. 2007; Cox et al. 2008). In addition, estimating the inundation caused by tsunami waves was performed in order to examine tsunami hazard mitigation practices (Pelinovsky et al. 1999). Numerical simulations have been well performed and broadly accepted, but these models have limited usage because a huge computational time and cost is needed.

1.3.1.2 WAVE FORCE MODELS

It is clear that the design of coastal structures in a tsunami-hazard zone should take into account loading from tsunamis if it is to be considered safe. Structural damage from tsunamis is caused by water-borne debris and by direct hydrostatic, and, in particular, hydrodynamic, forces. Experimental and numerical studies (e.g. Neelamani et al. 1999; FEMA-P646 2008; Wilson et al. 2009) or incident wave conditions (Ramsden 1996) demonstrate that the tsunami wave height is directly related to the wave forces exerted on a coastal structure.

Palermo et al (2009) carried out the experimental test in a large-scale flume and stated that the tsunami loading should be considered in design problems. Myrhaug et al (2009) provided a practical method consisting of only hydrodynamic forces to estimate the drag force on a vegetation field and the method was compared with the non-linear waves equations based on Stokes second order wave theory. Lukkunapraist et al (2009), Coastal Construction Manual (FEMA 55 2000), and ASCE (2005) proposed different equations based on fluid mechanics and experimental test data. FEMA P646 (2008) stated that tsunami wave force should be considered for the design of coastal structures, especially vertical evacuation structures. Approximate tsunami wave loading can be computed using a set of approximation equations proposed in FEMA P646 (2008). This approach provides an equivalent force expressed as a function of tsunami wave height. Despite continued scientific research, it remains very difficult to investigate the actual wave force, i.e. the actual wave pressure distribution, when the wave hits the structure mainly due to the combined water and air makeup of the tsunami bore. Thus, the formulas proposed in

FEMA P646 (2008) are assumed to be acceptable in computing tsunami wave forces to reduce the complexity of calculations within this dissertation.

1.3.2 EARTHQUAKES

1.3.2.1 OVERWIEW

Since modern seismic record keeping began in 1900, studies on earthquakes have been significantly improved to better understand mechanics and successfully reduced the earthquake damage. Many researchers have carried out experimental tests and numerical approaches to help better understand the structural behavior under earthquake loadings. Many documents have been published as an outcome of these studies. The National Earthquake Hazards Reduction Program (NEHRP) has been organized to reduce risks to life and property from earthquakes since 1977. The Federal Emergency Management Agency (FEMA) was also established to support and improve the capability to prepare for and protect against hazards including earthquakes.

Experimental studies involving wood have ranged from static to pseudo-dynamic as well as full-scale shake table studies. Recently, a significant seismic full-scale six-story condominium building's experiment test, especially focused on engineering wood construction, has been successfully completed as the part of the four-year five-university NEESWood project team led by van de Lindt (2011). This has been tested on the E-Defense (Miki City, Japan) shake table, the largest 3-D shake table in the world, to accommodate the height and payload of the mid-rise building in June 2010 (Pei et al. 2010). Numerical models, especially related to wood-materials, have been included the

study of three-dimensional structural components such as shear walls, roof and floor diaphragms, and its connectors and fasteners, under static and monotonic or cyclic loadings (He 2002; Du 2003; Folz and Filiatrault 2004a, b; van de Lindt 2004; Collins et al. 2005a; Judd 2005; Pei and van de Lindt 2008; Xu and Dolan 2009b). Overall, its development has included elastic and inelastic response of the structures (e.g. see Hart and Wong 2000; Chopra 2007 for details).

Meanwhile, scientists have introduced seismic protective devices such as base isolation systems and viscous dampers. Base isolation systems for protecting a building from the damage of an earthquake have become a practical strategy for earthquake-resistant design and have been installed in structures at the interface between the structure and the foundation to reduce inertia forces on the structure from earthquakes. Viscous dampers have been placed in buildings and bridges to dissipate the energy input to the structure from either wind or earthquake forces. These techniques have matured and are known as passive structural control techniques.

1.3.2.2 FRAGILITIES

In earthquake engineering, probabilistic relationships between earthquake ground motion intensity and structural damage are known as fragilities. Fragility curves describe the conditional probabilities of sustaining different degrees of damage at given levels of ground motion intensity. Thus, the development of fragility curves and damage probability matrices requires the characterization of the ground motion and the identification of the different degrees of structural damage.

Shinozuka et al (2000) presented a statistical analysis of structural fragility curves for both empirical and analytical approach. He utilized bridge damage data obtained from the 1995 Kobe earthquake for constructing fragility curves. Rosowsky and Ellingwood (2002) and Ellingwood et al (2004) developed a fragility analysis methodology for assessing the response of light-frame wood construction exposed to stipulated extreme windstorms and earthquakes. Li and Ellingwood (2006) developed probabilistic risk assessment methods to assess performance and reliability of low-rise light-frame wood residential construction in the United States subjected to hurricane hazards. Banerjee and Shinozuka (2008) proposed a mechanistic model for seismic damage ability of concrete bridges in the form of fragility curves in such a way that the model can be calibrated with the empirical fragility curves constructed on the basis of the damage data from the 1994 Northridge earthquake.

Park and van de Lindt (2009) developed a fragility formulation, which provided a method to assess the seismic vulnerability of a structure using existing shake table test data. A performance-based wind engineering approach that built on the logic of the Ellingwood et al (2004) study was based on fragility curves and was proposed by van de Lindt and Dao (2009). Koshimura et al (2009) applied a fragility analysis for tsunami hazard based on numerical simulations, observations, and data from the 2004 Indian Ocean tsunami disaster.

The majority of the above studies have successively relied upon experimental data in order to provide an accurate approach to both hazard and resistance for earthquakes and

wind fragility development. The ability to accurately characterize tsunami hazard is somewhat lacking due to the rarity of these natural phenomena and, as mentioned above, the exact loading is believed to vary significantly depending on numerous physical variables.

1.3.3 STRUCTURAL ANALYSIS

1.3.3.1 FINITE ELEMENT METHOD

The Finite Element Method (FEM) has become the prevalent technique used in structural analysis studies over the last several decades. The development and application of numerical models for wood structures, which have nonlinear behavior, has been relatively slow. In recent years, significant work to develop models suitable for nonlinear and dynamic analysis of light-frame wood buildings with high accuracy has been completed.

Dolan (1989) and White and Dolan (1995) developed a finite element program to perform nonlinear dynamic analysis of wood shearwalls with the introduction of non-linear hysteresis model for sheathing-to-framing connectors. Filiatrault (Filiatrault 1990) used a displacement-based energy formulation with the non-linear load-slip characteristics of sheathing-to-framing connectors in order to develop a two-dimensional shear wall model for both static and dynamic analysis. Tarabia (1994) and Tarabia and Itani (1997) presented a general three-dimension model of light-frame wood building using finite element method. In his model, five elements: framing elements, sheathing elements, sheathing interface elements, framing connector elements, and fastener

elements were used to model diaphragm and shearwalls. Hysteresis models were proposed to simulate fastener elements.

Folz and Filiatrault (2001) proposed a numerical model, called CASHEW (Cyclic Analysis of SHEar Walls), using three structural components, which were rigid framing members, linear elastic sheathing panels, and nonlinear sheathing-to-framing connectors, in order to predict the load-displacement response and energy dissipation characteristics of wood shearwalls under cyclic loadings. Good agreements were shown with the experimental test by using the hysteretic model for the sheathing-to-framing connector. Later, they developed a program, called SAWS (Seismic Analysis of Woodframe Structures), to predict the dynamic characteristics, quasi-static pushover, and seismic response of woodframe buildings. In their model, the three-dimensional building is degenerated into a two-dimensional planar model using a non-linear hysteretic spring (Folz and Filiatrault 2004a, b).

Judd (2005) and Judd and Fonseca (2005) developed a new analytical model for sheathing-to-framing connectors based on the CASHEW model for wood shearwalls and diaphragms by using a commercial software ABAQUS. In the ABAQUS program, wood framings are represented using linear beam elements, sheathing panels are represented using plane stress elements, chord splice connections are represented using linear spring elements, and new hysteresis model, implemented using user-defined elements. Collins et al (2005a, b) proposed a detailed three-dimensional numerical model based on finite element method by using a commercial software ANSYS. Shearwalls were modeled

using sheathing panels as shell elements, wood-framing as beam elements, and the connectors as the customized hysteretic spring elements. Then, each shearwall was replaced using sub-modeling technique to reduce the complexity of the model during analysis.

Using a nonlinear hysteretic spring element to model the sheathing-to-frame connector's behavior using finite element method is an acceptable approach when analyzing woodframe structures (Folz and Filiatrault 2001; He 2002; Du 2003; Folz and Filiatrault 2004a, b; Collins et al. 2005a; Judd 2005; Pei and van de Lindt 2008; Xu and Dolan 2009a, b).

1.3.3.2 HYSTERESIS MODEL FOR CONNECTOR

In order to complete the structural analysis using the finite element method, the sheathing-to-frame connectors should be modeled properly to propagate their nonlinear behavior to the system level because these connectors have dominated the response of woodframe structures under monotonic and cyclic loadings. To do this, hysteresis models have been recommended to represent the sheathing-to-frame connectors during the past several decades.

Since Foschi (1974) proposed a simple three-parameter model for the load-slip behavior of timber joints, many scientists have based monotonic and cyclic response of these connectors on that study. Dolan (1989) extended the work of Foschi (1974, 1977) and proposed a six-parameter model. Whilte and Dolan (1995) developed a hysteretic model

in order to simulate sheathing-to-framing connectors under monotonic and cyclic loadings. Tarabia (1994) proposed new hysteretic models including the axial resistance of connectors with the validation of experimental test data.

Folz and Filiatrault (2001) developed a new hysteretic model and called the CASHEW model. This model was extended from Stewart's (1987) and Dolan's (1989) model using a series of linear segments to model the loading and unloading paths off the envelop curve. This model included pinching behavior and strength and stiffness degradation under cyclic loading. Pang et al (2007) described a new evolutionary parameter hysteretic model, called the EPHM, based on the CASHEW model. In the EPHM, the authors improved the predictions of CASHEW by incorporating nonlinear loading and unloading paths with evolutionary hysteretic parameters.

1.4 OPTIMIZATION TECHNIQUES

Optimization techniques have been employed to develop an evacuation plan for single structures and for the community. To do this, a genetic algorithm has been adopted and it is a heuristic search procedure based on the mechanics of natural selection and genetics. It has been employed broadly to generate useful solutions to optimization and search problems over the 50 years due to the simple and robustness.

Since proposed by Holland (1975) and matured by Goldberg (1983, 1989), the genetic algorithm (GA) has been adopted extensively in many engineering optimization problems.

The application has variety such as shape and sizing optimization problem, structural design problems, estimating parameters, etc. Rajeev and Krishnamoorthy (1992) presented a simple genetic algorithm for designing structural systems with discrete variables. Hajela and Lee (1995) presented a stochastic search procedure based on genetic algorithm to develop optimal topologies of load bearing truss structures. Rajan (1995) proposed an approach based on a genetic algorithm to optimize the size, shape, and topology design of space trusses.

Recently, Kongsomsaksakul et al (2005) studied optimal shelter locations for flood evacuation planning using genetic algorithms. The shelter location was determined to minimize the evacuation time based on the several pre-defined locations. Doerner et al (2009) proposed a heuristic approach based on GA to make location planning for public facilities in tsunami-prone coastal areas. An objective function was formulated using three criteria such as a weighted mean of a minimum and maximum coverage, risk by possible tsunami events, and costs. The model was then applied to Southern Sri Lanka region.

1.5 ORGANIZATION OF DISSERTATION

The remainder of this dissertation presents the theory and methodology for the development of an evacuation planning methodology for a single light-frame wood structure and for entire communities from tsunamis using a numerical approach. Chapter 2 presents the theory and mathematical formulations for seismic and tsunami analysis, a

hysteretic model, a calculation of tsunami wave forces, a fragility analysis, and the optimization technique.

Chapter 3 provides the development of NAPSS (Nonlinear Analysis Program for Structural System) and SSTAP (Sequential Seismic and Tsunami Analysis Program), which is based on general finite element procedures for the nonlinear analysis of shear walls and entire structure. NAPSS is focused on computing the response of wood shearwalls and estimating the hysteretic parameters. SSTAP is focused on a response of structure.

Chapter 4 provides a tsunami fragility formulation and application for the single residential structure and its extension to the community level. Also, the interaction between the earthquake and resulting tsunami hazard is investigated. An illustrative example is considered to verify the proposed approach. Detailed modeling of a single structure, the results of structural analysis, and fragility analysis for single structures are presented.

Chapter 5 presents a tsunami vertical evacuation methodology for a single structure and an entire coastal community as well. Initially, each single structure can be reinforced with a tsunami safe frame consisting of steel or reinforced concrete columns to increase the lateral stiffness of the structure and heighten the elevation in order to decrease the collapse risk of the buildings from tsunami wave loading. An optimization has been

carried out to find the optimum location of the shelter for a community. A detailed example and its modeling are presented.

Chapter 6 describes the tsunami reliability assessment of a community using fragilities and the statistical approach. An event tree analysis has been adopted to consider the possible scenarios and maximize the survival of people in the community.

Chapter 7 presents a summary and conclusions, keeping in mind the objectives for this dissertation. Additional observations and recommendations are also provided, and a list of pertinent future research is suggested.

CHAPTER 2

THEORY AND MATHEMATICAL FORMULATION

2.1 OVERVIEW

This chapter provides the theory and mathematical formulation for seismic and tsunami analysis, a fragility analysis, and the optimization technique used. The seismic analysis module utilized the well-known Newmark β method, model reduction technique, and hysteresis models to obtain a computational efficiency. Background on the Newmark β method and hysteretic models is included but discussion on the model reduction technique is explained in Chapter 3 where the development of the numerical model is explained. A quasi-static pushover analysis module for tsunamis is added including a calculation of tsunami wave loadings.

2.2 SEISMIC ANALYSIS

In 1959, Newmark (1959) presented a family of single-step numerical integration methods for the solution of structural dynamic problems for seismic loading. Over the past decades, the Newmark β method has been broadly adopted to solve dynamics problems in structural engineering. The derivation of the method begins with

D'Alembert's principle of dynamic equilibrium for a multi degrees of freedom (MDOF) system subjected to base ground motion written in the following general form:

$$[m]\{\ddot{u}\}+[c]\{\dot{u}\}+[f_s(u,\dot{u})]\{u\}=-[m]\{(\ddot{u}_g)_i\} \tag{2-1}$$

where $[m]$ is a mass matrix of system, $\{\ddot{u}\}$ is a acceleration vector of mass relative to base, $[c]$ is a equivalent viscous damping matrix of system, $\{\dot{u}\}$ is a velocity vector of mass relative to base, $[f_s(u,\dot{u})]$ is a stiffness matrix of system which can have the linear or nonlinear behavior based on the characteristics of system, $\{u\}$ is a displacement vector of mass relative to base, and $\{(\ddot{u}_g)_i\}$ is a base ground acceleration vector given by a set of discrete values $(\ddot{u}_g)_i=\ddot{u}_g(t_i)$, $i=0\ldots N$.

Two assumptions about the variation of acceleration over a time step were developed by Newmark (1959) which is constant or linear. Initially, the variation of acceleration is assumed to be constant within a small increment of time, called constant average acceleration method and illustrated in Figure 2.1. The acceleration at time interval τ between t_i and t_{i+1} can be expressed as:

$$\ddot{u}(\tau)=\frac{1}{2}\left(\ddot{u}_{i+1}+\ddot{u}_i\right) \tag{2-2}$$

Then, integrating of Equation (2-2) twice can produce the following two expressions, respectively:

$$\dot{u}(\tau)=\dot{u}_i+\frac{\tau}{2}\left(\ddot{u}_{i+1}+\ddot{u}_i\right),\ \ u(\tau)=u_i+\dot{u}_i\tau+\frac{\tau^2}{4}\left(\ddot{u}_{i+1}+\ddot{u}_i\right) \tag{2-3}$$

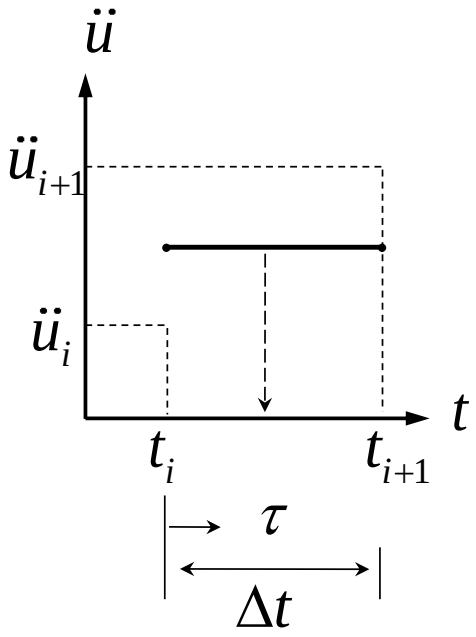

Figure 2.1: The constant averaged acceleration method.

The substitution of $\tau=\Delta t$, which is time $i+1$, in Equation (2-3) can yield the following:

$$\dot{u}_{i+1}=\dot{u}_i+\frac{\Delta t}{2}\left(\ddot{u}_{i+1}+\ddot{u}_i\right),\ \ u_{i+1}=u_i+\dot{u}_i\left(\Delta t\right)+\frac{\left(\Delta t\right)^2}{4}\left(\ddot{u}_{i+1}+\ddot{u}_i\right) \tag{2-4}$$

A linear variation of acceleration from time t_i to time t_{i+1} is assumed to be linear, is called the linear acceleration method and is shown in Figure 2.2. The similar derivation can be repeated in here and then the variation of the acceleration can be expressed as:

$$\ddot{u}(\tau) = \ddot{u}_i + \frac{\tau}{\Delta t}\left(\ddot{u}_{i+1} - \ddot{u}_i\right) \tag{2-5}$$

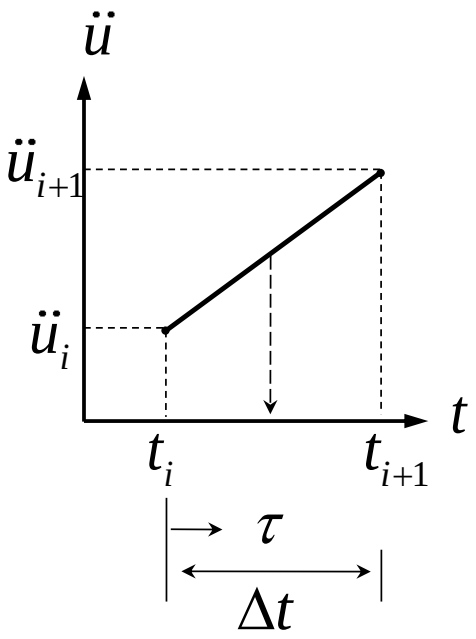

Figure 2.2: The linear acceleration method.

Then, integrating of Equation (2-5) twice can produce the following two expressions, respectively:

$$\dot{u}(\tau) = \dot{u}_i + \ddot{u}_i\tau + \frac{\tau^2}{2\Delta t}\left(\ddot{u}_{i+1} - \ddot{u}_i\right),\ u(\tau) = u_i + \dot{u}_i\tau + \ddot{u}_i\frac{\tau^2}{2} + \frac{\tau^3}{6\Delta t}\left(\ddot{u}_{i+1} - \ddot{u}_i\right) \tag{2-6}$$

Then, the substitution of $\tau = \Delta t$ into Equation (2-6) can give as the following equation:

$$\dot{u}_{i+1} = \dot{u}_i + \frac{\Delta t}{2}\left(\ddot{u}_{i+1} + \ddot{u}_i\right),\ u_{i+1} = u_i + \dot{u}_i\left(\Delta t\right) + \frac{\left(\Delta t\right)^2}{6}\left(\ddot{u}_{i+1} + 2\ddot{u}_i\right) \tag{2-7}$$

Therefore, two expressions in Equation (2-4) and Equation (2-7) can be written as the standard Newmark form, respectively:

$$\dot{u}_{i+1} = \dot{u}_i + [(1-\gamma)\Delta t]\ddot{u}_i + (\gamma\Delta t)\ddot{u}_{i+1} \tag{2-8}$$

$$u_{i+1} = u_i + (\Delta t)\dot{u}_i + [(0.5-\beta)(\Delta t)^2]\ddot{u}_i + [\beta(\Delta t)^2]\ddot{u}_{i+1} \tag{2-9}$$

where the parameters β and γ define the variation of acceleration over a time step and determine the stability and accuracy characteristics of the method.

Equation (2-1) can be reformulated by using Equation (2-10) to avoid iteration and to use incremental quantities. Equation (2-1) is then converted into the Equation (2-11), an incremental form as following:

$$\Delta u_i \equiv u_{i+1} - u_i, \quad \Delta\dot{u}_i \equiv \dot{u}_{i+1} - \dot{u}_i, \quad \Delta\ddot{u}_i \equiv \ddot{u}_{i+1} - \ddot{u}_i, \quad \Delta(\ddot{u}_g)_i \equiv (\ddot{u}_g)_{i+1} - (\ddot{u}_g)_i \tag{2-10}$$

$$[m]\{\Delta\ddot{u}_i\} + [c]\{\Delta\dot{u}_i\} + [f_s]\{\Delta u_i\} = -[m]\{\Delta(\ddot{u}_g)_i\} \tag{2-11}$$

where the response is determined at the discrete time instant t_i, denoted as time i: the displacement, velocity, and acceleration of the system are u_i, $\dot{u}_i$, and $\ddot{u}_i$, in equation of motion, respectively.

Equation (2-8) and Equation (2-9) can be arranged into incremental form:

$$\Delta\dot{u}_i = (\Delta t)\ddot{u}_i + (\gamma\Delta t)\Delta\ddot{u}_i \tag{2-12}$$

$$\Delta u_i = (\Delta t)\dot{u}_i + \frac{(\Delta t)^2}{2}\ddot{u}_i + \beta(\Delta t)^2\Delta\ddot{u}_i \tag{2-13}$$

Then, the acceleration incremental can be formulated the following form:

$$\Delta\ddot{u}_i = \frac{1}{\beta\ (\Delta t)^2}\Delta u_i - \frac{1}{\beta\Delta t}\dot{u}_i - \frac{1}{2\beta}\ddot{u}_i \tag{2-14}$$

Substitution of Equation (2-14) into Equation (2-12) gives the following equation:

$$\Delta\dot{u}_i = \frac{\gamma}{\beta\,\Delta t}\Delta u_i - \frac{\gamma}{\beta}\dot{u}_i + \Delta t(1-\frac{\gamma}{2\beta})\ddot{u}_i \tag{2-15}$$

Also, substitution from Equation (2-13) to Equation (2-15) into Equation (2-11) produces the following form:

$$(K_{effective})\Delta u + (-FAC_1)\dot{u}_i + (-FAC_2)\ddot{u}_i = -[m]\Delta(\ddot{u}_g)_i \tag{2-16}$$

where $K_{effective} = \frac{[m]}{\beta(\Delta t)^2} + \gamma\frac{[c]}{\beta\Delta t} + f_s$, $FAC_1 = \frac{[m]}{\beta\Delta t} + \gamma\frac{[c]}{\beta}$,

and $FAC_2 = \frac{[m]}{2\beta} - (1-\frac{\gamma}{2\beta})[c]\Delta t$.

Finally, increments in displacement and velocity can be computed based on the following forms:

$$\Delta u_i = \frac{(FAC_1)\dot{u}_i + (FAC_2)\ddot{u}_i - [m]\Delta(\ddot{u}_g)_i}{(K_{effective})} \tag{2-17}$$

$$\Delta \dot{u}_i = (FAC_3)\Delta u_i - (FAC_4)\dot{u}_i + (FAC_5)\ddot{u}_i \tag{2-18}$$

where $FAC_3 = \frac{\gamma}{\beta \Delta t}$, $FAC_4 = \frac{\gamma}{\beta}$, and $FAC_5 = (1 - \frac{\gamma}{2\beta})\Delta t$.

The increments of displacement and velocity can be computed from Equation (2-17) and Equation (2-18). Then, the response of system at next time step can be calculated from the sum of the response of current time step and the increments. After that the acceleration can be obtained from the equation of motion at time *i*+1 by using Equation (2-1). This approach requires a differential equation at time t_{i+1} after the solution at time t_i is found. Thus, it is the implicit method and requires the solution of a set of linear equations at each time step. Overall procedure of Newmark β method is depicted in Figure 2.3. In this dissertation, the constant average acceleration method, which gives unconditional stability for any time step, has been adopted. The parameter of two Newmark β methods is summarized in Table 2.1.

Table 2.1: Two parameters of Newmark β method.

Name	γ	β
Linear	$\frac{1}{2}$	$\frac{1}{6}$
Constant averaged	$\frac{1}{2}$	$\frac{1}{4}$

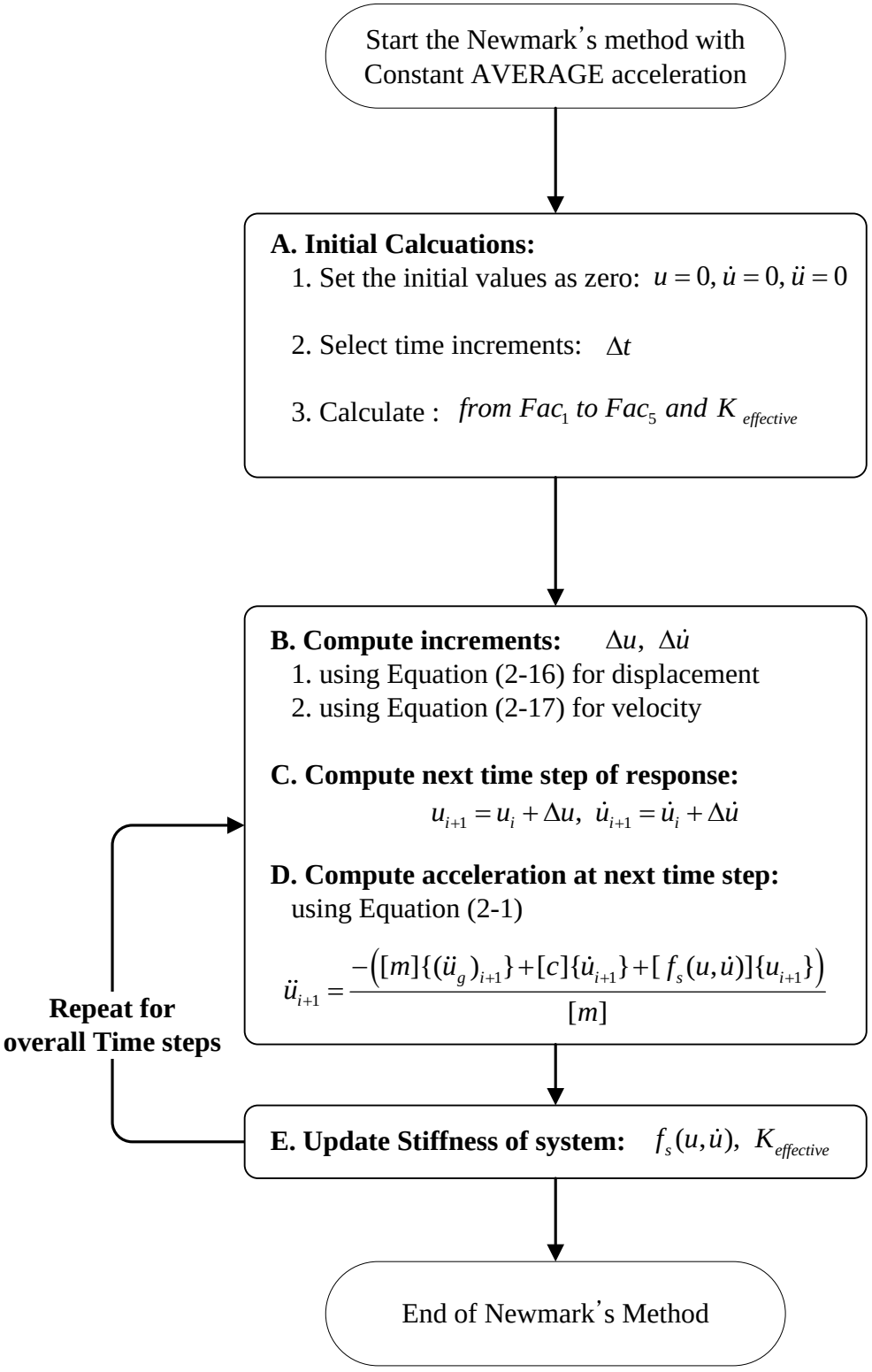

Figure 2.3: Overview of the Newmark β method.

Finally, the Newmark β method can be expressed implicitly as the only unconditionally stable method for the seismic analysis of practical engineering problems. The method has been implemented into the program, called SSTAP. Detailed explanation of building the system matrix and its development procedure of SSTAP are discussed in Chapter 3.

2.3 TSUNAMI ANALYSIS

A nonlinear pushover analysis has been adopted to analyze structures under tsunami load in this dissertation. The load is simplified and the equivalency procedure to obtain a deformation similar to that caused by a wave when pushing at the top of the wall will be explained later. The seismic analysis method mentioned above can be adopted again with the modification of a forcing function. Equation (2-19) can be employed to perform the tsunami analysis and it is identically equal to Equation (2-1) except that the right-hand side of the equation is now simply the pushover forcing function $P(t)$.

$$[m]\{\ddot{u}\}+[c]\{\dot{u}\}+[f_s(u,\dot{u})]\{u\}=P(t) \tag{2-19}$$

Then, the same procedure outlined from Equation (2-10) to Equation (2-18) can be employed in order to perform a unidirectional quasi-static pushover analysis by using $P(t)$, defined the following form:

$$P(t)=\frac{1}{2}\left[1-\cos\left(\frac{\pi t}{T_p}\right)\right]*P_{max}\,, \qquad 0\le t\le T_p \tag{2-20}$$

where $P(t)$ represents the temporal variation in the monotonically increasing, applied pushover load, P_{max} defined as the magnitude of the maximum lateral load. The maximum pushover load can be determined from the computed equivalent tsunami wave loading, applied to the structure, where T_p is the duration of the applied loading.

During analysis, two values can be used to define the P_{max}: (1) is to assume the value from the computed tsunami wave force and (2) is to take the maximum load-carrying capacity of the structure. The second approach, P_{max}, is defined as Equation (2-21) to ensure that the lateral load-carrying capacity of the structure is reached during the pushover analysis.

$$P_{max} = (0.05 * H_T) * \frac{P_1}{\Delta_1} \tag{2-21}$$

where H_T is the total height of the structure, P_1 is a lateral load of unit magnitude, and Δ_1 is the corresponding top of roof displacement obtained from a linear quasi-static analysis. In Equation (2-21), the load-carrying capacity of the structure is assumed to be the load needed to produce a 5% drift, defined as an approximate maximum drift before collapsing, in the structure under a linear elastic response. It should be noted that the maximum load is needed to define a load range during the non-linear analysis, thus it is

felt to be reasonable that the maximum drift from the linear elastic response could be a proper value.

2.4 HYSTERESIS MODEL

In order to most accurately represent the structures, a hysteretic model should be used. Generally, a hysteresis model defines the shape of the force-deformation loops with a set of empirical rules to allow one to perform nonlinear static and dynamic analysis. There is a full range of complexities for hysteretic models ranging from a simple elasto-plastic model (see Chopra 2007 for an example) to a model capable of full strength and stiffness degradation (Folz and Filiatrault 2001).

2.4.1 BILINEAR HYSTERETIC MODEL

A bilinear model is very similar to the simple elasto-plastic model, but it also accounts for the strain hardening effect in steel and reinforced concrete using non-zero post-yield stiffness and wood as well. As shown in Figure 2.4, the bilinear hysteresis can be expressed as a function of initial stiffness until yielding, the ratio of the stiffness after yielding to pre-yield stiffness, and the yield displacement.

It can be identically equal to the elasto-plastic model when the scaling factor of the stiffness after yielding is set to zero.

$$P = \begin{cases} K_0 * \delta & : |\delta| < \delta_y \\ K_0 * (\alpha\delta + (1-\alpha)\delta_y) & : |\delta| \geq \delta_y \\ 0 & : |\delta| \geq \delta_F \end{cases} \quad (2\text{-}22)$$

where K_0 is an initial stiffness, α is a yielding scaling factor ranging from 0 to 1, δ_y is a yielding displacement, δ_{UN} is a last unloading displacement (in following Figure 2.4), and δ_F is an arbitrarily defined failure displacement for applications.

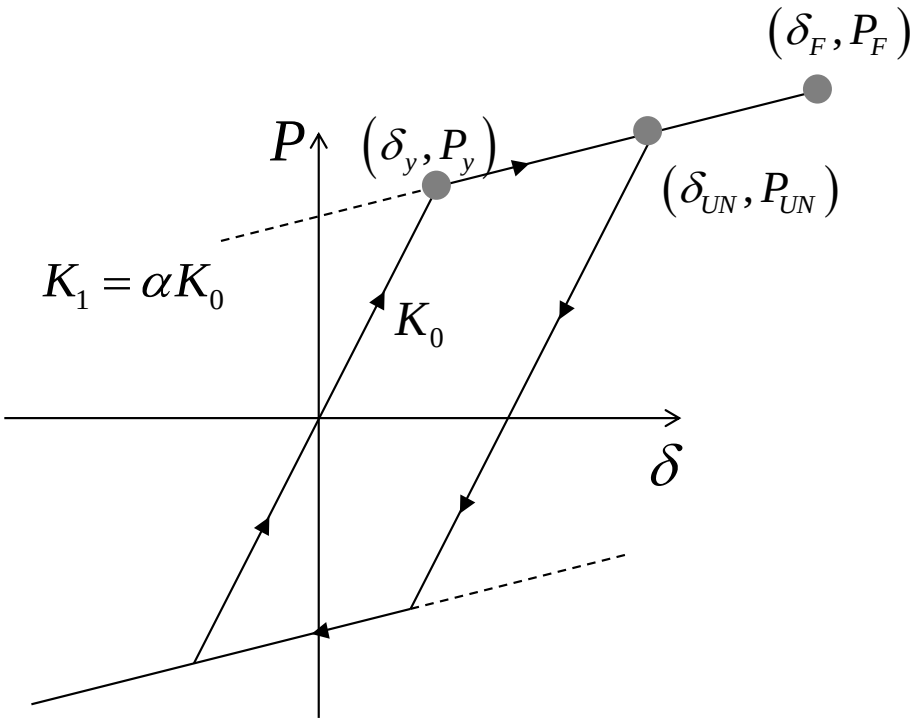

Figure 2.4: The parameters of a bilinear hysteretic model.

2.4.2 CUREE HYSTERETIC MODEL

The CUREE model, also known as modified Stewart model or CASHEW, has been developed as part of the CUREE (Consortium of Universities for Research in Earthquake

Engineering) Wood-frame research project. Initially, Folz and Filiatrault (2001) modified the exponential envelop curve used by Dolan (1989) to include hysteretic characteristics of a Stewart model (1987). The CUREE model has been employed to simulate the shear behavior of single sheathing-to-framing fasteners in wood shearwalls model and an equivalent single degree of freedom (DOF) model an entire wood shearwalls.

A force-deformation response of a sheathing-to-framing connector has a highly nonlinear behavior under monotonic and cyclic loading. Initially, as loading is increased, the connector deformed and its connection starts losing the capacity in proportion to the loading due to the nonlinearity of wood material, i.e. the wood is crushed by the connector gradually. If the loading continues after yielding of the connector, prior to failure the strength of the connection decreases with increasing displacement due to the connector withdrawal. The force-deformation curve under monotonic loading, shown in Figure 2.5, can be formulated as Equation (2-23), in order to capture the crushing between the wood framing and sheathing along with yielding of the connector.

$$P = \begin{cases} sign(\delta)\left(P_0 + r_1 K_0 |\delta|\right)\left[1 - \exp(-K_0 |\delta| / P_0)\right], & : |\delta| \le |\delta_u| \\ sign(\delta) P_u + r_2 K_0 \left[\delta - sign(\delta)\delta_u\right], & : |\delta_u| < |\delta| \le |\delta_F| \\ 0, & : |\delta| > |\delta_F| \end{cases} \qquad (2\text{-}23)$$

where K_0 is an initial stiffness, P_0 is an initial force, r_1 is a secondary stiffness factor, r_2 is a tertiary stiffness factor, δ_u is a ultimate displacement, and δ_F is a failure displacement, defined as the displacement occurs when the connector fails.

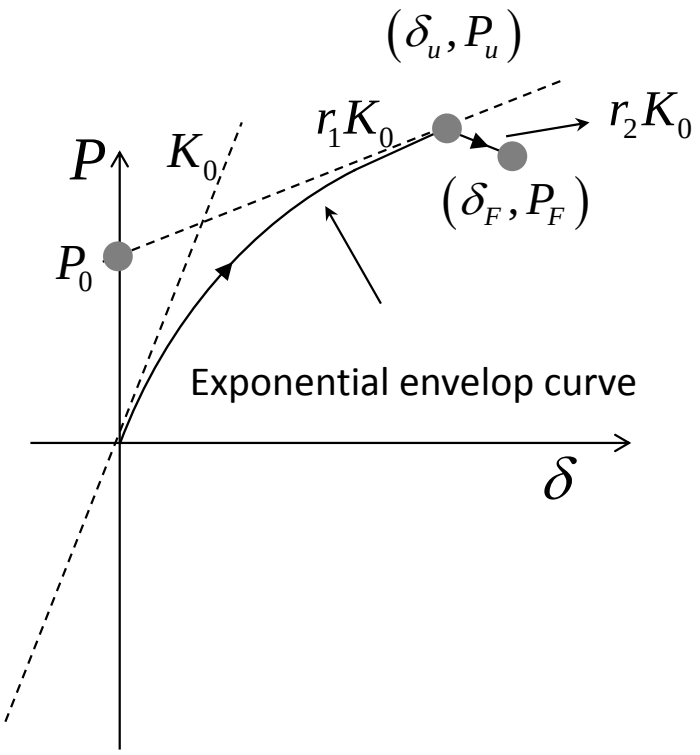

Figure 2.5: Force-deformation curve of CUREE model under monotonic loading.

Next, if the loading is reversed, i.e. under cyclic loading, the connector behaves as a pinched hysteresis loop. During the reversed-cyclic loading, hysteresis behavior is idealized by using a predefined set of load-paths to describe unloading, loading, and reloading. Initially, the loading rules follow the monotonic backbone curve described above. Unloading rules can be defined as piecewise linear by using two degrading stiffnesses, r_3K_0 and r_4K_0. During unloading, the connector loses partial contact with the surrounding wood due to permanent deformation caused by previous loading. Reloading after unloading exhibits a pinching stiffness K_P where pinching force P_I corresponds to zero-displacement and the reversal load path follows the unloading stiffness. The stiffness and strength degradation are defined using Equation (2-24).

$$K_P = K_0 \left(\frac{P_0}{\beta K_0 \delta_{UN}} \right)^{\alpha} \tag{2-24}$$

where K_0 is an initial stiffness, F_0 is an initial force, α and β are the degree of stiffness degradation parameters, and δ_{UN} is a last unloading displacement.

Therefore, the CUREE model, depicted in Figure 2.6, can be defined as the function of ten-parameter hysteretic model with loading and unloading rules.

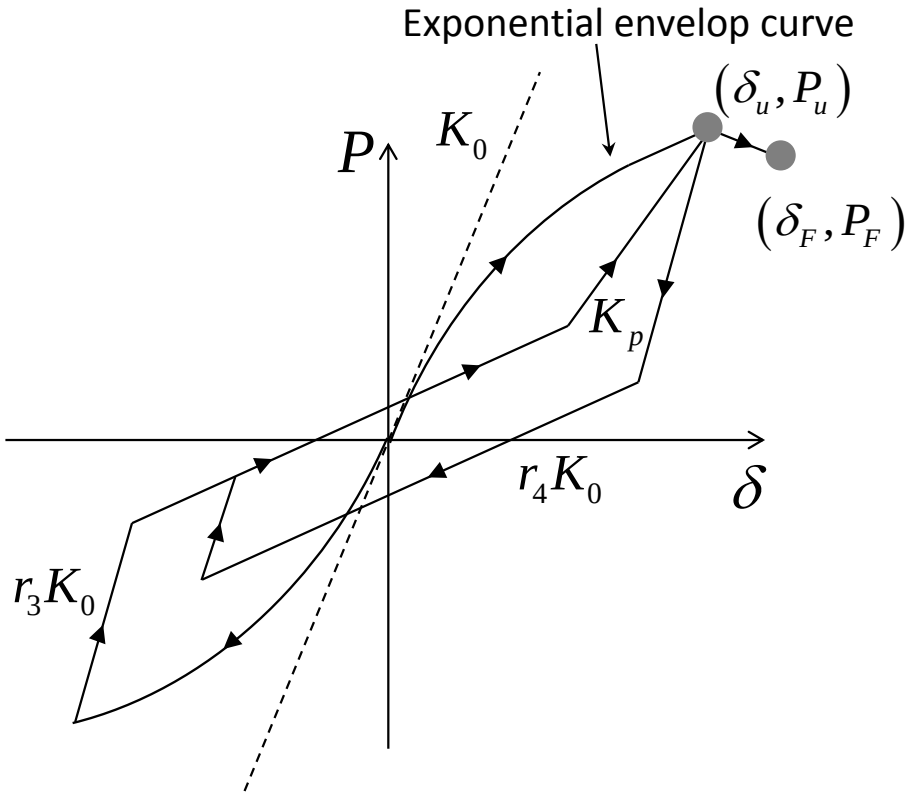

Figure 2.6: Force-deformation curve of CUREE Model under cyclic loading.

2.5 WAVE FORCE MODELS

Clear terminology related to tsunamis is imperative to form a clear understanding of the problem at hand. Inundation, or inundation distance, is the horizontal distance inland measured perpendicular to the shoreline, generally. The inundation line is measured horizontally from the mean sea level line. Run-up can be defined two ways: (1) is the horizontal distance from the elevation of maximum inundation line to the sea level at the time of the tsunami and (2) is measured ideally at a point that is a local maximum of the horizontal inundation. Tsunami wave height, or tsunami height, is defined as the difference between the elevation of the highest local water mark and the elevation of the sea level at the time of the tsunami (UNESCO 2008; USGS 2011b).

The Federal Emergency Management Agency's document FEMA P646 (2008) also defines tsunami terminology qualitatively and quantitatively. Tsunami inundation elevation is the distance measured from sea level, at the location of the maximum tsunami penetration. Tsunami run-up is the rush of tsunami waves up a slope, terrain, or structure. Tsunami run-up height is the distance from the elevation of maximum tsunami penetration to the elevation of the shoreline at the time of tsunami attack. Wave height is the vertical distance between the successive local maximum and minimum elevations in a wave profile (FEMA P646, 2008).

Figure 2.7 depicts the physical meanings of these terms used throughout this dissertation. The tsunami wave height, or tsunami height, is defined as the difference between the

elevation of the highest local water mark and the elevation of the sea level at the time of the tsunami in this dissertation work (UNESCO 2008; USGS 2011b).

FEMA P646 (2008) defined eight different types of forces that can potentially act on a structure, three of which are considered in this study: (1) hydrostatic forces, (2) hydrodynamic forces, and (3) impulsive forces.

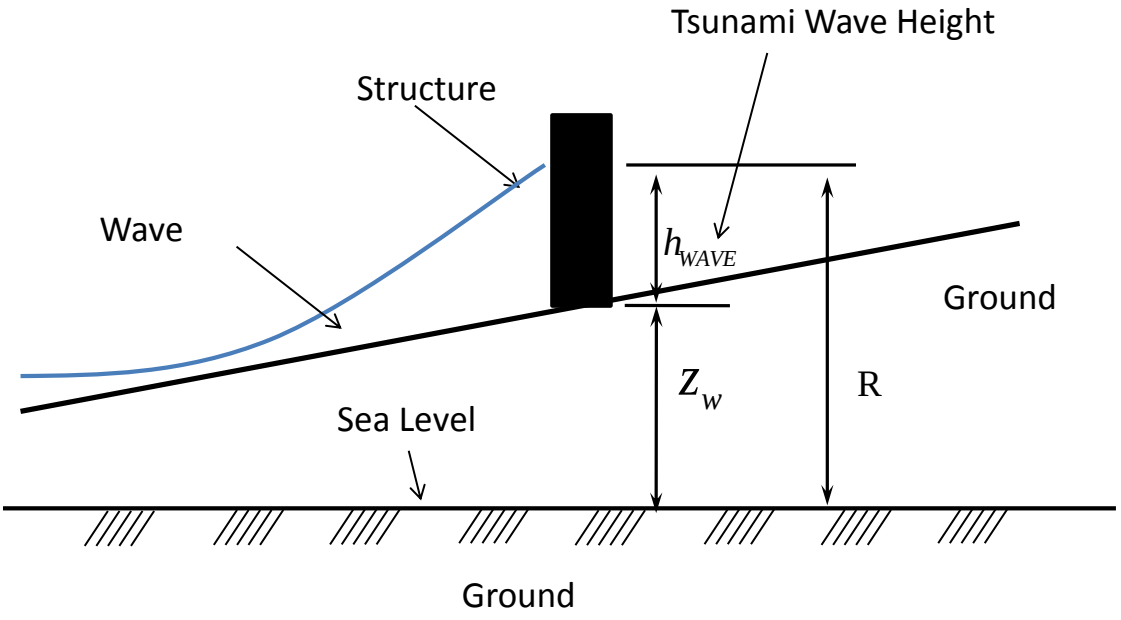

Figure 2.7: Schematic explanation of tsunami terminology.

The other forces, such as debris forces, are beyond the scope of this work but at least one project is underway by other researchers. Hydrostatic forces act when standing or slowly moving water is against a structure. It can be computed as:

$$F_h = \frac{1}{2}\rho_s g B (h_{WAVE})^2 \quad (2\text{-}25)$$

where ρ_s is the fluid density including sediment, 1200 kg/m^3 = 2.33 slugs/ft^3, g is the gravitational acceleration, B is the width of the structure or structural component, and h_{WAVE} is the maximum water height above the base of the wall at the structure location. This h_{WAVE} can be computed using the following equation:

$$h_{WAVE} = 1.3R^* - z_w = R - z_w \quad (2\text{-}26)$$

where R^* is the maximum tsunami run-up elevation taken as the estimated maximum inundation elevation at the structure from a detailed numerical simulation model, or the ground elevation at maximum penetration of the tsunami from available tsunami inundation maps. The design run-up elevation R is taken as 1.3 times the predicted maximum run-up elevation.

When water flows around a structure, hydrodynamic forces can be computed using Equation (2-27):

$$F_d = \frac{1}{2}\rho_s C_d B (hu^2)_{max} \quad (2\text{-}27)$$

where ρ_s is the fluid density including sediment, 1200 kg/m^3 = 2.33 slugs/ft^3, C_d is the drag coefficient, *B* is the width of the structure in the plane normal to the direction of flow, *h* is flow depth, and *u* is flow velocity at the location of the structure.

Impulsive forces are caused by the leading edge of a surge of water impacting a structure. It is conservatively recommended that the impulsive forces be taken as 1.5 times the hydrodynamic force and can be computed as follows:

$$F_s = 1.5F_d \tag{2-28}$$

Detailed explanations of these three forces can be found in FEMA P646 (2008). Thus, the tsunami wave forces can be computed as the summation of these three forces and expressed as:

$$TWF = F_h + F_d + F_s \tag{2-29}$$

where TWF is the total tsunami wave force, F_h is the hydrostatic force, F_d is the hydrodynamic force, and F_s is the impulsive force.

2.5.1 EQUIVALENT FORCE FOR TSUNAMI WAVE FORCE

A model reduction technique has been adopted in order to provide efficiency in computational time and cost but it has a limitation in applying the load condition on the

structure. Initially, the building model is degenerated from a three-dimension model to a two-dimension planar model. Then, each shearwall is converted into the nonlinear hysteretic spring model (such as the CUREE or bilinear model discussed earlier), which means the nodal point exists only at floor level. Thus, the computed wave force, which typically exists anywhere along the height of the structure, cannot be directly applied to the structure. Therefore, an equivalent force must be computed for the tsunami wave forces. Specifically, a point force that produces the same building response as the tsunami wave load is needed. Figure 2.8 shows the overall procedure of computation of equivalent forces.

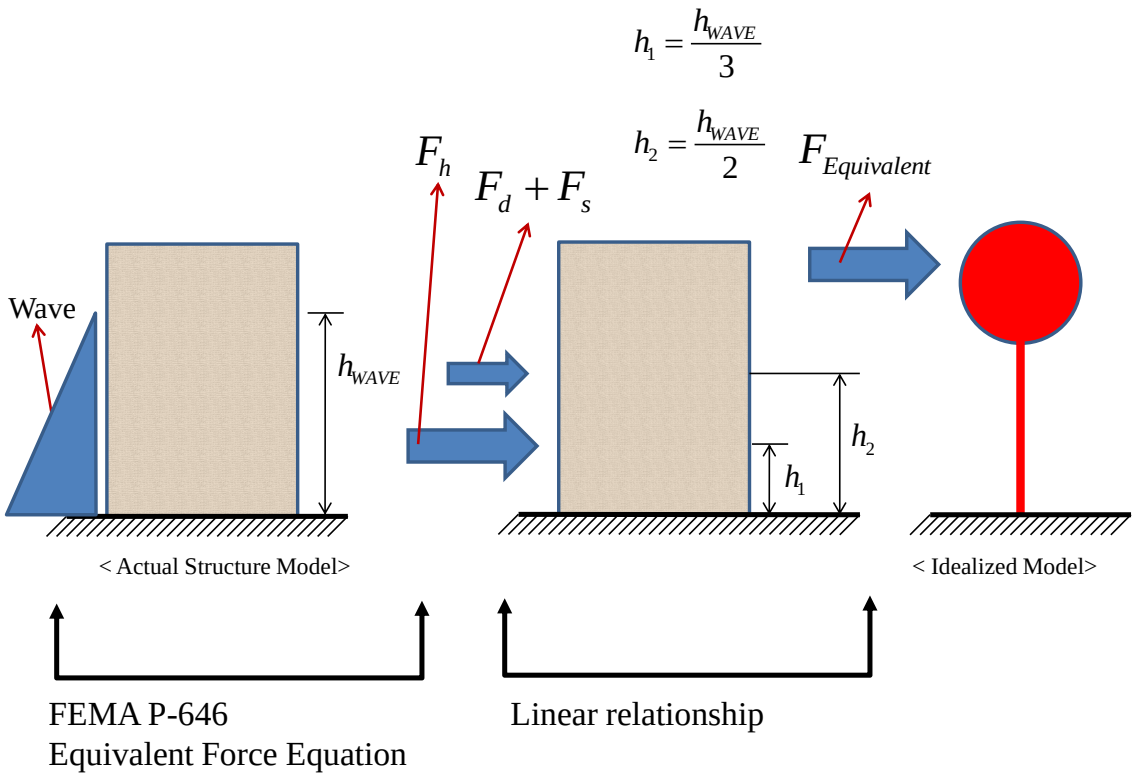

Figure 2.8: Overall schematic procedure of computation of equivalent force.

From FEMA P646 (2008), three wave forces are applied at different locations over the height of the structure. For a given tsunami wave height, hydrostatic wave forces are applied at a height equal to one-third the height of the tsunami wave height and the other two wave forces are generally applied at a height equal to half of tsunami wave height. Then, the relationship between the three tsunami wave forces and equivalent force can be assumed to be linear. Despite continued scientific research, it remains very difficult to investigate the actual wave force, i.e. the actual wave pressure distribution, when the wave hits the structure mainly due to the combined water and air makeup of the tsunami bore. Therefore, the computed wave forces are not well established with accuracy but can at least provide an approximate approach at this stage that is believed to be on the conservative side for design.

Assume the structure can be treated as a vertical cantilever beam and the forces can be dealt with as point loads on a beam considering the exact applying location. Each floor is substituted by the supporting conditions or nodal points. Then, deformations of the beam can be solved by using finite element procedure or other structural analysis methods. Typical beam's formulas, shown in Figure 2.9, are employed to calculate a deformation at a specific location by using the following form:

$$d = \begin{cases} \dfrac{Px^2}{6EI}(3a - x) & : 0 < x < a \\ \dfrac{Pa^2}{6EI}(3x - a) & : a < x < L \end{cases} \qquad (2\text{-}30)$$

where *d* is a deformation at location *x*, *x* is the target location, *a* is the location of the force *P*, *EI* are the material properties (the product of the modulus of elasticity and the moment of inertia), and *L* is the length.

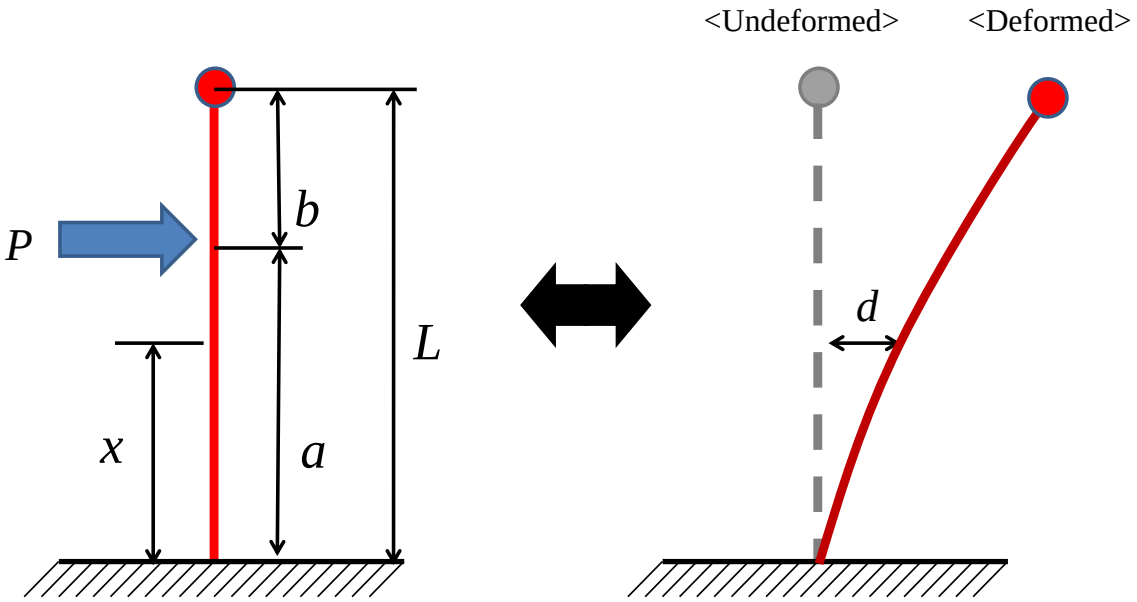

Figure 2.9: Deformation of specific location.

A typical two-story structure was selected as an illustrative example to show how to compute the equivalent forces from the three wave forces. Initially, the structure can be treated as a cantilever beam having two nodal points, as shown in Figure 2.10.

Two deformations at floor level, caused by wave forces, can be computed by using Equation (2-30). Then, the deformations caused by two equivalent forces, depicted in Figure 2.11 and Figure 2.12, can be also computed.

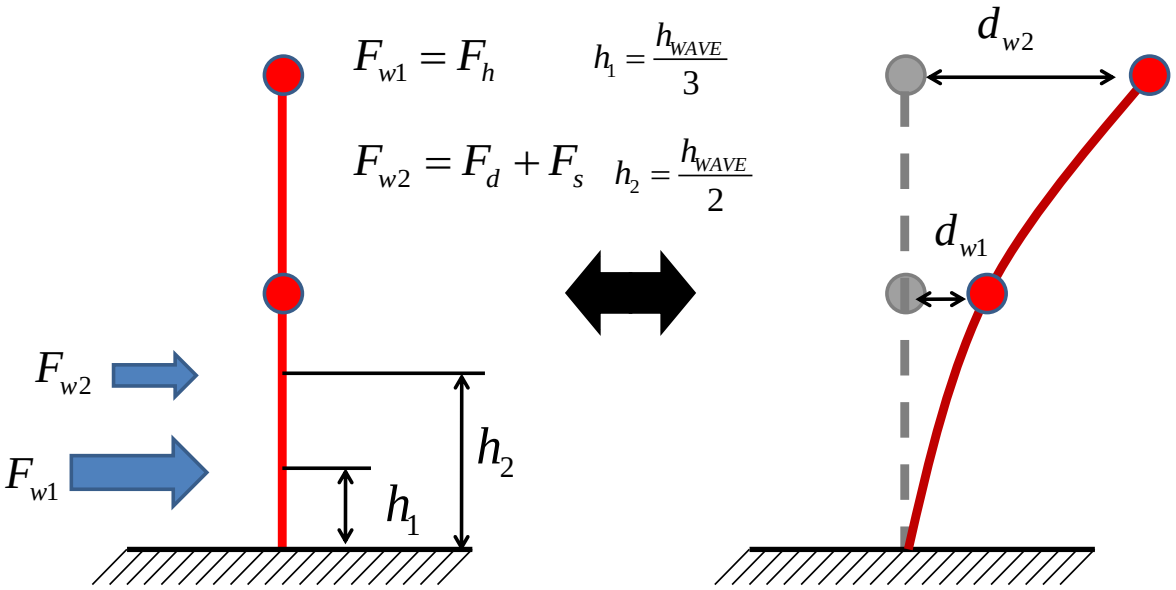

Figure 2.10: Schematic deformation of a typical two-story structure.

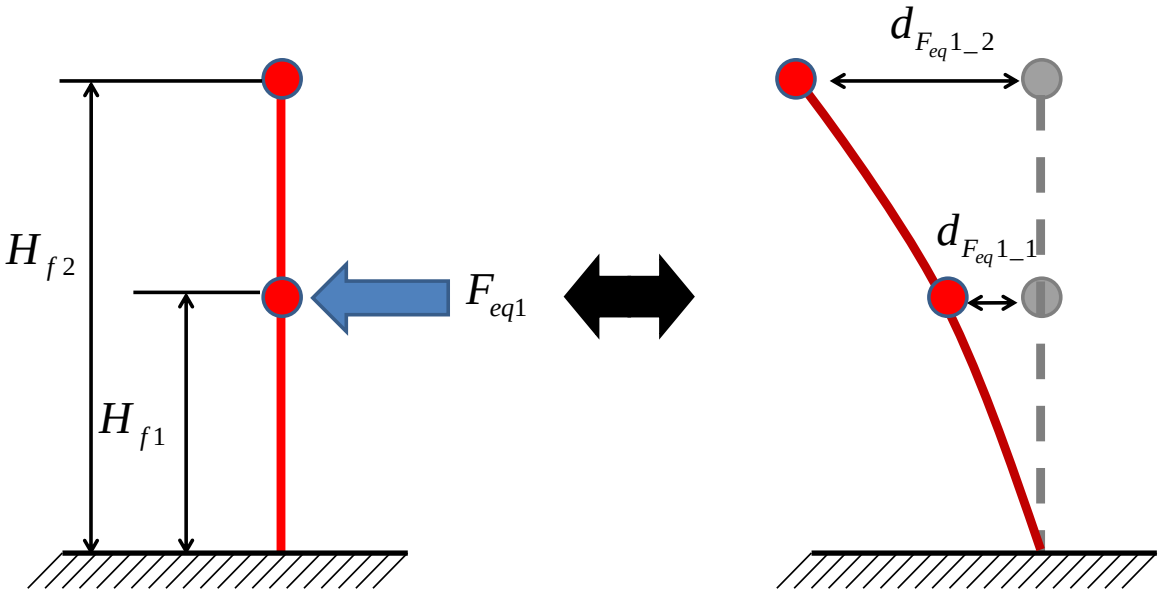

Figure 2.11: Schematic view of deformation caused by force F_{eq1}.

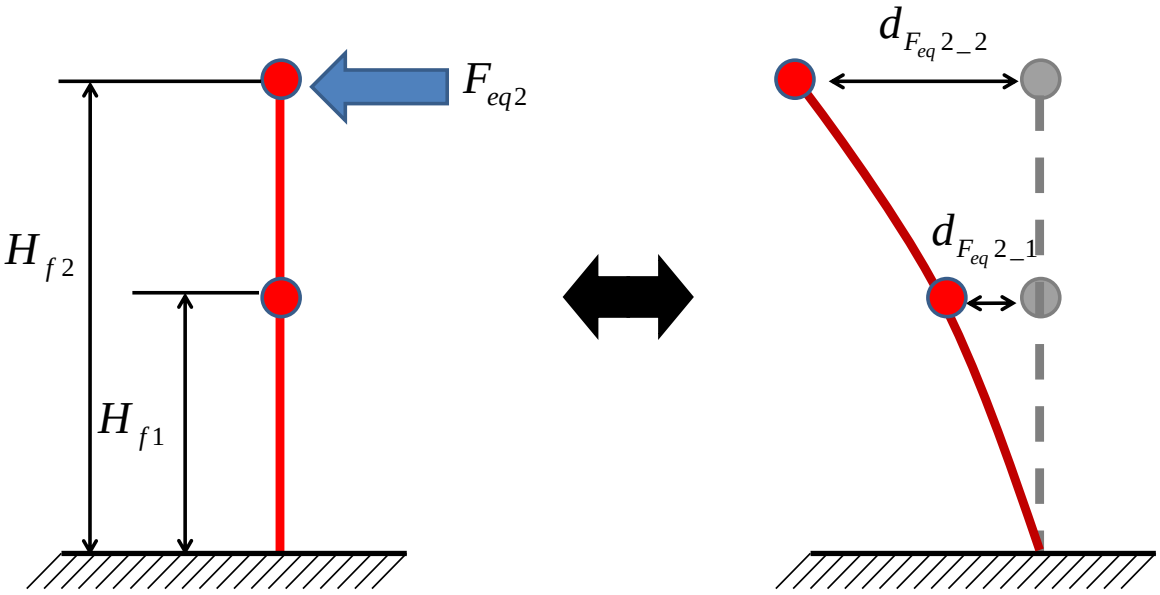

Figure 2.12: Schematic view of deformation caused by force F_{eq2}.

Finally, two deformations caused by wave forces should be equal to the summation of the deformation caused by equivalent forces due to the force equilibrium at each node, i.e. each floor level. Thus, it can be written as the following form:

$$d_{w1} = f_{eq1} * d_{f_{eq}1\_1} + f_{eq2} * d_{f_{eq}2\_1}$$
$$d_{w2} = f_{eq1} * d_{f_{eq}1\_2} + f_{eq2} * d_{f_{eq}2\_2} \quad (2\text{-}31)$$

where (d_{w1} and d_{w2}) are the deformations caused by wave forces, (f_{eq1} and f_{eq2}) are the equivalent forces per unit width, ($d_{f_{eq}1\_1}$ and $d_{f_{eq}1\_2}$) are the deformations at the location 1 and 2 caused by the equivalent force f_{eq1}, and ($d_{f_{eq}2\_1}$ and $d_{f_{eq}2\_2}$) are the deformations at the location 1 and 2 caused by the equivalent force f_{eq2}, respectively.

In addition, Equation (2-31) can be generally expressed as:

$$\left(d_w\right)_i = \sum_{j=1}^{N_F} \left(f_{eq}\right)_j * \left(d_{f_{eq}}\right)_{j\_i} \quad , i = 1, \cdots N_F \tag{2-32}$$

where $\left(d_w\right)_i$ is the deformation caused by wave forces at nodal point location *i*, $\left(f_{eq}\right)_j$ is the equivalent force at nodal point location *j*, $\left(d_{f_{eq}}\right)_{j\_i}$ is the deformation at the nodal point location *i* caused by equivalent force *j*, and N_F is the number of floors.

In its most general matrix form, it can be written as:

$$\left\{d_w\right\} = [d_{f_{eq}}]\left\{f_{eq}\right\} \tag{2-33}$$

where d_w can be defined as $\left\{\left(d_w\right)_1 \quad \left(d_w\right)_2 \quad \cdots \quad \left(d_w\right)_{N_F}\right\}^T$,

$\left\{f_{eq}\right\}$ can be defined as $\left\{\left(f_{eq}\right)_1 \quad \left(f_{eq}\right)_2 \quad \cdots \quad \left(f_{eq}\right)_{N_F}\right\}^T$, and

$\left[d_{f_{eq}}\right]$ can be defined as $\begin{bmatrix} \left(d_{f_{eq}}\right)_{1\_1} & \left(d_{f_{eq}}\right)_{2\_1} & \cdots & \left(d_{f_{eq}}\right)_{N_F\_1} \\ \left(d_{f_{eq}}\right)_{1\_2} & \left(d_{f_{eq}}\right)_{2\_2} & & \vdots \\ \vdots & & \ddots & \\ \left(d_{f_{eq}}\right)_{1\_N_F} & \cdots & & \left(d_{f_{eq}}\right)_{N_F\_N_F} \end{bmatrix}$.

Finally, equivalent forces can be computed by solving the matrices. It is noted that the computed equivalent forces are the forces for the unit width, so actual equivalent forces should be multiplied by the width of the structure in target direction.

$$\left\{F_{eq}\right\} = \left([d_{f_{eq}}]^T \left\{d_w\right\} \right) * W_{st} \tag{2-34}$$

where $\{F_{eq}\}$ is the computed equivalent force vector and W_{st} is a width of the structure in target direction, i.e. the direction of the coming wave.

2.6 FRAGILITY ANALYSIS

A fragility curve is a conditional statistical distribution that gives the probability of exceeding a specified threshold or achieving a specific condition, e.g. drift, damage, or collapse, as a function of hazard intensity. For earthquake hazard, intensity can be expressed in terms of spectral acceleration. For tsunami hazard, the wave height is felt to be the most logical measure of hazard intensity. Thus, a tsunami fragility will define the conditional probability of the demand (D) of the wave forces placed upon the structure exceeding the structural capacity (C) for a given level of tsunami wave height intensity (I), as shown in the following equation:

$$F = P[D \geq C \mid I] \tag{2-35}$$

where *F* represents a fragility probability under given conditions.

Generally, the lognormal distribution function is a convenient way to express a fragility curve and can be expressed as (Shinozuka et al. 2000; Ellingwood 2001; Rosowsky and Ellingwood 2002; Park and van de Lindt 2009):

$$F_R(x) = \Phi\left(\frac{\ln(x) - m_R}{\xi_R}\right) \tag{2-36}$$

where $\Phi(\cdot)$ is a standard normal distribution function, x is a spectral acceleration or a tsunami wave height, m_R is a median capacity, and ξ_R is a logarithmic standard deviation.

Recall that this dissertation focuses on the successive hazard of the earthquake and tsunami, thus the spectral acceleration (S_a) and tsunami wave height (h_{WAVE}) are selected as the x variable in Equation (2-36) for seismic and tsunami hazard, respectively. The two parameters (m_R = median capacity and ξ_R = logarithmic standard deviation) can be easily computed using a simple fitting technique to minimize the error terms based on least square methods.

2.7 OPITMIZATION TECHNIQUE

In Chapter 5, an optimization algorithm will be applied. Genetic algorithms (GAs) are adopted in this dissertation to find an optimal location of shelter(s) for the evacuation planning for a community, e.g. planning of vertical evacuation.

A general constrained optimization problem can be expressed as:

$$Minimize \quad f(x) \tag{2-37}$$

$$\text{Subject to} \begin{cases} g_i(x) \le 0 & : \quad i = 1, 2, ...q \\ h_j(x) = 0 & : \quad j = q+1, q+2, ...m \end{cases} \tag{2-38}$$

where $f(x)$ is a objective function which is various for the purpose of the problem, $g(x)$ is inequality constraints, q is the number of the inequality constrains, $h(x)$ is equality constraints, m-q is the number of equality constraints.

The general optimization problem is to find the solution subjected to one or more inequality and equality constraints. There is no known method to determining the global maximum or minimum solution; only if the objective function and the constraints satisfy certain properties then it can be one of the global optimum solutions. Thus, it is important to handle such constraints (Goldberg 1989; Arora 2004; Yeniay 2005). To do this, the penalty functions which help eliminate infeasible solutions during the procedure are adopted and the penalized objective function can be written as:

$$f_p(x) = f(x) + \sum_{i=1}^{m} C_i (P_i)^{\beta} \tag{2-39}$$

$$(P)_i^{\beta} = \begin{cases} \delta_i g_i(x) & : \quad i = 1, 2, \ldots\ldots, q \\ |h_i(x)| & : \quad j = q+1, \ldots, m \end{cases} \tag{2-40}$$

$$\delta_i = \begin{cases} 1 & : \quad \text{if } i^{th} \text{ constraints is violoated } (g_i(x) > 0) \\ 0 & : \quad \text{otherwise } (g_i(x) \leq 0) \end{cases} \tag{2-41}$$

where $f_p(x)$ is a penalized objective function, $f(x)$ is the (un-penalized) objective function, C_i is a constant imposed for violation of i^{th} constraint with values of relatively large number used, β is a user-defined exponent with values of 1 or 2 often used, δ_i is a kronecker's delta function, and constraints 1 through *q* are inequality constraints, so the penalty will only be activated when the constraint is violated, while constraints *q*+1 through *m* are equality constraints which will activate the penalty if there are any values (Arora 2004; Yeniay 2005).

Genetic Algorithms are stochastic search improvement-seeking algorithms based on the mechanics of natural genetics and have been employed in many optimization problems in order to overcome the shortcoming of classical calculus-based methods. Generally, calculus-based methods require the gradient of the objective function or the existence of derivatives in order to find local optima by solving the nonlinear set of equations. This is a severe limitation even if the numerical approximation of the derivative is allowed. Genetic Algorithms do not require the presence of these derivatives, i.e. finding derivatives with numerically methods or the gradient of the function. In addition, the

continuity of design variables is not a necessary condition, which is initially assumed in calculus-based optimization methods (Goldberg 1989).

In GAs, the problem can be represented as a population of strings, which is a set of binary bit strings of 0s and 1s for defining a solution to the problem. Each binary bit in this string can represent some characteristic of the solution or the whole string can represent an integer or float number. The basic mechanics in GAs is Darwinian evolution: weak traits are eliminated from the population and strong traits survive and are mixed by recombination in order to form better generation through evaluating and mating. To do this, the population, defined as a set of chromosomes, is randomly generated to make an initial solution of problems covering the entire range of the possible solution space. Four operators, which are defined as selection, reproduction, crossover, and mutation operators, are then employed to mimic the concept of Darwinian evolution.

Selection is process that a proportion of the existing population is selected to breed a new generation during each successive generation by using fitness-based measurement, similar to natural selection. The fitness, objective function, can be represented by some measure of profit, utility, or goodness to maximize or minimize. In nature, it can be determined by a creature's ability to survive predators, pestilence, and other such obstacles to survive. The next step is the reproduction operator, which generates an offspring of solutions from selected chromosomes. Each chromosome can be dealt a parent, i.e. either a father or mother. During the process, two important operators, crossover and mutation, are needed to evolve the solutions in order to seek the best one(s).

Crossover means that taking two random chromosomes from those already selected to form the next generation and exchanges randomly selected strings between them. After a crossover is performed, then mutation takes place. Mutation randomly changes the new offspring which switches a few randomly chosen bits from 0 to 1 or 1 to 0 in order to restore diversity that may be lost from the repeated application of the selection and crossover operators, and prevent all solutions falling into an optimum of solved problem. The overall procedure is depicted in Figure 2.13.

A roulette wheel rule, selecting a chromosome according to the weight of its fitness, can be adopted as a selection operator. This means that chromosomes with a higher value have a higher probability of contributing one or more offspring in the next generation. A schematic overview of the roulette wheel rule is shown in Figure 2.14.

Also, the use of a one-point crossover rule, which is to choose one point randomly, and everything before this point copy from a first parent and then everything after that point copy is from the second parent. This can be adopted as the crossover operator in this study. There are many crossover rules and specific crossover can improve the performance of the optimization. A schematic overview of one-point crossover roulette wheel rule can be shown in Figure 2.15.

Genetic algorithms are adopted in this dissertation for two purposes: 1) estimation of hysteretic parameters in structural analysis and 2) evacuation planning for a community, e.g. planning of vertical evacuation.

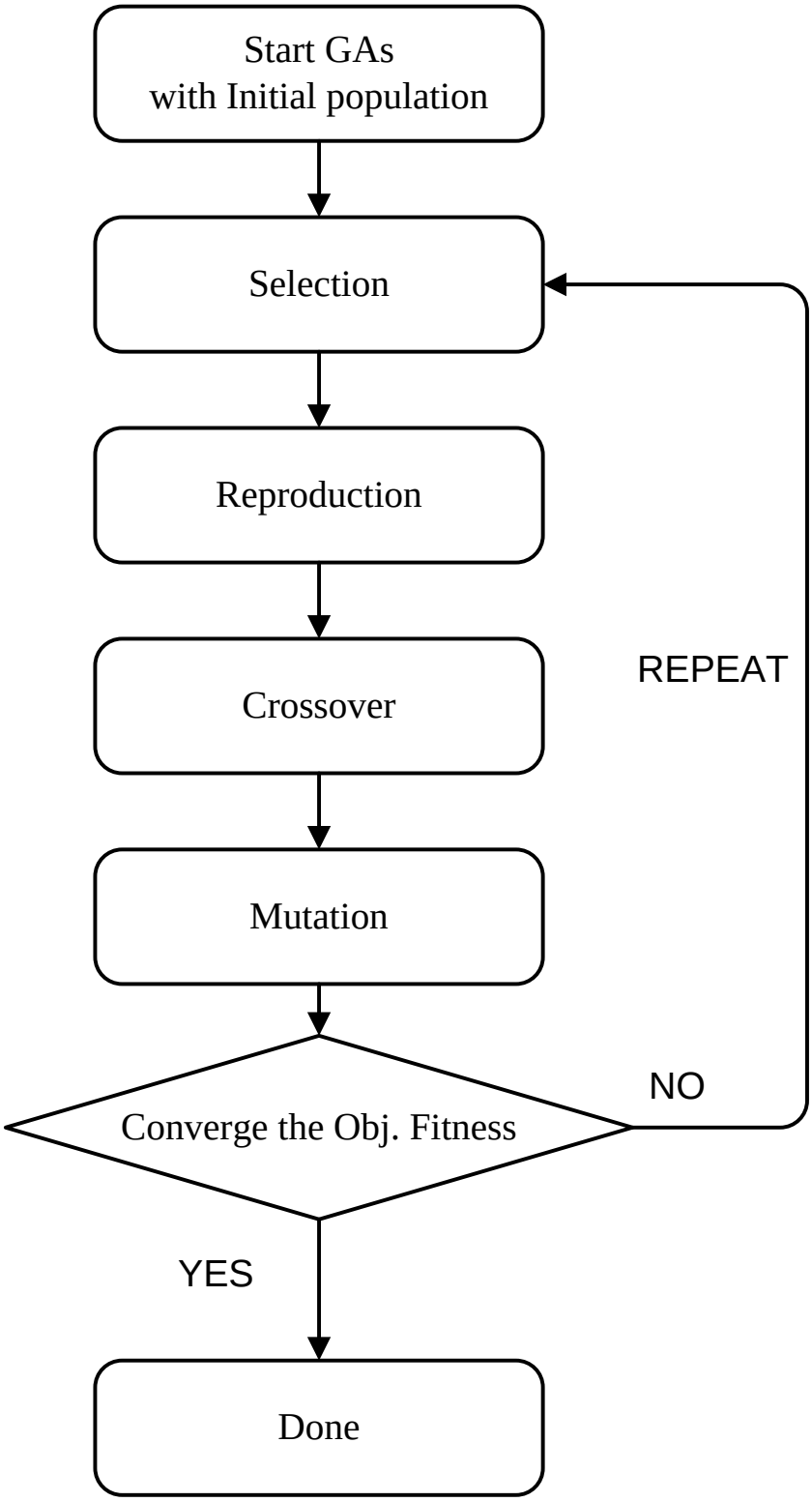

Figure 2.13: Overall procedure for Genetic Algorithms.

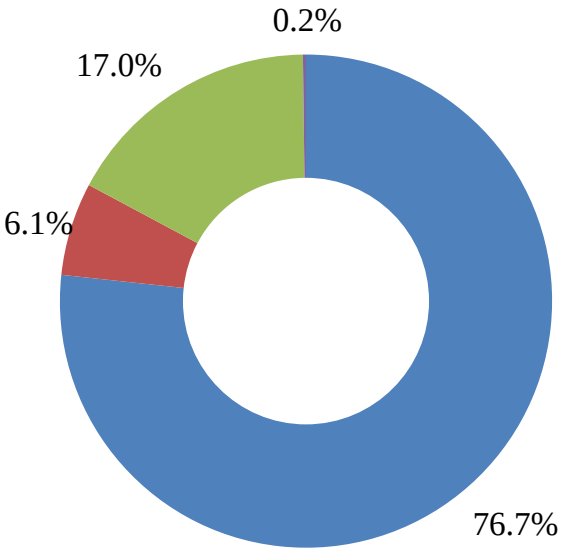

Population	Fitness	Weight
1	34225	0.767
2	2704	0.061
3	7569	0.170
4	100	0.002
Sum	44598	1.000

Figure 2.14: Overview of the roulette wheel rule selection method.

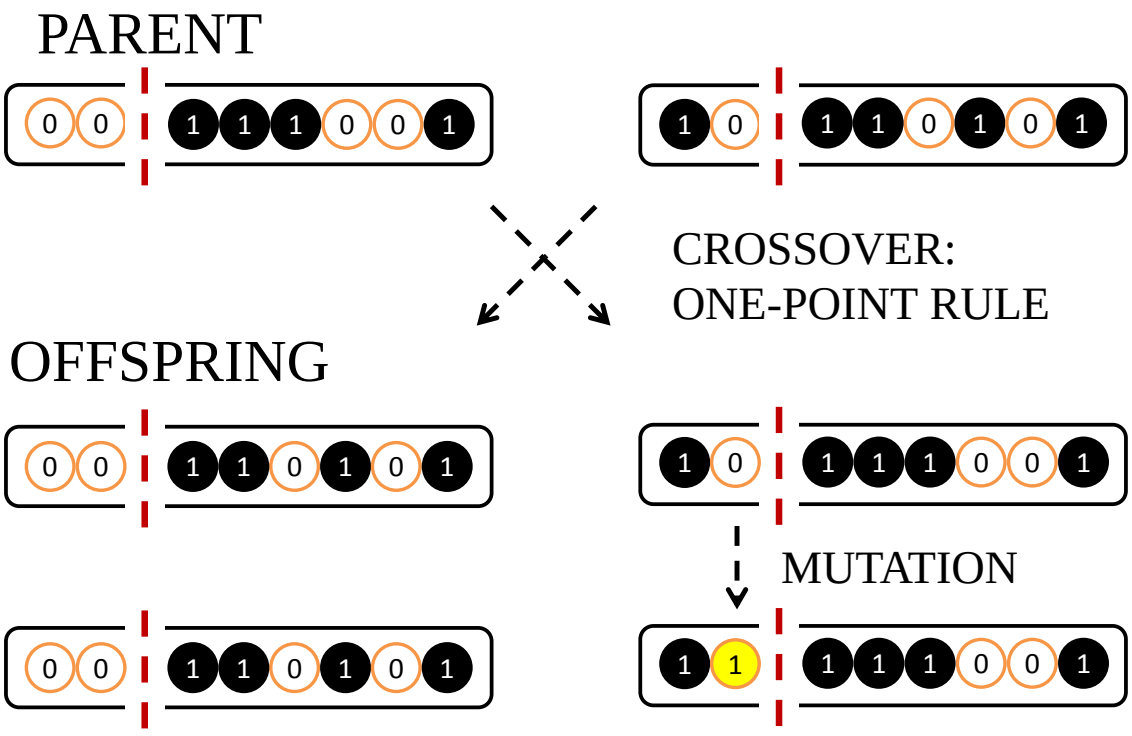

Figure 2.15: Schematic view of crossover and mutation operator.

CHAPTER 3

NUMERICAL MODEL DEVELOPMENT

3.1 OVERVIEW

This chapter presents the development of NAPSS (**N**onlinear **A**nalysis **P**rogram for **S**tructural **S**ystem) and SSTAP (**S**equential **S**eismic and **T**sunami **A**nalysis **P**rogram). NAPSS is especially focused on modeling the response of wood shearwalls and estimating the hysteretic parameters.

Due to the implementation of a general finite element procedure, NAPSS can be easily extended to solve general structural analysis problems for nonlinear behavior of three-dimensional structures and handle arbitrary load conditions such as nodal loads, pressure loads, distributed loads, etc. This consideration provides an advantage in applying loads associated with tsunami wave loading.

SSTAP was developed by using model reduction techniques, hysteretic spring models, and a basic finite element approach to compute the structural response of a degenerated model under seismic and tsunami wave loading.

3.2 PRELIMINARIES OF SHEAR WALL ANALYSIS PROGRAM

To obtain computational efficiency, each shearwall model is modeled as one nonlinear hysteretic spring at the system level. To do this, a special module capable of analyzing a wall model is needed. However, a large number of numerical models have been developed to predict the response of wood shearwalls, but many have weakness capturing the detailed interaction and load sharing between the components of the shear wall under monotonic and cyclic loadings. More sophisticated finite element models have been developed to overcome the limitation of these numerical models. Typically, three elements are used in accurate wood shear wall finite element models: (1) sheathing-to-framing connectors represent spring elements with nonlinear load-deformation characteristics; (2) the wood framing is modeled using beam elements with linear elastic relationship; and (3) the sheathing panel is represented by plane stress elements or plate-bending elements also in the linear elastic range. Additionally, gap and bearing elements have been introduced along the interface between the sheathing panels, and the end posts and sill plate. In addition, nonlinear behavior of wood framing and connectors for framing-to-framing have been introduced and implemented to improve the accuracy of the analysis results. It has been shown that these elements more fully model the inter-component response within the wall but a large amount of computational effort is needed because of the increased model complexity, particularly with the full building model.

A typical wood shearwall is modeled by using several typical structural elements in this dissertation work. Frame elements are used to model wood framing members. Sheathing panel is represented by shell elements. Sheathing-to-framing connectors are modeled by

using hysteretic spring elements. A schematic overview of typical wood shearwall is shown in Figure 3.1. All elements have six degrees of freedom (DOF) per node, three translations and three rotations, in order to build a three dimensional structural model, keep the consistency of elements, and to connect with other types of elements easily.

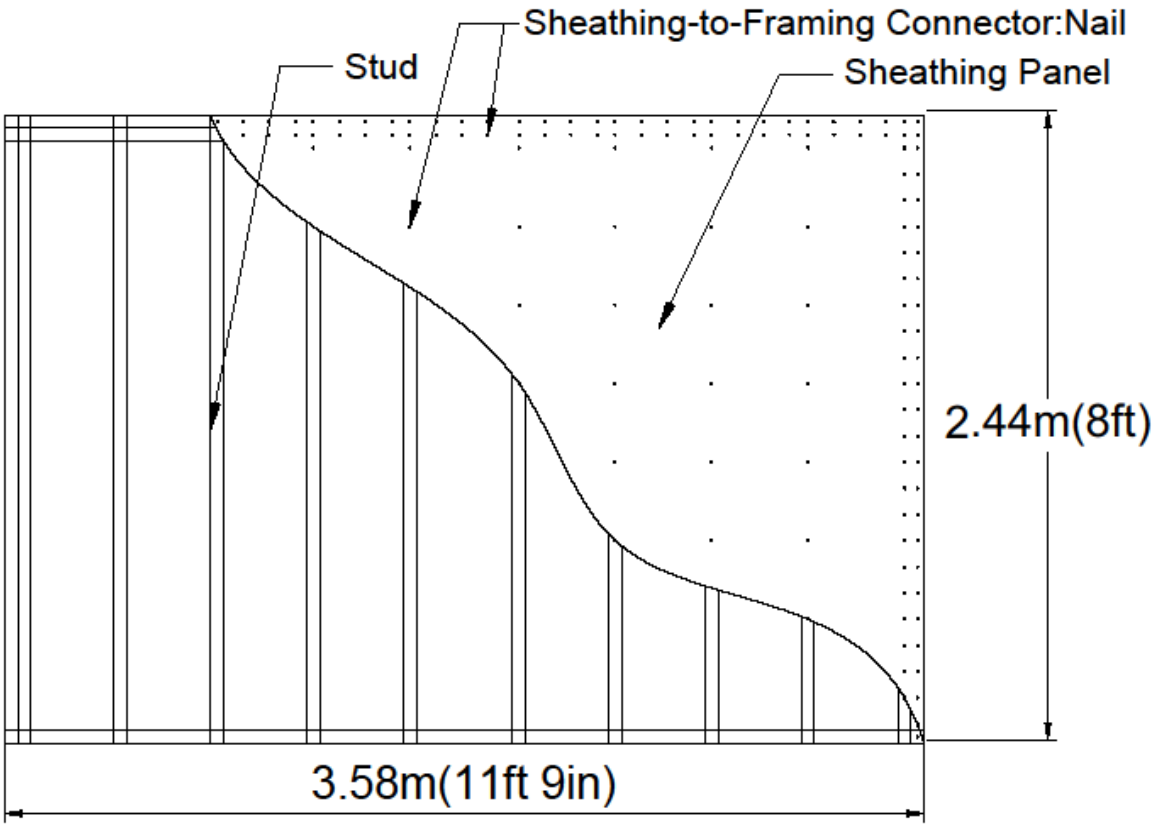

Figure 3.1: Schematic view of typical wood shearwall.

The principle of virtual work (PVW), a well-known approach in engineering, is applied to derive the equation of equilibrium for an element and then can obtain formulas for the element stiffness matrix and for load vectors associated with initial strains, body forces, and surface tractions. It can be stated in the following form:

$$\int \{\delta\varepsilon\}^T \{\sigma\} dV = \int \{\delta \mathrm{u}\}^T \{F\} dV + \int \{\delta \mathrm{u}\}^T \{\Phi\} dS \tag{3-1}$$

where $\{\delta\varepsilon\}$ is the vector of strain-displacement, $\{\delta u\}$ is the vector of virtual displacement defined as $\{\delta \mathrm{u}\} = \lfloor \delta u \quad \delta v \quad \delta w \rfloor^T$, $\{F\}$ is the body force vector over volume *V*, and $\{\Phi\}$ is surface traction forces on surface *S*. It should be noted that concentrated loads on nodal points can be expressed as surface tractions over a very small area, thus they are included in the surface traction force term.

Displacement vector $\{\mathrm{u}\}$ are interpolated over an element by using a shape function of the element. If the element type is determined, then a shape function can be selected to express the possible shape of the element. So each element has different shape functions and the displacement vector can be formulated as:

$$\{\mathrm{u}\} = [N]\{d\} \tag{3-2}$$

where $\{\mathrm{u}\} = \lfloor u \quad v \quad w \rfloor^T$, $[N]$ is the shape function, and $\{\mathrm{d}\}$ is the nodal displacement DOF of an element.

Strains can be determined from displacements as:

$$\{\varepsilon\} = [\partial]\{\mathrm{u}\} \tag{3-3}$$

Substituting Equation (3-2) into Equation (3-3) gives:

$$\{\varepsilon\} = [B]\{d\} \tag{3-4}$$

where $\{\varepsilon\} = \{\varepsilon_x \quad \varepsilon_y \quad \varepsilon_z \quad \gamma_{xy} \quad \gamma_{yz} \quad \gamma_{zx}\}^T$ is a strain vector for element, $[B] = [\partial][N]$, and $[\partial]$ can be defined as:

$$[\partial] = \begin{bmatrix} \frac{\partial}{\partial x} & 0 & 0 & \frac{\partial}{\partial y} & 0 & \frac{\partial}{\partial z} \\ 0 & \frac{\partial}{\partial y} & 0 & \frac{\partial}{\partial x} & \frac{\partial}{\partial z} & 0 \\ 0 & 0 & \frac{\partial}{\partial z} & 0 & \frac{\partial}{\partial y} & \frac{\partial}{\partial x} \end{bmatrix}^T \tag{3-5}$$

Virtual displacements and strains can be defined using Equation (3-2) to Equation (3-4) as:

$$\{\delta \mathrm{u}\}^T = \{\delta d\}^T [N]^T \tag{3-6}$$

$$\{\delta \varepsilon\}^T = \{\delta d\}^T [B]^T \tag{3-7}$$

Then, stress-strain relations can be defined as:

$$\{\sigma\} = [E]\{\varepsilon\} + \{\sigma_0\} \tag{3-8}$$

where $\{\sigma_0\} = -[E]\{\varepsilon_0\}$ is an initial stress vector of an element, i.e. stress due to a temperature change, $\{\sigma\}$ is a stress vector of an element, $\{\varepsilon\}$ is a strain vector of an element, and $[E]$ is a constitutive matrix of an element.

Substituting Equation (3-6), Equation (3-7), and Equation (3-8) into Equation (3-1) gives the following form:

$$\{\delta d\}^T \left(\begin{array}{c} \int [B]^T [E][B] dV \{d\} + \int [B]^T \{\sigma_0\} dV \\ - \int [N]^T \{F\} dV - \int [N]^T \{\Phi\} dS \end{array} \right) = 0 \qquad (3\text{-}9)$$

Equation (3-9) must be true for any admissible virtual displacement $\{\delta d\}$ from the equilibrium configuration, thus system matrices of an element can be formulated by:

$$[k_e]\{d\} = \{r_e\} \qquad (3\text{-}10)$$

where $[k_e] = \int [B]^T [E][B] dV$ is a local stiffness matrix of an element and $\{r_e\}$ is a local force vector of an element.

The vector of loads is applied to the nodes at the element level, due to all sources but element deformation can be defined as the following form:

$$\{r_e\} = \{r_F\} + \{r_S\} + \{r_I\} \tag{3-11}$$

where $\{r_F\} = \int [N]^T \{F\} dV$ is the element body force vector, $\{r_S\} = \int [N]^T \{\Phi\} dS$ is the element surface traction force vector, and $\{r_I\}$ is the initial stress or strain force vector, i.e. can be expressed as $\{r_I\} = -\int [B]^T \{\sigma_0\} dV$ or $\{r_I\} = \int [B]^T [E] \{\varepsilon_0\} dV$.

To build system matrices for a structure, each element matrix, i.e. stiffness matrix and force vector, in local coordinate system should be converted into global coordinates using a transformation matrix. Then system matrices in the global coordinate system of a structure can be obtained by using an assembly procedure. Displacement and force of an element in the local coordinate system can be expressed in the global coordinate system by multiplying transformation matrix of an element

$$\{d_e\} = [T]\{D\} \tag{3-12}$$

$$\{r_e\} = [T]\{R\} \tag{3-13}$$

where $[T]$ is a transformation matrix of an element, $\{d_e\}$, $\{r_e\}$, $\{D\}$, and $\{R\}$ is a displacement and force vector in the local and global coordinate system, respectively.

Substituting Equation (3-12) and Equation (3-13) into Equation (3-10), and multiplying each side by $[T]^T$ gives:

$$[k_e]([T]\{D\}) = ([T]\{R\}) \tag{3-14}$$

$$\left([T]^T [k_e][T]\right)\{D\} = \{R\} \tag{3-15}$$

The stiffness matrix and force vector of a structure in global coordinate system can be defined as following equations:

$$[K] = \sum_{i=1}^{N_{els}} \left([T]^T [k_e][T]\right)_i \tag{3-16}$$

$$\{R\} = \sum_{i=1}^{N_{els}} \left([T]^T \{r_e\}\right)_i \tag{3-17}$$

Finally, it can be expressed in the following form:

$$[K]\{D\} = \{R\} \tag{3-18}$$

where $[K]$ is the global stiffness matrix of a structure system, $\{D\}$ is the global deformation or displacement vector of a structure system, and $\{R\}$ is the global force vector of a structure system.

Using this basic FEM formulation, NAPSS is successfully developed and it can handle wall system modeling level including every connector (i.e. nails), wood studs and framings, and sheathing panels under monotonic and cyclic loadings. Detailed discussion of each element is followed and the Newton-Raphson numerical technique is utilized to

perform nonlinear analysis due to the fastener's nonlinearity. Therefore, an individual wall can be analyzed and then its hysteretic parameter can be determined based on the response of the analysis. An example of NAPSS is explained in Chapter 4. Also, a detailed explanation of the principle of virtual work and its derivations can be found in any graduate level finite element books (Bathe 1996; Cook et al. 2002; Zienkiewicz and Taylor 2005). Further formulation including frame elements, shell elements, spring elements, and nonlinear solver can be found in Appendix A of this dissertation.

3.3 SEQUENTIAL SEISMIC AND TSUNAMI ANALYSIS PROGRAM

A model reduction technique was adopted in this dissertation work in order to perform the structural analysis. Focusing on the role of shearwalls in lateral resistance under lateral loading, each shearwall can be substituted by zero-height spring elements connecting the floor and roof diaphragms together. Then, the actual three-dimensional structural model can be degenerated into a two-dimensional planar model. All diaphragms in the structural model are assumed to have infinite in-plane stiffness.

The response of the structure can be defined in terms of only three degrees of freedom (DOF) per floor, two translations, U and V, and one rotation, Θ, (Folz and Filiatrault 2001, 2004a, b; Pei and van de Lindt 2008). The relationship between local and global DOF of each shearwall can be expressed as:

$$\begin{Bmatrix} u_1 \\ v_1 \\ \theta_1 \\ u_2 \\ v_2 \\ \theta_2 \end{Bmatrix} = \begin{bmatrix} 1 & 0 & -y & 0 & 0 & 0 \\ & 1 & x & 0 & 0 & 0 \\ & & 1 & 0 & 0 & 0 \\ & & & 1 & 0 & -y \\ & symm & & & 1 & x \\ & & & & & 1 \end{bmatrix} \begin{Bmatrix} U_1 \\ V_1 \\ \Theta_1 \\ U_2 \\ V_2 \\ \Theta_2 \end{Bmatrix} = [T]\{D\} \tag{3-19}$$

where (u, v, and θ) and (U, V, and Θ) are the local and global coordinate displacements, respectively, and (x and y) are the distances from the position of wall to the center of mass of its floor.

To analyze the structure, each shearwall is analyzed or modeled using NAPSS. Then, each shearwall can be immediately substituted by zero-height spring elements with estimated hysteretic parameters, as described above. Once the substitution is completed, the entire structural system consists of several spring elements as the same number of shearwalls. These procedures have been implemented into SSTAP in order to conduct seismic and tsunami analysis.

A typical assembly and system matrix approach of the finite element method is adopted here. To do this, the transformation matrix, in Equation (3-19), is needed to change from local to global coordinates. The equivalent spring element stiffness of a single shearwall can be defined for each wall direction and then transferred into global coordinate system as well by:

$$[K_x]=\begin{bmatrix} K_s & 0 & 0 & -K_s & 0 & 0 \\ & 0 & 0 & 0 & 0 & 0 \\ & & 0 & 0 & 0 & 0 \\ & & & K_s & 0 & 0 \\ & & symm & & 0 & 0 \\ & & & & & 0 \end{bmatrix}, [K_y]=\begin{bmatrix} 0 & 0 & 0 & 0 & 0 & 0 \\ & K_s & 0 & 0 & -K_s & 0 \\ & & 0 & 0 & 0 & 0 \\ & & & 0 & 0 & 0 \\ & & symm & & K_s & 0 \\ & & & & & 0 \end{bmatrix} \quad (3\text{-}20)$$

$$[K]=\sum_{ix=1}^{N_x}\left([T_{ix}]^T[K_{ix}][T_{ix}]\right)+\sum_{jy=1}^{N_y}\left([T_{jy}]^T[K_{jy}][T_{jy}]\right) \quad (3\text{-}21)$$

where K_s is the stiffness of each spring element, N_x and N_y are the number of each direction's shearwall, and T_{ix} and T_{iy} are the transformation matrix for each shearwall.

In Equation (3-21) , the coordinates in the transformation matrices T_{ix} and T_{iy} identify the point of attachment of the SDOF shear element to the diaphragm. Extension of the formulation of the global force vector and stiffness matrix to multi-story building structure is straightforward. The structural configuration of a typical woodframe structure, as an illustrative purpose, and its numerical model layout in SSTAP is shown in Figure 3.2.

The global mass matrix can be obtained through consideration of dynamic equilibrium and application of D'Alembert's principle. The global mass matrix for a single-story structure can be defined as:

$$[M]=\begin{bmatrix} m & 0 & -m*y_c \\ 0 & m & m*x_c \\ -m*y_c & m*x_c & I_0+m*(x_c{}^2+y_c{}^2) \end{bmatrix} \tag{3-22}$$

where m is the mass of the diaphragm, (x_c and y_c) are the relative distances between base floor and other floor of its center of mass, if only single floor system then (x_c and y_c) are equal to zero, and I_0 is the mass moment of inertia about the center of mass.

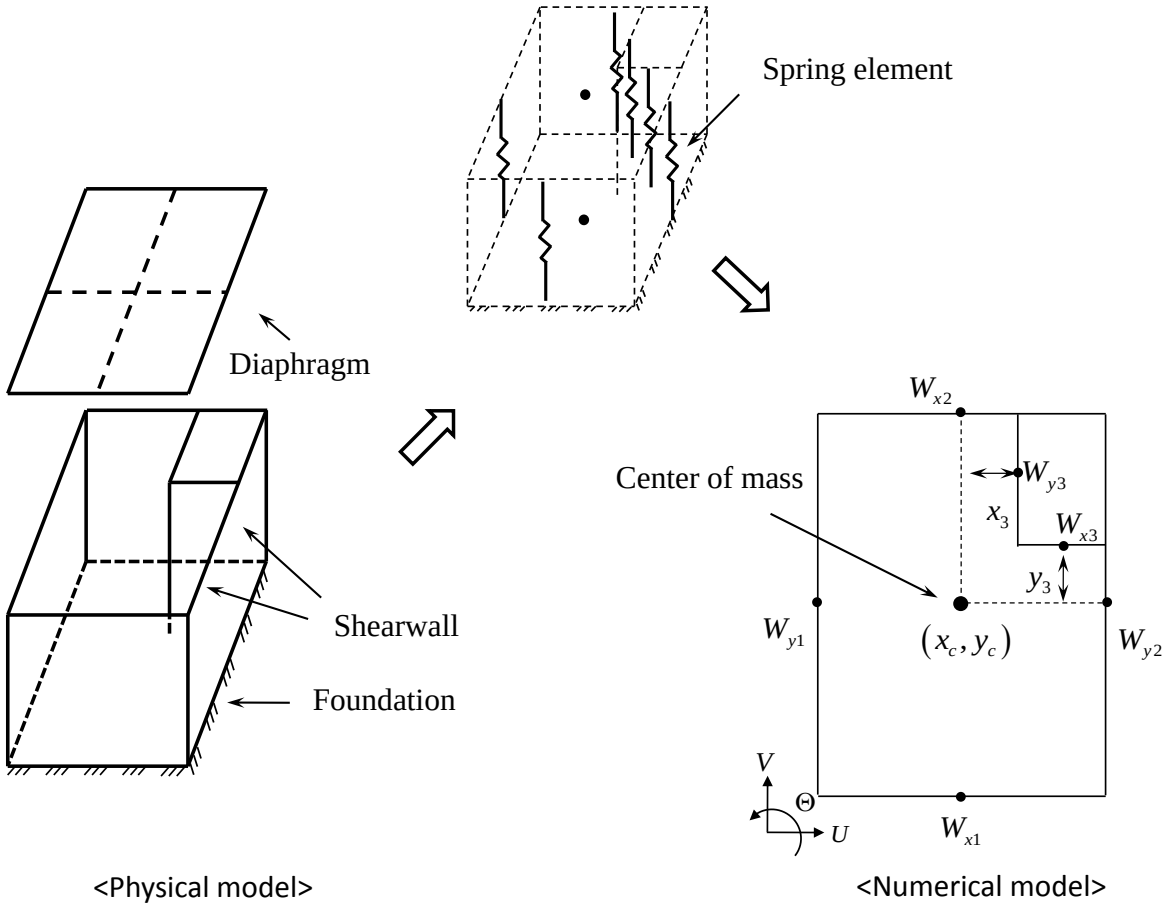

Figure 3.2: Overall procedure for degenerated modeling technique in SSTAP.

The contributing mass from the diaphragm is only represented in Equation (3-22). Additionally, mass associated with each shear wall or concentrated at a certain location can be represented by a discrete mass that includes rotational inertia and added appropriately to Equation (3-22). The global viscous damping matrix [*C*] accounts for all supplemental energy dissipating mechanisms in the structure other than the hysteretic damping produced in the shear wall elements. In this formulation, the viscous damping matrix is assumed to follow modal damping technique, such that:

$$[C] = 2\xi\sqrt{[M]*[K]} \tag{3-23}$$

where [*C*] is the damping matrix of a structure and ζ is a damping ratio of a structure.

CHAPTER 4

TSUNAMI FRAGILITY FORMULATION AND APPLICATION

4.1 OVERVIEW

This chapter presents the development of a tsunami fragility formulation and its application to the proposed approach for a single structure and its extension to the community level optimization. The fragilities for a single structure have been developed. Initially, NAPSS is used to model a single wood shearwall and perform the nonlinear structural analysis. Then, hysteretic parameter estimation is carried out in order to substitute a single degree of freedom (SDOF) model for the wood shearwall. This procedure is repeated for each shearwall of the target structure. Once the replacement is done, the program called SSTAP is used to model the entire structure and analyze it. Then, the development of fragilities and their application is carried out, which includes the interaction between earthquake and tsunami hazard through their successive application of load.

Community fragilities can be constructed as a combination of each single structure's fragilities. As an illustrative example, three more single structures are considered and analyzed to reflect structural variants of a typical real community, i.e. structures in the community that have different sizes and structural components.

4.2 MODELING OF A SINGLE WOOD SHEARWALL

Consider a typical wood shear wall having a 2.44 meter (96 inch) width and 2.44 meter (96 inch) height, shown in Figure 4.1, for explanatory purpose.

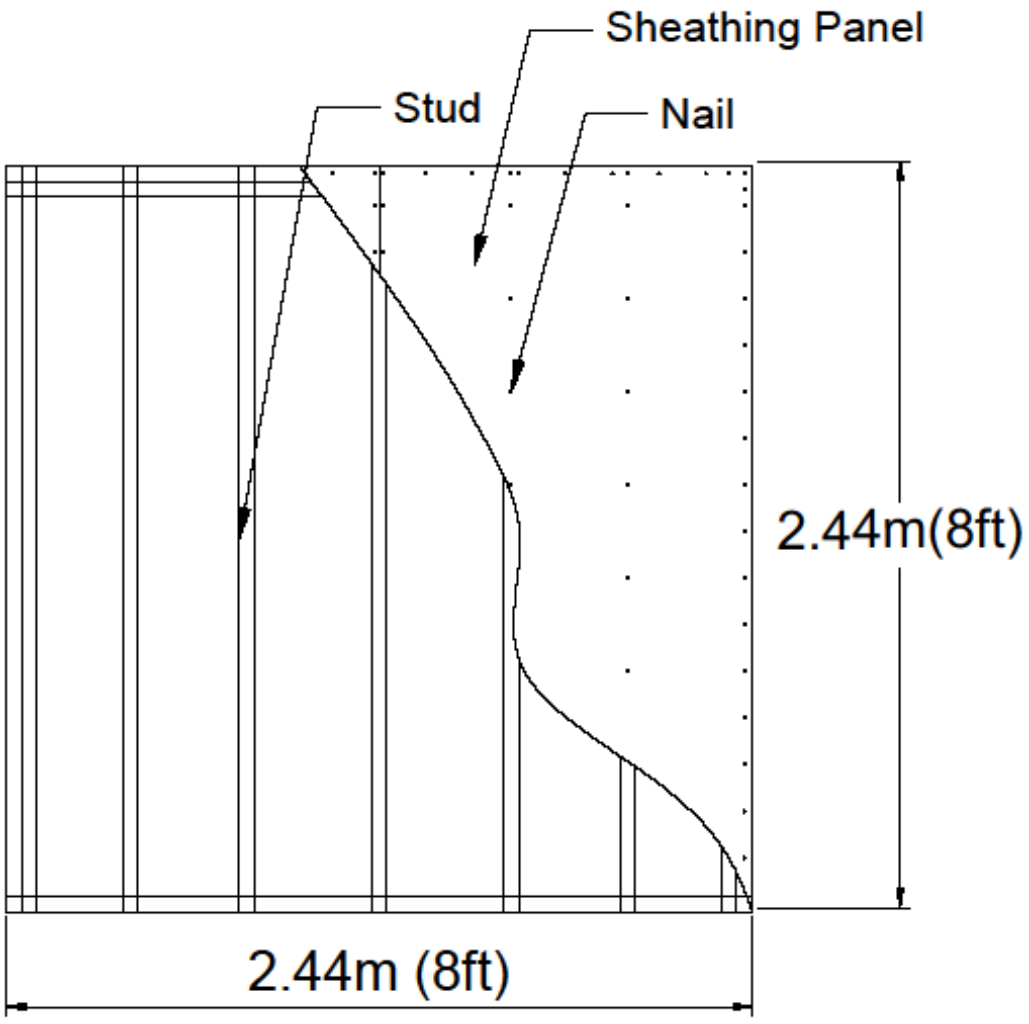

Figure 4.1: Schematic overview of a typical wood shearwall.

The wall had 9.53 mm (3/8 inch) thick oriented strand board (OSB) sheathing panels that were attached to framing using 8D common nails spaced at 152 mm (6 inch) on center along the panel edges and 304 mm (12 inch) on center in the panel field lines. Framing

consisted of double top plates using two 38.1 x 88.9 mm (2 x 4 inch nominal) members, and 38.1 x 88.9 mm (2 x 4 inch nominal) studs spaced 406.4 mm (16 inch) on center (Durham 1998; Judd 2005). It was modeled by using three basic finite elements, namely frame, shell, and spring elements. Nonlinear hysteretic spring elements were used to simulate the nonlinear behavior of the connector elements, i.e. a nail in this case. These details are summarized in Table 4.1.

Table 4.1: Structural configurations of the example wood shearwall.

Structural Component	Material Properties		
	Elastic Modulus	Shear Modulus	Dimension
Double Plate stud	9.65 *GPa* (1400 *ksi*)	0.5 *GPa* (73.0 *ksi*)	38.1 x 88.9 *mm* (2.0 x 4.0 *inch*)
Plywood Sheathing	12.4 *GPa* (1800 *ksi*)	0.62 *GPa* (90 *ksi*)	9.53 *mm* (0.375 *inch*)

	Hysteretic Parameters				
	K_0 (*kN/mm*)	F_0 (*kN*)	F_i (*kN*)	D_u (*mm*)	R_1
Sheathing-to-Framing Connector	0.561	0.751	0.141	12.5	0.061
	R_2	R_3	R_4	α	β
	-0.078	1.40	0.143	0.8	1.1

The analysis results of the wood shearwall under monotonic and reversed cyclic loading conditions are illustrated in Figure 4.2 and Figure 4.3, respectively.

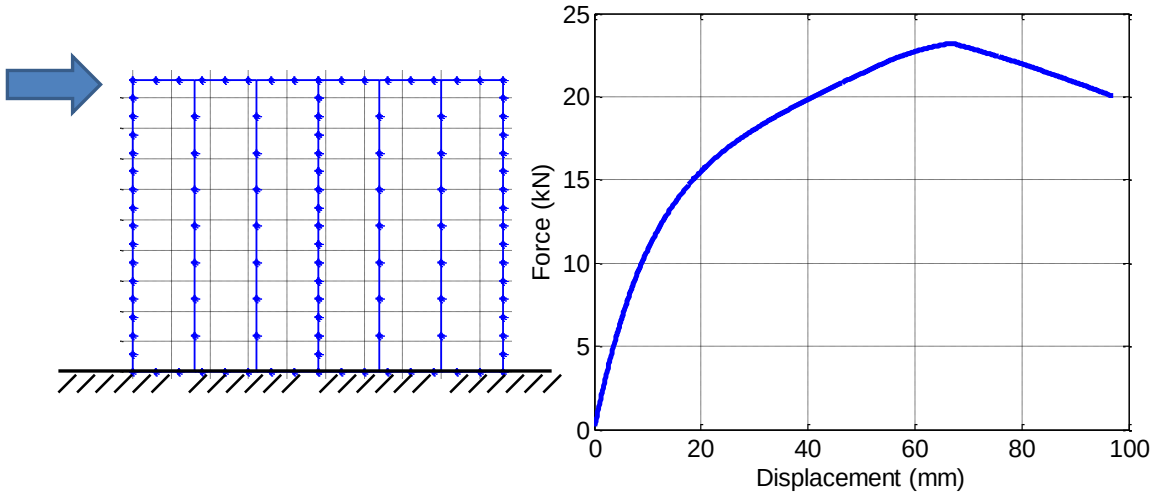

Figure 4.2: Analysis result of a wood shearwall under monotonic loading.

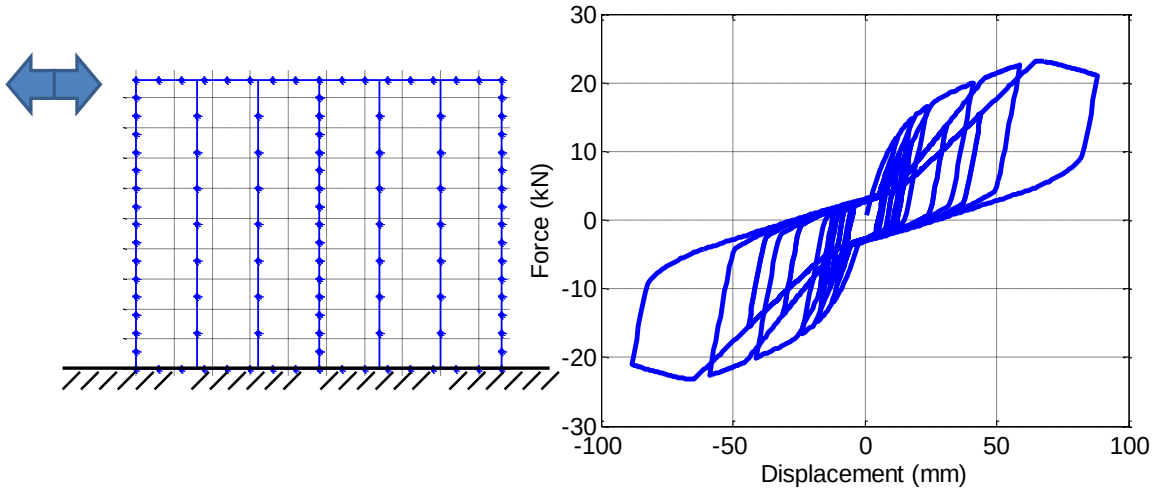

Figure 4.3: Analysis result of a wood shearwall under reversed cyclic loading.

The parameter estimation is needed to replace the wood shearwall with an equivalent SDOF, i.e. one hysteretic spring element, and the result is summarized in Table 4.2. This procedure is repeated for the rest of all shearwalls in each of the structures.

Table 4.2: The CUREE parameter for the single shearwall.

Hysteretic Parameters				
K_0 (kN/mm)	F_0 (kN)	F_i (kN)	D_u (mm)	R_1
1.63149	14.92655	2.87212	66.78479	0.07866
R_2	R_3	R_4	α	β
-0.06918	1.27586	0.07430	0.78944	1.08651

Typically, one single wall has a resistance capacity for both transverse and shear direction, but in most lateral analyses it is assumed that the wall can resist only force the shear direction. It should be noted that this assumption of counting on only the shear capacity of the walls, is not technically correct, particularly where tsunami loading is concerned. Even though the walls have been categorized into shearwalls, they resist lateral load in the shear and transverse direction. However, the transverse directional resistance capacity is relatively small. Thus, in the interest of design it is felt to be logical to neglect the capacity of the walls in the transverse direction because their contribution

in resisting lateral loads in the system is small. Additionally, this assumption provides a conservative approach in current design practices (Tarabia and Itani 1997).

4.3 SINGLE STRUCTURE MODELING

A two-story light-frame wood structure was selected as an illustrative example. Each component of the building was modeled using the ten-parameter CUREE hysteresis model described earlier. The building was one unit of a two-story townhouse and its total living area was approximately 167 m^2 (1800 ft^2), and had an attached two-car garage. The height of the townhouse from the first floor slab to the roof eaves was 5.49 meter (18 feet) and its total weight was approximately 36.3 tons (80 kips). The exterior walls of the two-story example structure were covered on the outside with 22.23 cm (7/8 inch) thick stucco over 11.12 cm (7/16 inch) thick OSB sheathed shear walls and 12.7 cm (1/2 inch) thick gypsum wallboard (drywall) was on the inside. The floor plan for this example, shown in Figure 4.4, is from the NEESWood benchmark test (Christovasilis et al. 2007), but the capacity was based on that of a typical Pacific Northwest design.

There are twenty-four wood shearwalls with various structural configurations. Thirteen shearwalls are assigned for the 1st story and eleven shearwalls for the 2nd story. Each shearwall represents a single hysteretic spring element and they resist only in the shear direction.

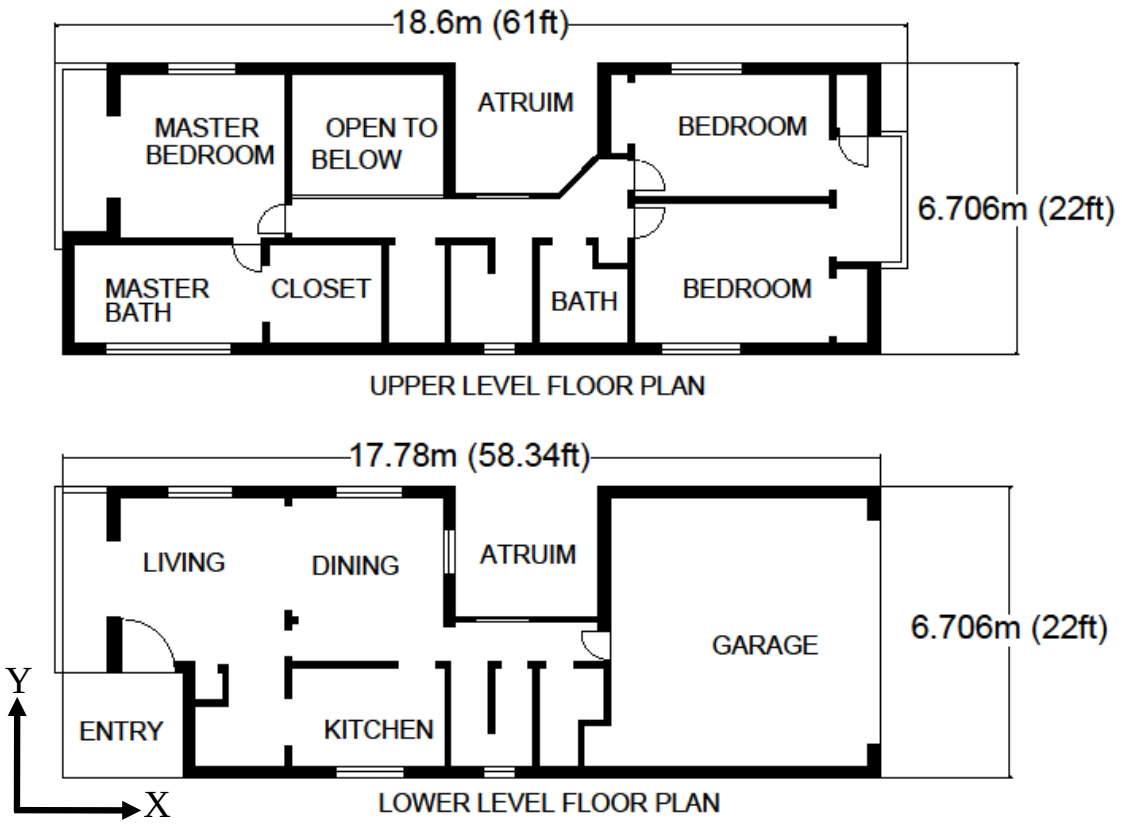

Figure 4.4: Floor plan of example residential building.

4.4 SINGLE STRUCTURE FRAGILITIES

Prior to computing the collapse fragility from tsunami loading, a nonlinear time history analysis for the earthquake that may have produced the tsunami is performed. Figure 4.5 provides a schematic overview of the two-stage analysis procedure used in this dissertation and the general shape of a fragility curve from this two-stage analysis. The tsunami loading characterized by FEMA P646 (2008) is used in the second stage of the analysis. In order to do this, a program was developed and termed SSTAP (**S**equential **S**eismic and **T**sunami **A**nalysis **P**rogram).

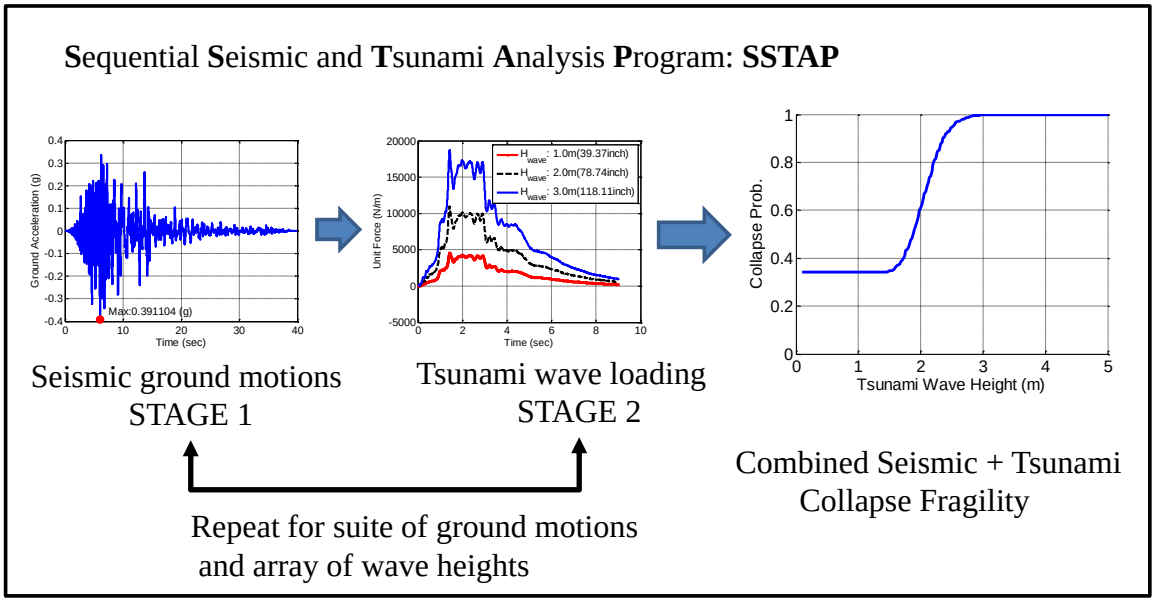

Figure 4.5: Schematic overview of the two-stage analysis procedure used in this study.

The design of coastal structures in a tsunami-hazard zone should take into account loading from tsunamis but the recurrence rates are still not well understood. In this dissertation, the issues of occurrence rate, i.e. tsunami hazard level, are not addressed. Rather, it is assumed that the tsunami occurs and the collapse probabilities computed. This is one purpose of fragilities, namely that they are developed independently from the hazard or occurrence rate essentially making them general and applicable to different sites provided they are re-coupled with the occurrence probability at a given site. Approximate tsunami wave loading can be computed using a set of force equations proposed in FEMA P646 (2008), explained in Chapter 2. This approach provides an equivalent force expressed as a function of tsunami wave height.

In stage two of the analysis procedure, a nonlinear static pushover analysis is performed using these computed tsunami wave loads based on the tsunami wave height under

investigation. The computed wave forces are converted into an equivalent force and then applied to the SDOF system at the top of the wall, which is computed using basic force equilibrium. If the computed tsunami wave loading exceeds the structural capacity, the structure is assumed to have collapsed.

Two seismic intensity levels described in terms of spectral acceleration, which are commonly used in design and analysis, are the Design Basis Earthquake (DBE) and the Maximum Credible Earthquake (MCE), representing 10% and 2% exceedance probabilities in 50 years, respectively. All 44 ground motions (the 22 pairs summarized in Table 4.3) were used in stage one of the analysis for 44 earthquake analyses at each intensity level.

Then, using the "damaged" numerical model, which was numerically represented by maintaining the stiffness and strength degradation in the hysteretic springs, the tsunami analysis was performed to check the collapse of the structure under given wave heights. Variation in the tsunami wave heights was introduced by applying a range for the coefficient of variation (COV), i.e. the ratio of standard deviation to the mean. Thus, it is possible to generate a suite of tsunami wave heights using the COV. The tsunami wave heights were generated in 0.1 meter increments from 0.0 meters to 5.0 meters. Each of those was treated as the mean tsunami wave height for that analysis and the COV used to introduce dispersion about the mean.

Table 4.3: Summary of ATC-63's 22 ground motions (excerpted from FEMA-P695 2009).

ID No.	Earthquake			PGA Max(g)	
	M	Year	Name	Component1	Component2
1	6.7	1994	Northridge	0.42	0.52
2	6.7	1994	Northridge	0.41	0.48
3	7.1	1999	Duzce, Turkey	0.73	0.82
4	7.1	1999	Hector Mine	0.27	0.34
5	6.5	1979	Imperial Valley	0.24	0.35
6	6.5	1979	Imperial Valley	0.36	0.38
7	6.9	1995	Kobe, Japan	0.51	0.50
8	6.9	1995	Kobe, Japan	0.24	0.21
9	7.5	1999	Kocaeli, Turkey	0.31	0.36
10	7.5	1999	Kocaeli, Turkey	0.22	0.15
11	7.3	1992	Landers	0.24	0.15
12	7.3	1992	Landers	0.28	0.42
13	6.9	1989	Loma Prieta	0.53	0.44
14	6.9	1989	Loma Prieta	0.56	0.37
15	7.4	1990	Manjil, Iran	0.51	0.50
16	6.5	1987	Superstition Hills	0.36	0.26
17	6.5	1987	Superstition Hills	0.45	0.30
18	7.0	1992	Cape Mendocino	0.39	0.55
19	7.6	1999	Chi-Chi Taiwan	0.35	0.44
20	7.6	1999	Chi-Chi Taiwan	0.47	0.51
21	6.6	1971	San Fernando	0.21	0.17
22	6.5	1976	Friuli, Italy	0.35	0.31

A log-normal distribution was assumed for the tsunami wave height since log-normal distributions have been used extensively to introduce dispersion for other natural hazards and are used in fragility analysis. The coefficient of variation (COV) for tsunami wave heights was computed from the publicly accessible data described in Baldock et al. (2009) as 0.136 and is included as one of the COV values in the present study. That 13.6% variation was observed in a laboratory environment at Oregon State University where the tsunami was generated at exactly the same height and the wave basin topography was nominally identical. Thus, neglecting variation in the wave maker itself, it was felt to be reasonable to assume that when randomness in nature is introduced the COV is larger, i.e. 13.6% is a lower bound.

Two different types of fragility curves were generated for a single structure. The first type was constructed using only tsunami (pushover) analysis without a nonlinear time history analysis being performed first. The second type is the successive earthquake and tsunami analysis in order to quantify the influence and better understand how this type of successive loading affects fragilities. In order to analyze the system, initially a nonlinear time history analysis was performed using the earthquake record suite as described above. As mentioned earlier, the damage from a single earthquake was allowed to remain numerically by keeping the strength and stiffness degradation in the hysteresis model representing the lateral force resisting system(s) for the structure then the tsunami loading described earlier was applied in the form of a nonlinear pushover analysis, i.e. the effects of the interaction of two hazards and detailed explanation of their mutual effects is followed in Section 4.5. This provides a single analysis point in terms of collapse or

survival. This procedure was repeated for thousands of combinations of the two earthquake levels and tsunami. The seismic intensity was held constant at either DBE or MCE level and all 44 records scaled to that intensity level, but the wave height for the tsunami was allowed to possess a prescribed level of uncertainty in the form of the aforementioned COV. This results in thousands of successive combinations from which statistics and the resulting fragility can be computed.

Consider the city of Cannon Beach, Oregon in the Pacific Northwest of the United States. According to the United State Geological Survey (USGS 2011a), the design basis earthquake (DBE) and the maximum credible earthquake (MCE) for the city of Cannon Beach have seismic intensities of 0.89*g* and 1.34*g* spectral acceleration at 0.2sec, $\xi = 5\%$, respectively. Degradation effects of the combination of the two hazards, i.e. interaction of two hazards, are investigated and repeated for each of the earthquakes in the suite described earlier and then a nonlinear static pushover analysis is performed using the degraded backbone curve to represent the tsunami loads.

Figure 4.6 shows the results of three analyses. Specifically, the solid line represents the resulting collapse fragility when only the tsunami (no earthquake) is considered, the dash line represents the resulting collapse fragility when the DBE level of earthquake intensity and the tsunami is considered, and the dash-dot line represents the resulting collapse fragility when the MCE level of earthquake intensity and the tsunami is considered. From the fragility one can read that a 1.97 meter wave will collapse the building 50% of the time, whereas a 1.67 meter wave will collapse the building 50% of the time, if subjected

to the MCE level earthquake first. While this may seem a minimal difference at first inspection, this is with the lower bound COV wave height considered.

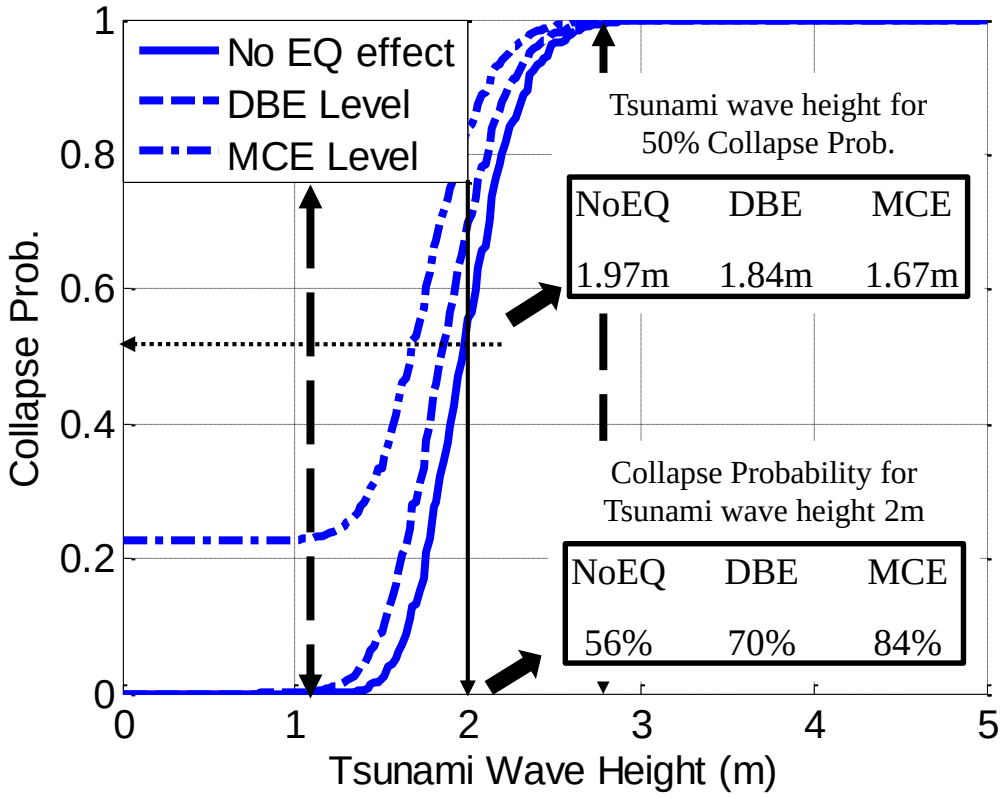

Figure 4.6: Collapse probability of 13.6% COV when wave coming narrow width (X direction) of two-story building.

One can also observe from Figure 4.6 that the lower portion of the fragility is the earthquake sensitive section, i.e. at MCE level there is a 22% chance of the earthquake collapsing the building prior to the tsunami reaching shore according to the model, used herein. Although these wave heights are not large by recent tsunami hazards, the methodology for successive earthquake-tsunami analysis is one of the main focuses of this dissertation and has applicability across a range of building materials and wave

heights.

Now, consider Figure 4.7 which shows the same plot but with a tsunami COV of 50% and in the Y-direction of the building. Initially, the resulting collapse fragility seems to be slightly different when only the tsunami (no earthquake) and the DBE level earthquake are considered. This can be explained in that the building has more shearwalls in the Y-direction, thus one can expect it to be stronger and able to survive at the DBE level earthquake without major damage that would have lead to the strength degradation of structural components, i.e. shearwalls. On the contrary, the width of the building in the Y-direction is wider than that of the other direction, thus it is more vulnerable to tsunami hazard (Y is parallel to the shoreline) because it will take significantly more wave force.

The building has a 50% chance of collapse, for example, for a 1.64 meter, 1.62 meter, and 1.42 meter wave for tsunami-only, DBE level, and MCE level case, respectively. There is only 0.04 meter difference between the tsunami case and the DBE level earthquake case, meaning there is no effect by the design basis earthquake. One can also observe from Figure 4.7 that the fragility shows only a 9% chance of the MCE level earthquake collapsing the building prior to the tsunami reaching shore.

From these basic results one can observe that the tsunami wave heights required to collapse a light-frame wood building decreased when the seismic intensity of the proceeding earthquake increases. The difference is not as notable as one might anticipate, but the trend is evident. The methodology presented herein could be used to statistically

determine requirements for vertical evacuation structures located in regions where near-field tsunamis are a risk such as the U.S. Pacific Northwest.

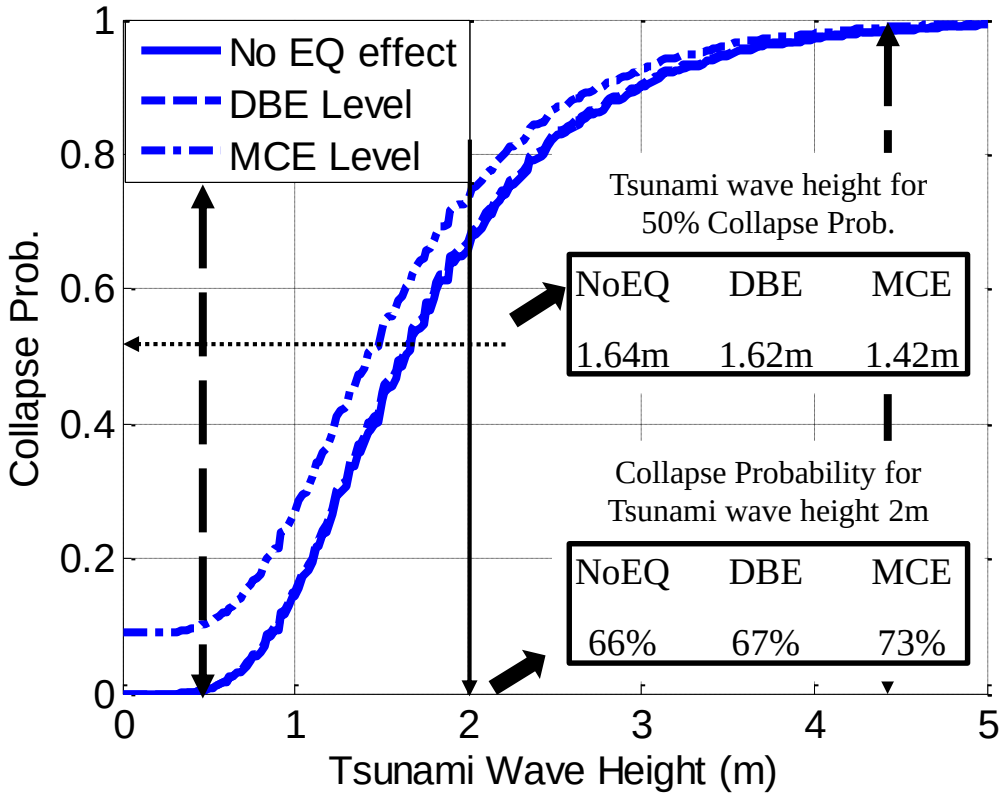

Figure 4.7: Collapse probability of 50.0% COV when wave coming wide width (Y direction) of two-story building.

4.5 INTERACTION OF TWO NATURAL HAZARDS

The understanding of how one hazard affects the other since they may occur rapidly in succession, i.e. without the ability to repair between the loadings, is investigated. Damage was allowed to accumulate in the numerical model so the successive effect of earthquake

loading and tsunami loading could be quantified. Figure 4.8 shows the effects of degradation, which is based on one ground motion from the suite of records.

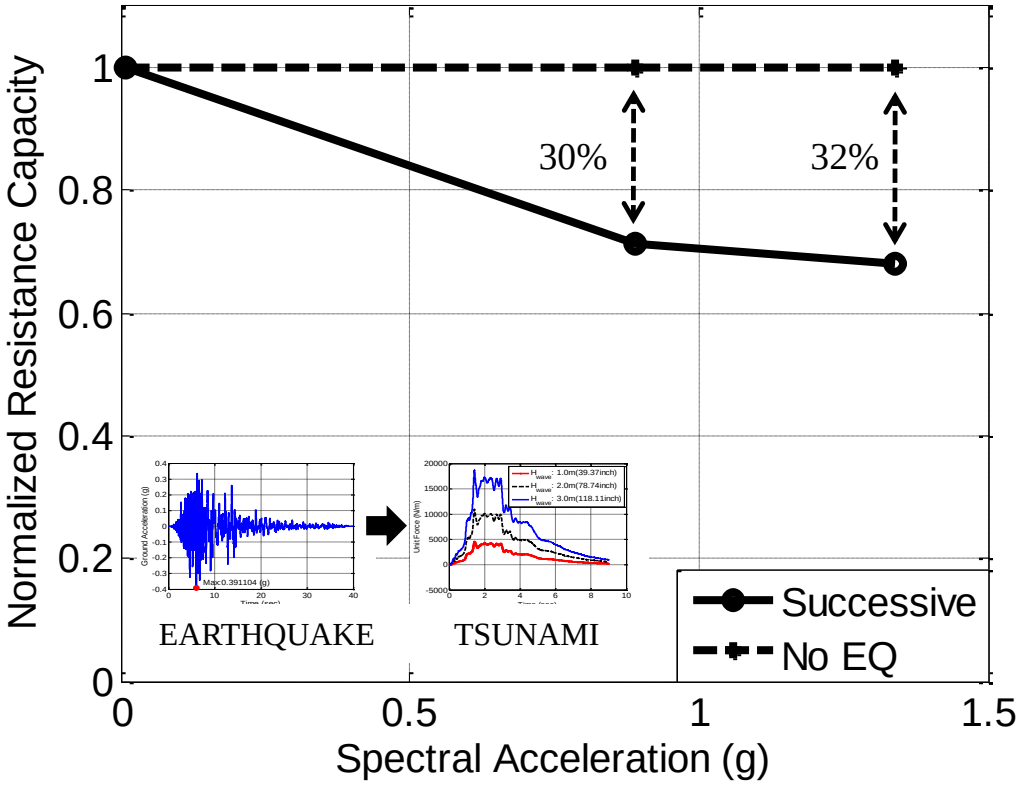

Figure 4.8: Degradation effects without any shearwalls failure case.

The dashed line represents the resistance of the building not considering seismic excitation, which will be unity (normalized). The solid line represents the successive earthquake and tsunami analysis results and shows the strength degradation for this particular earthquake. The normalized resistance capacity has the same values when seismic excitation is not considered but reduces gradually when earthquake and tsunami analysis are considered. Approximately, 30% of the resistance capacity is reduced when

the structure is subjected to the DBE (0.84*g*) level ground motion and 32% when MCE level (1.34*g*) is considered. However, Figure 4.8 depicts this reduction in structure capacity for only one earthquake within the suite of earthquakes.

Now consider another earthquake from the suite, whose results are shown in Figure 4.9. For this earthquake, one can see that the DBE level earthquake reduces the capacity by 54% and numerically fails the structure at a seismic intensity level even less than the MCE level.

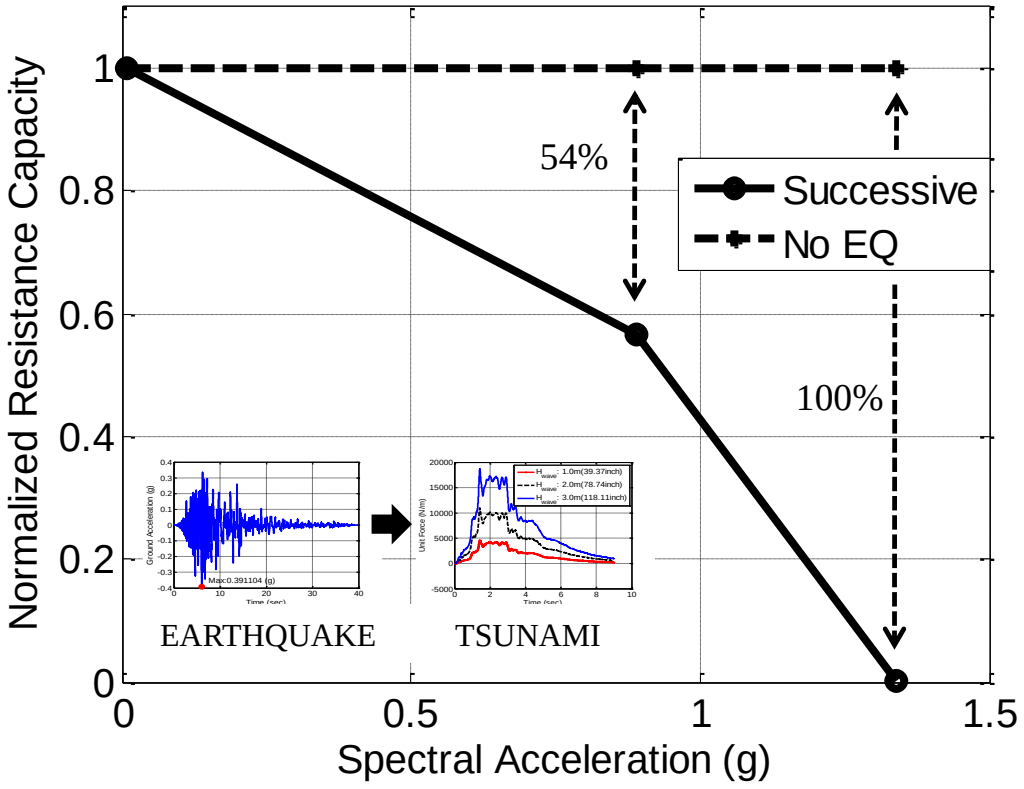

Figure 4.9: Degradation effects with shearwalls failure case.

From the results, it is felt to be important that the understanding of the interaction of the earthquake hazard and tsunami hazard due to their strong link and the possibility. From two figures, the structural capacity has been decreased significantly and this reduction caused to lead to the earlier structural collapse.

4.6 COMMUNITY FRAGILITIES: STRUCTURAL ASPECTS

In previous sections, the tsunami framework for a single building was developed and explained in detail. Another objective of this dissertation is to develop a methodology and procedure for development of a tsunami fragility framework and its extension to a coastal community. In order to do this, the community can be made from the combination of each building, thus the community fragility can also be constructed as a weighted summation of building fragilities. The building fragility for a coastal community can be computed by considering the relationship between a single building and the community. The relationships can be expressed by introducing a weighting factor as:

$$F_c = \sum_{i=1}^{n} \lambda_i^s F_i^s \tag{4-1}$$

where F_c is the fragility index for the community, F_i^s is the fragility index for the i^{th} structure, λ_i^s is the weighting factor defined as follows, and n is the number of total structures in the community.

The weighting factor can be simply defined as:

$$\lambda_i^s = \frac{I_i^s}{\sum_{i=1}^{n} I_i^s} \tag{4-2}$$

where λ_i^s is the weighting factor and I_i^s is an impact or importance parameter, which can be determined based on the number of people living in the structures, the overall area of the structures, and the importance of the structure in the community such as hospital, school, residential house, fire station, police station, etc. A schematic overview of the construction of the community fragilities from the combination of each single assembly is shown in Figure 4.10.

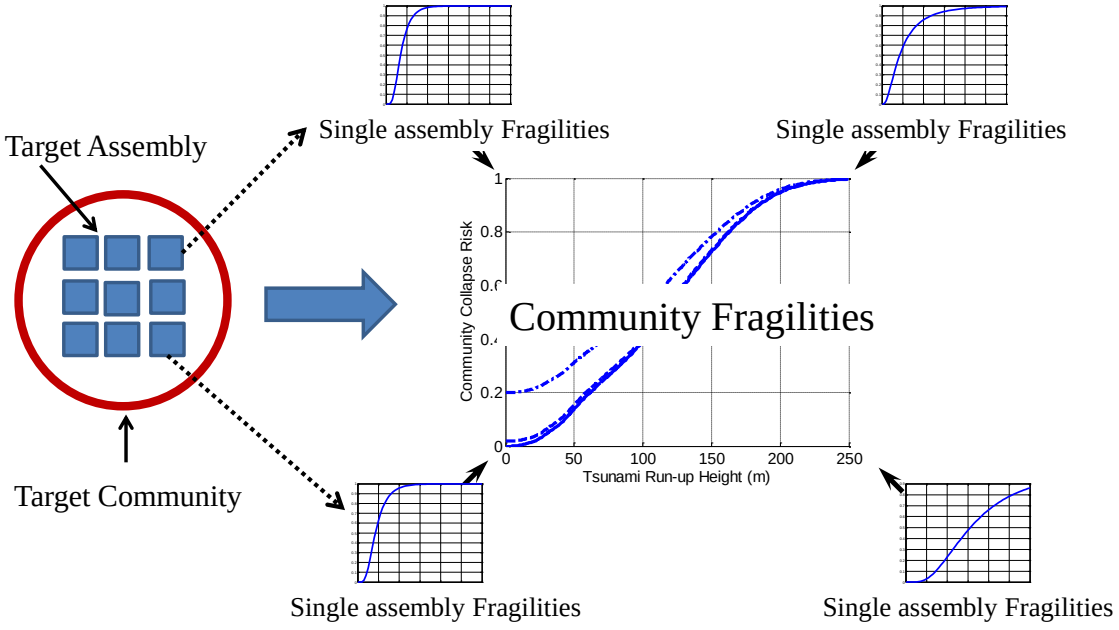

Figure 4.10: Schematic overview of constructing the community collapse risk fragilities.

The location of each single assembly in the community is an important factor due to the link between the tsunami wave forces, i.e. a house can have no damage from the tsunami if its location is far from the shoreline or at a high elevation. Thus, the proposed approach explained in the previous section can be applied directly to each single assembly and then individual fragilities obtained. Then the community fragilities are calculated using Equation (4-1).

The City of Cannon Beach along the northern Oregon coast was selected as an illustrative example shown in Figure 4.11. Residential houses are only considered in constructing the community fragilities as a simplification.

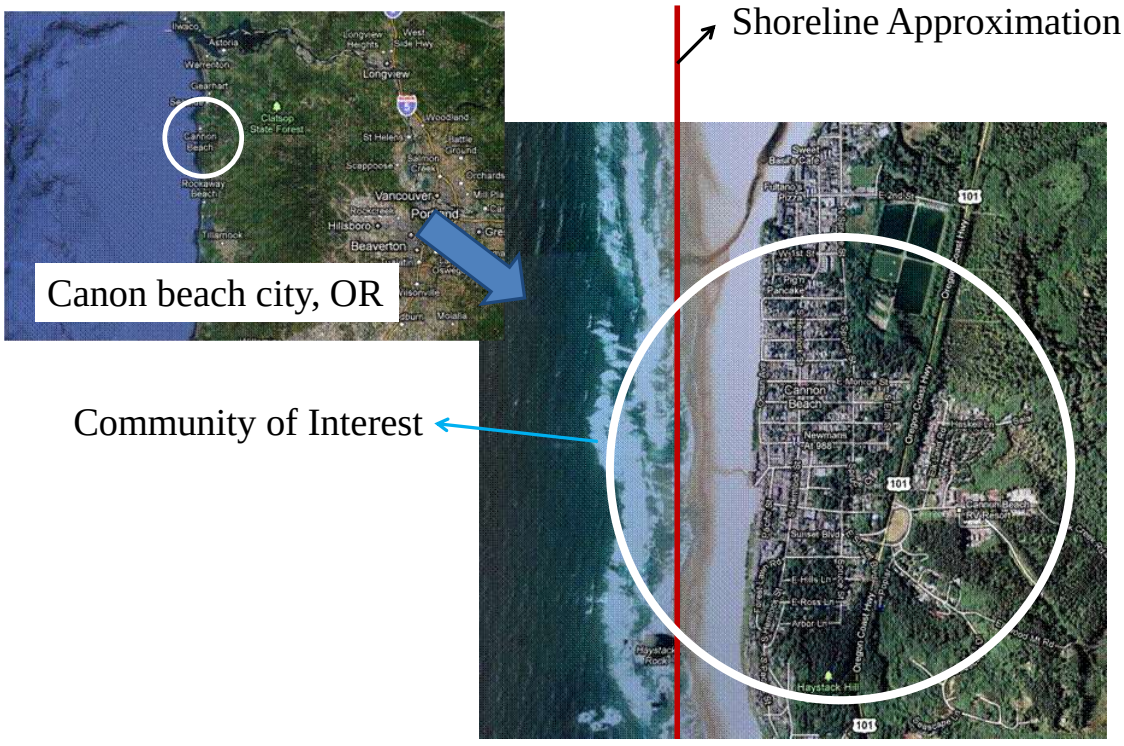

Figure 4.11: The City of Cannon Beach, Oregon, U.S.A.

Initially, the location of each individual house in the City of Cannon Beach is computed based on the satellite image and calibrated based on the south-west corner of the boundary of the city limitation. This point is designated as the origin. It is difficult to determine the exact elevation of individual houses in a community from the geographical two-dimensional images. A GIS (Geographical Information System) can be efficient with handling this problem if the resource is available. Approximately, the elevation was determined based on the shortest distance from the close shoreline to each residential house in the community.

A schematic overview of the City of Cannon Beach is illustrated in Figure 4.12. In Figure 4.12, the black solid line shows the boundary of the city and blue dots represent an individual residential house: approximately 1400 residential houses were identified in the study area. Detailed information of the residential houses can be found in Appendix H of this dissertation.

Now, in order to meet the variety of the structural configurations in the community, three more residential houses having varying floor plans are considered and analyzed using the proposed approach under the same conditions for seismic and tsunami analysis. The number of shearwalls in the residential house is assumed based on their floor plan and their capacities are also assumed based on typical Pacific Northwest construction. The example described in Section 4.3 is designated as Type A. Each example can consider either the narrow or the wide direction, i.e. the X- and Y- direction of the residential building depending on the orientation of the building to the shoreline. Thus, eight

different types of residential buildings can be best matched to each building in the satellite images for use in the community-level fragility analysis.

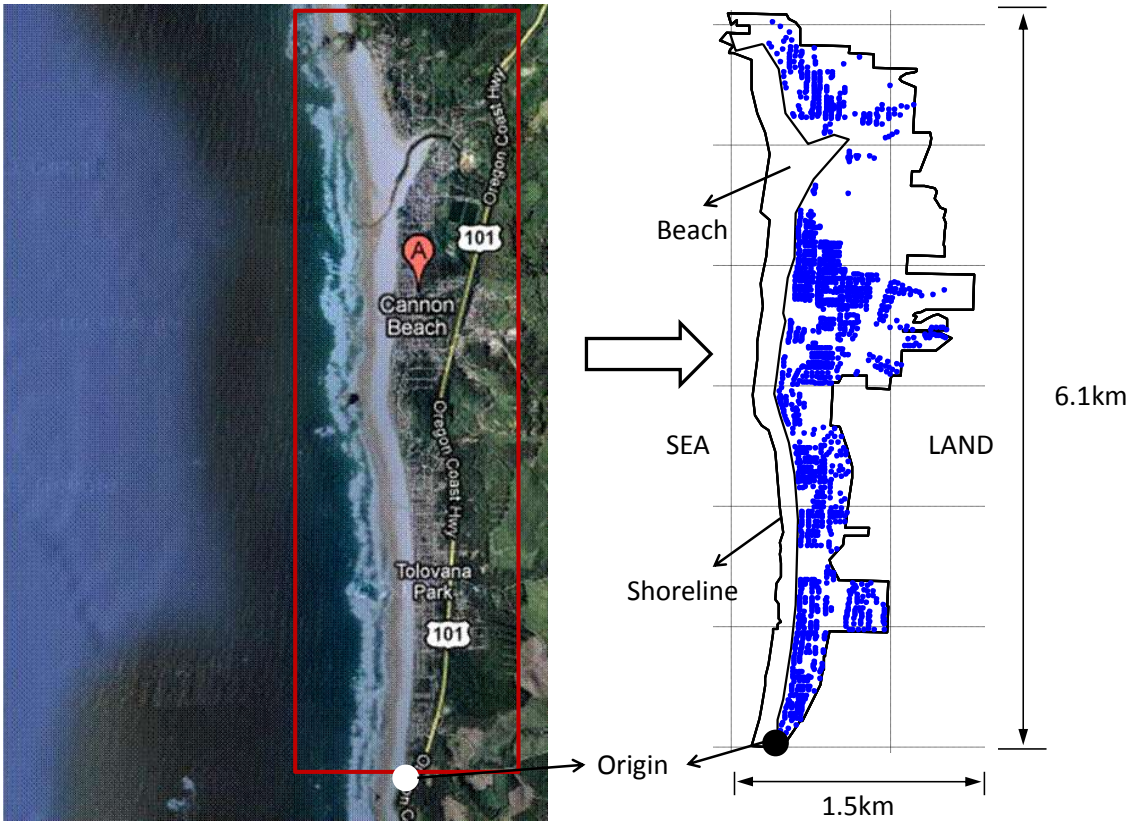

Figure 4.12: Schematic overview of the City of Cannon Beach, OR and dataset.

Type B is a one-story light-frame wood structure and represents a common two-bedroom and two-bathroom house. The building's total living area is approximately 113.53 m^2 (1222 ft^2) and its total weight is approximately 20.0 tons (44.05 kips). There are fifteen shearwalls; eight shearwalls are assigned for the X-direction having 10.37 meters (34 feet) width and seven shearwalls for the Y-direction having 12.35 meters (40.5 feet) width. The floor plan is shown in Figure 4.13.

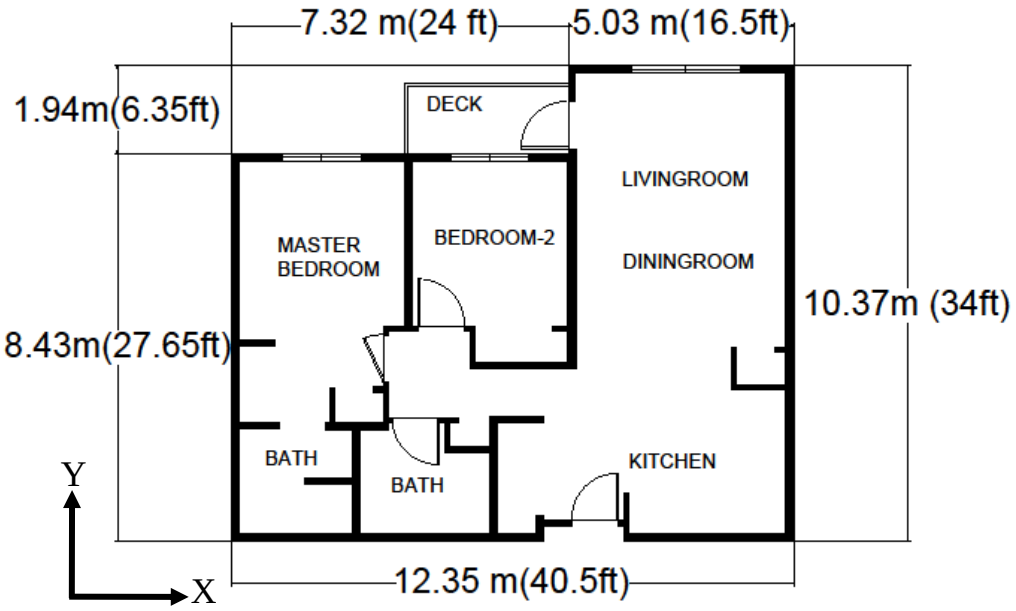

Figure 4.13: Floor plan for the Type B.

Type C is a one-story light-frame wood structure and represents a common one-bedroom and one-bathroom, bungalow style residential structure. The building's total living area is approximately 57.15 m^2 (615.97 ft^2) and its total weight is approximately 10.0 tons (22.06 kips). The building has ten shearwalls; six shearwalls are assigned for the X-direction having 6.73 meters (22.06 feet) width and four shearwalls for the Y-direction having 9.45 meters (31 feet) width. The floor plan is shown in Figure 4.14.

Type D is a one-story light-frame wood structure and represents a common three-bedroom and two-bathroom house with a two-car garage. The building's total living area is approximately 275.11 m^2 (2965.27 ft^2) and its total weight is approximately 48.57 tons (107.03 kips). The building has twenty-one shearwalls; ten shearwalls are assigned for

the X-direction having 14.06 meters (46.12 feet) width and eleven shearwalls for the Y-direction having 21.31 meters (69.95 feet) width. The floor plan is shown in Figure 4.15.

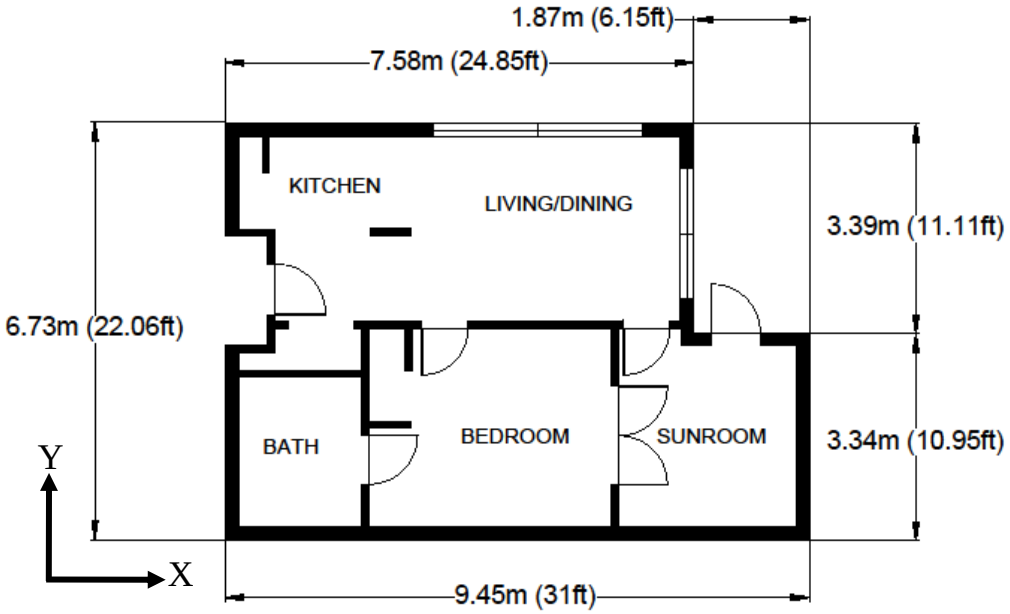

Figure 4.14: Floor plan for the Type C.

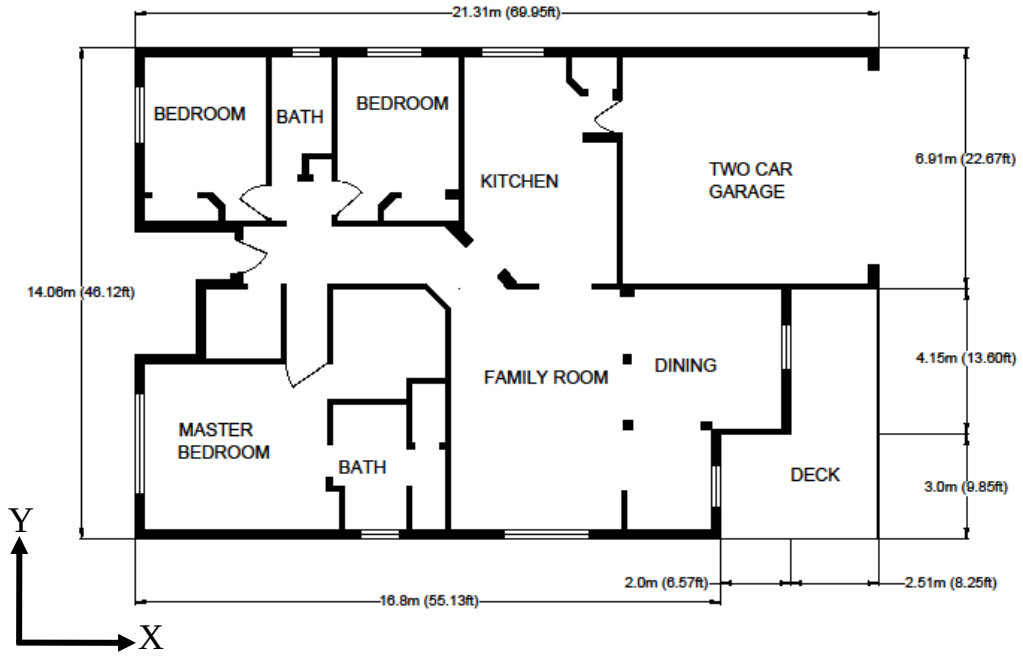

Figure 4.15: Floor plan for the Type D.

The results of fragilities for the above mentioned three residential buildings were also determined similar to the fragilities for structure Type A. The detailed fragility results for the three residential buildings can be found in Appendix E of this dissertation.

Community fragilities were constructed for each of these structures for two COV values for wave height, i.e. 13.6% and 50.0%. A type of single assembly was selected from the possible eight styles based on satellite images and then analyzed. The result of selections is tabulated in Table 4.4.

Table 4.4: Possible eight styles of residential building type for the community.

Style ID No.	Residential building		Allocated number of style
	Structure Type	Direction of wave	
1	A	X	101
2		Y	190
3	B	X	187
4		Y	207
5	C	X	216
6		Y	220
7	D	X	212
8		Y	89

Wave forces are computed from the generating tsunami wave run-up height. It should be noted that this wave force computing procedure should be repeated for every single assembly due to the various location of the entire single assembly, i.e. the elevation of each residential building varies depending on local topography and plays an important role in computing wave forces.

Each residential building has a collapse probability, which was computed from the earthquake hazard similar to an initial condition, i.e. DBE or MCE level earthquake intensity is considered as a previous hazard. This means that the community also has a seismic collapse probability of course, i.e. when a certain level, DBE or MCE level, earthquake occurs. Thus, the collapse probability from the previous hazard, i.e. earthquakes, is tabulated in Table 4.5.

Table 4.5: Collapse probability from only the earthquake hazards.

Style ID No.	Collapse Probability (%)	
	DBE Level	MCE Level
1	~ 0.	22.73
2	~ 0.	9.10
3	~ 0.	22.73
4	~ 0.	15.91
5	~ 0.	15.91
6	9.10	34.10
7	~ 0.	13.64
8	6.82	34.10

Community fragilities from the combination of the single structure fragilities are presented in Figure 4.16 when 13.6% COV is applied to generate the tsunami wave data. The solid line represents the resulting collapse fragility when only the tsunami (no earthquake) is considered, the dashed line represents the resulting collapse fragility when the DBE level for earthquake intensity and the tsunami is considered, and the dash-dot line represents the resulting collapse fragility when the MCE level earthquake intensity and the tsunami is considered.

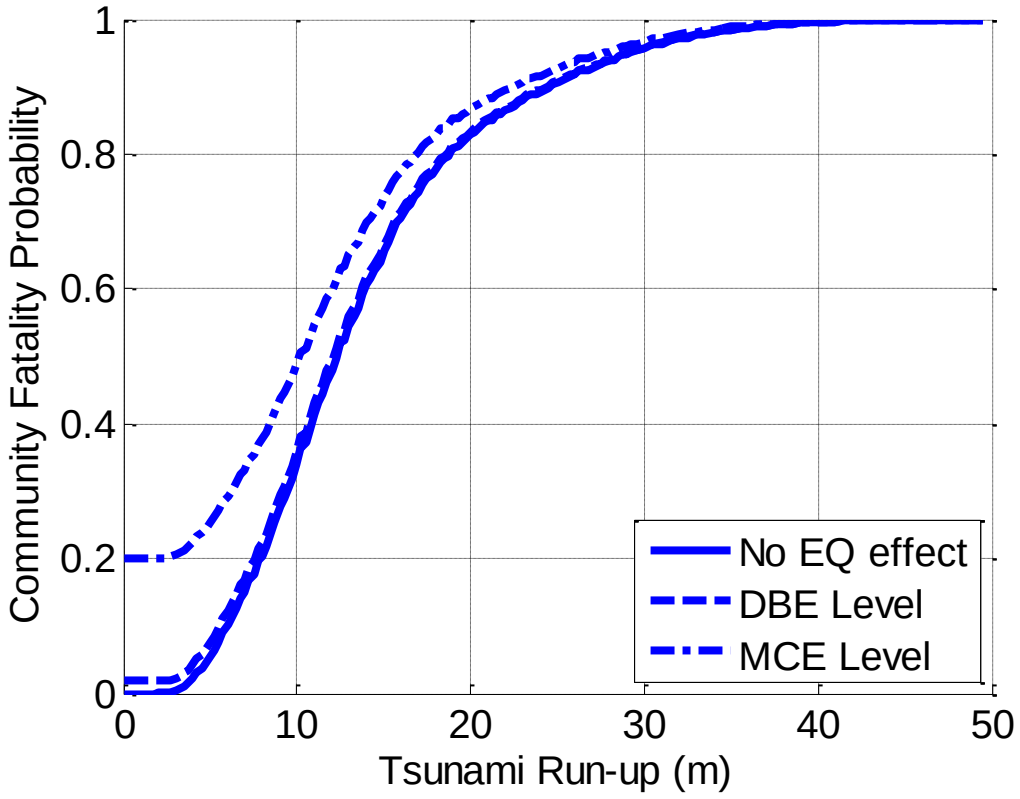

Figure 4.16: The fragilities for community for a wave COV of 13.6%.

From the figures, the collapse probability from the previous hazard, i.e. earthquakes, can be seen at DBE and MCE Level as having a 1.8% and 20.0%, respectively. If the

expected collapse probability is 50.0%, then one can see that the tsunami run-up height is 12.27 meters, 12.08 meters, and 10.17 meters when tsunami-only, DBE level earthquake, and MCE level earthquake is considered. If the tsunami run-up height is 10.0 meters then there would be a 33.9%, 35.6% and 48.7% collapse probability for tsunami-only, DBE level, and MCE level, respectively.

It should be noted that the label of x-axis in the figures are termed tsunami run-up height instead of tsunami wave height. The reason is that each house is subjected to a different tsunami wave height, typically defined as the vertical distance from the mean water elevation to the bottom of the structure, which is a function of their location in the community and topography. Thus, the tsunami run-up height was felt to be a more reasonable variable to express the wave height at the community. To better understand the difference between tsunami wave height and tsunami wave run-up height Figure 4.17 depicts all variables within the problem.

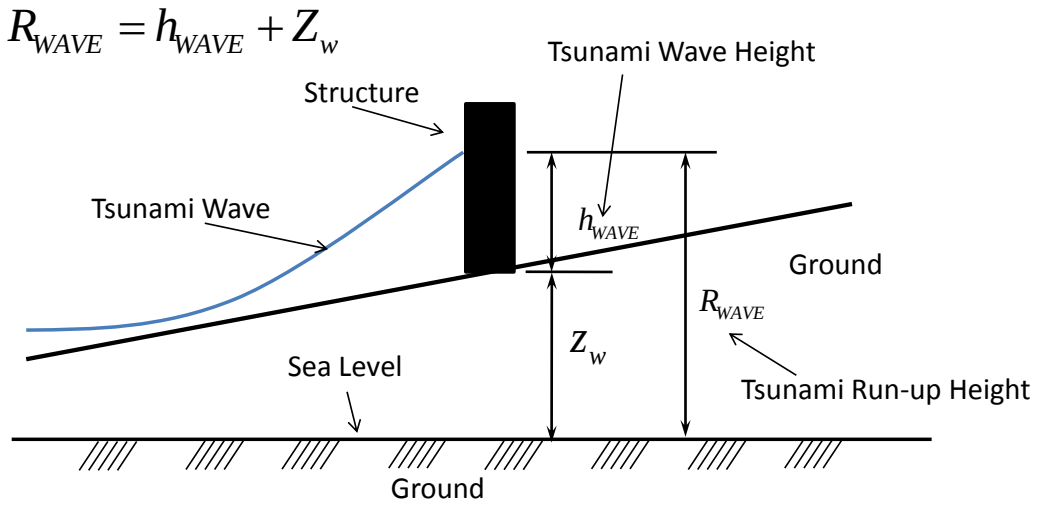

Figure 4.17: Definition of wave height and run-up height.

Now, the fragilities of the community considered for a wave having a 50.0% COV are presented in Figure 4.18. From the figures, the collapse probability from the previous hazard, i.e. earthquakes, can be seen at DBE and MCE level with 1.8% and 20.0%, respectively, which has same probability when 13.6% COV is considered. Run-up height of 13.60 meters, 13.31 meters, and 10.65 meters for tsunami-only, DBE level earthquake, and MCE level earthquake, respectively, correspond to a 50% probability of collapse. Looking at it from the other perspective, if the tsunami run-up height is expected to be only 10.0 meters, then one can see 31.6%, 33.2% and 46.4% probability of collapse for tsunami-only (no earthquake), DBE level, and MCE level, respectively.

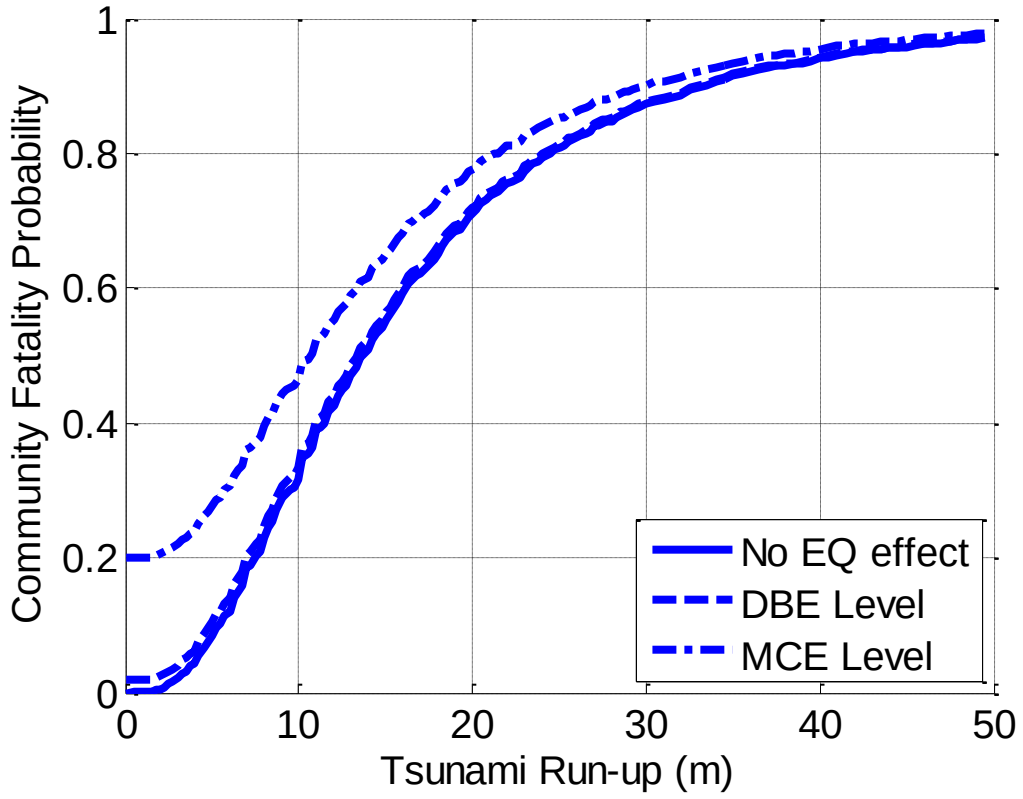

Figure 4.18: The fragilities for community for a wave COV of 50.0%.

From these results, one can observe that the tsunami wave heights required to collapse a light-frame wood building decreased when the seismic intensity of the proceeding earthquake increases, which is the same as the single assembly (shear wall) case as one would expect. The difference as a function of seismic intensity prior to the tsunami is not as notable as one might anticipate, but the trend is definite. The methodology presented herein could be used to statistically determine requirements for vertical evacuation structures located in regions where near-field tsunamis are a risk such as the U.S. Pacific Northwest.

CHAPTER 5

TSUNAMI VERTICAL EVACUATION METHODOLOGY

5.1 OVERVIEW

This chapter provides a tsunami vertical evacuation methodology for a single structure and for a coastal community. Initially, each structure is assumed to be able to be reinforced with a tsunami safe frame (TSF), which is similar to a safe room for a tornado hazard (FEMA-320 2008) in concept (i.e. protecting life of occupants), but is at the top level of the structure and rests on steel columns. The TSF may consist of steel or reinforced concrete columns to increase the stiffness of the structure but more importantly the objective is to elevate some portion of the building to a safe place in order to provide occupant safety while decreasing the collapse risk of the building. The approach can be applied to retrofit an existing structure, but would be significantly more costly then implementing the concept in new buildings.

Two methods are examined in this chapter in order to develop an evacuation plan for a community: (1) reinforcing of every house in the community which can be thought of as an upper bound and (2) constructing one or more shelter(s) to evacuate vertically and reduce the number of fatalities in the community.

An optimization technique is needed to find the best solution, therefore a program was developed and termed TOGA (**T**sunami evacuation **O**ptimization program using **G**enetic **A**lgorithms).

5.2 EVACUATION PLAN FOR SINGLE STRUCTURE

A single structure can be reinforced to survive when subjected to a certain level of natural hazards, i.e. earthquakes and tsunamis, and their combination. To do this, two methods are proposed: (1) reinforce the structural components to increase the stiffness and strength of the building; or (2) raise the elevation of the building. Both methods decrease the collapse risk of the single structure due to the reduction of the loading from the tsunami.

The initial idea is to reinforce the bottom of the structure with steel or reinforced concrete columns, termed herein as a TSF (Tsunami Safe Frame). This frame increases the stiffness of the location in a single room or single structure and allows the levels on top to serve as safe locations. Figure 5.1 shows a schematic of a two-story TSF with a vertical evacuation zone located at roof level.

If a structure is located at a high enough elevation to ensure it is out of the reach of the tsunami then it survives provided the columns can maintain stability. So, a second approach to be considered is simply heightening the elevation of a single structure within a community in order to reduce the tsunami wave height and subsequent forces, of course,

the elevation is a critical factor in computing wave forces. Figure 5.2 explains this approach schematically.

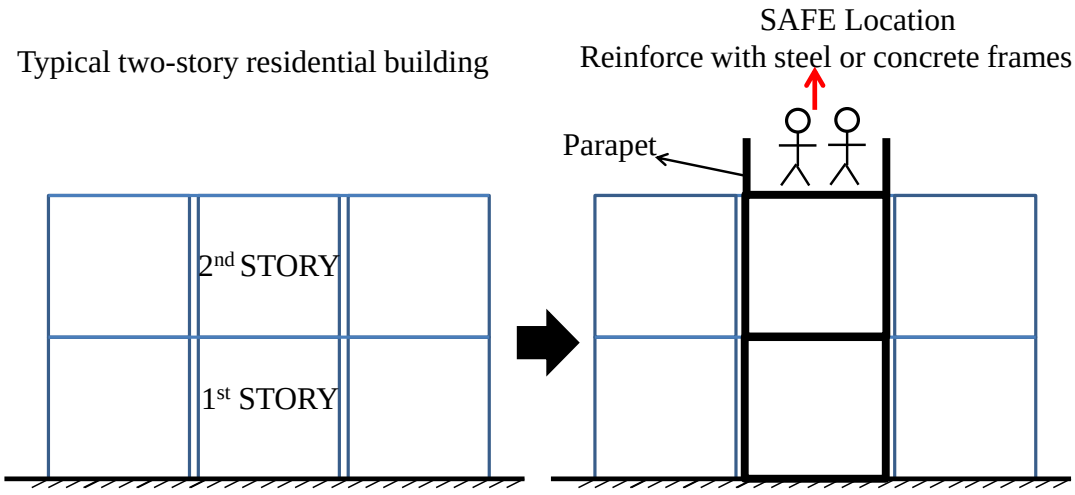

Figure 5.1: An example of a typical two-story house with a two-story TSF.

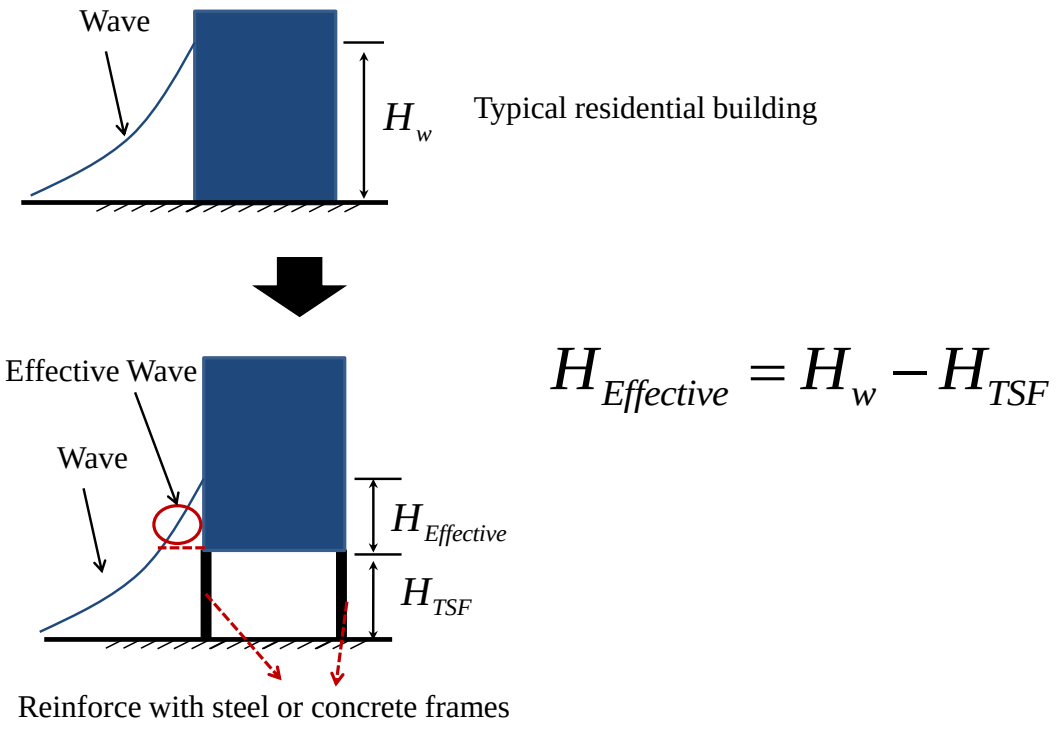

Figure 5.2: An example of typical residential building with reinforcement.

It should be noted that the connection between the TSF and the structure must be designed to avoid a connection failure in shear or uplift. The TSF is assumed to be a circular section type in order to reduce the tsunami wave forces, i.e. drag forces, and the width of the section is relatively small so the drag force is neglected compared to the width of the super-structure it is supporting. Therefore, no forces are applied to the TSF columns from the tsunami waves in the approach described herein.

It should also be mentioned that the large member for a TSF is definitely more efficient in resisting the lateral loading due to earthquake, but results in higher drag forces during tsunami wave loading due to the width of the section. Thus, additional research is needed to examine finding an optimal member, which can obtain a reasonable safety rate using optimization techniques, subjected to both the earthquake and the tsunami.

Recall the detailed floor plan for the Type A structure shown in Figure 4.4 of Chapter 4. This structure was selected as an illustrative example. Fragilities for this structure are constructed based on the various TSF elevation ranges from 0.0 meters to 5.0 meters for increments of 0.5 meters. In order to see the trend in collapse probability with respect to the various elevations consider the loading direction acting on the narrow direction of the structure with a target tsunami wave height of 2.0 meters and 13.6% COV for a wave height. Then, the collapse probability can be determined from the fragilities for each elevation. The resulting fragility is shown in Figure 5.3 and in tabular form in Table 5.1. In this figure, the solid line represents the resulting collapse fragility when only the tsunami (no earthquake) is considered, the dash line represents the resulting collapse

fragility when the DBE level of earthquake intensity and the tsunami is considered, and the dash-dot line represents the resulting collapse fragility when the MCE level of earthquake intensity and the tsunami are considered.

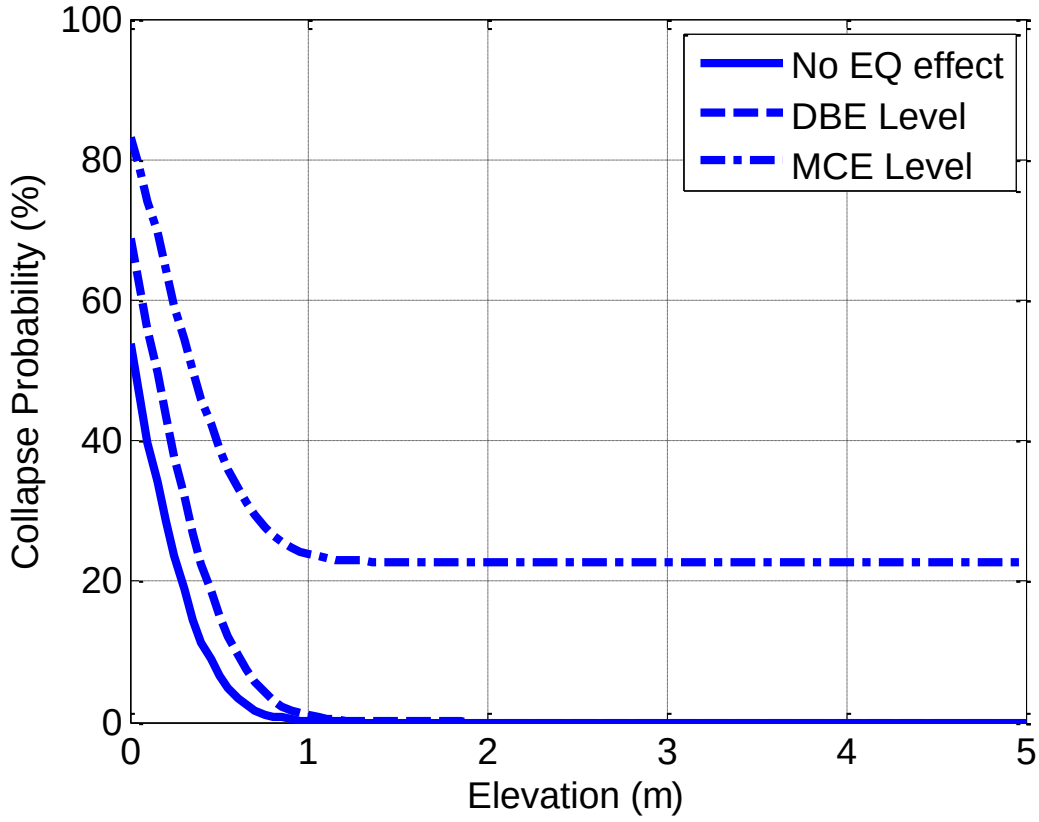

Figure 5.3: Collapse probability with respect to various elevations.

From Figure 5.3, one can read that even though the elevation is increased up to 5.0 meters, it still has a collapse probability of 22.73% when an MCE level earthquake intensity and tsunami are both considered. This can be explained in that the collapse probability of 22.73% comes from the earthquake hazard. Thus, if a stakeholder wants to reduce this collapse probability, they should redesign or reinforce this structure for

earthquake first and then consider an elevation increase. For the other cases, where the earthquake is smaller, the collapse probability can be reduced significantly with a proper amount of the elevation.

Table 5.1: Results of the collapse probability with respect to various elevations.

Elevation Increments (*m*)	Collapse Probability (%)		
	No EQ	DBE Level	MCE Level
0.00	53.70	68.76	83.11
0.25	23.55	37.65	59.18
0.50	6.60	15.06	39.00
0.75	1.05	4.26	27.82
1.00	0.25	0.90	23.80
1.50	~0.00	0.02	22.76
1.70	~0.00	~0.00	22.73
2.00	~0.00	~0.00	22.73
2.44	~0.00	~0.00	22.73

Additionally, the collapse probability can be decreased from 53.7% to 23.55% with 0.25 meter increments of the elevation when only tsunami hazard is considered. Also, it is reduced from 37.65% to 4.26% when the elevation is increased from 0.25 meters to 0.75 meters when the DBE level seismic intensity and tsunami are considered. If a height of

one story, i.e. 2.44 meter (96 in.), is selected as the elevation then the collapse probability is reduced significantly from 53.70% to nearly 0% for only the tsunami, from 68.76% to nearly 0% for DBE level seismic intensity, and from 83.11% to 22.73% for MCE level seismic intensity. This approach can be also applied to other structures, i.e. Type B, C, and D structure. Their results are also as expected and can be found in Appendix F of this dissertation.

It is obvious that the structural damage from tsunamis and risk of death can be significantly reduced by heightening the elevation while providing the needed amount of lateral capacity. Understanding the relationship between the reinforcement with a TSF and the collapse probability of a single structure can inform the planning of a community evacuation plan in order to decrease this risk of fatalities.

5.3 EVACUATION PLAN FOR COMMUNITY

In previous sections, the tsunami vertical evacuation framework for a single assembly was developed and explained in detail. Another objective of this dissertation is to develop a methodology and procedures for the tsunami vertical evacuation plan for the coastal structural systems with a focus on wood frame buildings and its extension to a community. The enhancement of each structure can be helpful in reducing the collapse risk and probability of fatalities for a community, thus this method can be suitable to assist in decision-making and planning for a tsunami evacuation plan for a community.

Although having the ability to shelter-in-place by going to the highest point in a building is ideal, it is typically cost prohibitive particularly for existing structures, FEMA-P646 recommended a combination of vertical evacuation facilities and the use of naturally high ground if it is available. Figure 5.4, excerpted from FEMA P-646 (2008), illustrates this concept.

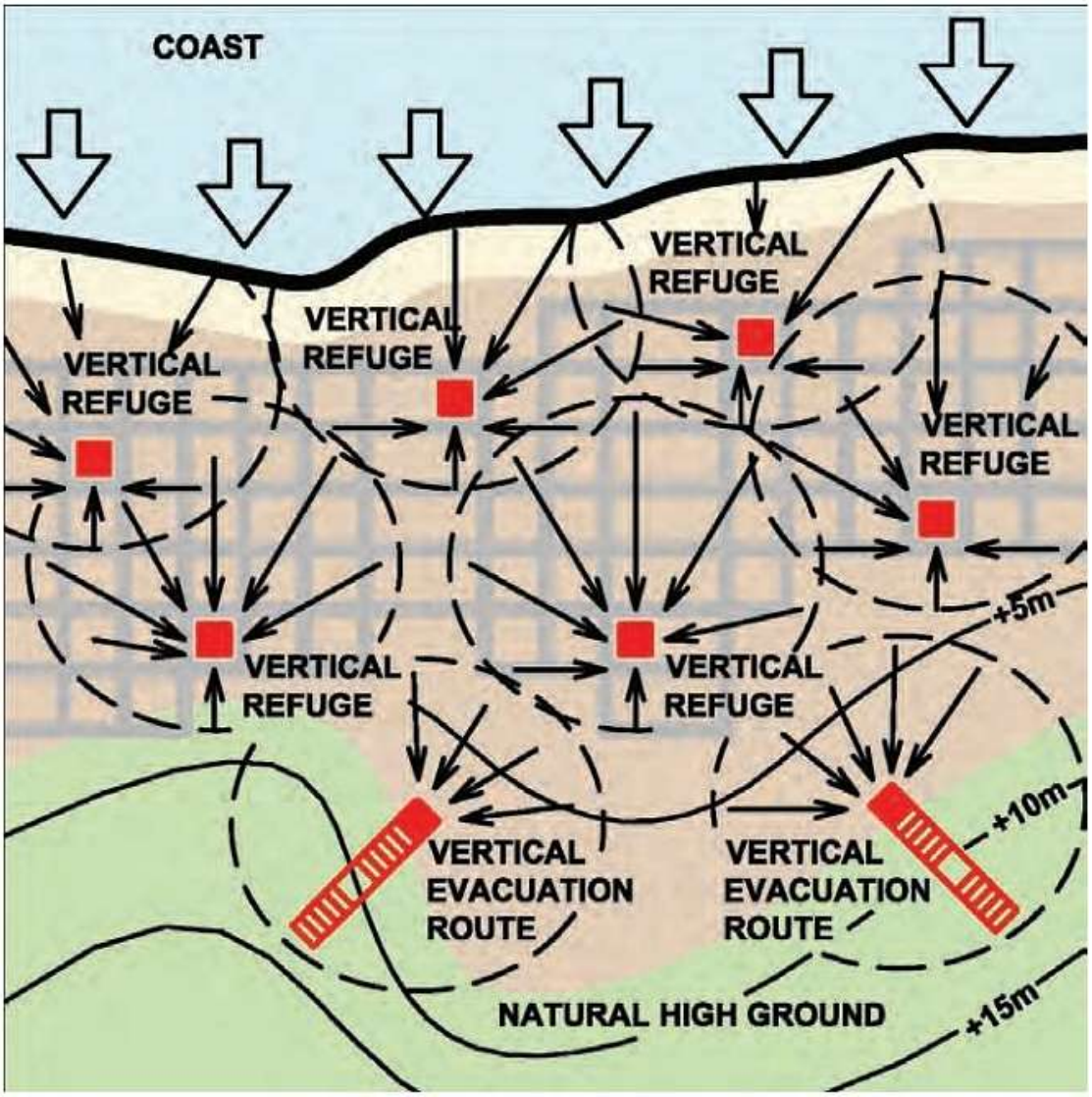

Figure 5.4: Shelters as an evacuation plan (excerpted from FEMA-P646 2008).

Shelter(s) can be located anywhere in the community, thus the location of the shelter must be determined to maximize survival while balancing cost or funding available. Of course, to examine this problem the number of persons to be admitted or accommodated and human walking (or running) speed for each age must be accounted for. Also included in the analysis is the optimal number of shelters for the entire community.

It should be noted that the shelter(s) do not always need to be new construction; rather they can be selected from existing structures in the community such as a city hall, hospital, school, fire station, etc, and a retrofit performed. In that case, the selected structure should be fortified properly to sever as a shelter.

An optimization technique, i.e. genetic algorithms in this dissertation, is applied to solve this problem. To do this, an objective function must be satisfied by minimizing a distance or elapsed time to evacuate from each structure to the shelters, i.e. minimizing the distance traveled for the community during an evacuation.

One large shelter which is large enough to serve all citizens of the community may not always be efficient when considering total time to “evacuate”. Therefore, two or more shelters may be needed to provide the optimal solution. In that case, a proper shelter location should be selected to obtain the shortest distance among the multiple shelters for the evacuees in a community.

There may exist initial conditions such as the capacity of the shelters, number of people beginning in each structure and its structure type, as well as boundary conditions for the community. These items can simply be treated as input data. Therefore, two data sets are introduced for the shelter and the single structure, as described in Table 5.2 and Table 5.3, respectively.

Table 5.2: Data set for the shelter.

Name	Variable	Remark
Coordinate	(x_{si}, y_{si})	Design variable
Admitted Capacity	AC_i	Given condition

Table 5.3: Data set for one single structure.

Name	Variable	Remark
Coordinate	$(x_i, \ y_i)$	Given condition
Assigned shelter number	S_i	For multi-shelter case only
Distance	L_i	Needs to be computed
Number of People	n_i	Given condition
People Type	A_i and Y_i	Adults and children have different walking speed

The goal of the optimization is to determine the optimal location for each of the shelters. The location vector can be expressed as:

$$X = \left\{ (x_1, y_1), (x_2, y_2), \cdots\cdots, \left(x_{N_{Shelter}}, y_{N_{Shelter}} \right) \right\} \tag{5-1}$$

where $N_{shelter}$ is the number of shelter.

The objective function for this problem, which is, of course, what is being minimized, can be expressed as:

$$f(x) = \sum_{i=1}^{N_{House}} L_i \tag{5-2}$$

where $f(x)$ is a objective function, N_{House} is the number of structures in the community, and L_i is the distance of the shelter and each structure in the community, defined as:

$$L_i = \sqrt{(x_i - x_s)^2 + (y_i - y_s)^2} \tag{5-3}$$

where (x_i and y_i) are the coordinates of each house and (x_s and y_s) are the coordinates of the shelter.

It should be noted that the distance calculation assumes they will take the shortest route, regardless of paths or roadways. In general, three coordinates are needed to express the exact location of a structure or shelter and the objective function could be extended by adding a z coordinate, i.e. height or elevation. In that case, the height of the single structure and shelter should be included in the calculation for distance. Typically, the range for heights in a coastal community may not be significant compared to horizontal distances and therefore only horizontal coordinates are used in the distance calculation.

TOGA is used to solve this problem numerically. The design variables are converted into a binary string array, i.e. the chromosome. The lower and upper bound of the design variable, i.e. the location of the shelter, is provided and can be determined from the community and then the size of the design variables can be computed as well.

It should be noted that if the community is too large, then the grid can be modified to reduce the size of the chromosome, which can reduce the computation cost significantly, but is not mandatory. In that case, the shelter is assumed to be located only at the grid point. The space of the grid can be selected as the half of the structural size of the shelter or arbitrary size.

As an illustrative example, consider a community that is a rectangular shape and idealized as 1.0 x 2.0 kilometers. One large shelter is assumed to be sufficient to serve the entire community. The location of the shelter is assumed to be located at the mid-point of the community area, (500m, 1000m) for illustration. The number of houses in this

community is assumed to be one hundred and their location is generated randomly, as illustrated in Figure 5.5.

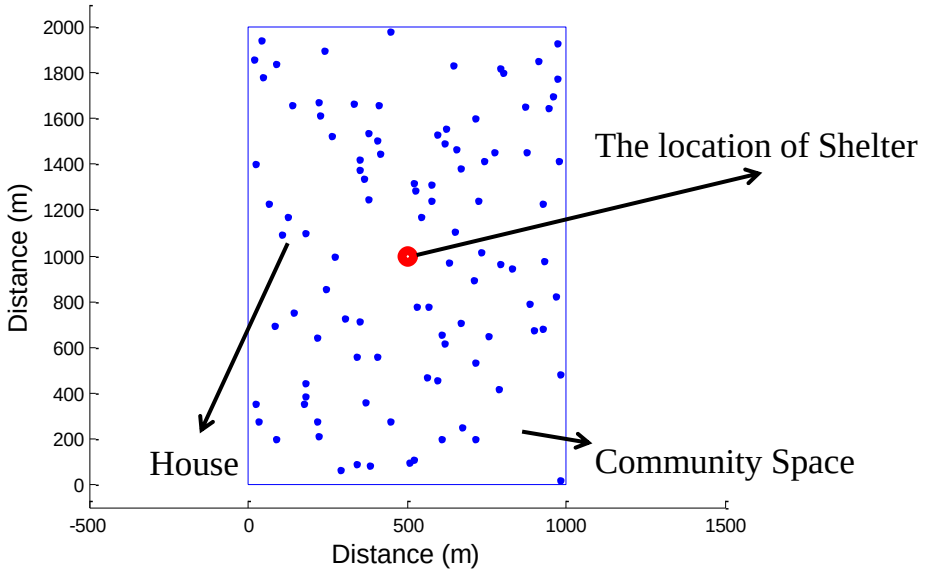

Figure 5.5: Schematic overview of an illustrative example.

The 21 binary strings can be represented by one design variable and are summarized in Table 5.4.

Table 5.4: Design configurations of the one shelter.

Design Variable	Lower / Upper bound	Binary	Size
x_i	0 / 1000 m (3281 ft)	2^{10} (1024)	10
y_i	0 / 2000 m (6562 ft)	2^{11} (2048)	11

The shelter is located at the middle of the community and is illustrated in Figure 5.6. It should be noted that the optimum location of the shelter may not be the mid-point of the community and more shelters may be needed to meet community evacuation requirements.

$$(x_1, y_1) = (500, 1000)$$

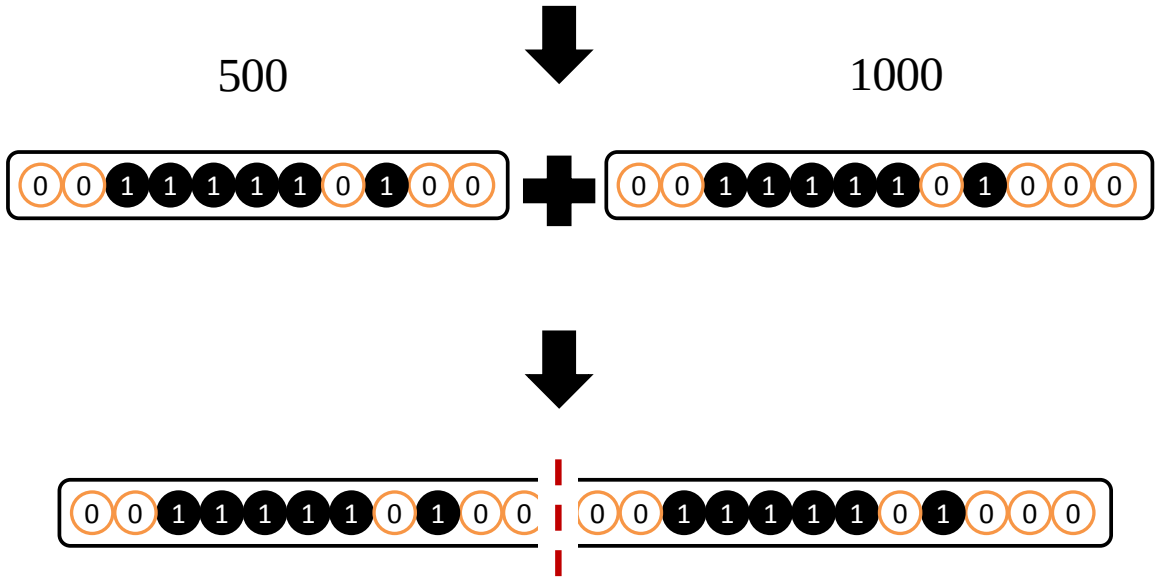

Figure 5.6: An example of a chromosome as array of binary strings.

Once the location of the shelter has been determined, the inverse of the fatality fragility, i.e. the survival fragility, can be computed based on the time to wave arrival at the community. To do this, human walking speed is used to provide a conservative estimate and applied as defined in Table 5.5 (Knoblauch et al. 1996).

Table 5.5: Human walking speed.

Age	Typical walking speed
Old (over 65)	1.253 m/sec (4.11 ft / sec)
Young (over 13)	1.509 m/sec (4.95 ft / sec)
Mean	1.381 m/sec (4.53 ft / sec)

With proper community education and training it is likely that many people would travel faster than typical, or average, walking speed. However, as mentioned, some will be ever slower because of delayed response or inability due to age and/or injury from the earthquake. In this dissertation the average walking speed is felt to be a good measure, albeit slightly conservative, of the time needed for community inhabitants to move from their home to the vertical (or other) evacuation shelter.

Each house is assumed to have four inhabitants and their walking speed is assumed to be the mean speed, 1.381 m/sec. It is noted that the people in the house can vary by gender and age. Their speed can also vary, so they are categorized into two groups in this study. Each person's evacuation time can be computed directly using Table 5.5.

The survival fragility is computed based on the shelter location which is in the middle of the community in the present example, i.e. without optimization, and shown in Figure 5.7 to illustrate the methodology.

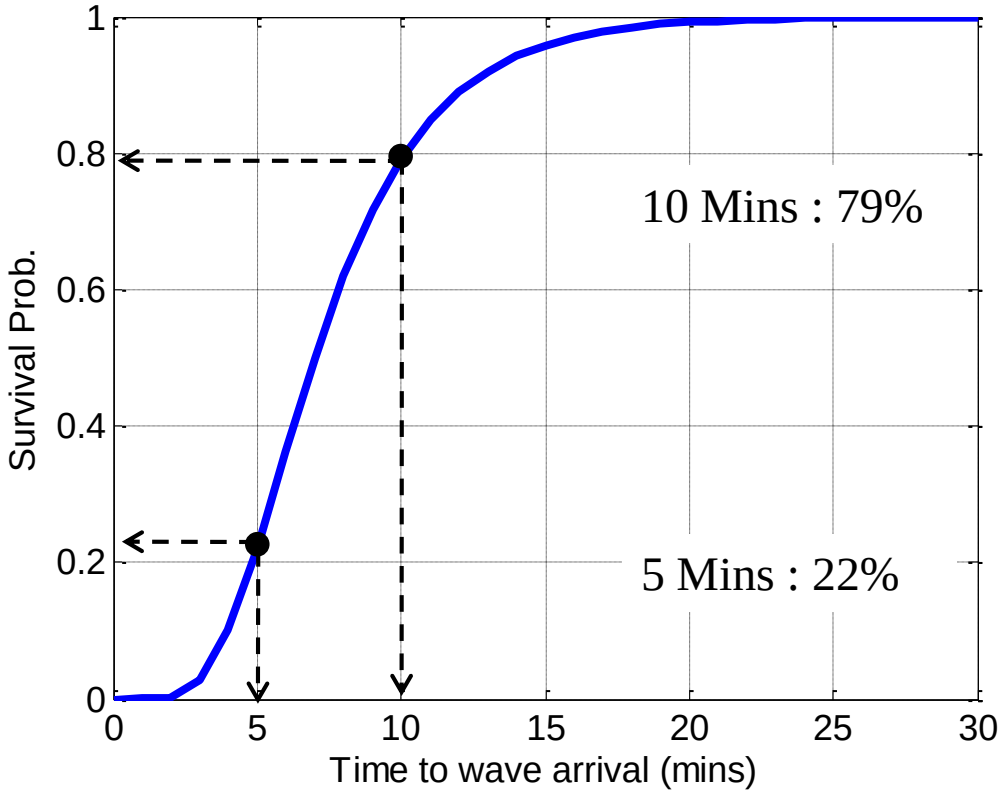

Figure 5.7: An example of a survival probability for one shelter.

From Figure 5.7, one can read that a 22% survival probability can be increased to 79% when the wave arrival time increases from 5 minutes to 10 minutes. This will be changed when the optimum location of the shelter(s) is found. The target survival probability of a specific tsunami arrival time can be selected as one of the constraints and can be expressed and normalized as:

$$\begin{aligned} g_1(x) &= S_{T_a} \le S_L \\ &= \frac{S_{T_a}}{S_L} - 1.0 \le 0 \end{aligned} \tag{5-4}$$

where S_{T_a} is the survival probability at a given tsunami arrival time T_a and S_L is the target survival probability.

Additionally, the number of shelters, their capacity, the shape of the community, and either the maximum distance or the maximum time to the shelter can all be constraints as well. These constraints can be selected and activated for the specific problem conditions within the methodology and can be expressed as:

$$\begin{aligned} g_2(x) &= N_S \le NS_L \\ &= \frac{N_S}{NS_L} - 1.0 \le 0 \end{aligned} \tag{5-5}$$

$$\begin{aligned} g_3(x) &= \max(H_i) \le H_L \\ &= \frac{\max(H_i)}{H_L} - 1.0 \le 0 \end{aligned} \tag{5-6}$$

$$\begin{aligned} g_4(x) &= \begin{cases} \max(L_i) \le L_L & : \text{ distance} \\ \max(L_i) * W_{speed} \le T_L & : \text{ time} \end{cases} \\ &= \begin{cases} \dfrac{\max(L_i)}{L_L} - 1.0 \le 0 & : \text{ distance} \\ \dfrac{\max(L_i) * W_{speed}}{T_L} - 1.0 \le 0 & : \text{ time} \end{cases} \end{aligned} \tag{5-7}$$

where N_S is the current number of shelter, NS_L is the possible number of shelter for the community, H_i is the number of people in one shelter, H_L is the maximum capacity per shelter, L_i is the shortest distance between the i^{th} house and a shelter,

W_{speed} is the human walking speed, and L_L and T_L is the limit of distance and time, respectively.

To handle an arbitrary community shape, the lower and upper bounds for the design variable are needed:

$$x_{L_i} \le x_i \le x_{H_i}, \quad y_{L_i} \le y_i \le y_{H_i} \tag{5-8}$$

where x_L , x_H , y_L ,and y_H are the lower and upper boundary of the x_i and y_i location, respectively. In this manner, the approach described above can handle an arbitrary community shape, i.e. outside of the regions can be treated as infeasible or a violation of the constraints and inside of the regions can be treated as satisfying the constraints.

The City of Cannon Beach, Oregon is selected as the illustrative example. Detailed descriptions can be found in Chapter 4, particularly Figure 4.11 and Figure 4.12. Optimization for a one, two, and three shelter case was performed and the results are presented in Table 5.6. The results of three analyses are combined into one and illustrated in the fragility plots in Figure 5.8.

As seen from Figure 5.8, the survival probability is increased as the number of shelters increases as expected. Also, when the time to tsunami wave arrival is assumed to be 20 minutes, one can read off the survival probabilities of the community. Based on these

results, one can understand how the number of shelters affects the survival probability of the members of a coastal community and determine the optimal number of shelters based on virtually any constraint. Finally, it can also provide useful information to better prepare vertical evacuation plans.

Table 5.6: Optimum location of the shelters.

Case	Shelter No.	Location (meter)
One Shelter	1	(390, 3731)
Two Shelters	1	(390,3748)
	2	(390, 1079)
Three Shelters	1	(320, 1055)
	2	(426, 3842)
	3	(239, 2255)

Suppose that there is a place with a high elevation near the community. The place is high enough to avoid tsunami inundation and suitable to stay. People in the community can escape to these place(s) from a tsunami.

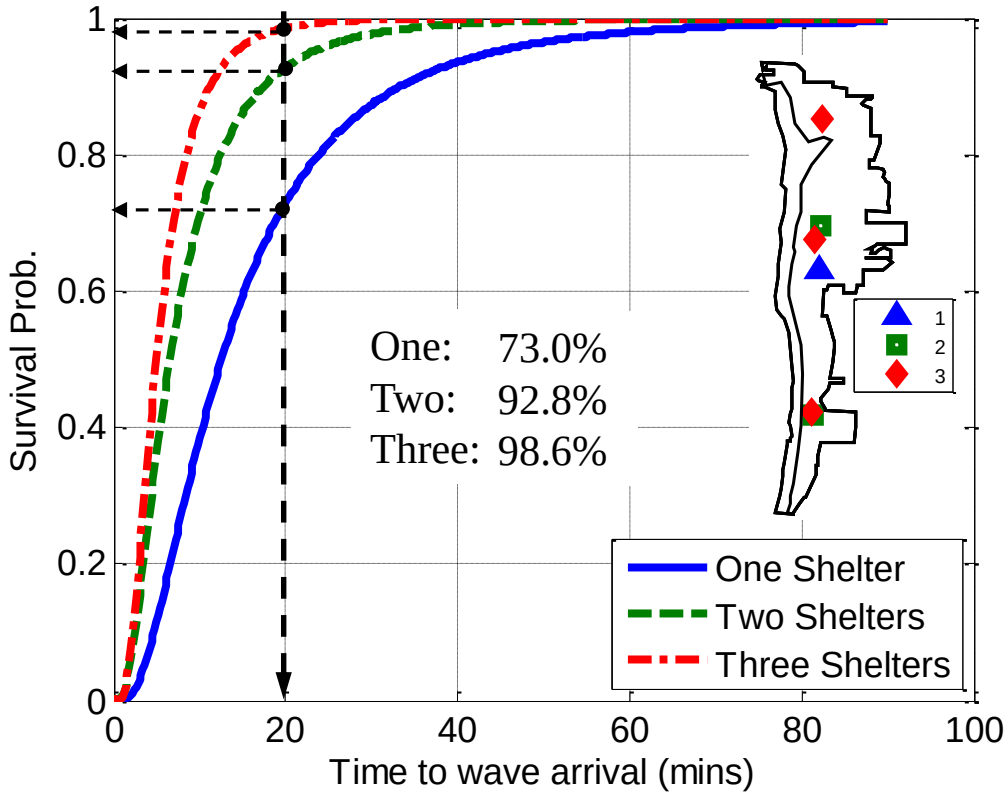

Figure 5.8: Fragility analysis results of the three cases.

To do this, the City of Cannon Beach is selected again as the illustrative example and the tsunami evacuation map from the city is illustrated in Figure 5.9, which contains the locations of high elevation near or within the city. In Figure 5.9, the left image is the tsunami evacuation map provided by the City of Cannon Beach and it shows the six places of high elevation to be used for vertical evacuation. The right image is a computer generated model showing the location of each house in the community. The black solid line shows the boundary of the city, and blue dots represent houses. The red dots represent an individual place of high elevation.

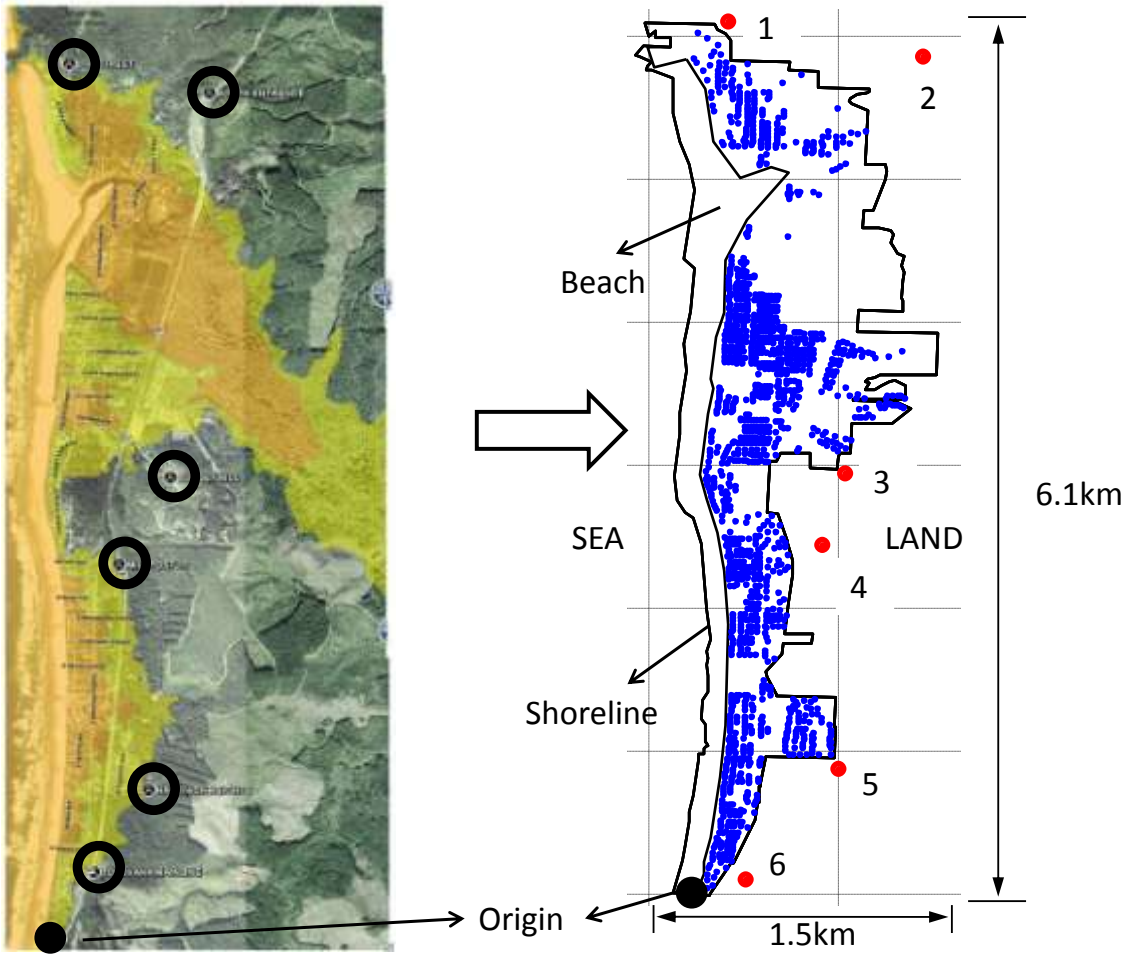

Figure 5.9: Location of the six safe places (The City of Cannon Beach 2011).

The location of the six safe places of high elevation is computed approximately based on the tsunami evacuation map and calibrated based on the south-west corner of the boundary of the city which is the same approach for computing the location of each residential building in the community in Chapter 4. The location of the six places of high-elevation is tabulated in Table 5.7. It should be mentioned that the location of the places may be different with the actual location due to the scale of the map, i.e. the map has been scaled down to show the entire community area.

Table 5.7: Location of the six safe places (The City of Cannon Beach 2011).

No.	Location (meter)	Name
1	(167, 6110)	8th Street
2	(1197, 5864)	North Entrance
3	(789, 2948)	Sunset Hill
4	(663, 2444)	Milepost 30
5	(751, 879)	Haystack Heights
6	(260, 105)	Tolovana Mainline

From Figure 5.9, one can know that the six safe places of high elevation for the vertical evacuation are located out of the city boundary which means it may take a long time to move to the proper places compared to shelters in the city. This is particularly true for people living close to the shoreline.

Fragilities for the community can also be constructed based on these six places of high elevation. One of the six safe places is assigned to each residential building based on obtaining the shortest distance between the house and the evacuation locations. Fragilities have been constructed, combined with three shelter cases shown in Figure 5.8, and are presented in Figure 5.10.

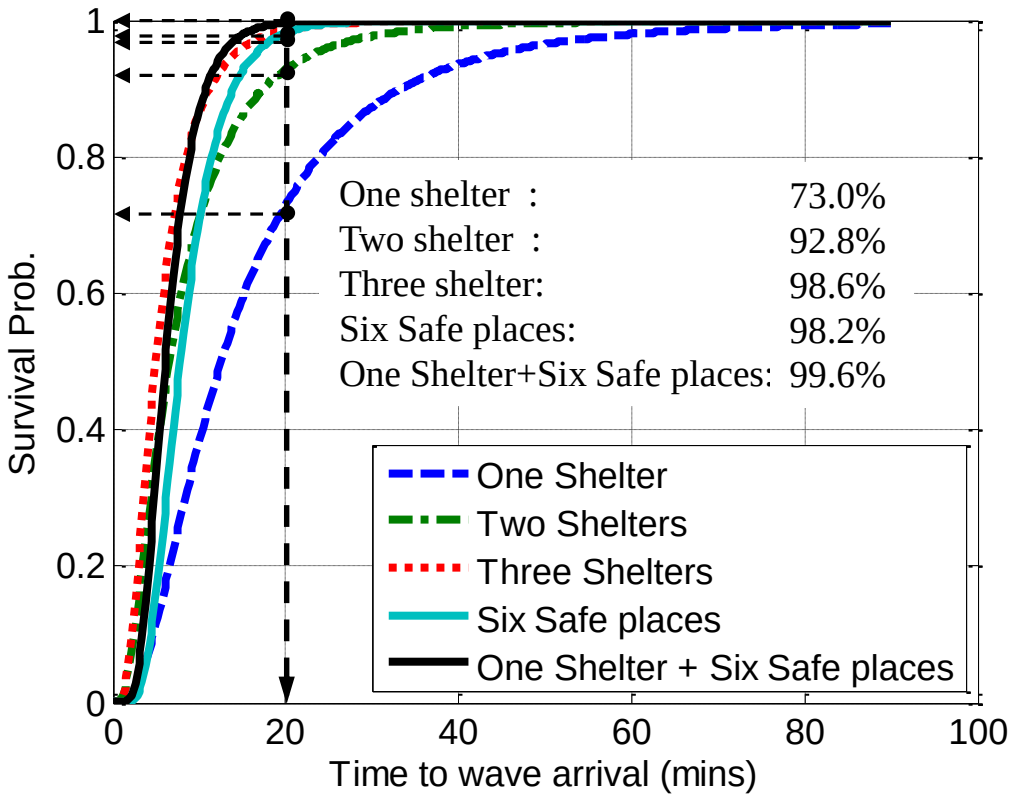

Figure 5.10: Fragility analysis results of the four cases.

The fact that the survival probability is increased proportionally to the number of shelters is shown in Figure 5.8. Thus, one can expect that the high elevation place gives a high survival probability because there are six places, i.e. the number of the high places is greater than that of the shelters which is three. However, it yields a survival probability higher than the one shelter case but lower than the two and three shelter cases primarily because of the location of the six safe places, i.e. the location has not been optimized.

What if the community has one shelter and six safe places, it yields a relatively high survival rate when the tsunami wave arrival time is greater than 10 minutes, but still it yields a lower than three shelter case when the time is less than 10 minutes due to the six places is located out of the city boundary.

Now, the time to tsunami wave arrival is assumed to be 20 minutes, one can read that the survival probability are computed as 73%, 92.8%, 98.6%, 98.2%, and 99.6% for one, two, three shelter case, six safe places case, and one shelter plus six safe places respectively. It shows the combination of one shelter and six safe places is the best solution in this case. However, the survival probability of the six safe places only case is little bit lower than three shelter case because the location of these six places was not optimized. The places of high elevation can be also helpful in increasing the survival probability but not as significantly compared to the addition of optimized shelters. Therefore, a combination of one shelter and a place of high elevation can be alternative if a construction cost is mattered, i.e. money for constructing a place of high elevation is much less than that for building a shelter.

Now, any residential building in this community can be elevated to improve the safety level of the community. This can be thought of as an extension of the community fragilities from the structural aspect using the methods proposed in Chapter 4 and its combination with a TSF. Three increments of the elevation such as zero, a height of one-story, i.e. 2.44 meters typically, and a height of two-story are applied. The community fragilities then have been reproduced with 13.6% COV for wave. The results of these analyses are summarized in Table 5.8.

From the tables, one can see a decreasing trend from 33.9% to 7.3% for tsunami-only, and from 35.6% to 9.3% for DBE level earthquake and tsunami, and from 48.7% to 26.8%

for MCE level earthquake and tsunami when the target tsunami wave run-up height is 10.0 meters.

Table 5.8: Difference between without and with TSF for a wave COV of 13.6%.

Earthquake Level	Community Fatality Probability (%) when 10.0 meter tsunami wave run-up height		
	No TSF	One-story TSF (2.44m)	Two-story TSF (4.88m)
No EQ	33.9	18.9	7.3
DBE Level	35.6	20.9	9.3
MCE Level	48.7	36.4	26.8

The results show that the collapse risk is decreased proportionally with the reinforcement using the TSF. This can be explained in that the single residential houses in this community are categorized into eight types with six of those types being one-story residential structures, thus the increment of 2.44 meters has a large influence on the fragilities as one might expect. Moreover, less than 10%, except the MCE level seismic intensity, of the community fatality probability was achieved for the two-story TSF case. Therefore, the reinforcement with the TSF plays an important role in reduction of community risk. In addition, even though the two-story TSF could not reduce much because the initial fatality came from the previous hazard, i.e. the earthquake. Going to a two-story TSF only slightly increases this benefit.

From the comparison between two hazard conditions, i.e. tsunami-only and MCE level earthquake intensity plus tsunami, one can see that when the intensity level of earthquake is increased the reduction of collapse risk between no TSF and having a TSF is decreased. The effects of TSF are not increased proportionally with the intensity level of the earthquake. This can be explained in that single houses in the community have influence on not only tsunamis but also earthquakes and their combinations. In other words, a single structure may already be collapsed from the earthquakes, i.e. MCE level earthquake, thus reinforcement with a TSF would not help to improve the collapse risk of the community.

Moreover, the improvement from using a TSF does not have an effect on every structure in this community due to variation in their location. Some of units may be influenced and some may not. If their location is far from the shoreline and they are spread over the community, then the effect may be quite a minor. If most of the residential buildings are located very closed to the shoreline, the effect may be significant.

The analysis results for the one-story TSF, is shown in Figure 5.11. From Figure 5.11, one can see that the community has the collapse probability of the previous hazards which was presented in Chapter 4.

Additionally, the community fragilities with 50.0% COV are also performed. The results are tabulated in Table 5.9 and seen in Figure 5.12.

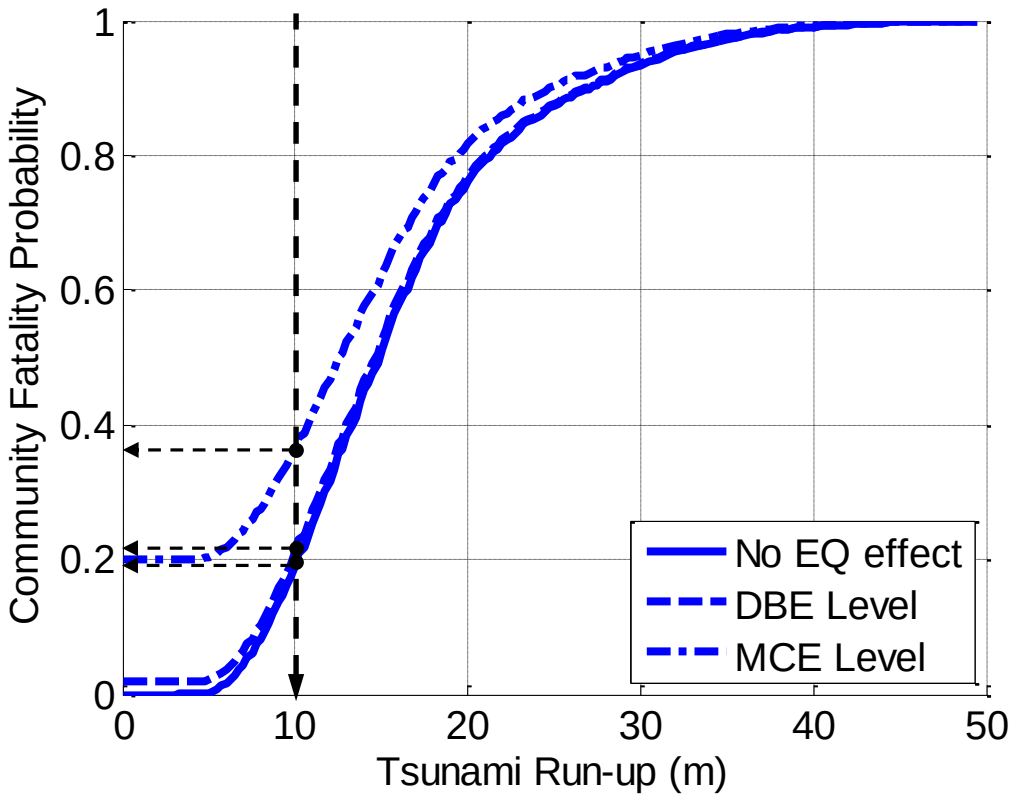

Figure 5.11: Community fragilities for a wave COV of 13.6% with one-story TSF case.

Table 5.9: Difference between without and with TSF for a wave COV of 50.0%.

Earthquake Level	Community Fatality Probability (%) when 10.0 meter tsunami wave run-up height		
	No TSF	One-story TSF (2.44m)	Two-story TSF (4.88m)
No EQ	31.6	20.7	12.8
DBE Level	33.2	22.5	14.6
MCE Level	46.4	37.4	30.8

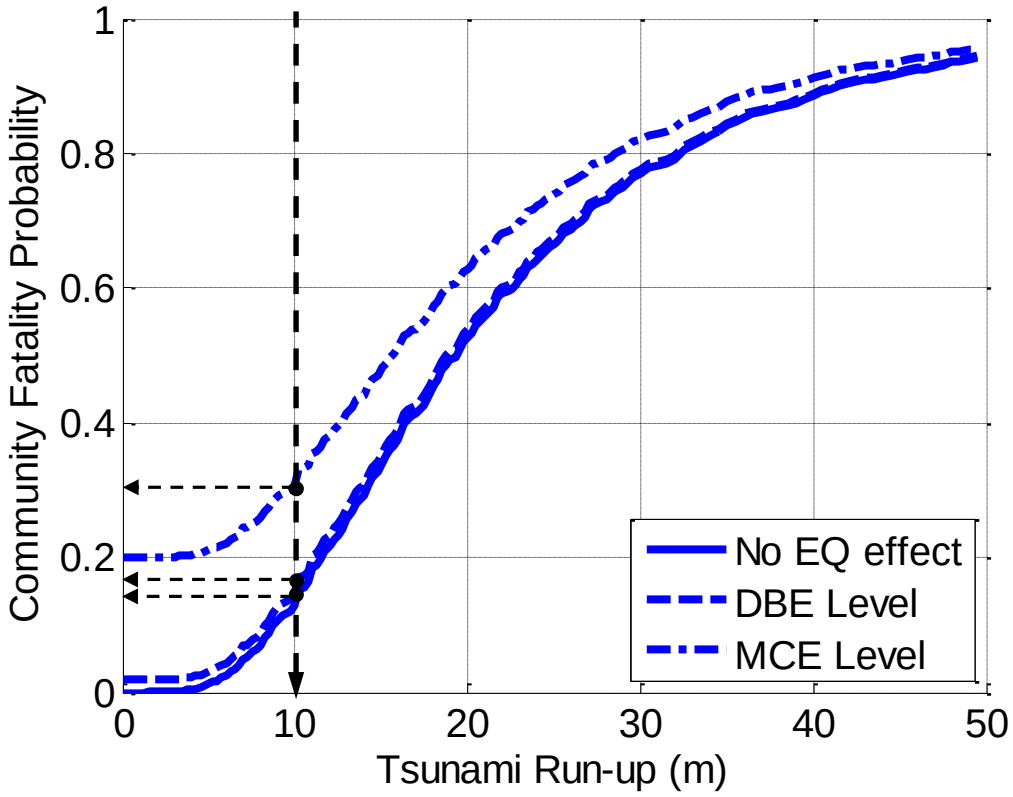

Figure 5.12: Community fragilities for a wave COV of 50.0% with two-story TSF case.

CHAPTER 6

TSUNAMI RELIABILITY ASSESSMENT OF THE COMMUNITY

6.1 OVERVIEW

This chapter presents the basic idea of how to assess the reliability of a community using fragilities. Initially, fragilities can be constructed using the methods proposed in Chapter 4 and Chapter 5. Then through statistical combinations the tsunami reliability of the community in consideration of possible events can be assessed. To do this, an event tree analysis is adopted. All possible scenarios can be summarized with the combination of initial or accidental events such as with or without shelters, collapse or survival of the shelter itself, survival or failure of the residential buildings, and evacuation or unsuccessful evacuation of the people to the shelter. Finally, a tsunami reliability assessment of the community can be evaluated considering all the possible scenarios.

6.2 TSUNAMI RELIABILITY ASSESSMENT METHODOLOGY

Fragilities for the single assembly and the community have been successfully performed in order to achieve one of the main focuses of this dissertation. Community fragilities have been developed through the combination of single assemblies. From Chapter 4, the

community fragilities have considered only structural aspects. Also the community fragilities, described in Chapter 5, have been constructed considering vertical evacuation shelter(s). At this point, one might surmise that the reliability of the community can be computed using the outcomes of the fragilities, especially focusing on the survival of the people in the community from both hazards.

To do this, event tree analysis is adopted. An event tree analysis (ETA) is an investigatory procedure that identifies all possible outcomes resulting from an initial event, taking into account where an event or condition is either true or false or whether an event has happened or not. The ETA provides an inductive approach to reliability assessment on account of showing the probability of results or conditions for a complex system. All relevant initial or accidental events can be determined by a preliminary analysis or some other techniques and then the ETA can be used to identify all potential accident scenarios in a complex system. By performing the ETA, the weakness of the design and procedure can be identified and probabilities of the possible outcomes can be determined as well.

The ETA can begin by identifying the possible events having on the tsunami reliability of the community. Initially, the vertical evacuation plan can be changed if the community has shelter(s). Thus, the existence / consideration of the shelter(s) can be accepted as the first event. The next possible event can be the survival or collapse of the shelter itself against the hazards, i.e. earthquakes, tsunamis, and their combination. The survival of a

single residential building is then next. Finally, vertical evacuation to one or more shelters and/or the escape to places of high elevation is the last event.

The combination of the possible four events focusing on the survival of people results in twelve possible scenarios which can be reduced to eight possible outcomes under the assumption that there are shelters that always survive the hazards, i.e. strong enough to resist the hazards. The possible scenarios are illustrated in Figure 6.1.

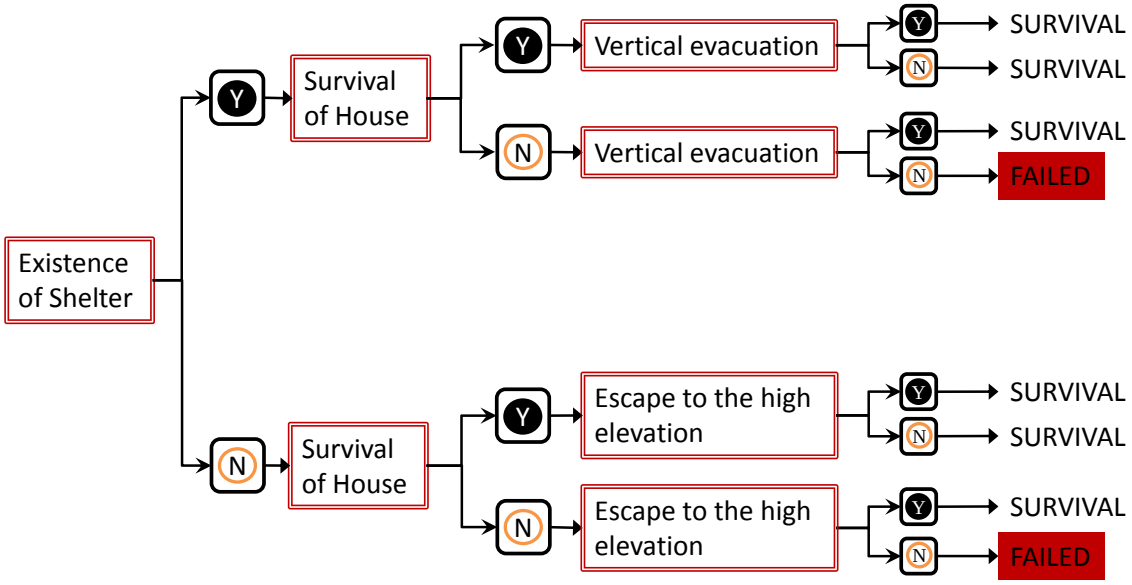

Figure 6.1: Possible scenarios for tsunami reliability assessment.

From Figure 6.1, one can know that there are two main events of concern; the survival of each single residential building which denotes event A and the success of the vertical evacuation to the shelter(s), or the escape to an area of high elevation which denotes event B. Therefore, all the possible scenarios, finally, can be expressed using the combination of two events, i.e. event A and event B.

There are only two scenarios namely, fail or survive. One is that the community has the shelter(s), each single residential building is collapsed under given the hazards, and the people in the single house are also failed to make vertical evacuation to the shelter within a given time, i.e. the elapsed time between the tsunami warning and the tsunami wave arrival at the community. The other is that there are no shelter(s) in this community, i.e. no shelter(s) means there is no structure for the purpose of covering or protecting from the hazards but the place like an high elevation ground may exist, each single residential buildings has been collapsed under given the hazards, and the people in the house failed to escape to places of high elevation before tsunami wave arrives at this community.

The two scenarios can be decoupled individually depending on the existence of the shelter(s) and considered independently to evaluate the tsunami reliability assessment of the community focusing on the survival of people. Each scenario can be analyzed using a statistical approach. The survival probability of the people in the community can be computed using the intersection of two events and expressed as:

$$P_S = 1 - P(A^C \cap B^C) \tag{6-1}$$

where P_S is the survival probability, A^C is the complementary of event A, its probability can defined as $P(A^C) = 1 - P(A)$, and B^C is the complementary of event B.

It should be noted that there are two judgments for survival; one is defined for the single buildings such that the structure can resist the hazards which can be determined by means

of performing a structural analysis and the other for the people in the house such that the people can vertically evacuate to the shelter(s) or escape to a place of high elevation within a short enough time.

6.3 APPLICATION TO THE COMMUNITY

The survival probability for people in the community was computed using the proposed approach. Three combinations of the hazards, i.e. tsunami hazard only, DBE level earthquake intensity, and MCE level earthquake intensity were used. The City of Cannon Beach, Oregon, was selected again as the illustrative example location to further examine the method.

Initially, it is computed under the condition that the one shelter and only tsunami hazard was considered. The optimum location of the shelter was extracted from the results of Chapter 5. Tsunami reliability is evaluated for two COV values for wave height as was done earlier, i.e. 13.6% and 50.0%. The tsunami run-up height is considered the range from 0.0 meters to 50.0 meters. Four wave arrival times are used; 0, 5, 10, and 20 minutes. It should be kept in mind that the wave height may often be only a few meters but the run-up height can be significantly higher as the tsunami bore climbs the slope of the ground.

The tsunami-only with a 13.6% COV for the wave height was considered initially and the results are presented in Figure 6.2. The solid line represents the resulting probability of

fatalities when the wave arrival time is 0 minutes essentially providing a bound and the dashed line represents the resulting probability of fatalities when 5 minutes wave arrival time is considered. The dash-dot line represents the resulting probability of fatalities when wave arrival time is 10 minutes, and the dotted line represents the resulting probability of fatalities when 20 minutes is considered as the wave arrival time.

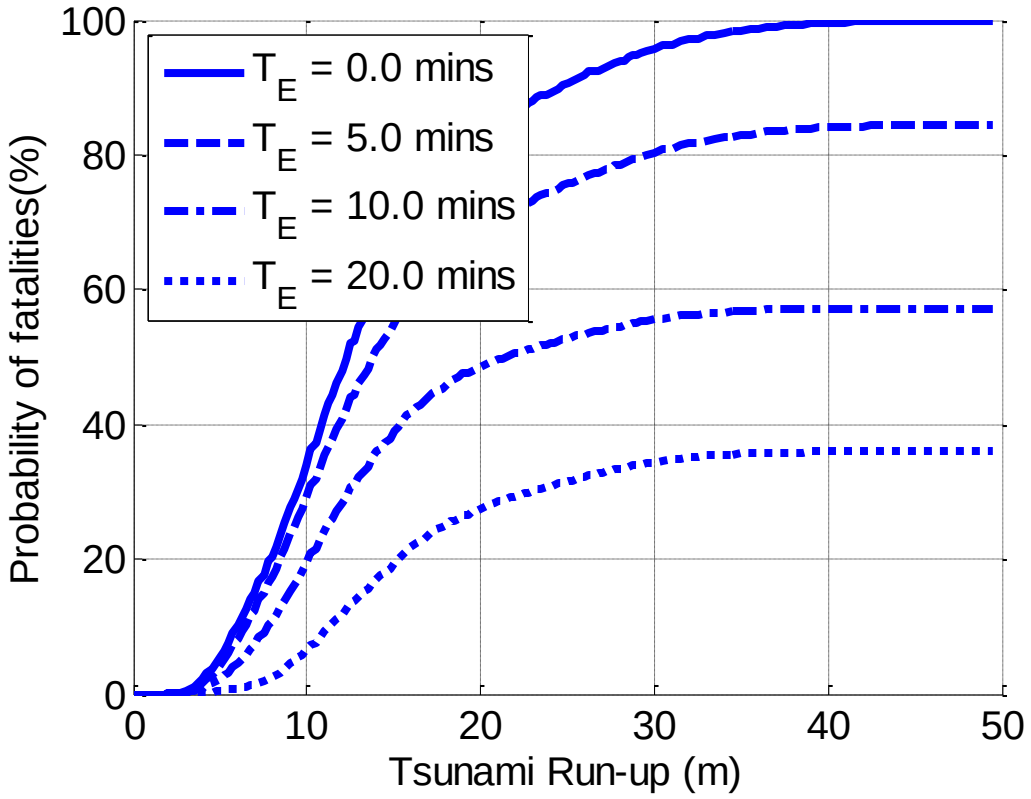

Figure 6.2: Probability of fatalities - one shelter, 13.6% COV, and tsunami-only.

One can see that the probability of fatalities for this community is significantly reduced (survival rate increased) with respect to increasing the amount of warning time provided to the community. Moreover, if the wave arrives after 20 minutes, the probability of fatalities is decreased from 100 % to 36% even though the tsunami run-up is 50 meters.

This is explained in that 20 minutes is enough time for the majority of people to evacuate to the shelter even though this community has only one shelter. This is means the construction of one shelter can significantly reduce the number of fatalities for a community.

Additionally, the results of the DBE and MCE earthquake cases are shown in Figure 6.3 and Figure 6.4, respectively.

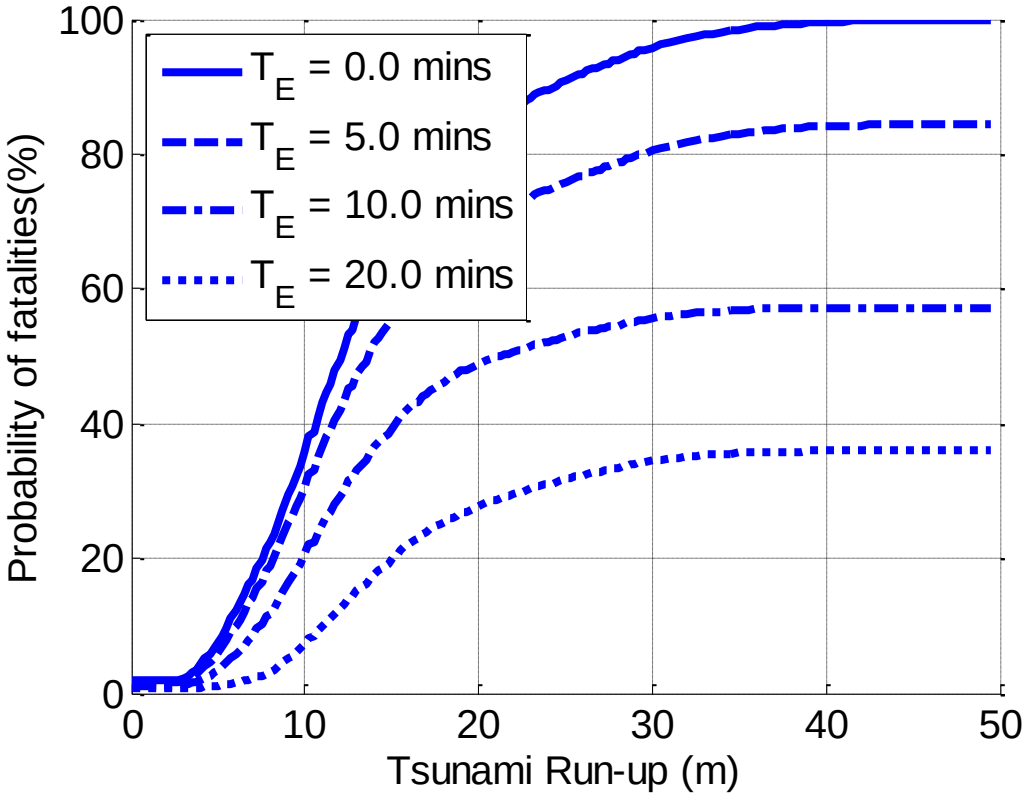

Figure 6.3: Probability of fatalities - one shelter, 13.6% COV, and DBE EQ.

In Figure 6.3, one can see that the probability of fatalities for this community has a similar trend but there is an initial collapse probability which would also result in

fatalities which came from the seismic hazard at MCE level and its value varies from 0.6% to 1.8% for each wave arrival time.

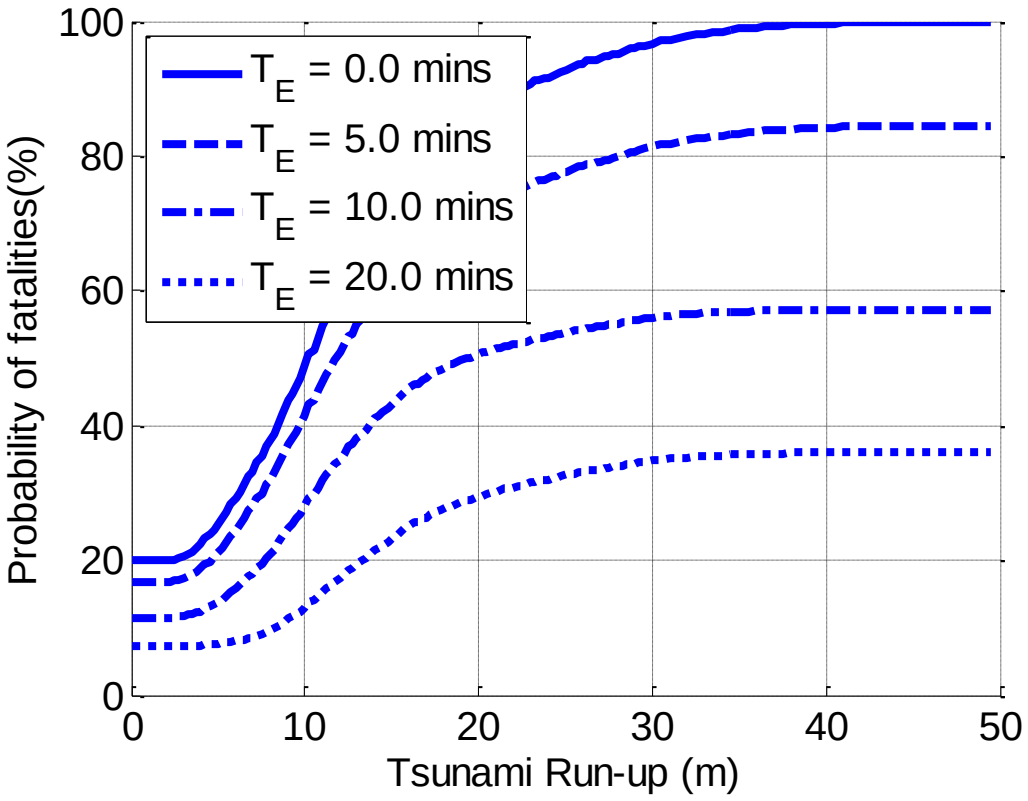

Figure 6.4: Probability of fatalities - one shelter, 13.6% COV, and MCE EQ.

In Figure 6.4, there is also the initial collapse risk of the buildings when the MCE level earthquake intensity is considered prior to the tsunami hazard. The initial collapse risk was reduced from 20% to 7.2% gradually for each wave arrival time. It can be explained in that the people in the single house can be evacuated to the shelter even though the house itself did not survive the earthquake, i.e. people felt the ground or structure's shaking, they escaped from the house immediately, and they evacuated to the shelter successfully.

The analysis is repeated for the two shelter case and the 13.6% wave height COV. Two results for the tsunami-only and MCE level earthquake considered are shown in Figure 6.5 and Figure 6.6, respectively.

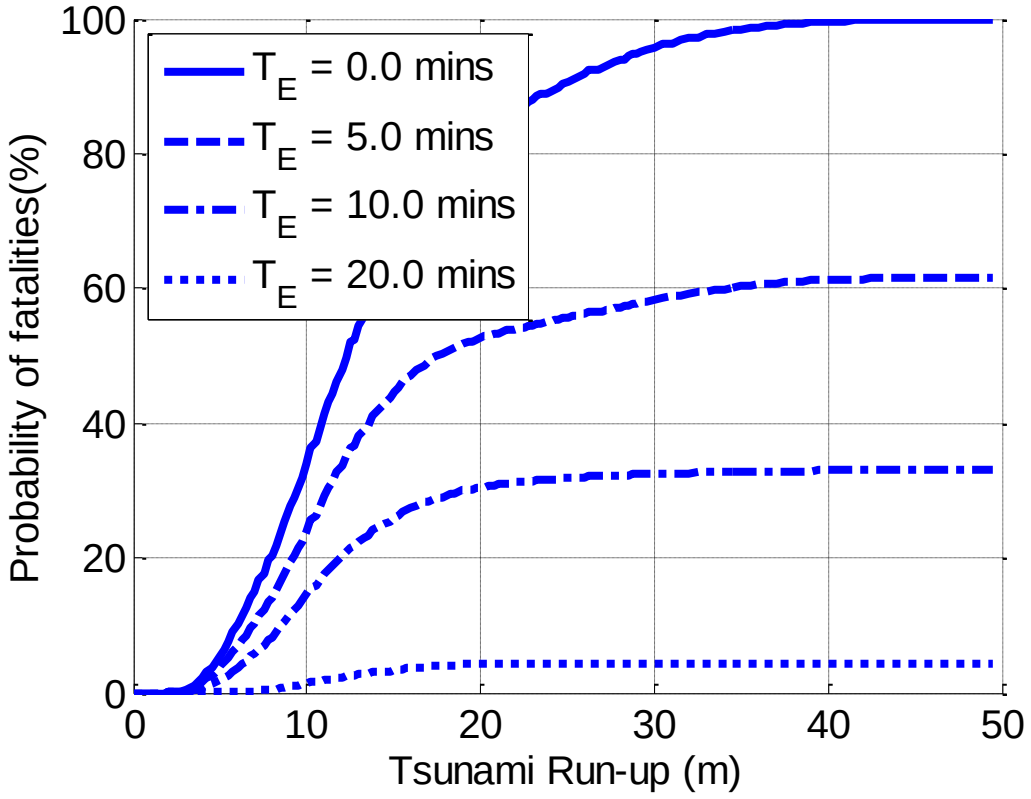

Figure 6.5: Probability of fatalities - two shelters, 13.6% COV, and tsunami-only.

In Figure 6.5, one can see that the reduction of the collapse risk has been accomplished significantly due to the vertical evacuation to the two shelters within a short time. The risk is only 4.43% which is a low probability when tsunami run-up height is 50 meters and wave arrival time is 20 minutes. Moreover, when comparing the one shelter case, the probability of fatalities for the community was decreased from 36% to 4.43%. The 4.43% collapse risk can be explained in that the 4.43% of the people could not evacuate to the

shelter. These trends can be seen for the other two cases. If a tsunami warning system is well established then the collapse risk of a community can be significantly reduced even though only one shelter is existed. Finally, the elimination of the collapse risk or fatalities can be obtained with an increase in the number of shelters.

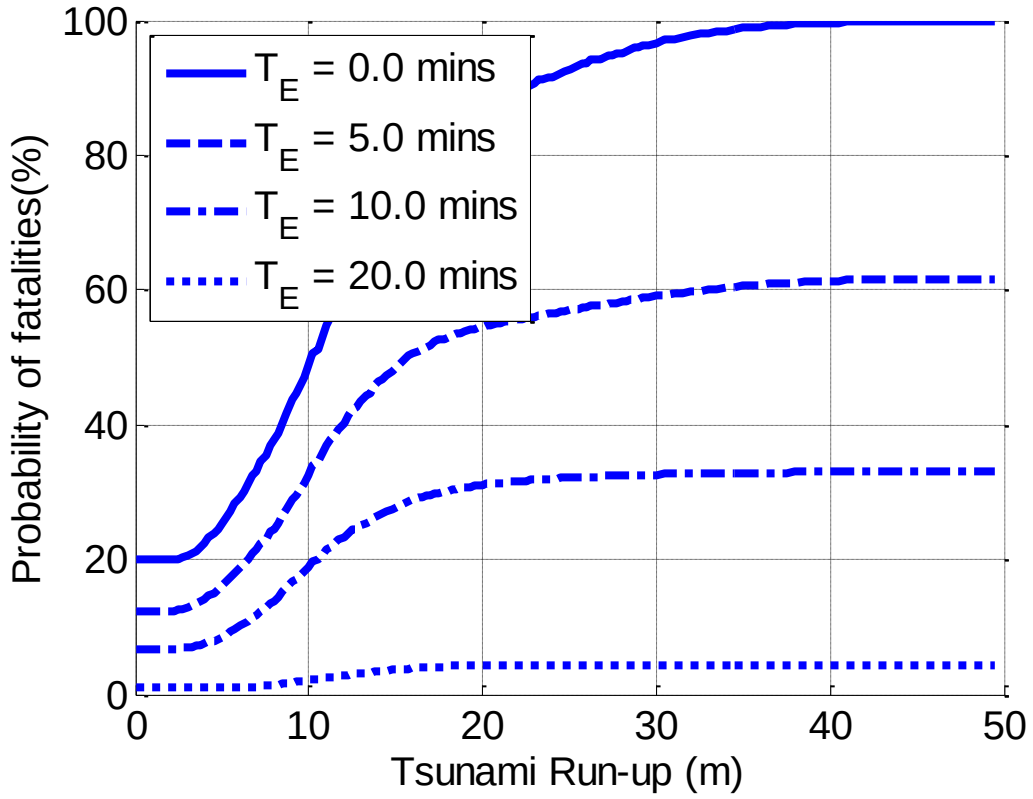

Figure 6.6: Probability of fatalities - two shelters, 13.6% COV, and MCE EQ.

The analysis is repeated for the three shelter case using both the 13.6% and 50.0% COV for the wave height considered. Two results, 13.6% COV for tsunami-only and 50.0% COV for MCE level earthquake intensity, can be shown in Figure 6.7 and Figure 6.8, respectively.

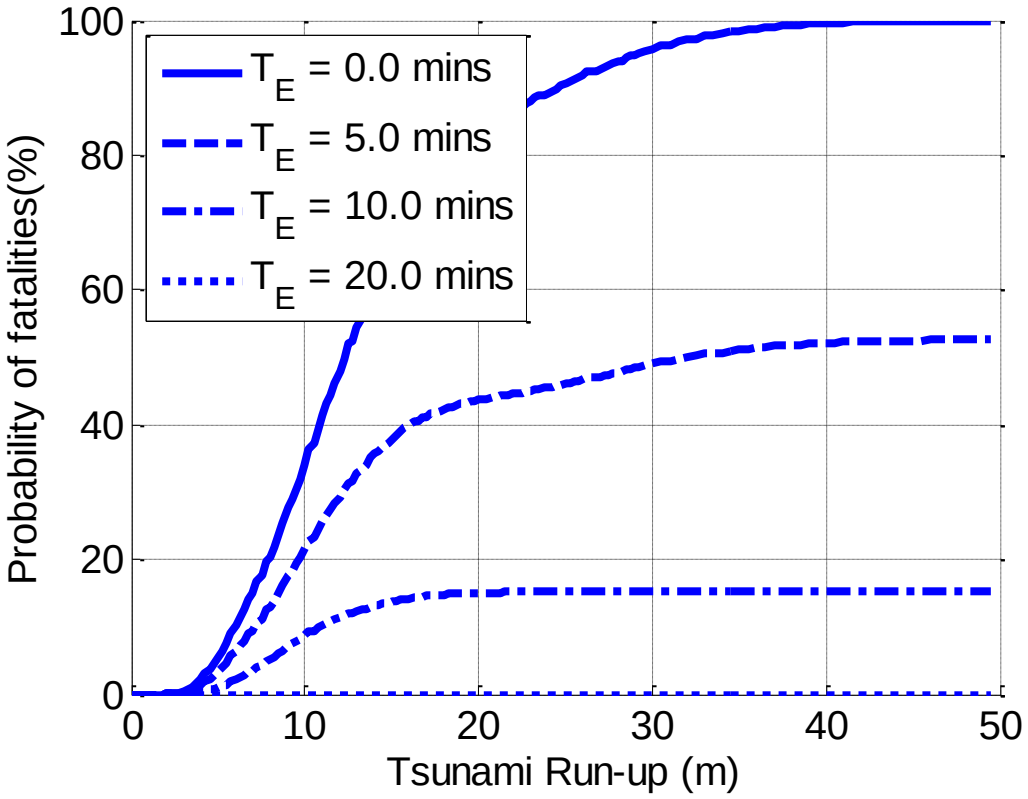

Figure 6.7: Probability of fatalities - three shelters, 13.6% COV, and tsunami-only.

The probability of fatalities for the community when tsunami run-up height is 50 meters is reduced to effectively 0% when the wave arrival time is 20 minutes. This can be explained in that this community has three shelters and they are located in the optimal location to provide vertical evacuation for all inhabitants within 20 minutes.

Lower fatality rates can be obtained through the increasing number of shelters but the construction and its cost is, of course, increased. Therefore, it can be concluded that if the community is located in a high tsunami hazard zone, more than one shelter is generally recommended.

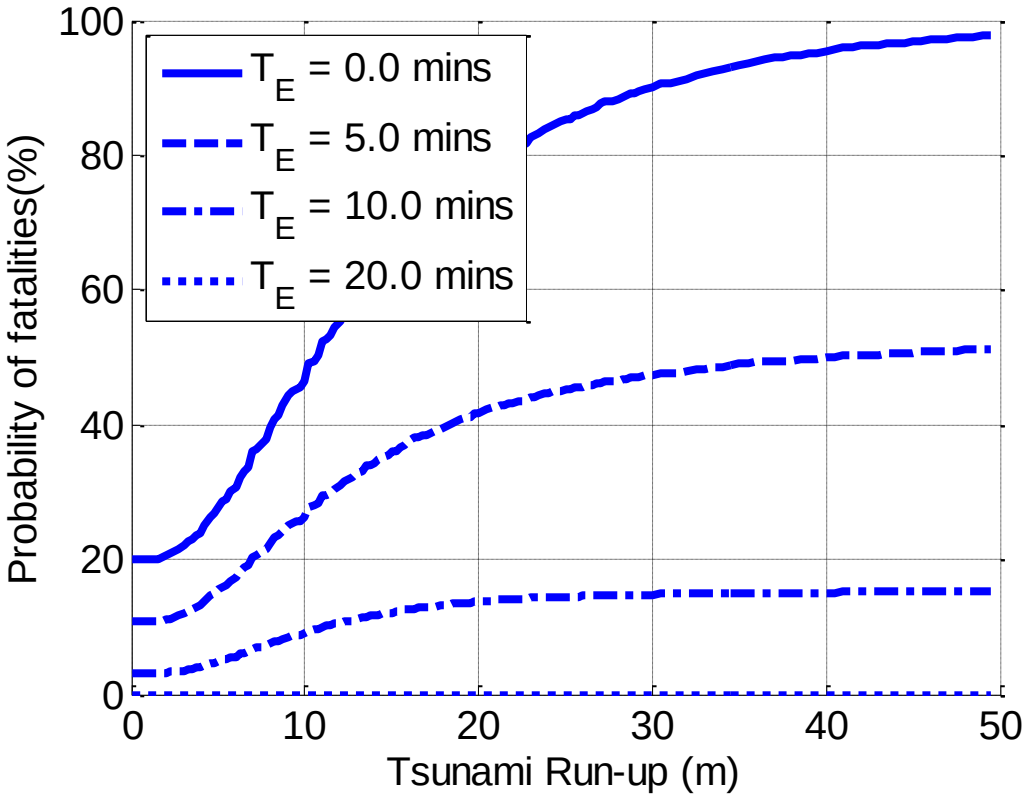

Figure 6.8: Probability of fatalities - three shelters, 50.0% COV, and MCE EQ.

Now, if the community has a place of high elevation instead of shelter(s), the analysis is similar to the previous cases. In this case, the expected time to escape to the place of high elevation instead of to the vertical evacuation shelter. The six high elevation place(s) extracted from the tsunami evacuation map provided by the City of Cannon Beach, Oregon, are again adopted for illustrative purposes. Detailed information can be found in Section 5.3 of Chapter 5, particularly Figure 5.9 and Table 5.7. The results are shown in Figure 6.9 and Figure 6.10.

From Figure 6.9, the probability of fatalities significantly decreases when arrival time changes 5 minutes to 10 minutes and it is equal to zero when arrival time is changed 20

minutes. This situation can be explained in that there are six places of high elevation to escape to within 10 to 20 minutes. The reason for the significant reduction can be explained in that the location of the six places is not distributed uniformly, i.e. not optimized but rather a function of the topography. Thus, it is almost impossible to escape within 5 minutes, moderate within 10 minutes, but quite possible within 20 minutes.

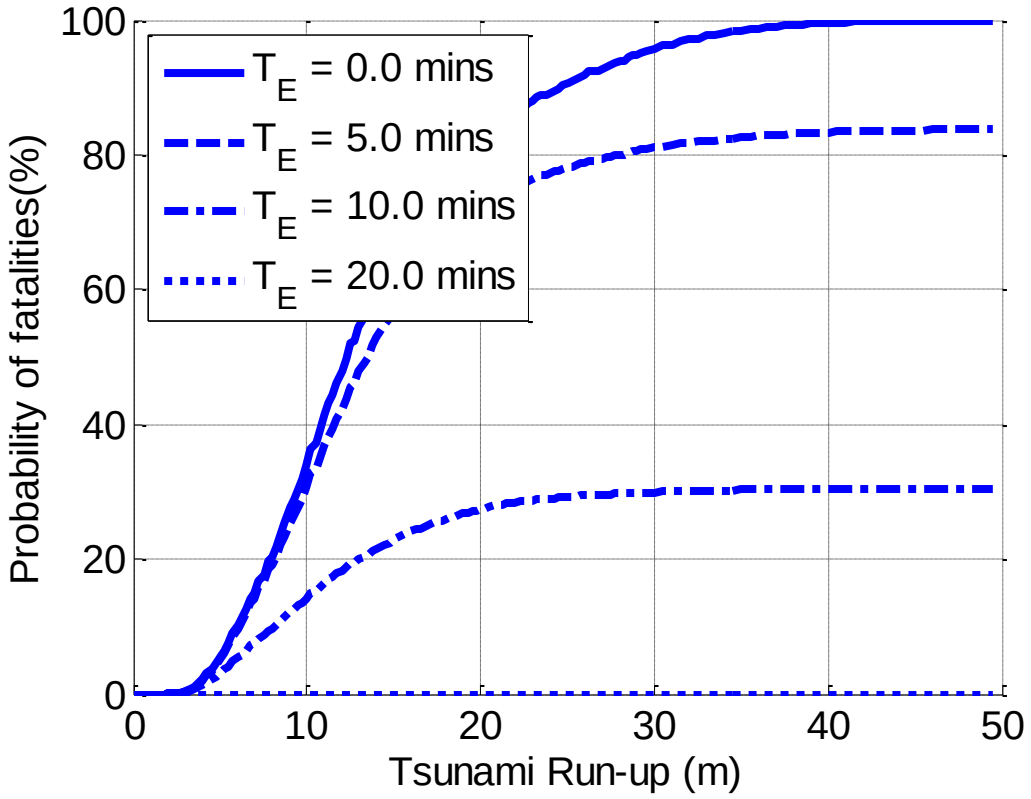

Figure 6.9: Probability of fatalities – six safe places, 13.6% COV, and tsunami-only.

Additionally, a similar trend can be seen in Figure 6.10. Even though the tsunami run-up height is large, i.e. 50 meters, there is zero probability of fatalities when the wave arrival time is 20 minutes. Therefore, if the tsunami warning system is well established and the warning provides 20 minutes notice then the six places of high elevation may be adequate.

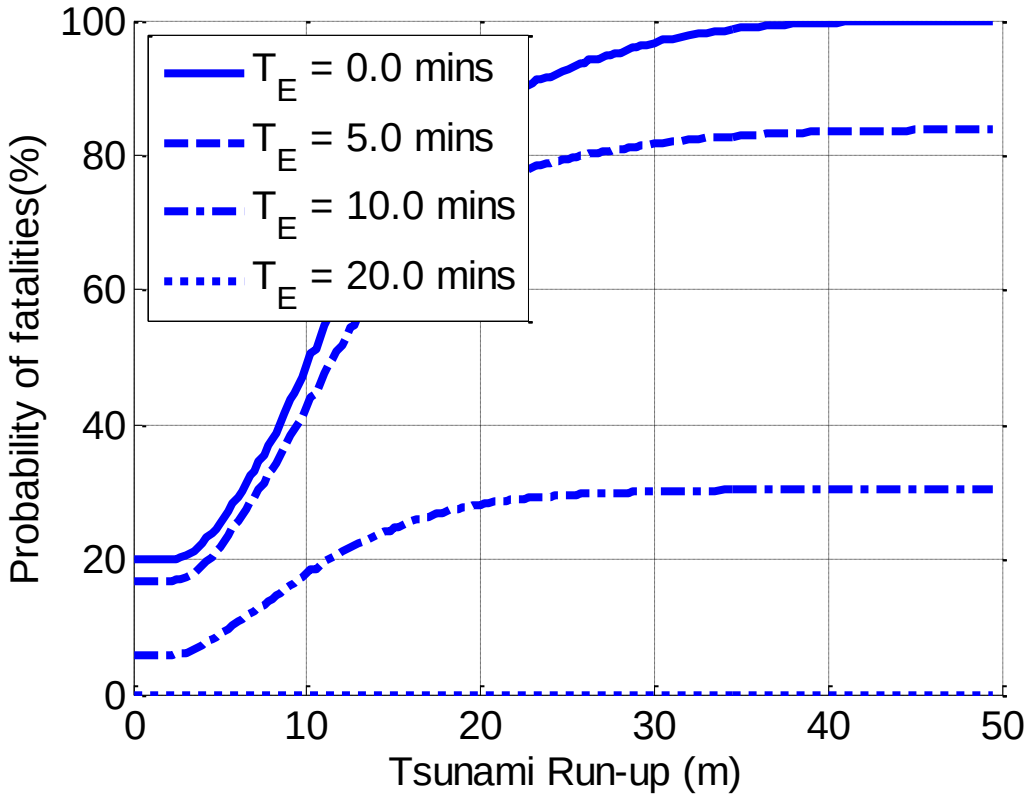

Figure 6.10: Probability of fatalities - six safe places, 13.6% COV, and MCE EQ.

The 50.0% COV for wave height combined with the MCE level earthquake intensity and tsunami is considered, is shown in Figure 6.11. Again, a similar trend can be observed. Therefore, it can be concluded that a well established tsunami warning system and shelter(s) or place(s) of high elevation can reduce the risk of fatalities in the community significantly.

To do mutual comparison, the results of the four cases with 13.6% COV value have been combined into Figure 6.12 and Figure 6.13, respectively. Two wave arrival times are considered which are 5 and 20 minutes.

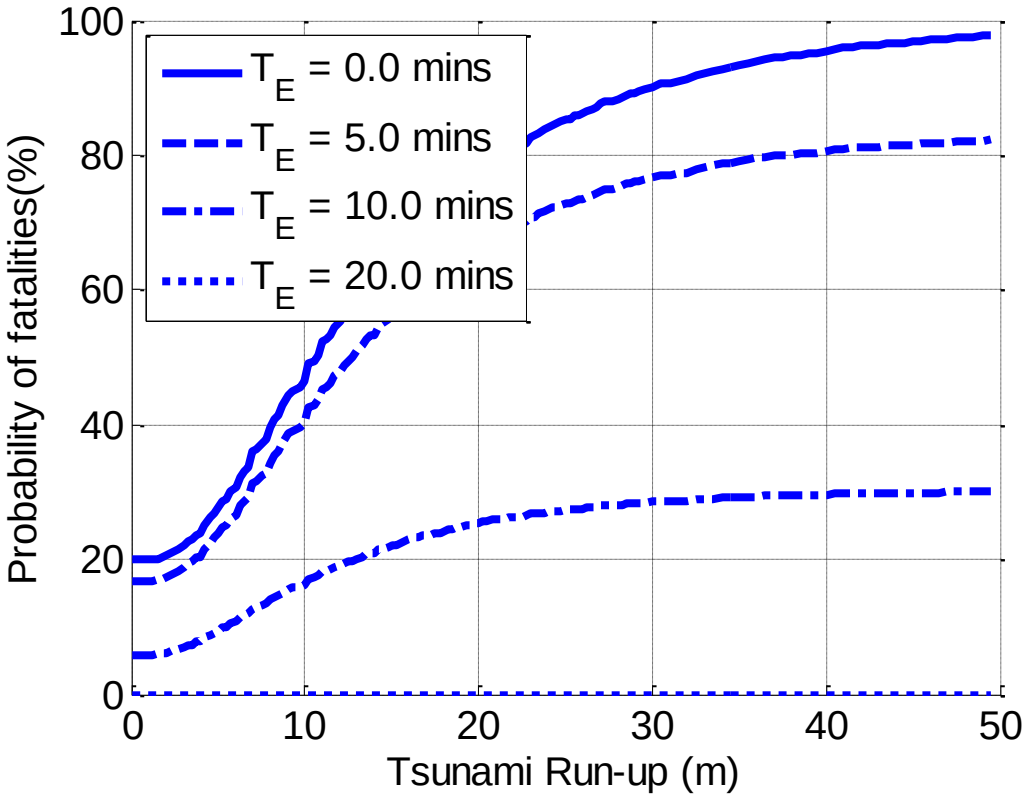

Figure 6.11: Probability of fatalities - six safe places, 50.0% COV, and MCE EQ.

From Figure 6.12, one can see that the two cases, one shelter and six high elevation places, are not efficient for the short wave arrival time, i.e. for instance 5 minutes.

The results of the four cases with 50.0% COV value have been also combined. Two wave arrival times are considered which are 5 and 20 minutes. In this case, overall collapse risk probability is reduced due to the high COV for wave height. Only one shelter has a relative high collapse risk compared. Additional figures can be found in Appendix G of this dissertation.

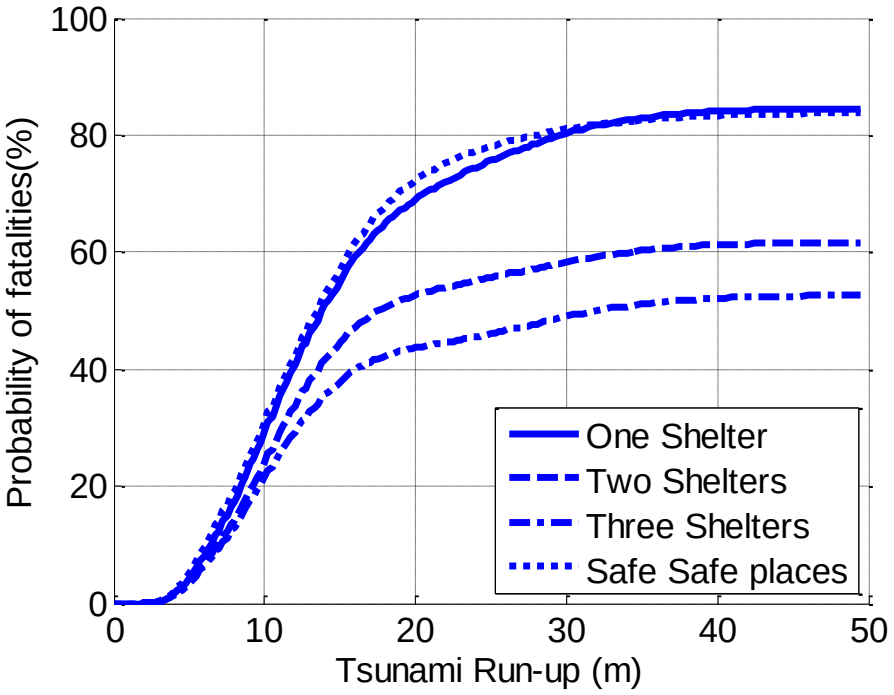

Figure 6.12: Combined four cases when 13.6% COV, no EQ, and 5 minutes.

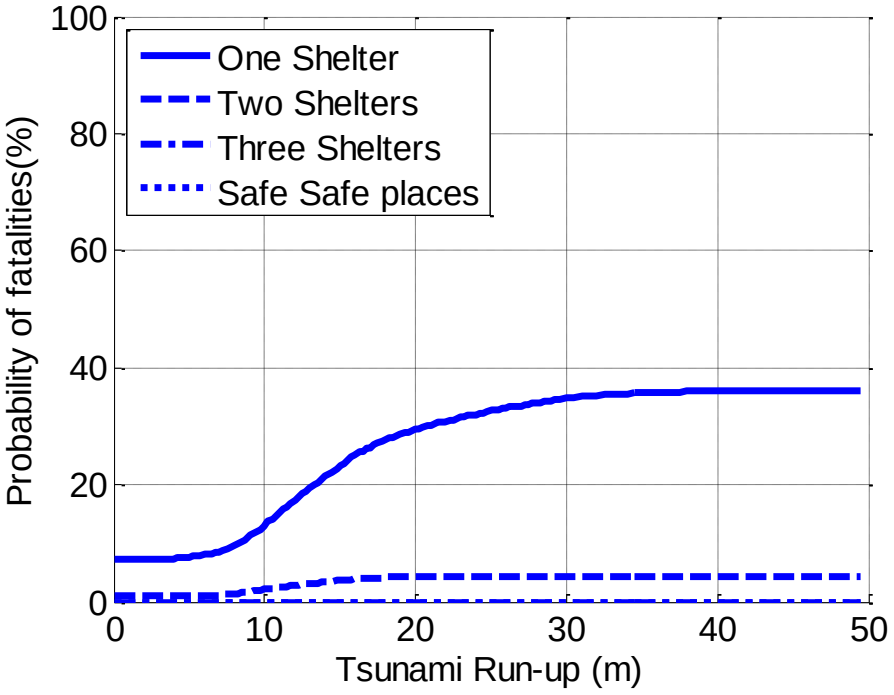

Figure 6.13: Combined four cases when 13.6% COV, MCE EQ, and 20 minutes.

CHAPTER 7

SUMMARY, CONCLUSIONS, AND RECOMMENDATIONS

7.1 OVERVIEW

This chapter summarizes the objectives of this dissertation and its outcomes. A wide range of numerical analyses were performed, including detailed finite element analysis, time domain analysis, and quasi-static analysis of single structural systems, to lead to development of fragilities for single structures to those for a coastal community.

7.2 SUMMARY AND CONCLUSIONS

Recall the objectives of this dissertation were: (1) to investigate tsunami wave forces on coastal structures, particularly residential coastal buildings; (2) to quantify the correlation between generating earthquakes and their tsunamis and their influence on structures; (3) to extend the current state-of-the-art models to predict the structural behavior and responses under successive earthquake and tsunami wave loadings; and (4) to provide a tsunami evacuation planning methodology for a coastal communities.

During the pursuit of the objective of this dissertation, a variety of numerical models and three computer programs, i.e. NAPSS, SSTAP, and TOGA, were developed. Two numerical models for structural analysis were developed as part of this dissertation research. NAPSS was developed using a general finite element formulation to perform non-linear static analysis under arbitrary loading conditions. It was intended to focus on wood shearwalls but applies to any typical linear or non-linear finite element problem. The other model SSTAP, has the capability of analyzing a structure by means of performing two numerical simulations either individually or in succession; (1) non-linear time history analysis for earthquakes; and (2) a quasi-static pushover analysis for tsunamis including computing the equivalent forces from the tsunami wave loading. These programs, when combined, allow one to understand how one hazard affects the other since they may occur rapidly in succession, i.e. without the ability to repair between the loadings.

Single structure fragilities were obtained by subjecting a structure to a suite of earthquake ground motions. After each motion, the numerically damaged structural model was subjected to non-linear pushover analysis with equivalent tsunami wave loading. The approach was then extended to the community level and an approach for determining the location and number of vertical evacuation sites demonstrated. Both the single structure cases and the community analyses were presented in terms of fragilities as a function of the parent earthquake level and evacuation time available. The intent was that the approach proposed herein can provide a framework regardless of structural model or hydrodynamic model used.

The implementation of nonlinear analysis and the proposed fragility approach has the potential to improve engineers' understanding of the interaction of waves and coastal structures. The illustrative example in this dissertation focused on residential buildings, but it is envisioned that the approach may be extended to other structure types that are modeled nonlinearly with strength and stiffness degradation.

The proposed tsunami vertical evacuation methodology was intended to provide key information to better understand and mitigate risk caused by earthquakes and tsunamis, thus it is possible to mitigate hazard for a community with only several large vertical evacuation shelters. It is able to provide a framework for vertical evacuation plan and for the mitigation of collapse risk and fatalities of structures and the community.

7.3 CONTRIBUTIONS

As an endeavor of this research, the following contributions to structural engineering, tsunami-engineering and design for coastal structures, with a particular focus on light-frame wood residential buildings, including vertical evacuation, were accomplished.

1) Tsunami loading for coastal structures was examined as an outcome of the work done in Chapter 2. The structures examined here are typical shape, which later helps to create data and tables for the design process. Three types of wave forces, i.e. hydrostatic, hydrodynamic, and impulsive forces, were investigated and were able to be converted to

equivalent forces. On-going experimental investigation by collaborators at Oregon State University is underway.

2) Extension of current state-of-the-art non-linear wood frame models to predict the structural behavior under successive earthquakes and tsunamis was performed in this study. To date, this successive analysis and wave occurrence was discussed and the need to investigate it has been stressed but research related directly to it was never performed. Inclusion of a realistic COV for the wave height was also unique to this study.

3) A procedure to predict seismic collapse plus tsunami risk by means of fragilities was a major contribution of this study. This was presented in order to demonstrate the risk for coastal communities subjected to earthquakes, tsunamis, and their rapid successive occurrence.

4) A logical fragility-based, or performance-based, procedure for vertical evacuation methodology for residential coastal buildings and community planning was developed. A mechanism to obtain a reduction in the collapse risk of a structure and more critically maximize survival for a community was another major outcome from this dissertation.

7.4 RECOMMENDATIONS FOR FUTURE WORK

Several limitations were found during this study due to the time and complexity with implementation of numerical model and its approach. The complexity and non-linear

behavior of the wood structures should be further investigated to improve the numerical analysis results. The assumption that diaphragm and its connection with typical shearwalls are rigid should be better modeled to more accurately analyze the structural system.

Due to the time and expense with such specimens, there was a limit on the number of experimental testes and number of design variables that could be properly explored. The lack of field observations for tsunami hazards is limitation. In order to use of the approach developed herein, several questions must be answered through additional research. Some of these topics and issues that need to be investigated are as follows:

1. More complex finite element must be carefully considered to improve the accuracy and better understanding of failure mechanism for light-frame wood structure under wave bore loading.
2. Additional study on the tsunami wave model could help to improve the understanding of the fluid-structure interaction behavior using experimental tests, field observation, and numerical approach.
3. A design process can be completed by means of building a database procedure to help with the decision making in wood construction and tsunami safe frames.
4. Extension to full structures and structure groups with the inclusion of drawdown and /or debris impact is needed to more fully understand the risk tsunami pose to coastal structures and quantify the applicability of vertical evacuation structures in the U.S. and around the world.

REFERENCES CITED

Arora, J. (2004). "Introduction to Optimum Design."2nd, Academic Press.

ASCE (2005). "Minimum Design Loads for Buildings and Other Structures." Reston,VA, ASCE/SEI 7-05,ASCE.

Baldock, T. E., D. Cox, et al. (2009). "Kinematics of breaking tsunami wavefronts: A data set from large scale laboratory experiments." *Coastal Engineering* 56: 506-516.

Banerjee, S. and M. Shinozuka (2008). "Mechanistic quantification of RC bridge damage states under earthquake through fragility analysis." *Probabilistic engineering mechanics* 23: 12-22.

Bathe, K.-J. (1996). "Finite Element Procedures."1st ed. Englewood Cliffs, NJ, Prentice Hall.

Batoz, J.-L. and G. Dhatt (1979). "Incremental displacement algorithms for nonlinear problems." *International Journal for Numerical Methods in Engineering* 14(8): 1262-1267.

Battjes, J. A. (1974). "Surf Similarity". 14th International Conference on Coastal Engineering.466-480

Choi, C.-K., T.-Y. Lee, et al. (2002). "Direct modification for non-conforming elements with drilling DOF." *International Journal for Numerical Methods in Engineering* 55: 1463-1476.

Chopra, A. K. (2007). "Dynamics of Structures: Theory and applications to earthquake engineering."3rd, Prentice Hall.

Collins, M., B. Kasal, et al. (2005a). "Three-Dimensional Model of Light Frame Wood Buildings. I : Model Description." *Journal of Structural Engineering* 131(4): 676-683.

Collins, M., B. Kasal, et al. (2005b). "Three-Dimensional Model of Light Frame Wood Buildings. II : Experimental Investigation and Validation of Analytical Model." *Journal of Structural Engineering* 131(4): 684-692.

Cook, R. D. (1994). "Four-Node 'flat' shell element:Drilling degrees of freedom,

Membrane-Bending coupling, Warped Geometry, and Behavior." *Computer and Structures* 50(4): 549-555.

Cook, R. D., D. S. Malkus, et al. (2002). "Concepts and applications of finite element analysis."4th ed. Hoboken, NJ, John Wiley & Sons, Inc.

Cox, D., T. Tomita, et al. (2008). "Tsunami Inundation with macro-roughness in the constructed environment". Proceedings of the 31st International Conference on Coastal Engineering, Hamburg, Germany.1421-1432

Crisfield, M. A. (1991). "Non-linear Finite Element Analysis of Solids and Structures."Vol.1.1st ed., John Wiley & Sons, Inc.

Doerner, K. F., W. J. Gutjahr, et al. (2009). "Multi-crietria location planning for public facilities in tsunami-prone coastal areas." *OR Spectrum* 31(3): 651-678.

Dolan, J. D. (1989). "The dynamic response of timber shear walls." Civil Engineering. Vancouver, British Columbia, The University of British Columbia. Doctor of Philosophy.

Dovey, H. H. (1974). "Extension of Three-dimensional Analysis to Shell Structures using the Finite Element Idealization." Mechanical Engineering, University of California at Berkeley. Ph.D.

Du, Y. (2003). "The Development and Use of a novel finite element for the evaluation of Embedded Fluid dampers within Light-Frame Timber Structures with seismic loading." Civil and Environmental Engineering, Washington State Unversity. Doctor of Philosophy.

Durham, J. P. (1998). "Seismic response of wood shearwalls with oversized oriented strand board panels." Civil Engineering, University of British Columbia. Master of Applied Science.

Ellingwood, B. R. (2001). "Earthquake risk assessment of building structures." *Reliability Engineering and System Safety* 74: 251-262.

Ellingwood, B. R., D. V. Rosowsky, et al. (2004). "Fragility assessment of light-frame wood construction subjected to wind and earthquake hazards." *Journal of Structural Engineering* 130(12): 1921-1930.

FEMA-55 (2000). "Coastal Construction Manual:Principles and Practices of Planning, Siting, Designing, Constructing, and Maintaining Residential Buildings in Coastal Areas." FEMA-55. Washington, D.C., Federal Emergency Management Agency.

FEMA-320 (2008). "Taking Shelter From the Storm: Building a Safe Room For Your Home or Small Business ". FEMA-320. Washington, D.C, Federal Emergency Management Agency.

FEMA-P646 (2008). "Guidelines for Design of Structures for Vertical Evacuation frm Tsunamis." Washington, D.C., Federal Emergency Management Agency.

FEMA-P695 (2009). "Quantification of Building Seismic Performance Factors." FEMA-P695. Washington, D.C., Federal Emergency Management Agency.

Filiatrault, A. (1990). "Static and Dynamic analysis of timber shear walls." *Canadian Journal of Civil Engineering* 17(4): 643-651.

Folz, B. and A. Filiatrault (2001). "Cyclic Analysis of Wood Shear Walls." *Journal of Structural Engineering* 127(4): 433-441.

Folz, B. and A. Filiatrault (2004a). "Seismic analysis of woodframe structures. I: Model formulation." *Journal of Structural Engineering* 130(9): 1353-1360.

Folz, B. and A. Filiatrault (2004b). "Seismic analysis of woodframe structures. II: Model implementation and verification." *Journal of Structural Engineering* 130(9): 1361-1370.

Foschi, R. O. (1974). "Load-slip characteristics of nails." *Wood science* 7(1): 69-74.

Foschi, R. O. (1977). "Analysis of wood diaphragms and trusses. I: Diaphragms." *Canadian Journal of Civil Engineering* 4(3): 345-352.

Goldberg, D. E. (1983). "Computer-aided gas pipeline operation using genetic algorithms and rule learning." Department of civil engineering. Ann Arbor, University of Michgan. Pholosophy of Doctor.

Goldberg, D. E. (1989). "Genetic Algorithms in Search, Optimization, and Machine Learning." Addison-Wesley Publishing Co.

Hajela, P. and E. Lee (1995). "Genetic algorithms in truss topological optimization." *International Journal for solids structures* 32(22): 3341-3357.

Hart, G. C. and K. Wong (2000). "Structural Dynamics for Structural Engineers."1st, Wiley.

He, M. (2002). "Numerical modeling of three-dimensional light wood-frame buildings." Wood Science, University of British Columbia. Doctor of Philosophy.

Holland, J. H. (1975). "Adaptation in natural and artificial systems." The MIT Press.

Holman, R. A. (1986). "Extreme value statistics for wave run-up on a natural beach." *Coastal Engineering* 9: 527-544.

Hughes, S. A. (2004). "Estimation of wave run-up on smooth, impermeable slopes unsing the wave momentum flux parameter." *Coastal Engineering* 51: 1085-1104.

Hughes, T. J. R. and F. Brezzi (1989). "On Drilling Degrees of Freedom." *Computer methods in applied mechanics and engineering* 72: 105-121.

Hughes, T. J. R., M. Cohen, et al. (1978). "Reduced and Selective integration techniques in the finite element analysis of plates." *Nuclear Engineering and Design* 46: 203-222.

Hunt, I. A. (1959). "Design of seawalls and breakwaters." *Journal of the Waterways and Harbors Division* 85(3): 123-152.

Ibrahimbegovic, A., R. L. Taylor, et al. (1990). "A Robust quadrilateral membrane finite element with drilling degrees of freedom." *International Journal for Numerical Methods in Engineering* 30: 445-457.

Japanese National Police Agency (2011, April 20). "Damage Situation and Police Countermeasures associated with 2011 Tohoku district - off the Pacific Ocean Earthquake." Retrieved May 17, 2011, from http://www.npa.go.jp/archive/keibi/biki/higaijokyo_e.pdf.

Judd, J. P. (2005). "Analytical Modeling of wood-frame shear walls and diaphragms." Civil and Environmental Engineering, Brigham Young University. Master of Science.

Judd, J. P. and F. S. Fonseca (2005). "Analytical model for sheathing-to-framing connections in wood shear walls and diaphragms." *Journal of Structural Engineering* 131(2): 345-352.

Kirby, J. T. (2009). "FUNWAVE (FUlly Nonlinear boussinesq WAVE model)." January, 2010, from http://chinacat.coastal.udel.edu/programs/funwave/funwave.html.

Knoblauch, R. L., M. T. Pietrucha, et al. (1996). "Field studies of Pedestrian Walking Speed and Start-Up Time." *Journal of the Transportation Research Board* 1538: 27-38.

Kobayashi, N. and E. A. Karjadi (1994). "Surf-Similarity Parameter for breaking solitary-wave Runup." *Journal of Waterway, Port, Coastal, and Ocean Engineering* 120(6): 645-650.

Kongsomsaksakul, S., A. Chen, et al. (2005). "Shelter Location-allocation model for Flood evacuation planning." *Journal of the Eastern Asia Society for Transportation Studies* 6: 4237-4252.

Koshimura, S., T. OIE, et al. (2009). "Developing fragility functions for tsunami damage estimation using numerical model and post-tsunami data from banda aceh, Indonesia." *Coastal Engineering Journal* 51(3): 243-273.

Li, Y. and B. R. Ellingwood (2006). "Hurricane damage to residential construction in the US: importance of uncertainty modeling in risk assessment." *Engineering Structures* 28:

1009-1018.

Liu, P. L.-F. (2009). "COBRAS (Cornell Breaking Waves and Structure) ". January, 2010, from http://ceeserver.cee.cornell.edu/cobras/defaults.htm.

Lukkunaprasit, P., A. Ruangrassamee, et al. (2009). "Tsunami loading on buildings with openings." *Science of Tsunami Hazards* 28(5): 303-310.

Lynett, P. (2007). "The Effect of a Shallow Water Obstruction on Long Wave Runup and Overland Flow Velocity." *Journal of Waterway, Port, Coastal, and Ocean Engineering* 133(6): 455-462.

Madsen, P. A. and D. R. Fuhrman (2008). "Run-up of tsunamis and long waves in terms of surf-similarity." *Coastal Engineering* 55: 209-223.

Malkus, D. S. and T. J. R. Hughes (1978). "Mixed finite element methods - reduced and selective integration techniques: a unification of concepts." *Computer methods in applied mechanics and engineering* 15: 63-81.

Myrhaug, D., L. E. Holmedal, et al. (2009). "Nonlinear random wave-induced drag force on a vegetation field " *Coastal Engineering* 56: 371-376.

Naganarayana, B. P. and G. Prathap (1989). "Force and moment corrections for the warped four-node quadrilateral plane shell element." *Computer and Structures* 33(4): 1107-1115.

Neelamani, S., H. Schuttrumpf, et al. (1999). "Prediction of wave pressures on smooth impermeable seawalls." *Ocean Engineering* 26: 739-765.

Newmark, N. M. (1959). "A method of computation for structural dynamics." *Journal of the Engineering Mechacnis Division* 85(EM3): 67-94.

NOAA (2011). Retrieved March, 2011, from http://stateofthecoast.noaa.gov/population/welcome.html.

Oñate, E., O. C. Zienkiewicz, et al. (1992). "A general methodology for deriving shear constrained Reissner-Mindlin plate elements." *International Journal for Numerical Methods in Engineering* 33(2): 345-367.

Palermo, D., I. Nistor, et al. (2009). "Tsunami loading of near-shoreline structure: a primer." *Canadian Journal of Civil Engineering* 36(11): 1804-1815.

Pang, W. C., D. R. Rosowsky, et al. (2007). "Evolutionary parameter hysteretic model for wood shear walls." *Journal of Structural Engineering* 133(8): 1118-1129.

Park, S. and J. W. van de Lindt (2009). "Formulation of Seismic Fragilities for a Wood-

Frame Building Based on Visually Determined Damage Indexes." *Journal of Performance of Constructed Facilities* 23(5): 346-352.

Pei, S. and J. W. van de Lindt (2008). "Manual of SAPWood for windows version 1.0."

Pei, S., J. W. van de Lindt, et al. (2010). "Seismic Testing of a Full-Scale Mid-Rise Buildings: The NEESWood Capstone Test." Colorado State University. Report NW-04.

Pelinovsky, E., E. Troshina, et al. (1999). "Runup of Tsunami Waves on a Vertical Wall in a Basin of Complex Topography." *Physics and Chemistry of the Earth(B)* 24(5): 431-436.

Rajan, S. D. (1995). "Sizing, Shape, and Topology design optimization of trusses using genetic algorithm." *Journal of Structural Engineering* 121(10): 1480-1487.

Rajeev, S. and C. S. Krishnamoorthy (1992). "Discrete optimization of structures using genetic algorithms." *Journal of Structural Engineering* 118(5): 1233-1250.

Ramm, E. (1981). "Strategies for tracing the nonlinear response near limit points." 2nd US-Europe Workshop "Nonlinear Finite Element Analysis in Structural Mechanics". W. Wunderlich, E. Stein and K. J. Bathe. Bochum, Springer-Verlag**:** 63-89.

Ramsden, J. D. (1996). "Forces on a vertical wall due to long waves, bores, and dry-bed surges." *Journal of Waterway, Port, Coastal, and Ocean Engineering* 122(3): 134-141.

Rose, J. D. (1994). "Performance of wood structural panel shear walls under cyclic(reversed) loading". Proc. Research Needs Workship on Analysis, Design, and Testing of Timbr Structures Under Seismic Loads, Forest Products Laboratory, University of Californa, Richmond, CA.129-141

Rosowsky, D. V. and B. R. Ellingwood (2002). "Performance-based engineering of wood frame housing: Fragility analysis methodology." *Journal of Structural Engineering* 128(1): 32-38.

Shinozuka, M., M. Q. Feng, et al. (2000). "Statistical analysis of fragility curves." *Journal of Engineering Mechanics* 126(12): 12241231.

Stewart, W. G. (1987). "The seismic design of plywood sheated shearwalls." Civil Engineering. Christchurch, New Zealand, Unversity of Canterbury. Doctor oh philosophy.

Synolakis, C. E. (1987). "The runup of solitary waves." *Journal of Fluid Mechanics* 185: 523-545.

Tarabia, A. M. (1994). "Response of light-frame buildings due to earthquake loadings." Civil and Evniromental Engineering. Pullman, Washington State University. Doctor of Philosophy.

Tarabia, A. M. and R. Y. Itani (1997). "Seismic Response of Light-Frame Wood Buildings." *Journal of Structural Engineering* 123(11): 1470-1477.

Taylor, R. L. (1987). "Finite element analysis of linear shell problem". Proceedings of the Mathematics of Finite Elements and Application VI - MAFELAP, Academic Press.191-203

The City of Cannon Beach, O., USA (2011). "Tsunami Evacuation Map." Retrieved August, 19th, 2011, from http://www.ci.cannon-beach.or.us/GIS_2011/CARTOMATION/index4.htm.

Tomita, T., K. Honda, et al. (2007). "Application of three-dimensional tsunami simulator to estimation of tsunami behavior around structures". Proceeding of the International Conference on Coastal Engineering, World Scientific.1677-1688

UNESCO (2008). "Tsunami Glossary." Intergovernmental Oceanographic Commission Technical Series 85. S. United Nations Educational, and Cultural Organization(UNESCO).

USGS (2011a). "U.S. Seismic Design Map ". Retrieved March, 2011, from https://geohazards.usgs.gov/secure/designmaps/us/.

USGS (2011b). "USGS Scientists in Samoa and American Samoa Studying Impacts of Recent Tsunami, October-November 2009." Retrieved April, 2011, from http://walrus.wr.usgs.gov/news/tsu-terms.html.

van de Lindt, J. W. (2004). "Evolution of Wood Shear Wall Testing, Modeling, and Reliability Analysis: Bibliography." *Practice Periodical on Structural Design and Construction* 9(1): 44-53.

van de Lindt, J. W. (2011). Retrieved March, 2011, from http://jwv.eng.ua.edu/.

van de Lindt, J. W. and T. N. Dao (2009). "Performance-Based Wind Engineering for Woodframe Buildings." *Journal of Structural Engineering* 135(2): 169-177.

White, M. W. and J. D. Dolan (1995). "Nonlinear Shear-Wall Analysis." *Journal of Structural Engineering* 121(11): 1629-1635.

Wilson, E. L. (1974). "The static condensation algorithm." *International Journal for Numerical Methods in Engineering* 8(1): 198-203.

Wilson, E. L., R. L. Taylor, et al. (1973). "Incompatible Displacement Models." New York, Academic Press.

Wilson, J. S., R. Gupta, et al. (2009). "Behavior of a One-Sixth Scale Wood-Framed Residential Structure under Wave Loading." *Journal of Performance of Constructed*

Facilities 23(5): 336-345.

Xu, J. and J. D. Dolan (2009a). "Development of a Wood-Frame Shear Wall Model in ABAQUS." *Journal of Structural Engineering* 135(8): 977-984.

Xu, J. and J. D. Dolan (2009b). "Development of Nailed Wood Joint Element in ABAQUS." *Journal of Structural Engineering* 135(8): 968-976.

Yeniay, O. (2005). "Penalty function methods for constrained optimization with genetic algorithms." *Mathematical and Computational Applications* 10(1): 45-56.

Zienkiewicz, O. C. and R. L. Taylor (2005). "The Finite Element Method."6th Ed., Butterworth-Heinemann.

Zienkiewicz, O. C., R. L. Taylor, et al. (1971). "Reduced Integration technique in general analysis plates and shells." *International Journal for Numerical Methods in Engineering* 3(2): 275-290.

APPENDIX A

FINITE ELEMNT PROCEDURES

A.1 OVERVIEW

Three finite elements such as frame, shell, and spring are developed using principal of virtual work to derivate element stiffness and force vector and transformation matrix was introduced as well.

Initially, frame elements have been developed based on three dimensional coordinates system. Additionally, shear deformation was then considered. Therefore, there are two types of element stiffness. Shell elements have been developed the combination of membrane element and plate-bending element based on three dimensional coordinates system. Warping effects and several numerical techniques was introduced to overcome the locking effect which is the defect of the classical membrane and plate-bending elements. Spring elements are introduced to represent the connector and improved to handle the non-linear behavior of the connector.

A non-linear solver is needed and developed by means of Newton-Raphson iteration technique and an incremental-iterative displacement control solution strategy.

A.2 FRAME ELEMENTS

A typical three-dimensional frame, shown in Figure A.1, is used to represent wood-framing components in shearwalls. It has two nodes and each node has six DOF, three translational and three rotational DOF in the *x*, *y*, and *z* direction, respectively.

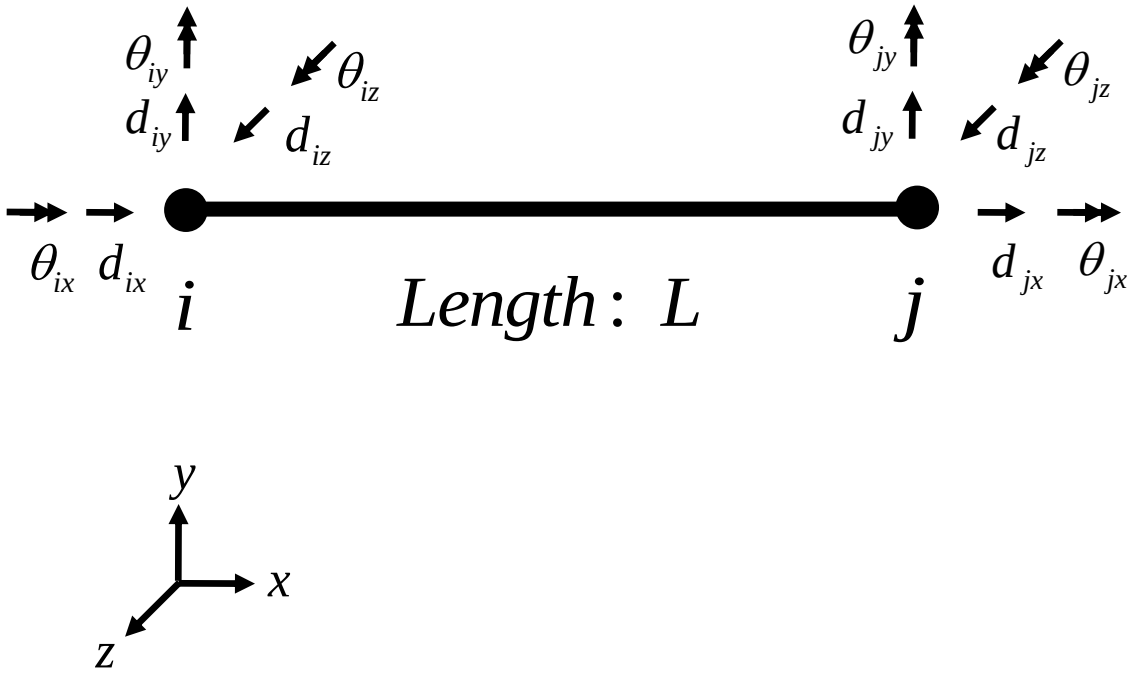

Figure A.1: Frame element in local coordinate system with twelve DOFs.

A.2.1 ELEMENT STIFFNESS MATRIX

The stiffness matrix in local coordinate system can be derived by using either principle of virtual work (PVW) or direct stiffness method, which makes use of the member' stiffness relations between forces and displacements. Shear-deformation is neglected, thus Euler-Bernoulli beam is selected. The stiffness matrix can be expressed as the following form:

$$[k_e] = \begin{bmatrix} \frac{EA}{L} & 0 & 0 & 0 & 0 & 0 & -\frac{EA}{L} & 0 & 0 & 0 & 0 & 0 \\ & \frac{12EI_z}{L^3} & 0 & 0 & 0 & \frac{6EI_z}{L^2} & 0 & -\frac{12EI_z}{L^3} & 0 & 0 & 0 & \frac{6EI_z}{L^2} \\ & & \frac{12EI_y}{L^3} & 0 & -\frac{6EI_y}{L^2} & 0 & 0 & 0 & -\frac{12EI_y}{L^3} & 0 & -\frac{6EI_y}{L^2} & 0 \\ & & & \frac{GJ}{L} & 0 & 0 & 0 & 0 & 0 & -\frac{GJ}{L} & 0 & 0 \\ & & & & \frac{4EI_y}{L} & 0 & 0 & 0 & \frac{6EI_y}{L^2} & 0 & \frac{2EI_y}{L} & 0 \\ & & & & & \frac{4EI_z}{L} & 0 & -\frac{6EI_z}{L^2} & 0 & 0 & 0 & \frac{2EI_z}{L} \\ & & & & & & \frac{EA}{L} & 0 & 0 & 0 & 0 & 0 \\ & & & & & & & \frac{12EI_z}{L^3} & 0 & 0 & 0 & -\frac{6EI_z}{L^2} \\ & & & & & & & & \frac{12EI_y}{L^3} & 0 & \frac{6EI_y}{L^2} & 0 \\ & & & symm & & & & & & \frac{GJ}{L} & 0 & 0 \\ & & & & & & & & & & \frac{4EI_y}{L} & 0 \\ & & & & & & & & & & & \frac{4EI_z}{L} \end{bmatrix} \quad \text{(A-1)}$$

where A is the cross-sectional area of an element, E is the elastic modulus of an element, G is the shear modulus of an element, L is the length of an element, I_y and I_z are the moment of inertia in local y and z direction, and J is the torsional constant of an element.

A.2.2 FORCE VECTOR

Frame elements can have a concentrated load on nodal point and a distributed load with component w on an element as a type of surface loads, depicted in Figure A.2.

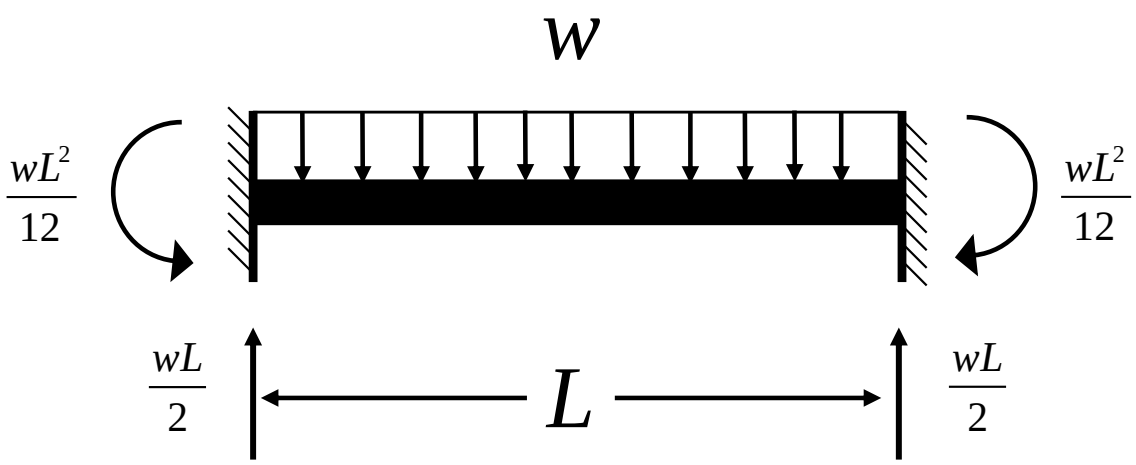

Figure A.2: End reactions of member under uniform distributed load.

When a uniformly distributed load with w applied on the member, the force vector in local coordinate system is formulated as

$$\{r_S\} = \left\{0 \quad \frac{w_y L}{2} \quad \frac{w_z L}{2} \quad 0 \quad \frac{-w_z L^2}{12} \quad \frac{w_y L^2}{12} \quad 0 \quad \frac{w_y L}{2} \quad \frac{w_z L}{2} \quad 0 \quad \frac{w_z L^2}{12} \quad \frac{-w_y L^2}{12}\right\}^T \qquad \text{(A-2)}$$

where w_y and w_z are the uniformly distributed load in local y and z directions, respectively, L is the length of the member.

Nodal concentrated forces are also applied to this element and these loads are transferred into components in global coordinate system by using transformation matrix.

A.2.3 TRANSFORMATION MATRIX

Transformation matrix is needed to determine system matrices in global coordinate system in order to assembly a system matrix of a structure.

Initially, the local *x-axis* can be defined along the line from the nodes 1 and 2 of an element. However, the local *x-axis* can rotate about the axis of the element, thus additionally one more point, as a reference point, is needed to establish the local coordinate system. This point can be located anywhere in the local *x-y* plane except on the *x-axis*. Thus, the local *y-axis* is to line in the plane defined by points 1, 2, and 3. Finally, the local *z-axis* is then automatically defined from the fact that *x*, *y*, and *z* form a right-handed system, shown in Figure A.3.

Transformation matrix [T] can be defined as the following form:

$$[T]=\begin{bmatrix}[\lambda] & [0] & [0] & [0]\\ [0] & [\lambda] & [0] & [0]\\ [0] & [0] & [\lambda] & [0]\\ [0] & [0] & [0] & [\lambda]\end{bmatrix} \tag{A-3}$$

where $[0]$ is a zero matrix defined as $[0]=\begin{bmatrix}0 & 0 & 0\\ 0 & 0 & 0\\ 0 & 0 & 0\end{bmatrix}$ and $[\lambda]$ is a direction cosine matrix defined as $[\lambda]=\begin{bmatrix}l_1 & m_1 & n_1\\ l_2 & m_2 & n_2\\ l_3 & m_3 & n_3\end{bmatrix}$, l_1, m_1, and n_1 are the cosines of the angles between the local *x-axis* and the global *X-axis*, *Y-axis*, and *Z-axis*, respectively. Similarly,

l_2, m_2, and n_2 are the cosines of the angles associated with local *y-axis* and l_3, m_3, and n_3 are the cosines of the angles associated with local *z-axis*.

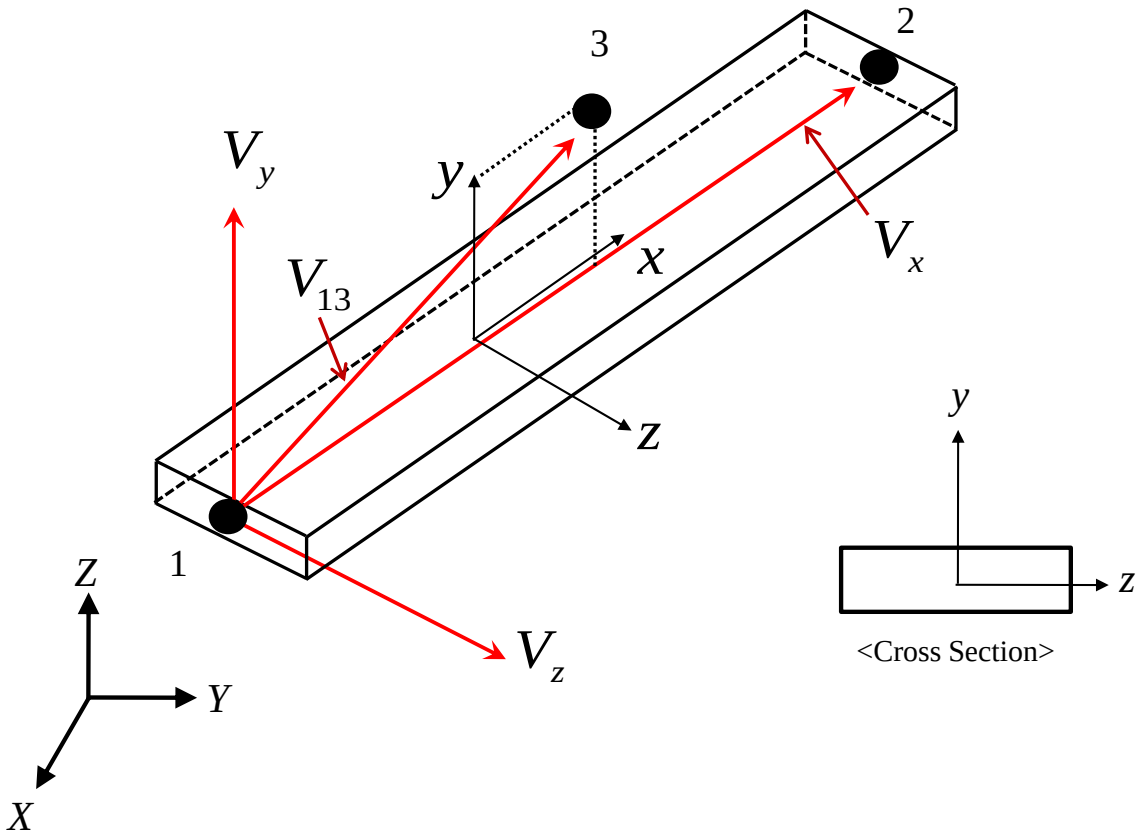

Figure A.3: Local and global coordinate systems of the frame element.

This direction cosine matrix can be obtained from the coordinates of the points 1, 2, and 3 as follows:

$$l_1 = \frac{x_2 - x_1}{L_e}, \quad m_1 = \frac{y_2 - y_1}{L_e}, \quad n_1 = \frac{z_2 - z_1}{L_e} \tag{A-4}$$

where (x_1, y_1, and z_1) are coordinate components of point 1, (x_2, y_2, and z_2) are coordinate components of point 2, and L_e is a length or distance between point 1 and point 2 of an element defined as $L_e = \sqrt{(x_2 - x_1)^2 + (y_2 - y_1)^2 + (z_2 - z_1)^2}$.

Rest of two direction cosine matrices can be computed from vector calculations. Let $V_x = \{l_1 \quad m_1 \quad n_1\}^T$ denote the unit vector along the local *x-axis*. Then the unit vector along the point 1 and point 3 can be defined as:

$$V_R = \left\{ \frac{x_3 - x_1}{L_R} \quad \frac{y_3 - y_1}{L_R} \quad \frac{z_3 - z_1}{L_R} \right\}^T \tag{A-5}$$

where (x_3, y_3, and z_3) are coordinate components of point 3 and L_R is a distance between point 1 and point 3 defined as $L_R = \sqrt{(x_3 - x_1)^2 + (y_3 - y_1)^2 + (z_3 - z_1)^2}$.

The unit vector along the local *z-axis*, which can be obtained from cross product of V_x and V_R, is given by the following form:

$$V_z = \{l_3 \quad m_3 \quad n_3\}^T = \frac{V_x \times V_R}{|V_x \times V_R|} \tag{A-6}$$

Finally, the direction cosines along local *y-axis*, which can be computed from cross product of V_z and V_x , are given by the following form:

$$V_y = \begin{Bmatrix} l_2 & m_2 & n_2 \end{Bmatrix}^T = V_z \times V_x \tag{A-7}$$

A.2.4 SHEAR DEFORMATION

Typically, there are two theories for beam elements, Euler-Bernoulli beam theory and Timoshenko beam theory which is included a shear deformation. The difference between two theories is that the transverse shear stress is whether taken into account or not. As usual, Euler-Bernoulli beam theory gives a good result if a beam is slender or thin also Timoshenko beam theory is good for thick beams.

$$[k_e] = \begin{bmatrix}
\frac{EA}{L} & 0 & 0 & 0 & 0 & 0 & -\frac{EA}{L} & 0 & 0 & 0 & 0 & 0 \\
 & \frac{12EI_z}{L^3(1+K_{sy})} & 0 & 0 & 0 & \frac{6EI_z}{L^2(1+K_{sy})} & 0 & -\frac{12EI_z}{L^3(1+K_{sy})} & 0 & 0 & 0 & \frac{6EI_z}{L^2(1+K_{sy})} \\
 & & \frac{12EI_y}{L^3(1+K_{sz})} & 0 & -\frac{6EI_y}{L^2(1+K_{sz})} & 0 & 0 & 0 & -\frac{12EI_y}{L^3(1+K_{sz})} & 0 & -\frac{6EI_y}{L^2(1+K_{sz})} & 0 \\
 & & & \frac{GJ}{L} & 0 & 0 & 0 & 0 & 0 & -\frac{GJ}{L} & 0 & 0 \\
 & & & & \frac{(4+K_{sz})EI_y}{L(1+K_{sz})} & 0 & 0 & 0 & \frac{6EI_y}{L^2(1+K_{sz})} & 0 & \frac{(2-K_{sz})EI_y}{L(1+K_{sz})} & 0 \\
 & & & & & \frac{(4+K_{sy})EI_z}{L(1+K_{sy})} & 0 & -\frac{6EI_z}{L^2(1+K_{sy})} & 0 & 0 & 0 & \frac{(2-K_{sy})EI_z}{L(1+K_{sy})} \\
 & & & & & & \frac{EA}{L} & 0 & 0 & 0 & 0 & 0 \\
 & & & & & & & \frac{12EI_z}{L^3(1+K_{sy})} & 0 & 0 & 0 & -\frac{6EI_z}{L^2(1+K_{sy})} \\
 & & & & & & & & \frac{12EI_y}{L^3(1+K_{sz})} & 0 & \frac{6EI_y}{L^2(1+K_{sz})} & 0 \\
 & & & symm & & & & & & \frac{GJ}{L} & 0 & 0 \\
 & & & & & & & & & & \frac{(4+K_{sz})EI_y}{L(1+K_{sz})} & 0 \\
 & & & & & & & & & & & \frac{(4+K_{sy})EI_z}{L(1+K_{sy})}
\end{bmatrix} \tag{A-8}$$

where K_{sy} and K_{sz} are the shear deformation coefficients and can be defined as $K_{sy} = \frac{12EI_z}{G*A_{sy}*L^2}$ and $K_{sz} = \frac{12EI_y}{G*A_{sz}*L^2}$, where A_{sy} and A_{sz} are the shear area of the given cross-section. The shear area term is provided based on the shape of cross-section. If the shape is rectangular section, for instance, then $A_s = \frac{5}{6}A$ is recommended.

A.3 SHELL ELEMENTS

A shell element is selected to represent a sheathing panel. The shell element has been formed by combination of the membrane and plate-bending elements, which is the flat shell element approach due to its simplicity in formulation and computational cost.

Over the last decades, two elements have been matured enough to overcome their weakness such as locking problems, the flexural behavior in distorted mesh, the spurious mechanism, and difficulty in connection with other types of elements. Incompatible or non-conforming modes, reduced and selective integration techniques, and other numerical schemes have been adopted to eliminate their limitations. Additionally, the connections with other elements can be possible to add the drilling-DOF.

Therefore, a six degree per node shell element, shown in Figure A.4, can be established and the possessing with six-DOF per node can be ensured successfully (Zienkiewicz et al. 1971; Hughes et al. 1978; Ibrahimbegovic et al. 1990; Choi et al. 2002).

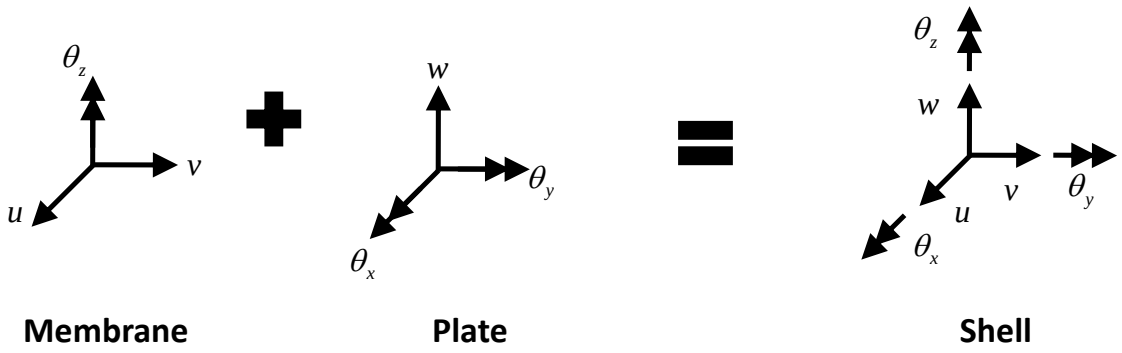

Figure A.4: The shell element with drilling DOF.

The incompatible mode technique, initially proposed by Wilson et al. (1973), is an approach to add more displacement modes in order to improve its behavior, shown in Figure A.5.

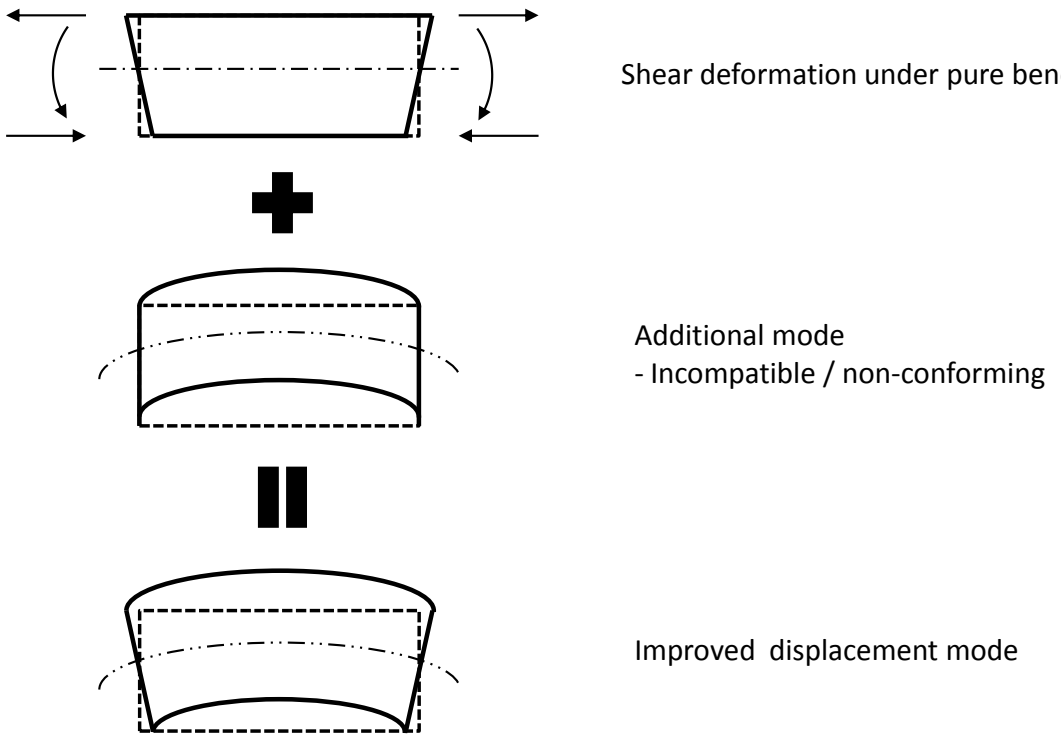

Figure A.5: An example of an improved bending behavior.

A.3.1 MEMBRANE ELEMENTS WITH DRILLING DOF

Typically, membrane elements have only two translational DOF (*u* and *v*) per node, shown in Figure A.6. To adopt a drilling DOF (θ_z), defined as an in-plane rotational DOF about the axis normal to the plane of the element, the mixed variational formulation, proposed by Hughes and Brezzi (1989), is used.

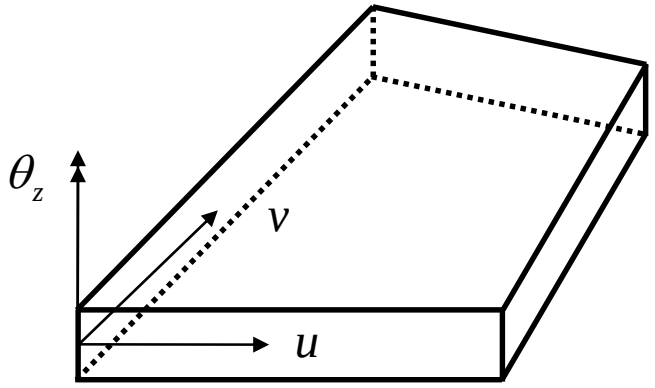

Figure A.6: Degree of freedom for Membrane elements with drilling DOF.

The formulation is presented with symmetric component of the displacement gradient and independent rotational field, which can separate kinematics variables of displacement and rotations (Hughes and Brezzi 1989; Ibrahimbegovic et al. 1990) and can be expressed the following form:

$$\Pi(u,\theta) = \frac{1}{2}\int_{\Omega}\left[symm\left(\nabla u\right)\right]\cdot\left[D\right]\cdot\left[symm\left(\nabla u\right)\right]d\Omega \; + \\ \frac{\mu}{2}\int_{\Omega}\left\{skew\left(\nabla u\right)-\theta\right\}^{T}\cdot\left\{skew\left(\nabla u\right)-\theta\right\}d\Omega - \int_{\Omega}\left\{u\right\}^{T}\cdot\left\{f\right\}d\Omega \tag{A-9}$$

where u is a displacement field vector, θ is a rotational field vector, D is constitutive matrix, μ is a shear modulus, and $\left[symm(\nabla u)\right]$ and $\left\{skew(\nabla u)\right\}$ are related to symmetric gradient matrix and skew-symmetric gradient vector, respectively, defined as following form:

$$symm(\nabla u) = \begin{bmatrix} \frac{\partial}{\partial x} & 0 & \frac{\partial}{\partial y} \\ 0 & \frac{\partial}{\partial y} & \frac{\partial}{\partial x} \end{bmatrix}^T \tag{A-10}$$

$$skew(\nabla u) = \frac{1}{2}\left\{ -\frac{\partial}{\partial y} \quad \frac{\partial}{\partial x} \right\} \tag{A-11}$$

The shape function for the displacement with introduction of incompatible mode and rotation fields can be expressed as the following form:

$$u = \begin{Bmatrix} u \\ v \end{Bmatrix} = \sum_{i=1}^{n} N_i \begin{Bmatrix} u_i \\ v_i \end{Bmatrix} + \sum_{j=1}^{m} \bar{N}_j \begin{Bmatrix} \bar{u}_j \\ \bar{v}_j \end{Bmatrix} = \sum_{i=1}^{n} N_i u_i + \sum_{j=1}^{m} \bar{N}_j \bar{u}_j \tag{A-12}$$

$$\theta = \{\theta_z\} = \sum_{i=1}^{n} N_i \{\theta_{zi}\} \tag{A-13}$$

where (N_i, u_i, and n) is a shape function, displacement DOF, and the number of nodes per elements related to the compatible modes, respectively, ($\bar{N}_j$, $\bar{u}_j$, and m) is a shape function, displacement DOF, and the number of nodes per elements related to the incompatible modes, respectively, and θ is the rotational DOF. Detailed explanation of

the shape functions for compatible and incompatible mode can be found in Appendix B of this dissertation.

The symmetric matrix and skew vector can be expressed by using the shape functions as following form:

$$\begin{aligned} symm(\nabla u) &= \sum_{i=1}^{n} symm(\nabla N_i u_i) + \sum_{j=1}^{m} symm(\nabla \bar{N}_j \bar{u}_j) \\ &= \sum_{i=1}^{n} B_i u_i + \sum_{j=1}^{m} \bar{B}_j \bar{u}_j \end{aligned} \tag{A-14}$$

$$\begin{aligned} skew(\nabla u) - \theta &= \sum_{i=1}^{n} skew(\nabla N_i u_i) - \sum_{j=1}^{m} skew(\nabla \bar{N}_j \bar{u}_j) - \sum_{i=1}^{n} N_i \theta_i \\ &= \sum_{i=1}^{n} G_i u_i - \sum_{j=1}^{m} \bar{G}_j \bar{u}_j - \sum_{i=1}^{n} N_i \theta_i \end{aligned} \tag{A-15}$$

where B_i and $\bar{B}_j$ are the strain-displacement matrices of compatible and incompatible part, respectively, G_i and $\bar{G}_j$ are the strain-rotation matrices of compatible and incompatible part, respectively, and N_i is the shape function vector. They can be defined as the following form:

$$\left[B_i\right] = \begin{bmatrix} N_{i,x} & 0 & N_{i,y} \\ 0 & N_{i,y} & N_{i,x} \end{bmatrix}^T \tag{A-16}$$

$$\left[\bar{B}_j\right] = \begin{bmatrix} \bar{N}_{j,x} & 0 & \bar{N}_{j,y} \\ 0 & \bar{N}_{j,y} & \bar{N}_{j,x} \end{bmatrix}^T \tag{A-17}$$

$$\{G_i\} = \frac{1}{2}\begin{Bmatrix} N_{i,y} & -N_{i,x} \end{Bmatrix} \tag{A-18}$$

$$\{\bar{G}_j\} = \frac{1}{2}\begin{Bmatrix} \bar{N}_{j,y} & -\bar{N}_{j,x} \end{Bmatrix} \tag{A-19}$$

where $N_{i,x}$ is a derivation of i^{th} shape function with respect to x, denote $N_{i,x} = \frac{\partial N_i}{\partial x}$, and the other terms also denote $N_{i,y} = \frac{\partial N_i}{\partial y}$, $\bar{N}_{j,x} = \frac{\partial \bar{N}_j}{\partial x}$, and $\bar{N}_{j,y} = \frac{\partial \bar{N}_j}{\partial y}$, respectively.

It is noted that $\bar{B}$ and $\bar{G}$ matrix cannot always pass the patch test due to their incompatible modes, so modification is needed numerically. The direct modification scheme can be adopted (Choi et al. 2002 and explained in Appendix C) then these modified matrices can be defined as the following form:

$$\left[\bar{B}_j^*\right] = \begin{bmatrix} \left(\bar{N}_{j,x}\right)^* & 0 & \left(\bar{N}_{j,y}\right)^* \\ 0 & \left(\bar{N}_{j,y}\right)^* & \left(\bar{N}_{j,x}\right)^* \end{bmatrix}^T \tag{A-20}$$

$$\{\bar{G}_j^*\} = \frac{1}{2}\begin{Bmatrix} \left(\bar{N}_{j,y}\right)^* & -\left(\bar{N}_{j,x}\right)^* \end{Bmatrix} \tag{A-21}$$

The, similar approach of PVW can be applied to determine element stiffness matrix and then the stiffness matrix of the elements can be written as:

$$[k_e] = \begin{bmatrix} [k_{CC}] & [k_{CI}] \\ [k_{CI}]^T & [k_{II}] \end{bmatrix} \tag{A-22}$$

where $[k_{CC}]$ represents a compatible matrix only, $[k_{CI}]$ represents a compatible and incompatible mixed matrix, and $[k_{II}]$ represents a incompatible matrix only, where they can be defined as

$$[k_{CC}] = \int_V \begin{bmatrix} [B]^T [D][B] & [0] \\ [0] & [0] \end{bmatrix} dV + \mu \int_V \begin{bmatrix} \{G\}^T \{G\} & \{G\}^T \{N\} \\ \{N\}^T \{G\} & \{N\}^T \{N\} \end{bmatrix} dV \tag{A-23}$$

$$[k_{CI}] = \int_V \begin{bmatrix} [B]^T [D][\bar{B}^*] \\ [0] \end{bmatrix} dV + \mu \int_V \begin{bmatrix} \{G\}^T \{\bar{G}^*\} \\ \{N\}^T \{\bar{G}^*\} \end{bmatrix} dV \tag{A-24}$$

$$[k_{II}] = \int_V [\bar{B}^*]^T [D][\bar{B}^*] dV + \mu \int_V \{\bar{G}^*\}^T \{\bar{G}^*\} dV \tag{A-25}$$

One can think these matrices are oversized due to the introduction of incompatible mode. They can be reduced back to typical size of an membrane matrix by using static condensation algorithm (Wilson 1974; Cook et al. 2002). Finally, membrane stiffness matrix can be reformulated from Equation (A-22):

$$[k_{membrane}] = [k_{CC}] - [k_{CI}][k_{II}]^{-1}[k_{CI}]^T \tag{A-26}$$

The numerical integration technique is needed to compute the stiffness (Zienkiewicz et al. 1971; Hughes et al. 1978; Malkus and Hughes 1978). Especially, reduced and selective

integration techniques are used in membrane elements to overcome the locking problems and to compute incompatible parts, especially related to strain-displacement matrix.

The four additional incompatible modes are adopted to improve the membrane elements behavior and summarized in Table A.1. Detailed explanation of the incompatible mode and the integration scheme can be found in Appendix B and Appendix D of this dissertation, respectively.

Table A.1: Additional modes and integration schemes for Membrane elements.

Incompatible Mode	Integration Schemes			
	$[k_{CC}]$	$[k_{CI}]$	$[k_{II}]$	
			$\left[\bar{B}^*\right]^T[D]\left[\bar{B}^*\right]$	$\left[\bar{G}^*\right]^T\left[\bar{G}^*\right]$
$\bar{N}_1, \bar{N}_2, \bar{N}_4$, and $\bar{N}_5$	2x2	3x3	5-point	2x2

A.3.2 REISSNER-MINDLIN PLATE-BENDING ELEMENTS

The Reissner-Mindlin plate theory has been widely accepted to derive the formulation of plate-bending element. Typically the elements having three DOF per node, one displacement *w* and two rotations θ_x and θ_y at the mid-surface, can be also improved by the introduction of the incompatible modes, shown in Figure A.7.

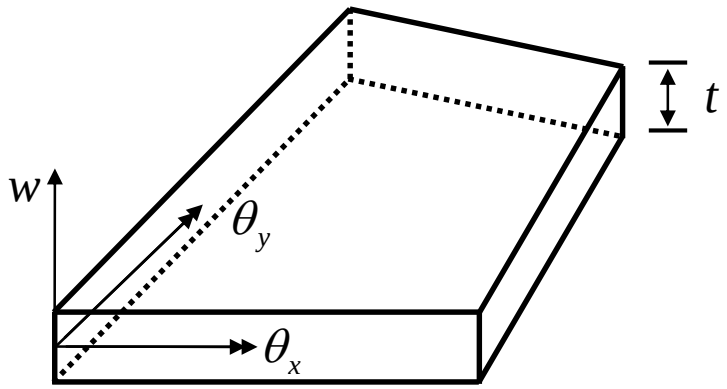

Figure A.7: Degree of freedom for Reissner-Mindlin plate-bending elements.

The similar procedure mentioned earlier can be adopted in here. Initially, the shape functions for the elements can be defined as the following form:

$$u = \begin{Bmatrix} w \\ \theta_x \\ \theta_y \end{Bmatrix} = \sum_{i=1}^{n} N_i \begin{Bmatrix} w_i \\ \theta_{xi} \\ \theta_{yi} \end{Bmatrix} + \sum_{j=1}^{m} \bar{N}_j \begin{Bmatrix} 0 \\ \bar{\theta}_{xj} \\ \bar{\theta}_{yj} \end{Bmatrix} = \sum_{i=1}^{n} N_i u_i + \sum_{j=1}^{m} \bar{N}_j \bar{u}_j \tag{A-27}$$

Then, the curvatures can be given by the following form:

$$\kappa = \begin{Bmatrix} \kappa_x \\ \kappa_y \\ \kappa_{xy} \end{Bmatrix} = \begin{Bmatrix} -\theta_{y,x} \\ \theta_{x,y} \\ -\theta_{y,y} + \theta_{x,x} \end{Bmatrix} \tag{A-28}$$

where $\theta_{x,y}$ is the derivation of *x* rotational DOF with respect to *y*, $\theta_{y,x}$ is the derivation of *y* rotational DOF with respect to *x*, $\theta_{x,x}$ is the derivation of *x* rotational DOF with

respect to *x*, $\theta_{y,y}$ is the derivation of *y* rotational DOF with respect to *y*, and can be defined as the following form:

$$\theta_{x,x} = \frac{\partial \theta_x}{\partial x} \quad , \quad \theta_{x,y} = \frac{\partial \theta_x}{\partial y} \tag{A-29}$$

$$\theta_{y,x} = \frac{\partial \theta_y}{\partial x} \quad , \quad \theta_{y,y} = \frac{\partial \theta_y}{\partial y} \tag{A-30}$$

Generally, the strain of the plate-bending elements is typically separated into two components, i.e. curvature and transverse shear strain parts, and it can be written as:

$$\varepsilon = -z \begin{Bmatrix} \kappa_x \\ \kappa_y \\ \kappa_{xy} \end{Bmatrix} = \sum_{i=1}^{n} B_{bi} u_i + \sum_{j=1}^{m} \overline{B}_{bj} \overline{u}_j \tag{A-31}$$

$$\gamma = \begin{Bmatrix} \gamma_{yz} \\ \gamma_{xz} \end{Bmatrix} = \begin{Bmatrix} \dfrac{\partial w}{\partial y} - \theta_x \\ \dfrac{\partial w}{\partial x} + \theta_y \end{Bmatrix} = \sum_{i=1}^{n} B_{si} u_i + \sum_{j=1}^{m} \overline{B}_{sj} \overline{u}_j \tag{A-32}$$

where B_{bi} and $\overline{B}_{bj}$ are the strain-displacement matrix of the curvature components for compatible and incompatible part, respectively, and B_{si} and $\overline{B}_{sj}$ are the strain-displacement matrix of the transverse shear components for compatible and incompatible part, respectively, where B_{bi}, $\overline{B}_{bj}$, B_{bi}, and $\overline{B}_{sj}$ can be defined as the following form:

$$\left[B_{bi}\right]=\begin{bmatrix}0 & 0 & zN_{i,x}\\ 0 & -zN_{i,y} & 0\\ 0 & zN_{i,x} & -zN_{i,y}\end{bmatrix},\quad \left[\bar{B}_{bj}\right]=\begin{bmatrix}0 & 0 & z\bar{N}_{j,x}\\ 0 & -z\bar{N}_{j,y} & 0\\ 0 & z\bar{N}_{j,x} & -z\bar{N}_{j,y}\end{bmatrix} \tag{A-33}$$

$$\left[B_{si}\right]=\begin{bmatrix}N_{i,y} & -N_i & 0\\ N_{i,x} & 0 & N_i\end{bmatrix},\ \left[\bar{B}_{sj}\right]=\begin{bmatrix}\bar{N}_{j,y} & -\bar{N}_j & 0\\ \bar{N}_{j,x} & 0 & \bar{N}_j\end{bmatrix} \tag{A-34}$$

The strain-displacement relation matrix is also needed to modify to pass the patch test. Thus, the modified matrix can be expressed:

$$\left[\left(\bar{B}_{bj}\right)^*\right]=\begin{bmatrix}0 & 0 & z\left(\bar{N}_{j,x}\right)^*\\ 0 & -z\left(\bar{N}_{j,y}\right)^* & 0\\ 0 & z\left(\bar{N}_{j,x}\right)^* & -z\left(\bar{N}_{j,y}\right)^*\end{bmatrix} \tag{A-35}$$

$$\left[\left(\bar{B}_{sj}\right)^*\right]=\begin{bmatrix}\left(\bar{N}_{j,y}\right)^* & -\left(\bar{N}_j\right)^* & 0\\ \left(\bar{N}_{j,x}\right)^* & 0 & \left(\bar{N}_j\right)^*\end{bmatrix} \tag{A-36}$$

To overcome the problems of Reissner-Mindlin plate-bending elements, such as shear locking which is the excessive flexural stiffness due to the transverse displacement constraint, various remedy has been proposed, like the introduction of reduced or selective integration techniques or the use of constrained substitutive shear strain fields (Oñate et al. 1992). The natural shear strains can be assumed as a linear relationship, for the four node rectangular element, using the natural coordinate system, ξ, η:

$$\bar{\gamma} = \begin{Bmatrix} \gamma_\xi \\ \gamma_\eta \end{Bmatrix} = \begin{bmatrix} 1 & \eta & 0 & 0 \\ 0 & 0 & 1 & \xi \end{bmatrix} \begin{Bmatrix} \alpha_1 \\ \alpha_2 \\ \alpha_3 \\ \alpha_4 \end{Bmatrix} = A\alpha \tag{A-37}$$

The Cartesian shear strains can be directly obtained as:

$$\gamma = \begin{Bmatrix} \gamma_{yz} \\ \gamma_{xz} \end{Bmatrix} = J^{-1}\bar{\gamma} \tag{A-38}$$

where *J* is the standard 2x2 Jacobian matrix of the transformation $(x, y) \rightarrow (\xi, \eta)$.

Then, the tangential shear strains along the element at edge *j-k* can be also computed from the natural shear strains:

$$\gamma_{edge}^{j-k} = \left(\cos \beta_{edge}^{j-k}\right)\gamma_\xi + \left(\sin \beta_{edge}^{j-k}\right)\gamma_\eta \tag{A-39}$$

where β_{edge}^{j-k} is the angle that the direction of the element edge *j-k* forms with ξ direction.

The tangential shear strains γ_{edge} are sampled at four selected points along natural directions (ξ, η), as shown in Figure A.8.

Thus, substituting Equation (A-39) in Equation (A-37) and sampling the resulting equation at i^{th} sampling points on the edge *j-k* the following system of equations can be obtained:

$$P\left(\xi_i, \eta_i, \beta_{edge}^{j-k}\right)\alpha = \gamma_{edge} \tag{A-40}$$

$$\alpha = P^{-1} \cdot \gamma_{edge} \tag{A-41}$$

where γ_{edge} contains the prescribed shear strains at the sampling points and denotes $\gamma_{edge} = \left\{\gamma_{edge}^{1-2} \quad \gamma_{edge}^{3-4} \quad \gamma_{edge}^{2-3} \quad \gamma_{edge}^{4-1}\right\}^T$.

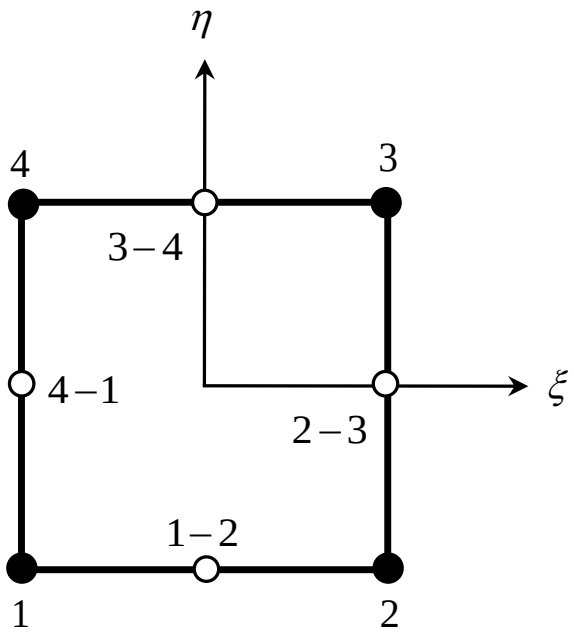

Figure A.8: Four sampling points for tangential shear strains.

The relationship between the tangential shear strains and the natural shear strains at sampling points can be explained by a simple transformation:

$$\gamma_{edge} = \begin{bmatrix} 1 & 0 & 0 & 0 & 0 & 0 & 0 & 0 \\ 0 & 0 & 1 & 0 & 0 & 0 & 0 & 0 \\ 0 & 0 & 0 & 0 & 1 & 0 & 0 & 0 \\ 0 & 0 & 0 & 0 & 0 & 0 & 0 & 1 \end{bmatrix} \begin{Bmatrix} \gamma_{\xi}^{1-2} \\ \gamma_{\eta}^{1-2} \\ \gamma_{\xi}^{3-4} \\ \gamma_{\eta}^{3-4} \\ \gamma_{\xi}^{2-3} \\ \gamma_{\eta}^{2-3} \\ \gamma_{\xi}^{4-1} \\ \gamma_{\eta}^{4-1} \end{Bmatrix} = T\tilde{\gamma} \qquad \text{(A-42)}$$

The natural shear strains can be transformed to the Cartesian shear strains at the sampling points by the use of the Jacobian matrix:

$$\tilde{\gamma} = \begin{Bmatrix} \gamma_{\xi}^{1-2} \\ \gamma_{\eta}^{1-2} \\ \gamma_{\xi}^{3-4} \\ \gamma_{\eta}^{3-4} \\ \gamma_{\xi}^{2-3} \\ \gamma_{\eta}^{2-3} \\ \gamma_{\xi}^{4-1} \\ \gamma_{\eta}^{4-1} \end{Bmatrix} = \begin{bmatrix} J_1^{1-2} & 0 & 0 & 0 & 0 & 0 & 0 & 0 \\ 0 & J_1^{1-2} & 0 & 0 & 0 & 0 & 0 & 0 \\ 0 & 0 & J_2^{3-4} & 0 & 0 & 0 & 0 & 0 \\ 0 & 0 & 0 & J_2^{3-4} & 0 & 0 & 0 & 0 \\ 0 & 0 & 0 & 0 & J_3^{2-3} & 0 & 0 & 0 \\ 0 & 0 & 0 & 0 & 0 & J_3^{2-3} & 0 & 0 \\ 0 & 0 & 0 & 0 & 0 & 0 & J_4^{4-1} & 0 \\ 0 & 0 & 0 & 0 & 0 & 0 & 0 & J_4^{4-1} \end{bmatrix} \begin{Bmatrix} \gamma_{yz}^{1-2} \\ \gamma_{xz}^{1-2} \\ \gamma_{yz}^{3-4} \\ \gamma_{xz}^{3-4} \\ \gamma_{yz}^{2-3} \\ \gamma_{xz}^{2-3} \\ \gamma_{yz}^{4-1} \\ \gamma_{xz}^{4-1} \end{Bmatrix} = C\hat{\gamma} \qquad \text{(A-43)}$$

where J_i^{j-k} is the standard 2x2 jacobian matrix the i^{th} sampling points located at *j*-*k* edge.

The Cartesian shear strains at the sampling points located at *j*-*k* edge are related to the nodal displacement by:

$$\hat{\gamma} = \begin{Bmatrix} \gamma_{yz}^{1-2} \\ \gamma_{xz}^{1-2} \\ \gamma_{yz}^{3-4} \\ \gamma_{xz}^{3-4} \\ \gamma_{yz}^{2-3} \\ \gamma_{xz}^{2-3} \\ \gamma_{yz}^{4-1} \\ \gamma_{xz}^{4-1} \end{Bmatrix} = \begin{bmatrix} B_s^{1-2} & 0 & 0 & 0 \\ 0 & B_s^{3-4} & 0 & 0 \\ 0 & 0 & B_s^{2-3} & 0 \\ 0 & 0 & 0 & B_s^{4-1} \end{bmatrix} \begin{Bmatrix} u_1 \\ u_2 \\ u_3 \\ u_4 \end{Bmatrix} = B_s u \tag{A-44}$$

where B_s^{j-k} is the standard shear strain matrix of Equation (A-34) and u_i is the displacement at i^{th} node, defined $u_i = \begin{Bmatrix} w_i & \theta_{xi} & \theta_{yi} \end{Bmatrix}^T$.

Therefore, the substitute shear strain matrix can be obtained from the combining Equation (A-37), Equation (A-38), and Equation (A-41) ~ Equation (A-44) :

$$\gamma = J^{-1} A\alpha = J^{-1} A P^{-1} \gamma_{edge} = J^{-1} A P^{-1} T \hat{\gamma} = J^{-1} A P^{-1} T C B_s u = \tilde{B}_s u \tag{A-45}$$

where $\tilde{B}_s = J^{-1} A P^{-1} T C B_s$.

Finally, the stiffness matrix of improved plate-bending element can be expressed as the following form:

$$\left[k_e\right]=\begin{bmatrix}\left[k_{CC}\right] & \left[k_{CI}\right]\\ \left[k_{CI}\right]^T & \left[k_{II}\right]\end{bmatrix} \tag{A-46}$$

where $\left[k_{CC}\right]$ represents a compatible matrix only, $\left[k_{CI}\right]$ represents a compatible and incompatible mixed matrix, and $\left[k_{II}\right]$ represents a incompatible matrix only, where they can be defined as

$$\left[k_{CC}\right]=\int_V\left[B_b\right]^T\left[D_b\right]\left[B_b\right]dV+\int_V\left[\tilde{B}_s\right]^T\left[D_s\right]\left[\tilde{B}_s\right]dV \tag{A-47}$$

$$\left[k_{CI}\right]=\int_V\left[B_b\right]^T\left[D_b\right]\left[\bar{B}_b^*\right]dV+\int_V\left[\tilde{B}_s\right]^T\left[D_s\right]\left[\bar{B}_s^*\right]dV \tag{A-48}$$

$$\left[k_{II}\right]=\int_V\left[\bar{B}_b^*\right]^T\left[D_b\right]\left[\bar{B}_b^*\right]dV+\int_V\left[\bar{B}_s^*\right]^T\left[D_s\right]\left[\bar{B}_s^*\right]dV \tag{A-49}$$

where D_b and D_s are the material property matrix for bending and shear rigidity, respectively.

The stiffness matrix is also oversized due to the introduction of incompatible mode, so the static condensation algorithm can be applied again to condense it. Then, Equation (A-46) can be reformulated:

$$\left[k_{plate}\right]=\left[k_{CC}\right]-\left[k_{CI}\right]\left[k_{II}\right]^{-1}\left[k_{CI}\right]^T \tag{A-50}$$

The additional incompatible modes and numerical integration schemes for bending and shear components, which are used to improve the elements behavior, are summarized in Table A.2.

Table A.2: Additional modes and integration schemes for Reissner-Mindlin plate-bending elements.

Incompatible Mode	Integration Schemes				
	$[k_{CC}]$	$[k_{CI}]$		$[k_{II}]$	
		Bending	Shear	Bending	Shear
$\bar{N}_1 \sim \bar{N}_3$, $\bar{N}_6$, and $\bar{N}_7$	2x2	3x3	2x2	3x3	2x2

Again, detailed explanation of shape function for compatible and incompatible modes, and its modified and the integration techniques can be found in Appendix B and Appendix D of this dissertation, respectively.

A.3.3 FLAT SHELL ELEMENTS

As mentioned earlier, flat shell elements can be established by the combination of membrane and plate-bending elements, so the stiffness matrix can be expressed as the following form:

$$\left[k_{flat}\right] = \begin{bmatrix} \left[k_{plate}\right] & 0 \\ 0 & \left[k_{membrane}\right] \end{bmatrix} \tag{A-51}$$

Typically, while all the nodes of the 3-node flat shell element are coplanar, nodes of a 4-node flat shell element in a warped mesh are not coplanar. To remove the problem, the rigid link correction, initially proposed by Taylor (1987), is needed. To do this, the mean plane is formed by center point of each side. The distance of mean plane and nodes are same (Naganarayana and Prathap 1989; Cook 1994). And then the stiffness matrix is constructed at a mean plane which is the projection of warped geometry, shown in Figure A.9.

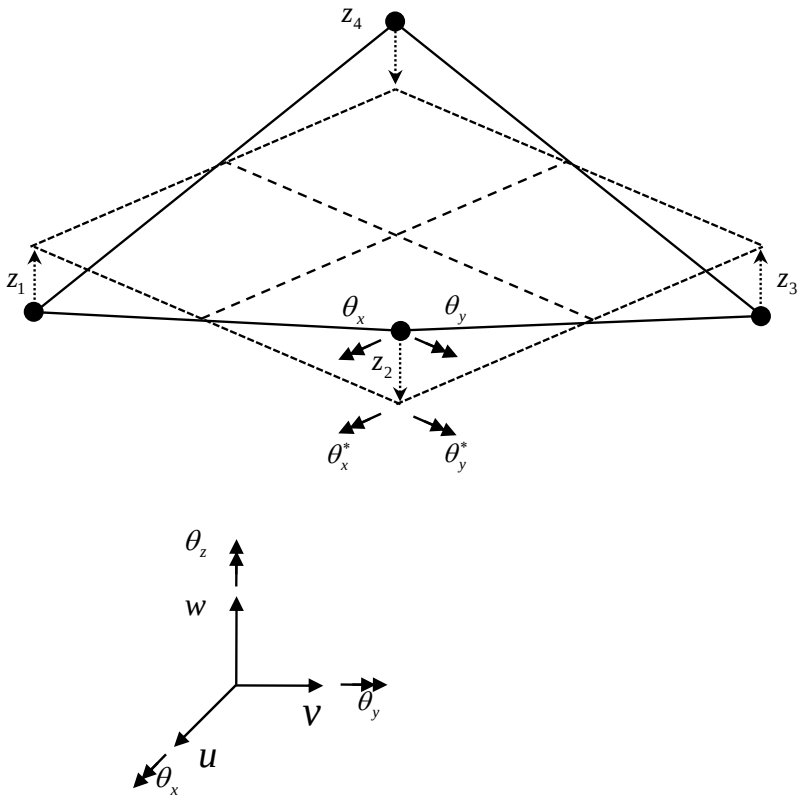

Figure A.9: Projection of warped Geometry.

The warped transformation matrix can be expressed as:

$$\left\{u_i^*\right\} = \begin{Bmatrix} u_i^* \\ v_i^* \\ w_i^* \\ \theta_{xi}^* \\ \theta_{yi}^* \\ \theta_{zi}^* \end{Bmatrix} = \begin{bmatrix} 1 & 0 & 0 & 0 & 0 & 0 \\ 0 & 1 & 0 & 0 & 0 & 0 \\ 0 & 0 & 1 & 0 & 0 & 0 \\ 0 & z_i & 0 & 1 & 0 & 0 \\ -z_i & 0 & 0 & 0 & 1 & 0 \\ 0 & 0 & 0 & 0 & 0 & 1 \end{bmatrix} \begin{Bmatrix} u_i \\ v_i \\ w_i \\ \theta_{xi} \\ \theta_{yi} \\ \theta_{zi} \end{Bmatrix} = \left[W\right]\left\{u_i\right\} \tag{A-52}$$

where z_i defines the warp at each node and quantities with a superscript u_i^* act on the flat projection.

The stiffness matrix including warped geometry effects can be expressed as:

$$\left[k_{local}\right] = \left[W\right]\left[k_{flat}\right]\left[W\right]^T \tag{A-53}$$

where $\left[W\right]$ is the warped transformation matrix.

A.3.4 FORCE VECTOR

Shell element can also have two types of load like a concentrated load on the nodal point and the distributed pressure on the surface. The pressure loads can be transformed into equivalent nodal loads by using the shape function of the element.

$$P = \int_S \{N\}^T \{\Phi\} dS \tag{A-54}$$

The equivalent load can be computed for an arbitrary load shapes by using Equation (A-54). The calculation can be quite a simple when the pressure is assumed to be applied only on the local *x*-*y* plane, i.e. force has only local *z* direction components. If the pressure loads has *w* magnitude and applied on the local *x*-*y* plane of the element, shown in Figure A.10, then the equivalent nodal loads can be calculated as:

$$P_i = \frac{1}{4} w \tag{A-55}$$

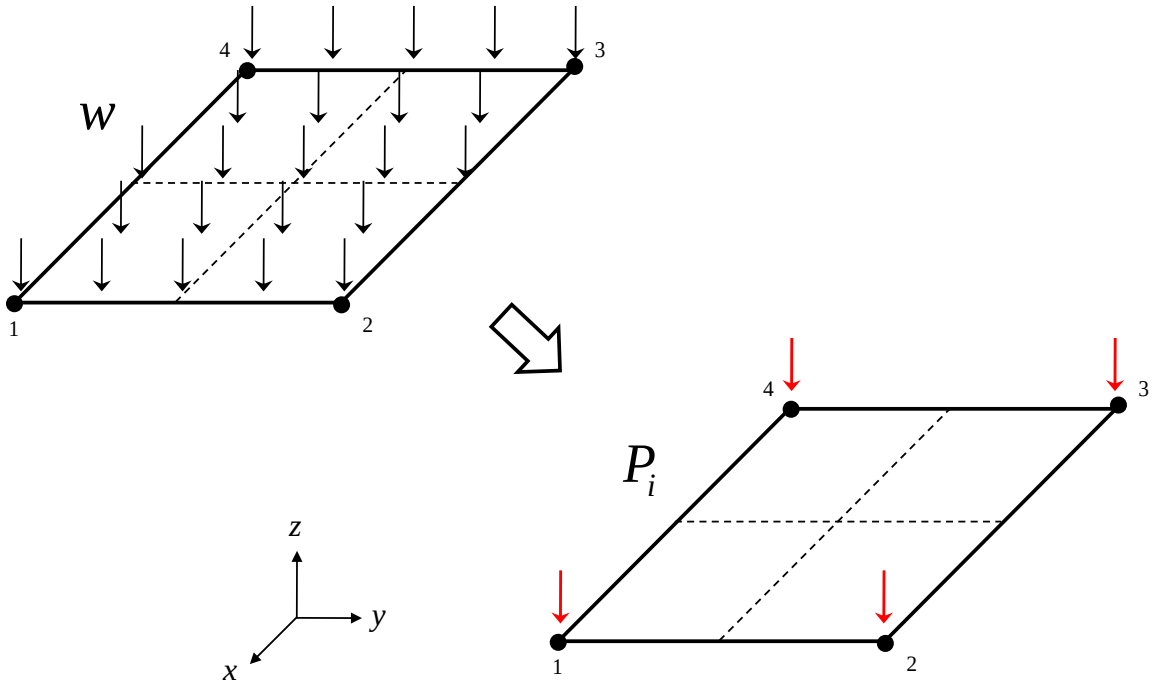

Figure A.10: Pressure loads and its equivalent nodal loads.

A.3.5 TRANSFORMATION MATRIX

Transformation matrix for the shell element can be obtained in similar approach described in the frame element. The only difference is that there is no need to define the reference point 3, as there are already four nodes for the shell element. The local and global coordinate system is in Figure A.11. Transformation matrix [T] can be defined as the following form:

$$[T]=\begin{bmatrix} [\lambda] & [0] & [0] & [0] \\ [0] & [\lambda] & [0] & [0] \\ [0] & [0] & [\lambda] & [0] \\ [0] & [0] & [0] & [\lambda] \end{bmatrix} \tag{A-56}$$

where $[0]$ is a 3×3 zero matrix, $[\lambda]$ is a direction cosine matrix exactly same as the direction cosine matrix of the frame element, see Equation (A-3) for detailed explanation.

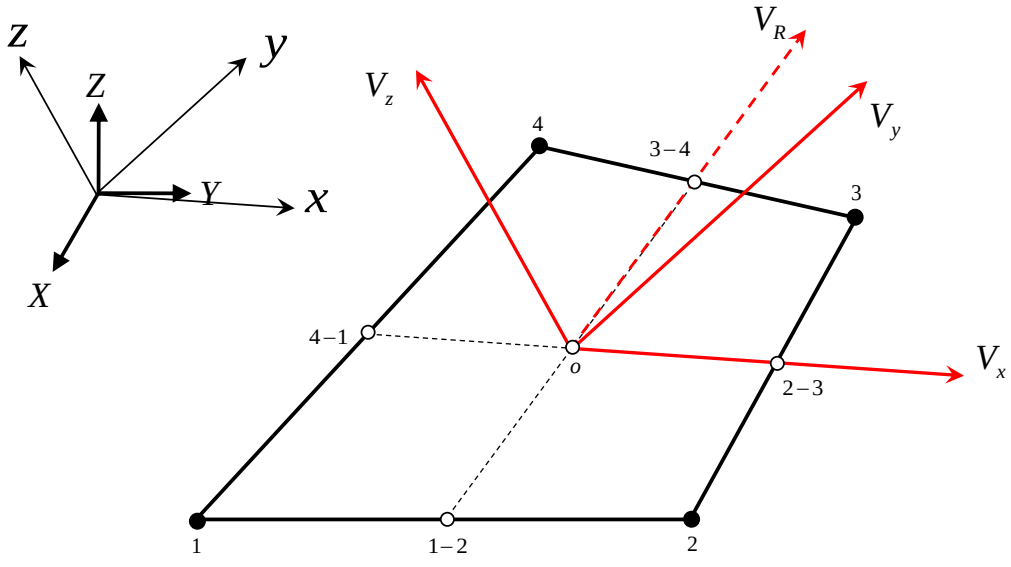

Figure A.11: Local and global coordinate systems of the shell element.

The direction cosine matrix can be obtained from the coordinates of the mid-point of the sides 2-3 and center point as follows:

$$l_1 = \frac{x_{2-3} - x_o}{L_e}, \quad m_1 = \frac{y_{2-3} - y_o}{L_e}, \quad n_1 = \frac{z_{2-3} - z_o}{L_e} \tag{A-57}$$

where (x_{2-3}, y_{2-3}, and z_{2-3}) are coordinate components of the mid-point of the node 2 and 3, defined as $x_{2-3} = \frac{x_2 + x_3}{2}$ and the same way to the y_{2-3} and z_{2-3}, (x_o, y_o, and z_o) are coordinate components of the center point, and L_e is a distance between the mid-point 2-3 and the center point defined as $L_e = \sqrt{\left(x_{2-3} - x_o\right)^2 + \left(y_{2-3} - y_o\right)^2 + \left(z_{2-3} - z_o\right)^2}$.

Rest of two direction cosine matrices can be computed from vector calculations. Let $V_x = \{l_1 \quad m_1 \quad n_1\}^T$ denote the unit vector along the local *x-axis*. Then the reference unit vector along the mid-point of the node 3 and 4 and the center point can be defined as:

$$V_R = \left\{ \frac{x_{3-4} - x_o}{L_R} \quad \frac{y_{3-4} - y_o}{L_R} \quad \frac{z_{3-4} - z_o}{L_R} \right\}^T \tag{A-58}$$

where (x_{3-4}, y_{3-4}, and z_{3-4}) are coordinate components of the mid-point of the node 3 and 4, and L_R is a distance between the mid-point 3-4 and the center point defined as $L_R = \sqrt{\left(x_{3-4} - x_o\right)^2 + \left(y_{3-4} - y_o\right)^2 + \left(z_{3-4} - z_o\right)^2}$.

The unit vector along the local *z-axis* , which can be obtained from cross product of V_x and V_R , is given by the following form:

$$V_z = \{l_3 \quad m_3 \quad n_3\}^T = \frac{V_x \times V_R}{|V_x \times V_R|} \tag{A-59}$$

Finally, the direction cosines along local *y-axis* , which can be computed from cross product of V_z and V_x, are given by the following form:

$$V_y = \{l_2 \quad m_2 \quad n_2\}^T = V_z \times V_x \tag{A-60}$$

A.4 SPRING ELEMENTS

A sheathing-to-framing connector can be represented as a two-node element, depicted in Figure A.12.

One is the location of the nail head in the sheathing panel and the other is the location of the nail tail in the wood framing. The connector has a rotational resistance but it is relatively small enough to be neglected (Folz and Filiatrault 2001; Judd and Fonseca 2005). Thus, it can have three DOF corresponding to in- and out-plane translations. One might think that the connector can have a rotational stiffness as a small value to obtain numerical stability issue. In this case an element can be six DOFs per each node.

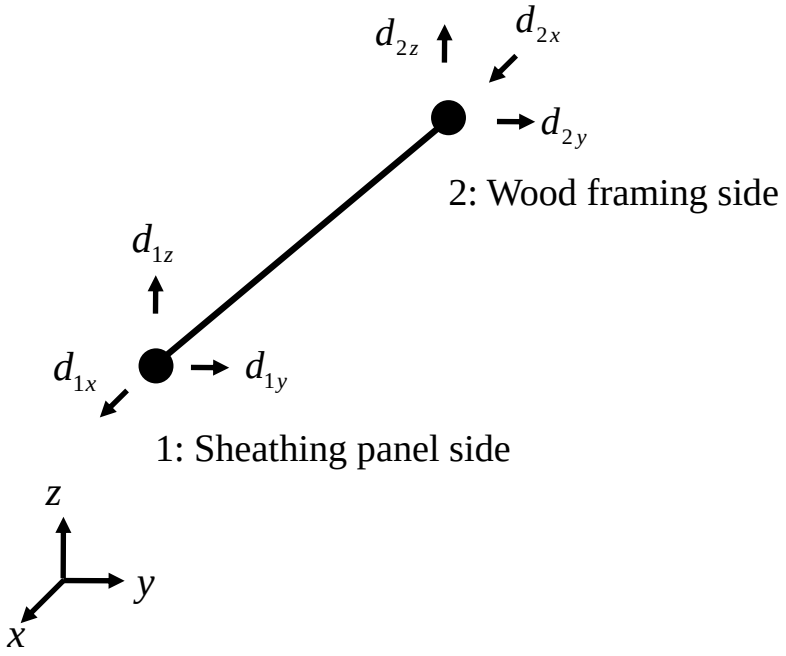

Figure A.12: A sheathing-to-framing connector element.

Then, the structural behavior of the connector can be modeled by using nonlinear hysteretic spring model to simulate its load-deformation characteristics (Folz and Filiatrault 2001; Judd 2005; Xu and Dolan 2009b). In their work, the connector was represented using two hysteretic spring pair model as a shear element, shown in Figure A.13.

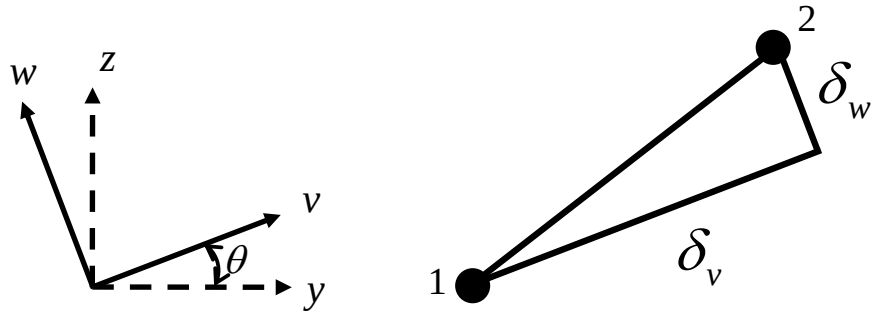

Figure A.13: The shear element as two directional spring pair model.

Additionally, axial stiffness is introduced to express a 3D element in this study. Thus, the connector can be established by using three individual hysteretic spring elements: one is for an axial direction which is local *x* coordinate and the others are for shear directions, local *y* and *z* coordinate system. Numerically, there is no link, related to stiffness and force, between axial direction and shear directions. But one can think that one of three direction's failure is directly related to the failure of the connector, thus this relation should be considered in model numerically.

A.4.1 ELEMENT STIFFENSS MATRIX

An element stiffness matrix can be built by using a combination of axial and shear stiffness. Typical spring / bar element was accepted to express axial component and oriented spring pair model was used to establish shear component. Shear deformations in this model can be separated into two components which are initial displacement trajectory component (*v*-direction) and off-directional component (*w*-direction), shown in Figure A.14. The initial displacement trajectory can be obtained as a deformation of linear static analysis or a displacement of time-history analysis at time zero (Judd 2005). The stiffness of each direction can be computed using CUREE model for shear directions. Thus, the element stiffness matrix of the connector can be expressed as the following form:

$$[k_e] = [k_{axial}] + [k_{shear}] = \begin{bmatrix} [k_s] & -[k_s] \\ -[k_s] & [k_s] \end{bmatrix} \tag{A-61}$$

where $[k_s] = \begin{bmatrix} k_{xx} & 0 & 0 & 0 & 0 & 0 \\ 0 & k_{yy} & k_{yz} & 0 & 0 & 0 \\ 0 & k_{zy} & k_{zz} & 0 & 0 & 0 \\ 0 & 0 & 0 & k_{\infty} & 0 & 0 \\ 0 & 0 & 0 & 0 & k_{\infty} & 0 \\ 0 & 0 & 0 & 0 & 0 & k_{\infty} \end{bmatrix}$, k_{∞} is a stabilizing stiffness, i.e. a small number, k_{xx} is a stiffness component of axial direction, i.e. stabilizing stiffness also, k_{yy}, k_{yz}, k_{zy}, and k_{zz} are stiffness components of shear direction, which can be defined as the following forms:

$$\begin{aligned} k_{yy} &= k_v \cos^2\theta + k_w \sin^2\theta \\ k_{yz} &= k_{zy} = (k_v - k_w)\cos\theta \sin\theta \\ k_{zz} &= k_v \sin^2\theta + k_w \cos^2\theta \end{aligned} \tag{A-62}$$

where k_v and k_w are stiffness component of *v*- and *w*- direction, respectively, and θ is the angle between the *v*- and *y*- direction, shown in Figure A.14.

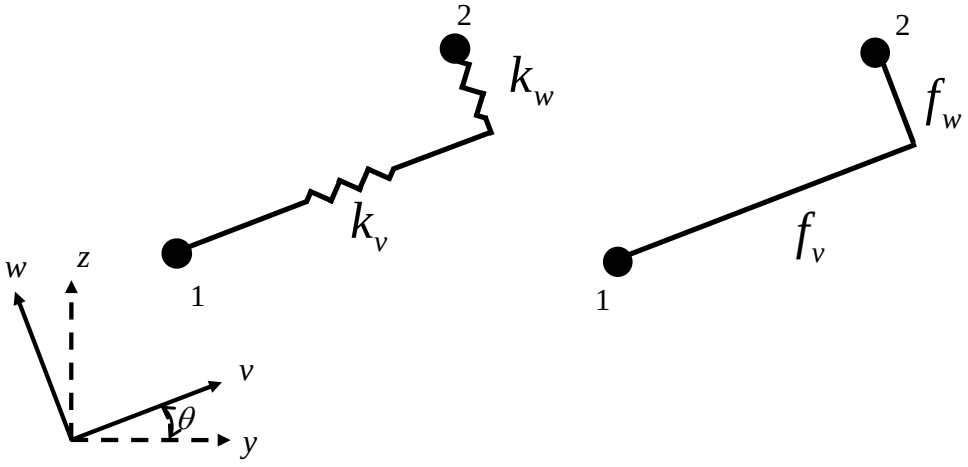

Figure A.14: Two components of the shear element.

Typically, the tangent stiffness of the fasteners, i.e. nail, is needed in solving a nonlinear system equation and they can be obtained from the instantaneous slope along the current branch of the hysteretic model to perform the nonlinear analysis.

A.4.2 FORCE VECTOR

Force vector can be also derived similar way like the stiffness matrix, i.e. the combinations of axial and shear forces, and it can be defined as the following form:

$$\{r_e\} = \{f_{axial}\} + \{f_{shear}\} = \begin{Bmatrix} f_s \\ -f_s \end{Bmatrix} \tag{A-63}$$

where $\{f_s\} = \{f_x \quad f_y \quad f_z \quad m_\infty \quad m_\infty \quad m_\infty\}^T$, m_∞ is a local moment related to the numerical stability, f_x is a axial force , and f_y and f_z are shear forces defined as

$$\begin{aligned} f_y &= f_v \cos\theta - f_w \sin\theta \\ f_z &= f_v \sin\theta + f_w \cos\theta \end{aligned} \tag{A-64}$$

where f_v and f_w are the force of *v* and *w* direction and θ is the angle between the *v*- and *y*- direction, shown in Figure A.14.

A.4.3 TRANSFORMATION MATRIX

Initially, two-node of the connector has the same nodal point and it has a zero length. Node of the connector can be the first point, i.e. point 1, and additional two more points are needed to determine a transformation matrix for the connector element, i.e. point 2 and 3 are needed. After that, local stiffness matrix and force vector of the connector can be followed typical transformation rule to obtain global coordinate system similar like the frame elements. Thus, the approach of the transformation matrix for the frame elements is accepted in here to define that for the connector.

A.5 NUMERICAL SOLVER FOR NONLINEARITY

The Newton-Raphson iteration technique has been adopted to solve the nonlinear system equation. Especially, an incremental-iterative displacement control solution strategy is adopted to analyze the wall structure under monotonic and cyclic loading conditions (Batoz and Dhatt 1979; Ramm 1981; Rose 1994). The incremental equilibrium equations at load-step i and i+1 can be expressed as:

$$^{(i+1)}K_T\,^{(i+1)}\Delta\delta = {}^{(i+1)}\Delta\lambda F_0 + {}^{(i)}R \tag{A-65}$$

$$^{(i)}R = {}^{(i)}F - {}^{(i)}K_S\,{}^{(i)}\delta \tag{A-66}$$

$$^{(i+1)}\Delta\delta = {}^{(i+1)}\Delta\lambda\Delta\delta^F + {}^{(i)}\Delta\lambda\Delta\delta^R \tag{A-67}$$

$$^{(i+1)}K_T\,^{(i+1)}\Delta\delta^F = F_0, \quad {}^{(i+1)}K_T\,{}^{(i+1)}\Delta\delta^R = {}^{(i)}R \tag{A-68}$$

where K_S is the global secant stiffness matrix, K_T is the global tangent stiffness matrix, $\Delta\lambda$ is the incremental load factor applied to the reference global load vector F_0, $\Delta\delta$ is the incremental global displacement, and *R* is the global residual force vector.

The load factor can be determined at prescribed displacement as:

$$^{(i+1)}\Delta\lambda = -\frac{^{(i+1)}\Delta\delta_p^R}{^{(i+1)}\Delta\delta_p^F} \tag{A-69}$$

where $^{(i+1)}\Delta\delta_p^F$ is the prescribed displacement at *i*+1 step of the reference load vector, i.e. a target displacement of the system in displacement control schemes, and $^{(i+1)}\Delta\delta_p^R$ is the displacement at *i*+1 step of the residual load vector.

Subsequent iterations are employed until a predefined convergence criterion is satisfied for a given displacement, shown in Figure A.15 (Batoz and Dhatt 1979; Ramm 1981; Crisfield 1991; Bathe 1996). Finally, the displacement and forces of the system can be computed:

$$^{(i+1)}\delta = ^{(i)}\delta + ^{(i+1)}\Delta\delta \tag{A-70}$$

$$^{(i+1)}F = ^{(i+1)}\Delta\lambda F_0 \tag{A-71}$$

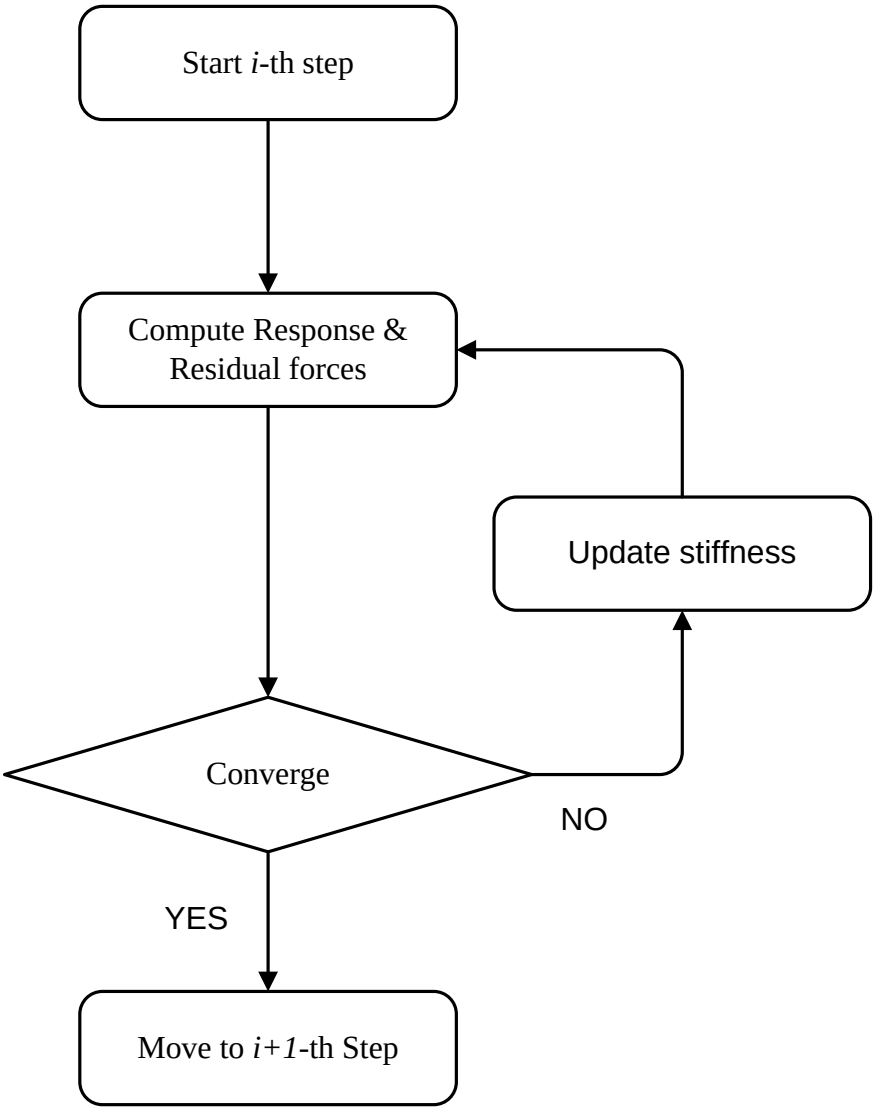

Figure A.15: Overall procedure for the non-linear Newton-Raphson iteration technique.

Generally, the Newton-Raphson iteration technique uses two kinds of convergence criteria: force based and displacement based. The force based convergence is defined as the ratio of the unbalanced load to incremental force; on the other hand, the displacement based convergence criterion is defined as the ratio of the first iteration to the last iteration displacements, adopted in this dissertation work:

$$\varepsilon_F = \frac{\left|\left\{{}^{(i)}R_j\right\}\right|}{\left|\left\{{}^{(i)}\Delta F\right\}\right|}, \quad \varepsilon_D = \frac{\left|\left\{{}^{(i)}\Delta\delta_j\right\}\right|}{\left|\left\{{}^{(i)}\Delta\delta_1\right\}\right|} \tag{A-72}$$

where ε is the convergence criterion, i and j denotes j^{th} substep of i^{th} step, R is the residual force vector, and other are explained in Figure A.16.

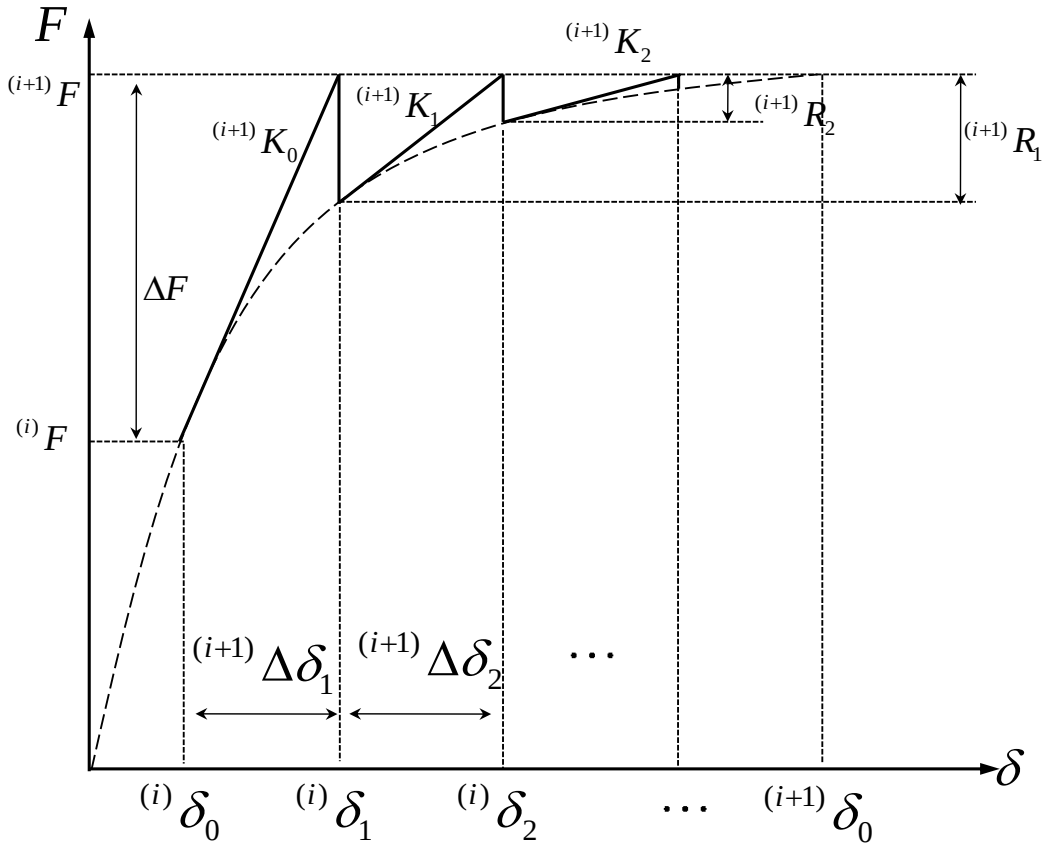

Figure A.16: Schematic view of the Newton-Raphson iteration technique.

APPENDIX B

SHAPE FUNCTIONS AND THEIR DERIVATIVES

B.1 OVERVIEW

Conforming mode shape functions, which are typical, and non-conforming mode shape functions are introduced and their derivatives are presented in here.

B.2 CONFORMING MODES SHAPE FUNCTIONS

Rectangular quadrilateral shape functions, tabulated in Table B.1 and illustrated in Figure B.1, are used to represent a conforming mode.

Table B.1: Conforming mode shape functions and their derivatives.

Shape Function	Derivative	
	with respect to ξ	with respect to η
$N_1 = \frac{1}{4}(1-\xi)(1-\eta)$	$\frac{\partial N_1}{\partial \xi} = \frac{1}{4}(-1+\eta)$	$\frac{\partial N_1}{\partial \eta} = \frac{1}{4}(-1+\xi)$
$N_2 = \frac{1}{4}(1+\xi)(1-\eta)$	$\frac{\partial N_2}{\partial \xi} = \frac{1}{4}(1-\eta)$	$\frac{\partial N_2}{\partial \eta} = \frac{1}{4}(-1-\xi)$
$N_3 = \frac{1}{4}(1+\xi)(1+\eta)$	$\frac{\partial N_3}{\partial \xi} = \frac{1}{4}(1+\eta)$	$\frac{\partial N_3}{\partial \eta} = \frac{1}{4}(1+\xi)$
$N_4 = \frac{1}{4}(1-\xi)(1+\eta)$	$\frac{\partial N_4}{\partial \xi} = \frac{1}{4}(-1-\eta)$	$\frac{\partial N_4}{\partial \eta} = \frac{1}{4}(1-\xi)$

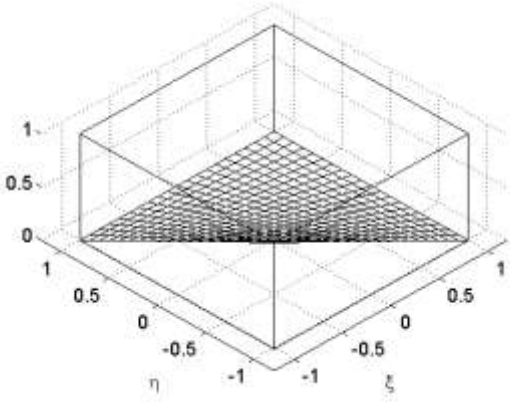

N_1

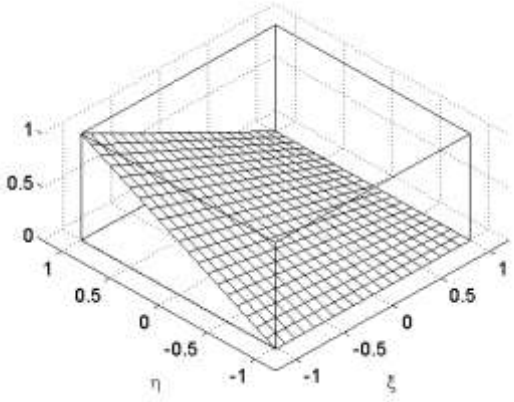

N_2

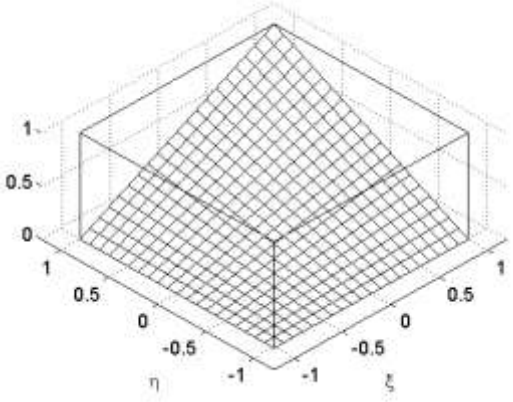

N_3

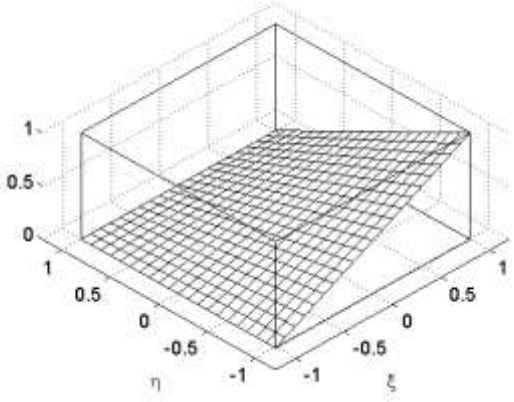

N_4

Figure B.1: Shape functions for conforming modes.

B.3 NON-CONFORMING MODES SHAPE FUNCTIONS

Shape functions for Non-conforming modes are used in this dissertation due to improve element efficiency. Seven shape functions are investigated in order to improve a performance of an element and to overcome their known drawbacks. Shape functions and their derivatives are summarized in Table B.2 and illustrated in Figure B.2.

Table B.2: Non-conforming modes shape functions and their derivatives.

Shape Function	Derivative	
	with respect to ξ	with respect to η
$\bar{N}_1 = (1-\xi^2)$	$\frac{\partial \bar{N}_1}{\partial \xi} = -2\xi$	$\frac{\partial \bar{N}_1}{\partial \eta} = 0$
$\bar{N}_2 = (1-\eta^2)$	$\frac{\partial \bar{N}_2}{\partial \xi} = 0$	$\frac{\partial \bar{N}_2}{\partial \eta} = -2\eta$
$\bar{N}_3 = (1-\xi^2)(1-\eta^2)$	$\frac{\partial \bar{N}_3}{\partial \xi} = -2\xi(1-\eta^2)$	$\frac{\partial \bar{N}_3}{\partial \eta} = -2\eta(1-\xi^2)$
$\bar{N}_4 = (1-\xi^2)\eta$	$\frac{\partial \bar{N}_4}{\partial \xi} = -2\xi\eta$	$\frac{\partial \bar{N}_4}{\partial \eta} = (1-\xi^2)$
$\bar{N}_5 = (1-\eta^2)\xi$	$\frac{\partial \bar{N}_5}{\partial \xi} = (1-\eta^2)$	$\frac{\partial \bar{N}_5}{\partial \eta} = -2\xi\eta$
$\bar{N}_6 = (1-\xi^2)\xi\eta$	$\frac{\partial \bar{N}_6}{\partial \xi} = \eta(1-3\xi^2)$	$\frac{\partial \bar{N}_6}{\partial \eta} = (1-\xi^2)\xi$
$\bar{N}_7 = (1-\eta^2)\xi\eta$	$\frac{\partial \bar{N}_7}{\partial \xi} = (1-\eta^2)\eta$	$\frac{\partial \bar{N}_7}{\partial \eta} = \xi(1-3\eta^2)$

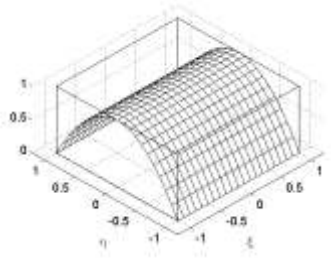

$\bar{N}_1$

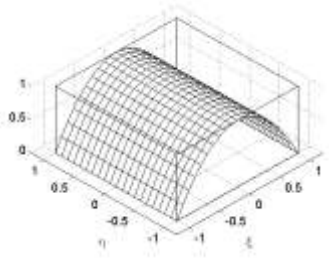

$\bar{N}_2$

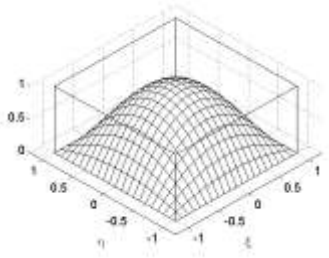

$\bar{N}_3$

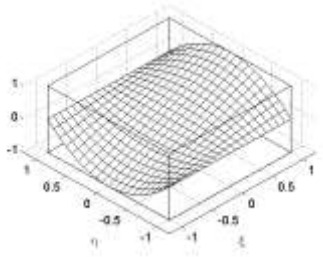

$\bar{N}_4$

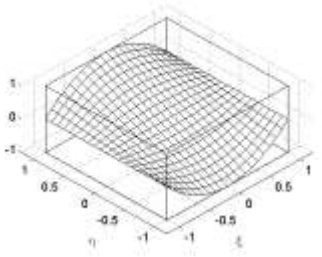

$\bar{N}_5$

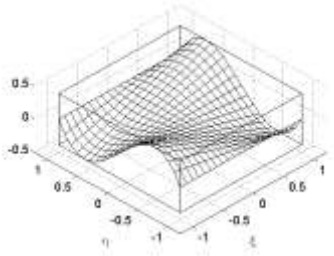

$\bar{N}_6$

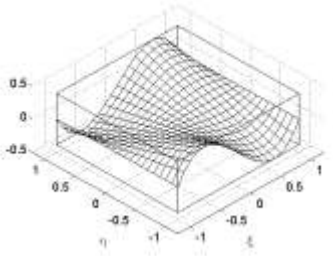

$\bar{N}_7$

Figure B.2: Shape functions for non-conforming modes.

APPENDIX C

DIRECT MODIFICATION SCHEME

C.1 OVERVIEW

The introduction of non-conforming modes improves the element behavior significantly but it may lead to fail in passing the patch test. To overcome this defect, direct modification scheme is proposed (Choi et al. 2002). Initially, the scheme corrects the strains due to non-conforming modes directly. Therefore, it always guarantees to pass the patch test and less computational cost.

C.2 DIRECT MODIFICATION SCHEME

Two types of correction constant are investigated. One is the derivative of the shape function and the other is the shape function itself. The correction constants for the derivative are able to make the integration of strain modes due to non-conforming displacements in an element domain zero, illustrated in Figure C.1. Therefore, the correction constant is shifted up or down by the amount, thus the summation is equal to zero.

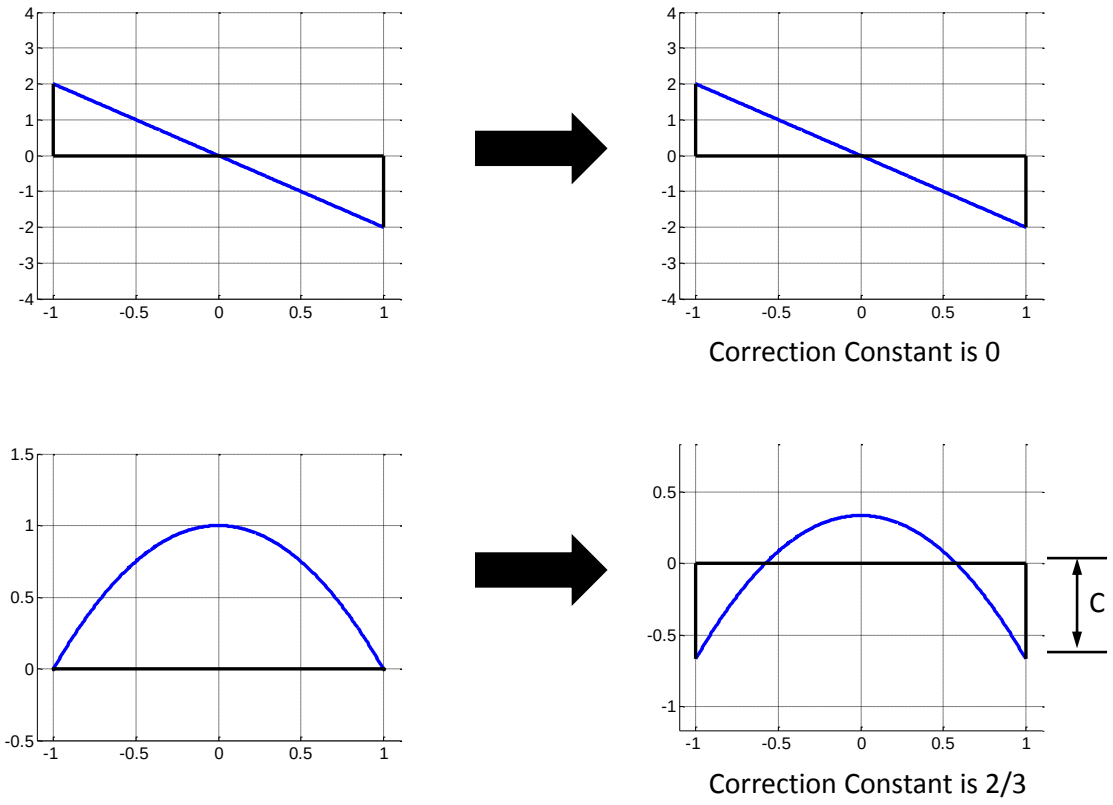

Figure C.1: Schematic overview of an introduction of correction constants.

The correction constants for derivatives can be expressed as:

$$\int_{-1}^{1}\int_{-1}^{1}\left(\frac{\partial \bar{N}_j}{\partial \xi_\alpha}+C_j^\alpha\right)d\xi d\eta = 0 \qquad \text{(C-1)}$$

where $\bar{N}_i$ is the shape function of non-conforming mode, C_i^α, i.e. C_i^ξ and C_i^η, is the correction constants and it can be evaluated numerically for each non-conforming modes.

$$C_j^{\alpha} = -\frac{1}{4}\int_{-1}^{1}\int_{-1}^{1}\frac{\partial \bar{N}_j}{\partial \xi_{\alpha}}d\xi d\eta \tag{C-2}$$

Derivatives of non-conforming modes with respect to the global coordinate system x_k can be obtained in a manner:

$$\left(\frac{\partial \bar{N}_j}{\partial x_k}\right)^{*} = \frac{|J(0,0)|}{|J(\xi,\eta)|}\sum_{\alpha=1}^{2}\left\{J_{k\alpha}^{-1}(0,0)\left(\frac{\partial \bar{N}_j}{\partial \xi_{\alpha}} + C_j^{\alpha}\right)\right\} \tag{C-3}$$

Especially, the correction constants for both the non-conforming mode shape function and its derivatives are needed when non-conforming modes are used in rotational fields. It can be expressed as following equation by adding a correction constant d_j to the non-conforming mode $\bar{N}_j$ directly:

$$\bar{N}_j^{*} = \bar{N}_j + d_j \tag{C-4}$$

$$\int_{\Omega}\bar{N}_j^{*}\partial\Omega = \int_{-1}^{1}\int_{-1}^{1}\left(\bar{N}_j + d_j\right)d\xi d\eta = 0 \tag{C-5}$$

$$d_j = -\frac{1}{4}\int_{-1}^{1}\int_{-1}^{1}\bar{N}_j d\xi d\eta = 0 \tag{C-6}$$

The correction constants are tabulated in Table C.1. Typically, the non-conforming modes can be categorized into three groups, which are basic, hierarchical, and higher order modes.

Table C.1: Correction constant for non-conforming modes.

Shape function	Correction constants			Groups
	C_j^{ξ}	C_j^{η}	d_j	
$\bar{N}_1$	0	0	$-\frac{2}{3}$	Basic
$\bar{N}_2$	0	0	$-\frac{2}{3}$	
$\bar{N}_3$	0	0	$-\frac{4}{9}$	
$\bar{N}_4$	0	$-\frac{2}{3}$	0	Hierarchical
$\bar{N}_5$	$-\frac{2}{3}$	0	0	
$\bar{N}_6$	0	0	0	Higher order
$\bar{N}_7$	0	0	0	

APPENDIX D

NUMERICAL INTEGRATION TECHNIQUE

The Gauss quadrature rule is used for numerical integration in evaluating the stiffness matrix at specific points, multiplying the resulting number by an appropriate weighting factor and adding results. Typical two dimensional Gauss quadrature rule can be expressed as:

$$I = \int_{-1}^{1}\int_{-1}^{1} \phi(\xi,\eta)d\xi d\eta \approx \int_{-1}^{1}\left[\sum_i W_i\phi(\xi_i,\eta)\right]d\eta$$
$$\approx \sum_j W_j\left[\sum_i W_i\phi(\xi_i,\eta_j)\right] = \sum_j W_j \sum_i W_i\phi(\xi_i,\eta_j) \quad \text{(D-1)}$$

where ξ_i, η_j are the gauss points and W_i, W_j are the weighting factors.

The sampling points and their weighting factors are tabulated in Table D.1. Detailed explanation can be found in many finite element books (Bathe 1996; Cook et al. 2002; Zienkiewicz and Taylor 2005). Additionally, modified five-point integration, proposed by Dovey (1974), are used. A location of the five sampling points is schematically illustrated in Figure D.1.The modified integration scheme is expressed as:

$$I^* = W_0\phi(0,0) + W_\alpha\phi(\pm\alpha, \pm\alpha) \qquad \text{(D-2)}$$

where W_0 and W_α are the weight factors.

The W_0 value is selected as 0.001 and then α and W_α can be computed by using the following equations:

$$W_\alpha = 1 - \frac{W_0}{4}, \qquad \alpha = \sqrt{\left(\frac{1}{3W_\alpha}\right)} \qquad \text{(D-3)}$$

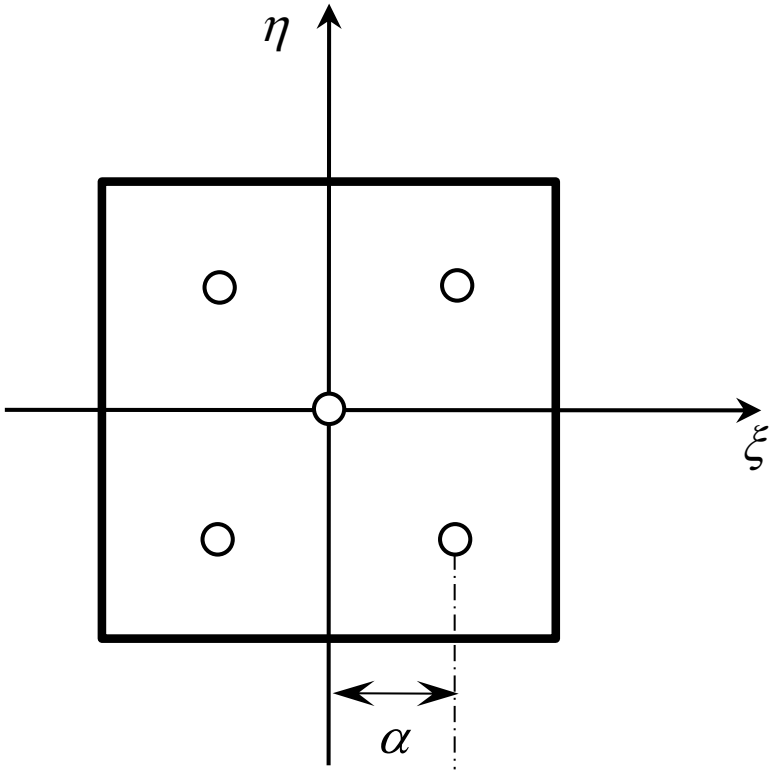

Figure D.1: The location of five points of modified integration scheme.

Table D.1: Gauss points and the weight factors.

Order	Sampling points	Weight factors
1	0.	2.
2	$\pm 0.57735\ 02691\ 89626 = \pm\sqrt{\frac{1}{3}}$	1.
3	$\pm 0.77459\ 66692\ 41483 = \pm\sqrt{\frac{3}{5}}$	$0.55555\ 55555\ 55555 = \frac{5}{9}$
	0.	$0.88888\ 88888\ 88888 = \frac{8}{9}$
4	$0.86113\ 63115\ 94953 = \pm\sqrt{\frac{\left(3+2\sqrt{\frac{6}{5}}\right)}{7}}$	$0.34785\ 48451\ 37454 = \frac{18-\sqrt{30}}{36}$
	$0.33998\ 10435\ 84856 = \pm\sqrt{\frac{\left(3-2\sqrt{\frac{6}{5}}\right)}{7}}$	$0.65214\ 51548\ 62546 = \frac{18+\sqrt{30}}{36}$

APPENDIX E

STRUCTURAL COLLAPSE FRAGILITIES

Four types of floor plan are considered in this dissertation. Their tsunami collapse fragilities, especially when the increment of elevation is equal to zero, are shown for giving more information. Initially, each structure has different width for each X and Y direction. Thus, as indicated earlier, it can be eight possible types totally. Also, two COV values, 13.6% and 50.0%, for wave height were considered. Each figure contains three analyses, i.e. tsunami-only (no earthquake), DBE level earthquake intensity, and MCE level earthquake intensity. Width of each structure is tabulated in Table E.1 and their collapse fragilities are summarized from Table E.2 to Table E.5, respectively.

Table E.1: Width of four structures for each side.

	Width of X-direction (*m*)	Width of Y-direction (*m*)
Type A	6.858	16.078
Type B	10.363	12.344
Type C	6.724	9.449
Type D	14.057	21.321

Table E.2: Structural collapse fragilities for Type A.

COV	X-direction	Y-direction
13.6%	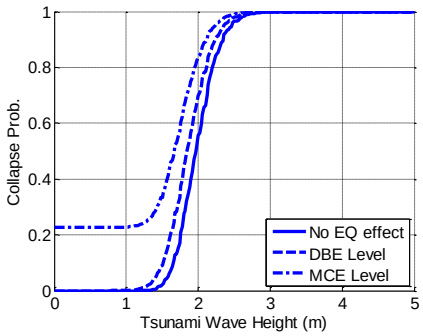	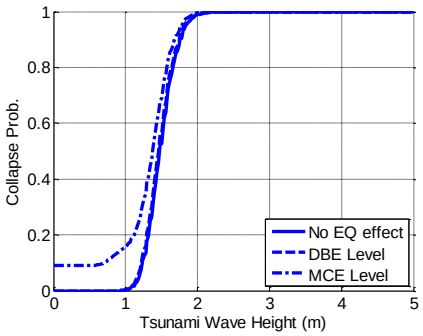
50.0%	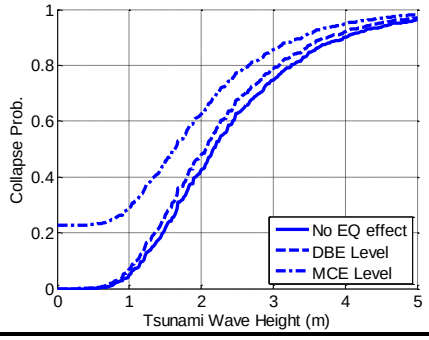	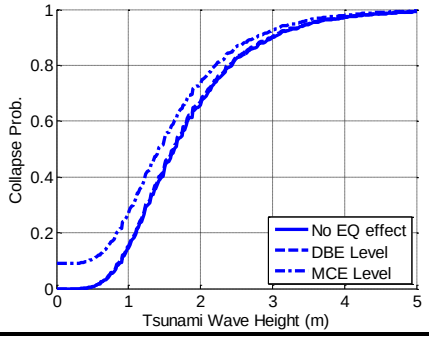

Table E.3: Structural collapse fragilities for Type B.

COV	X-direction	Y-direction
13.6%	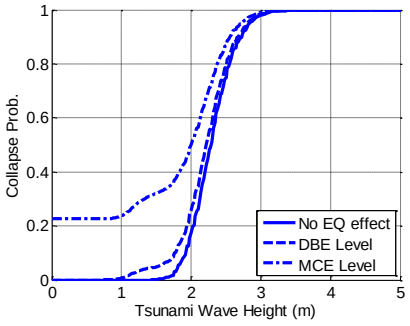	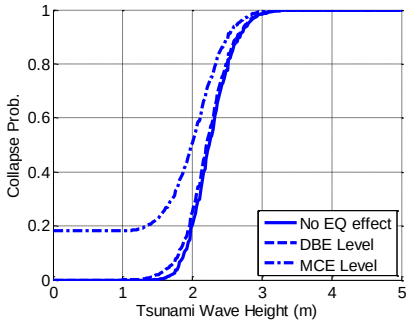
50.0%	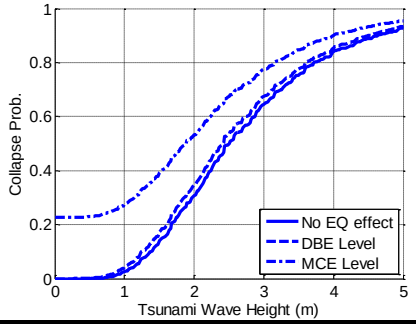	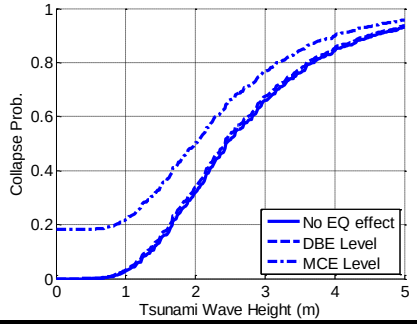

Table E.4: Structural collapse fragilities for Type C.

COV	X-direction	Y-direction
13.6%	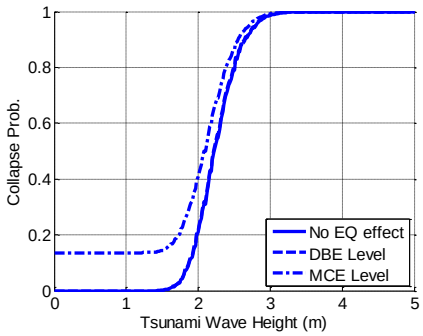	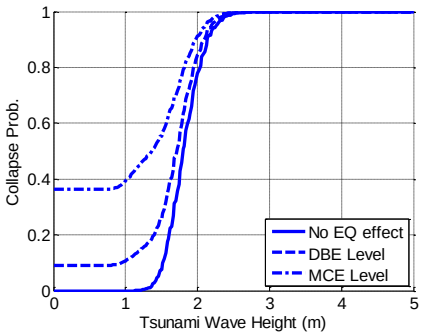
50.0%	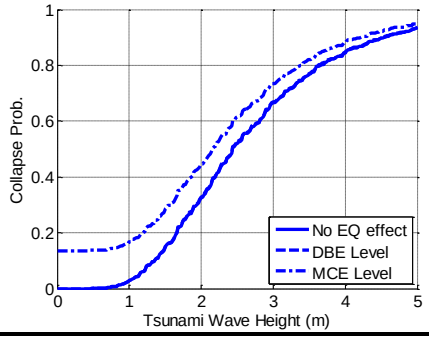	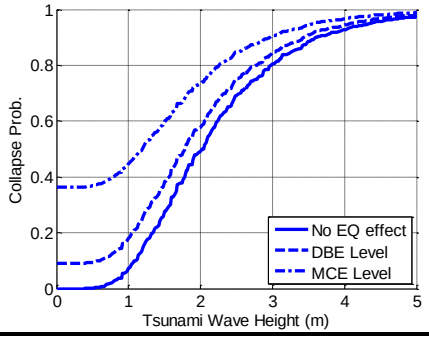

Table E.5: Structural collapse fragilities for Type D.

COV	X-direction	Y-direction
13.6%	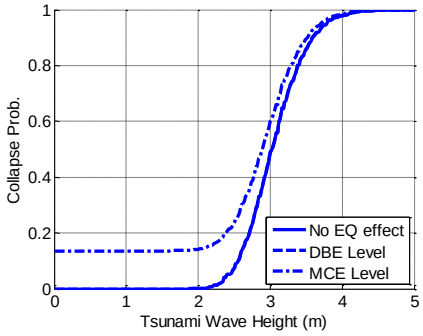	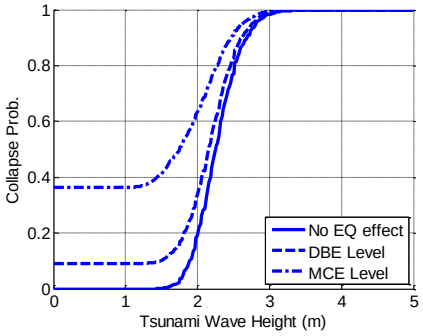
50.0%	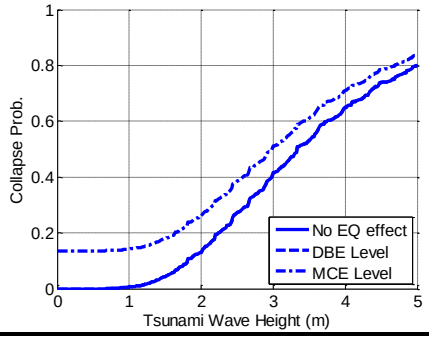	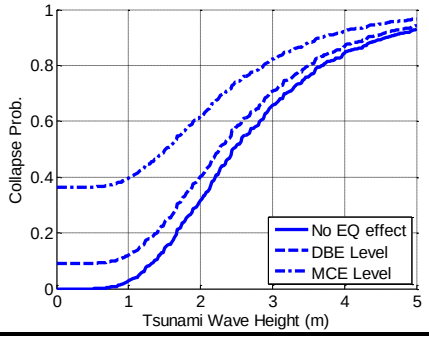

APPENDIX F

COLLAPSE FRAGILITIES WITH TSUNAMI SAFE FRAME

Each structure can be reinforced with TSF in order to reduce tsunami wave loading, as mentioned earlier. The relationship between structural collapse risk probabilities versus the TSF elevation were carried out through the collapse fragilities. Two COV values, 13.6% and 50.0%, for wave height were considered. Each figure contains three analyses, i.e. tsunami-only (no earthquake), DBE level earthquake intensity, and MCE level of earthquake intensity.

There are so many figures with respect to different target wave height, thus 2.0 meter wave height is selected as an illustrative example in order to show the trends when relatively high tsunami waves attack the structure, i.e. 2.0 meters is approximately close to one story height. Four types of structure were analyzed under three hazards levels, i.e. tsunami-only (no earthquake), DBE, and MCE level earthquake intensity. The results of each structure are tabulated in from Table F.1 to Table F.4, respectively.

Table F.1: Fragilities for Type A structure with various elevations TSF.

COV	X-direction	Y-direction
13.6%	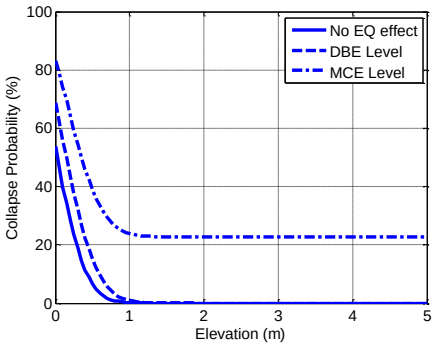	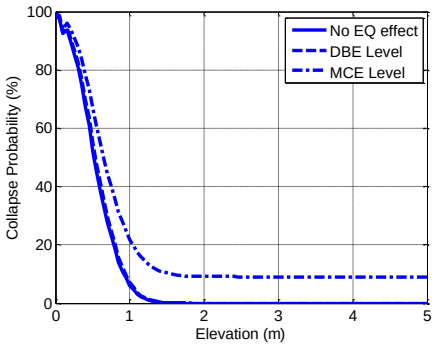
50.0%	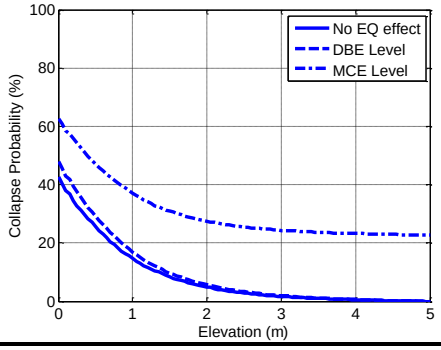	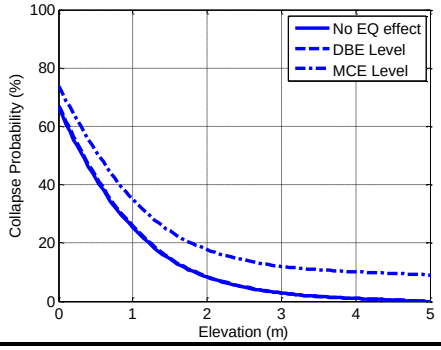

Table F.2: Fragilities for Type B structure with various elevations TSF.

COV	X-direction	Y-direction
13.6%	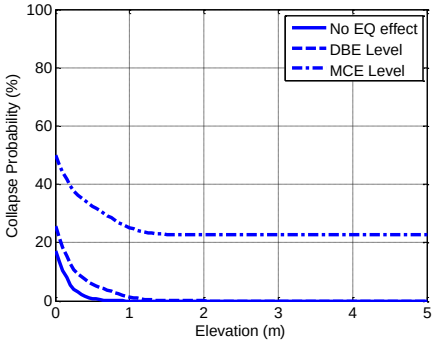	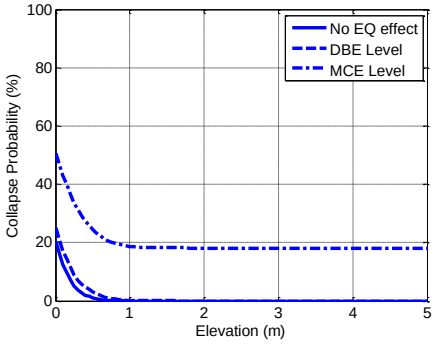
50.0%	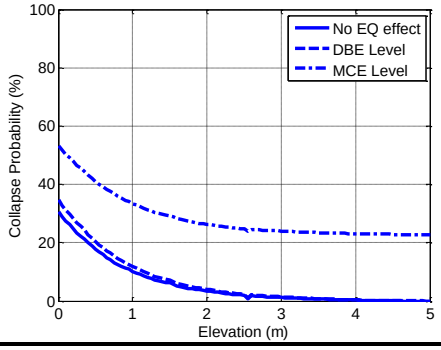	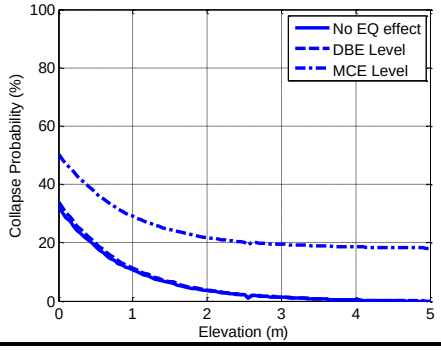

Table F.3: Fragilities for Type C structure with various elevations TSF.

COV	X-direction	Y-direction
13.6%	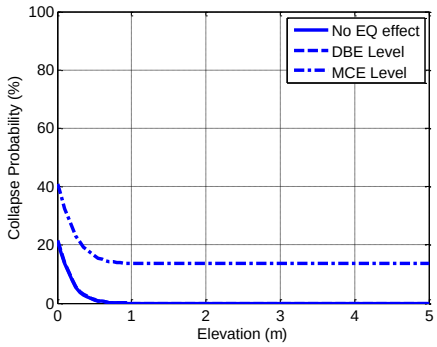	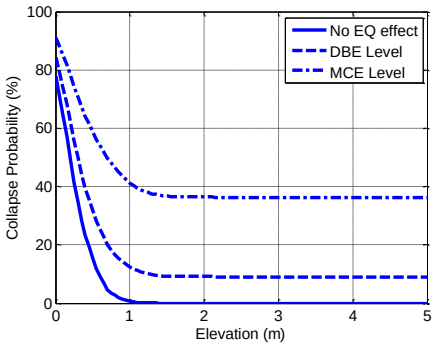
50.0%	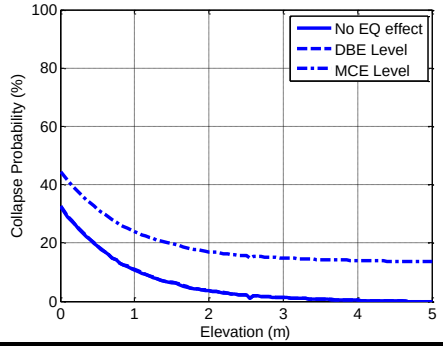	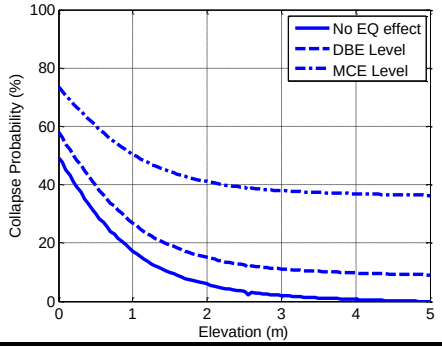

Table F.4: Fragilities for Type D structure with various elevations TSF.

COV	X-direction	Y-direction
13.6%	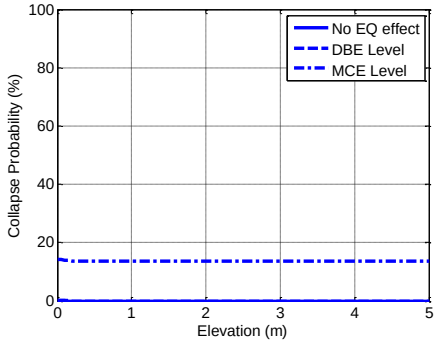	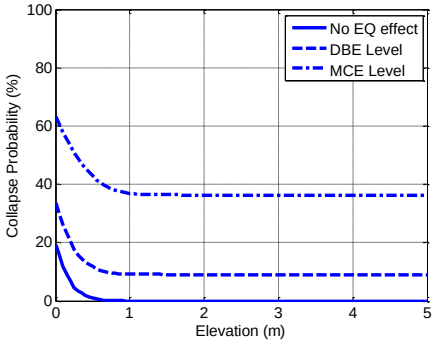
50.0%	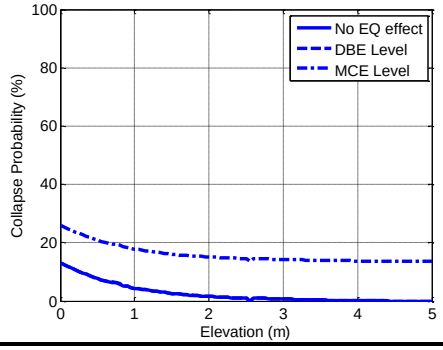	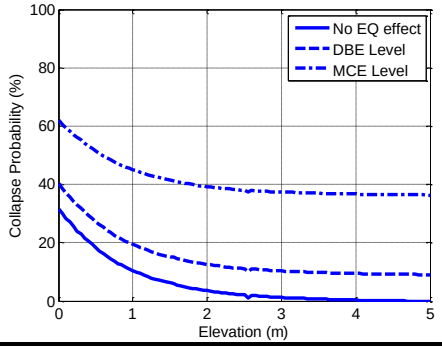

APPENDIX G

COMMUNITY FRAGILITIES WITH TSUNAMI SAFE FRAME

Probabilities of fatalities for the community fragilities were constructed when the community has shelter(s) or places of the high elevation including no TSF and the reinforcement of the one-story TSF for each residential building in the community. Four cases were carried out; one, two, and three shelters and six places of the high elevation. Two COV values were considered for each case.

Therefore, there are six fragility plots for each case, i.e. six plots for each shelter and each COV case. Additionally, the results were extracted and plotted again to help an easy comparison among the cases. Totally seventh-two figures are illustrated in here and they are tabulated into twelve tables. Detailed figures are shown in from Table G.1 to Table G.8. Two times, i.e. 5 and 20 minutes, were selected as an time to wave arrival and four figures, from Table G.9 to Table G.12, were constructed to help better understanding the relation among the four cases.

Table G.1: One shelter case for a wave COV of 13.6%.

EQ	0.00 meter Elevation	2.44 meter Elevation
NO EQ	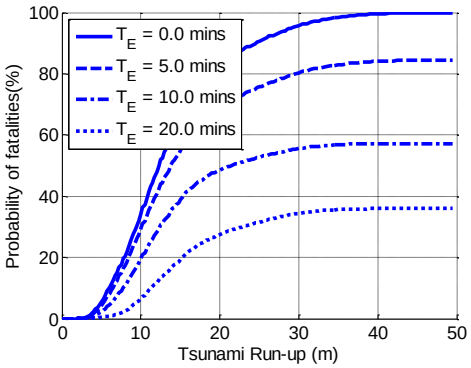	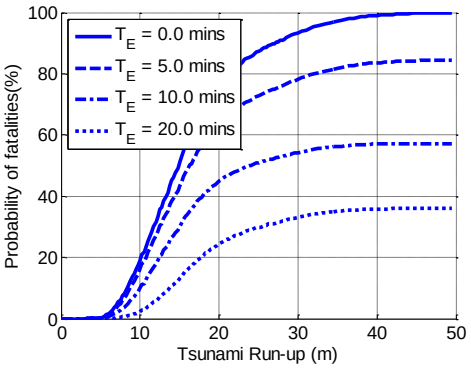
DBE	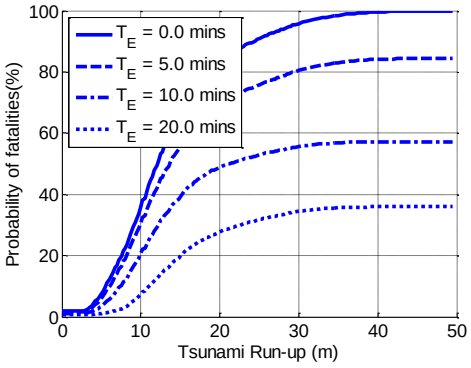	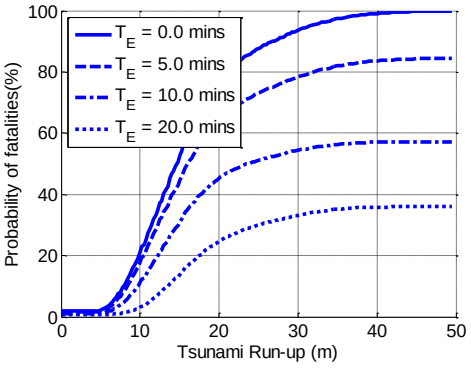
MCE	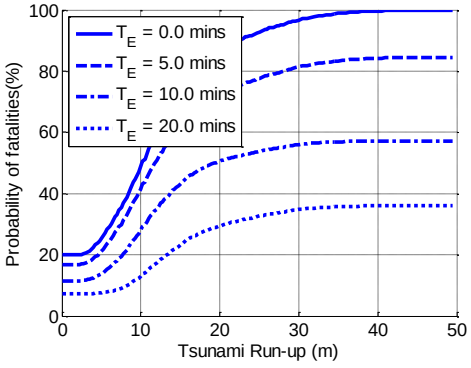	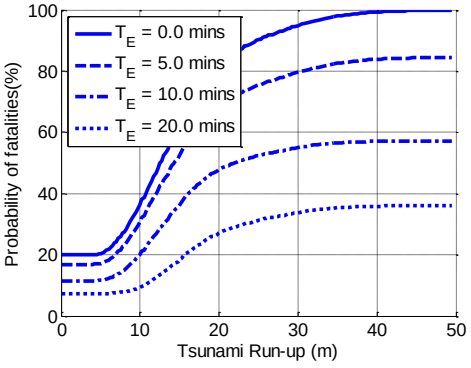

Table G.2: One shelter case for a wave COV of 50.0%.

EQ	0.00 meter Elevation	2.44 meter Elevation
NO EQ	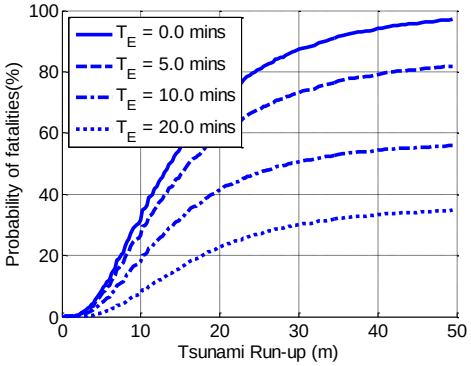	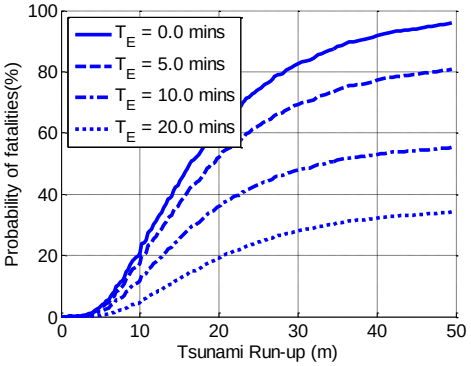
DBE	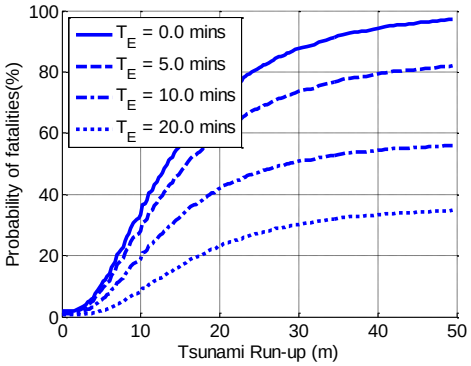	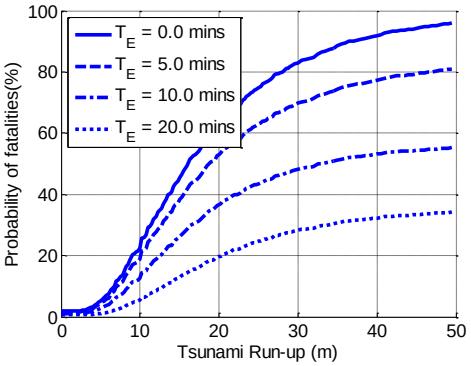
MCE	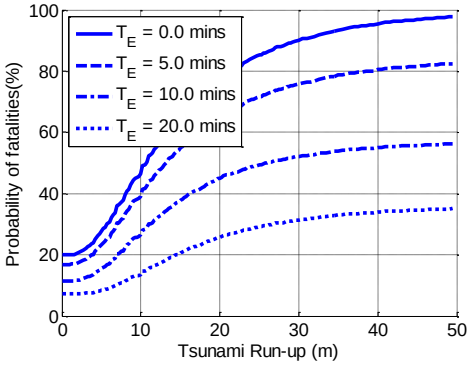	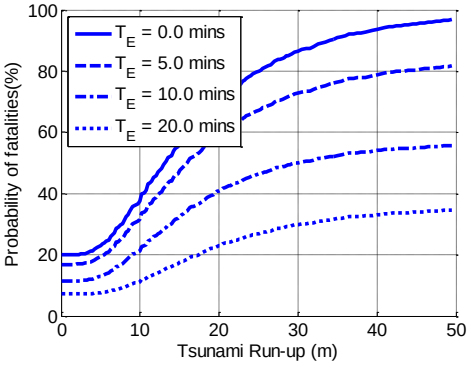

Table G.3: Two shelters case for a wave COV of 13.6%.

EQ	0.00 meter Elevation	2.44 meter Elevation
NO EQ	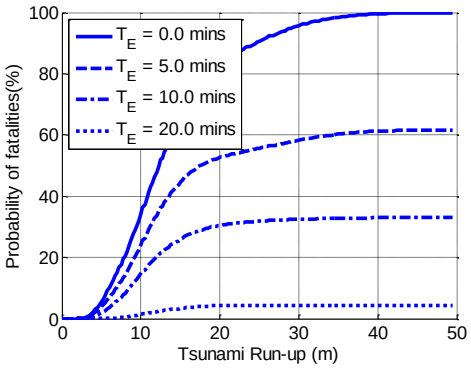	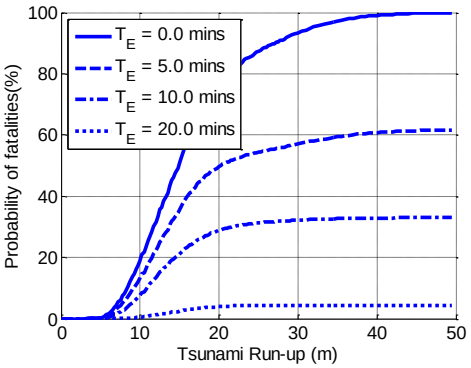
DBE	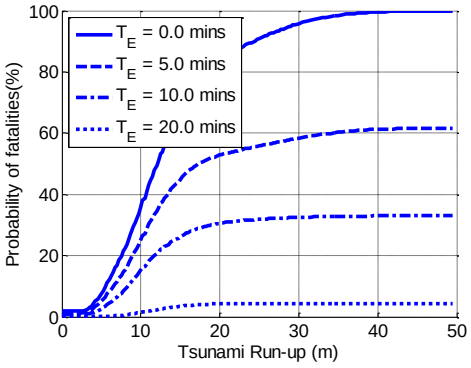	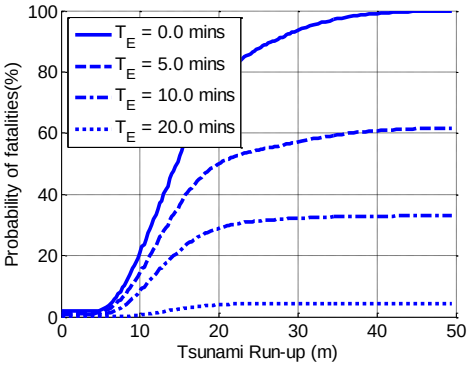
MCE	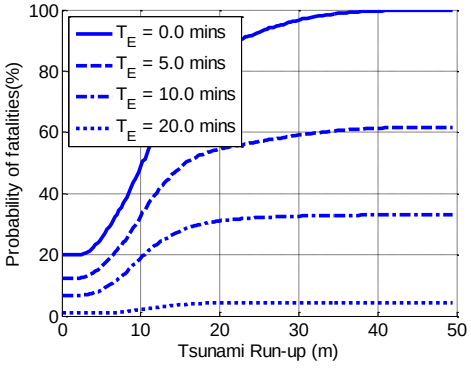	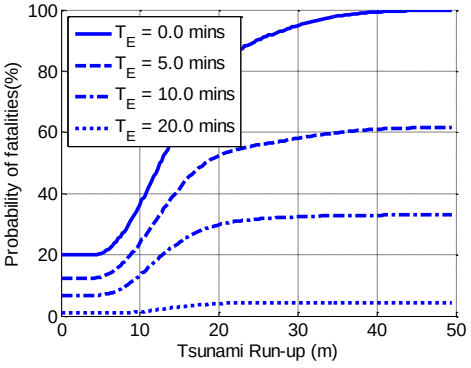

Table G.4: Two shelters case for a wave COV of 50.0%.

EQ	0.00 meter Elevation	2.44 meter Elevation
NO EQ	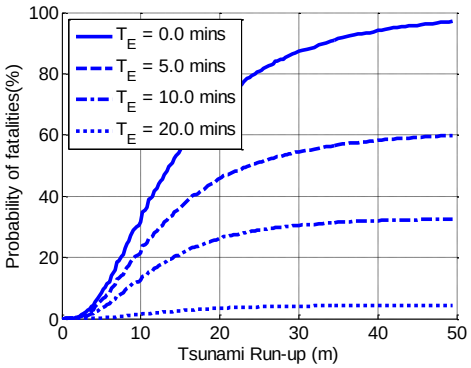	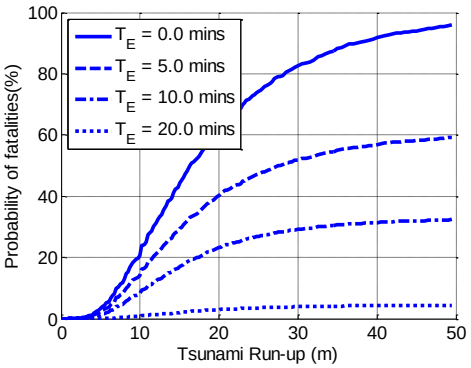
DBE	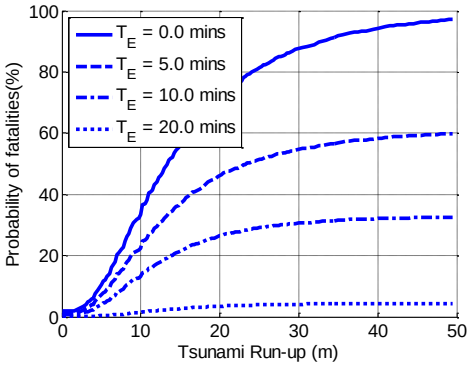	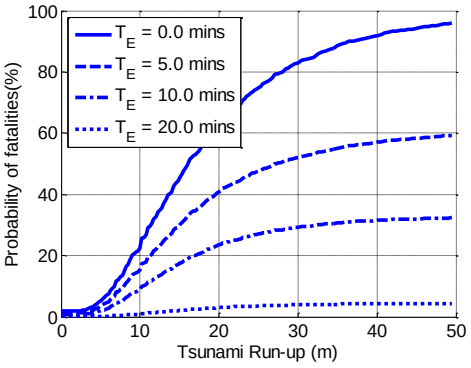
MCE	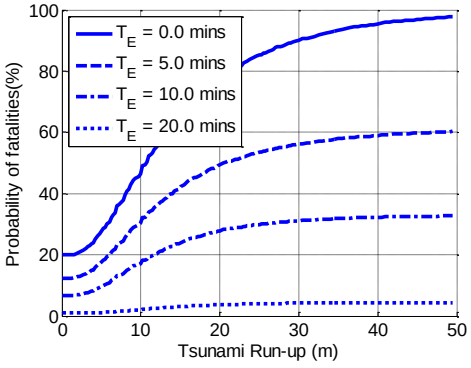	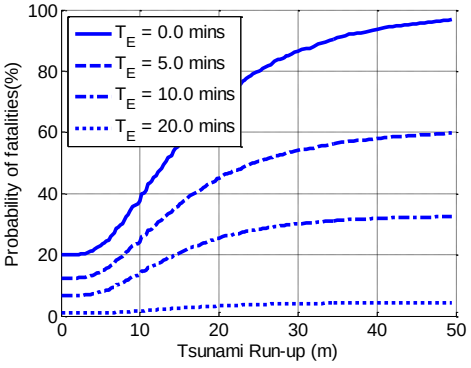

Table G.5: Three shelters case for a wave COV of 13.6%.

EQ	0.00 meter Elevation	2.44 meter Elevation
NO EQ	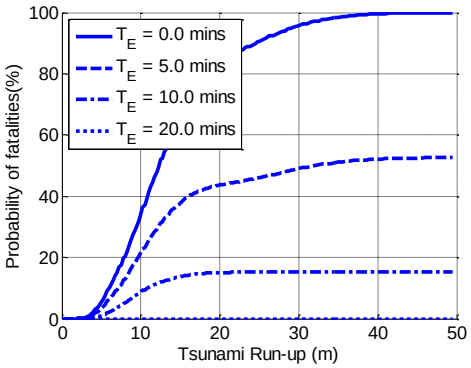	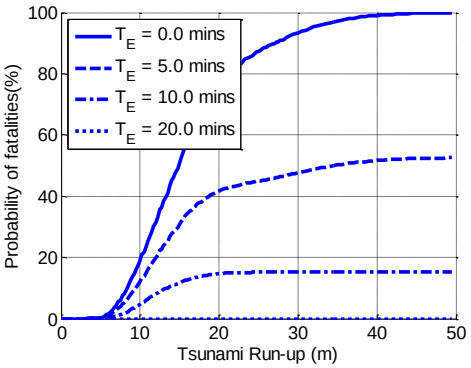
DBE	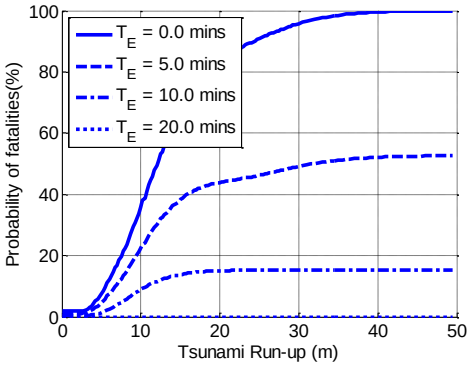	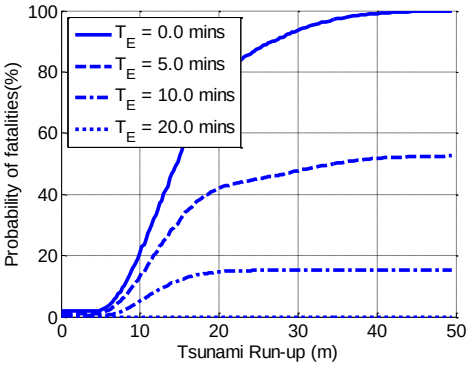
MCE	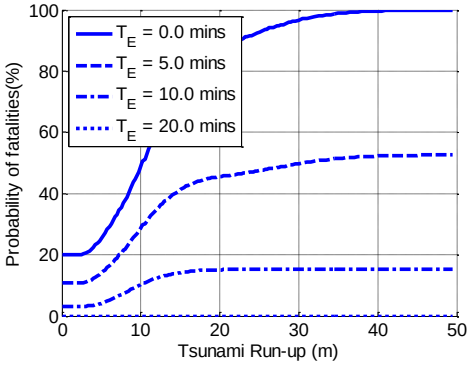	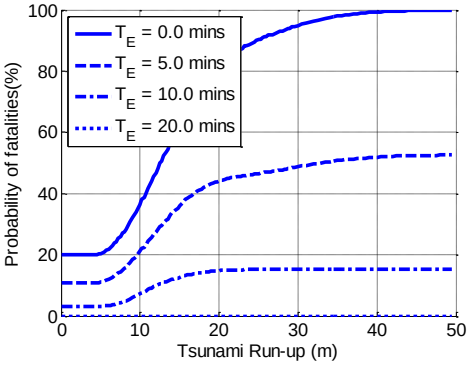

Table G.6: Three shelters case for a wave COV of 50.0%.

EQ	0.00 meter Elevation	2.44 meter Elevation
NO EQ	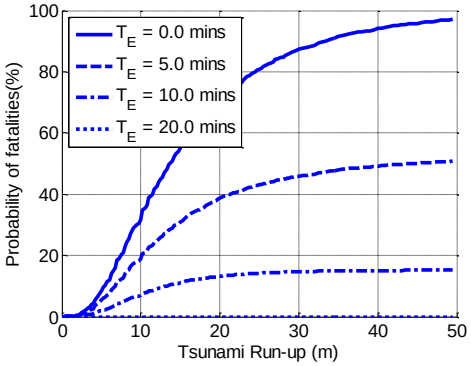	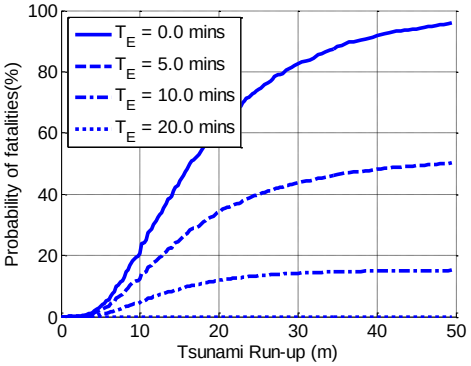
DBE	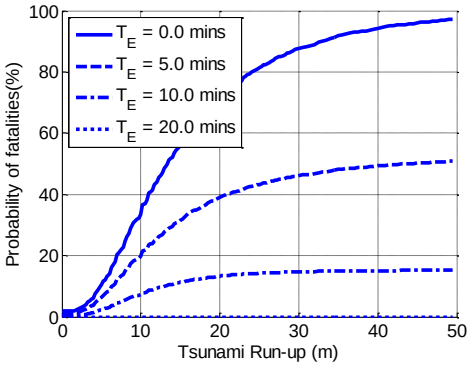	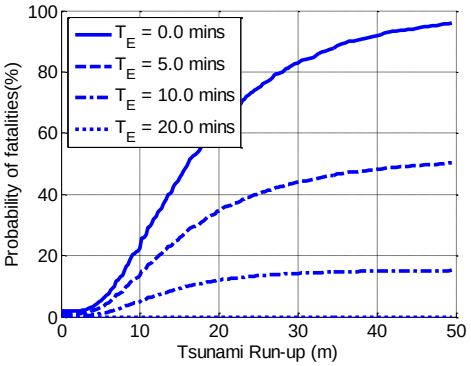
MCE	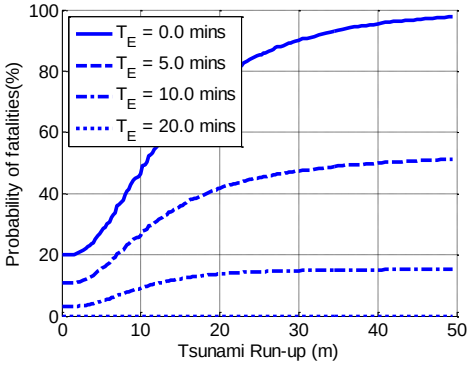	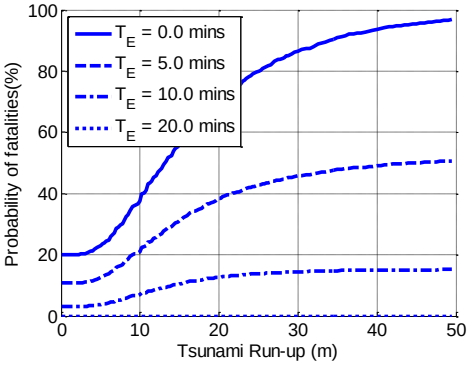

Table G.7: Six safe places of high elevation case for a wave COV of 13.6%.

EQ	0.00 meter Elevation	2.44 meter Elevation
NO EQ	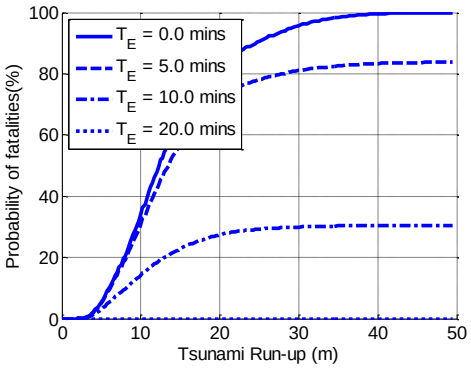	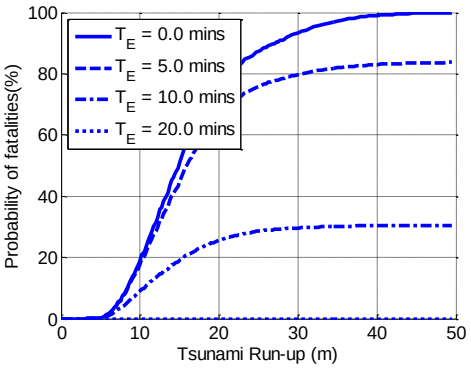
DBE	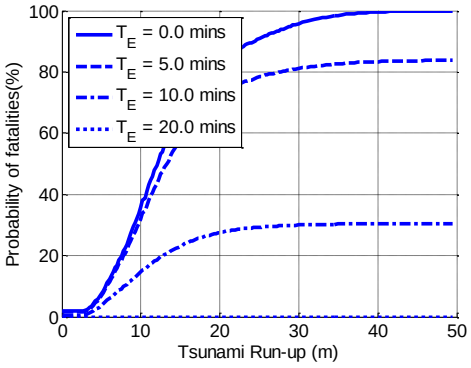	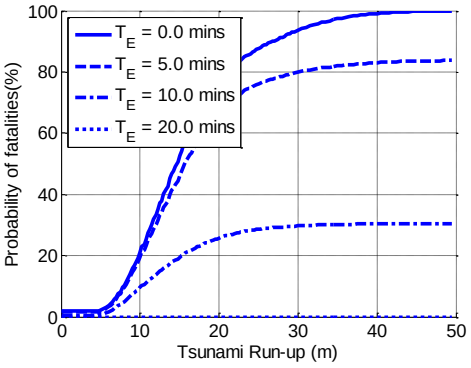
MCE	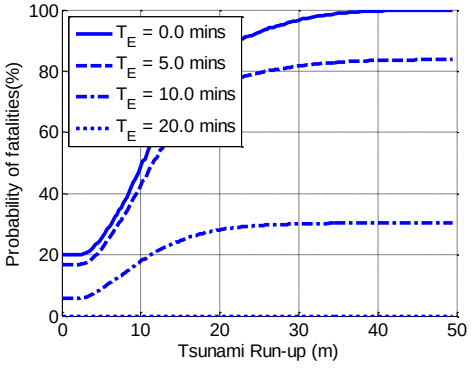	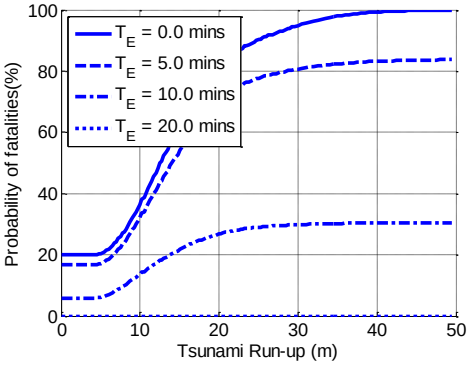

Table G.8: Six safe places of high elevation case for a wave COV of 50.0%.

EQ	0.00 meter Elevation	2.44 meter Elevation
NO EQ	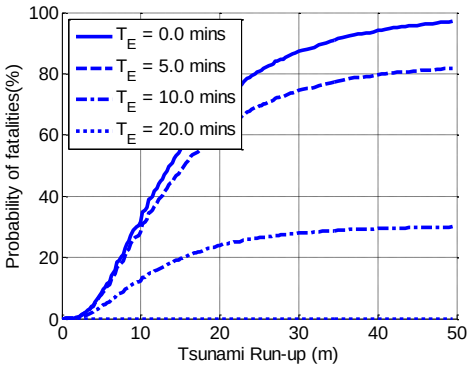	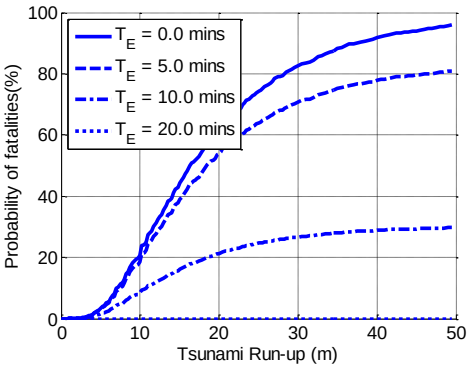
DBE	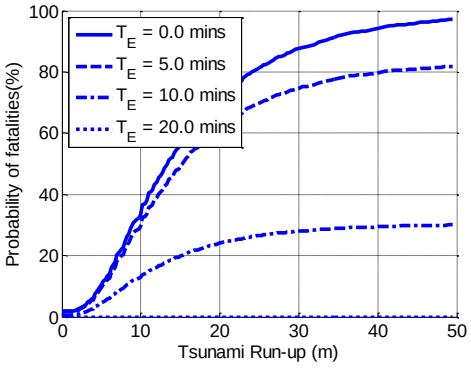	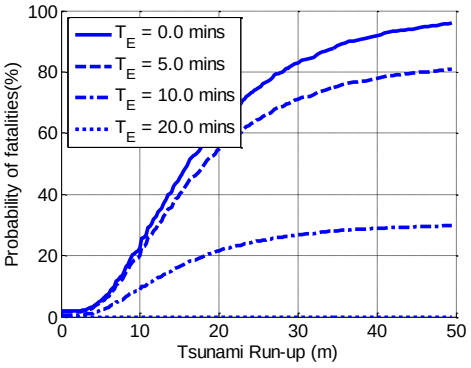
MCE	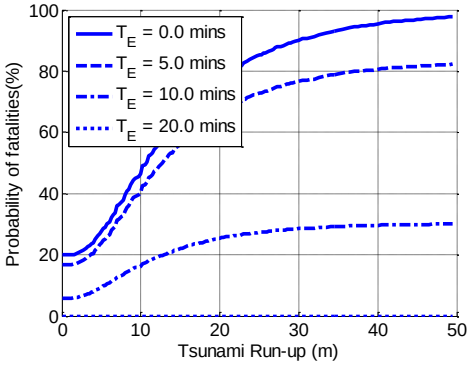	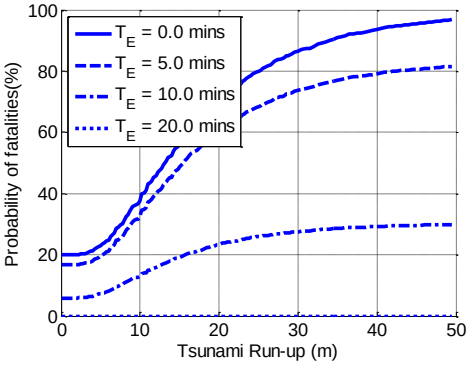

Table G.9: Time to wave arrival: 5 minutes, for a wave COV of 13.6%.

EQ	0.00 meter Elevation	2.44 meter Elevation
NO EQ	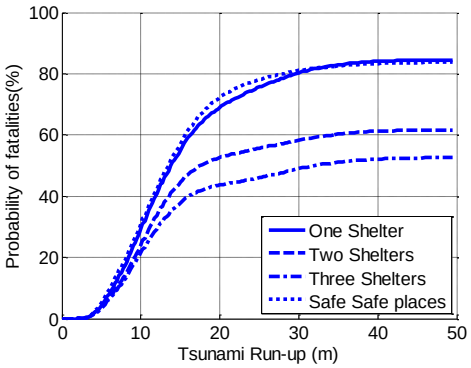	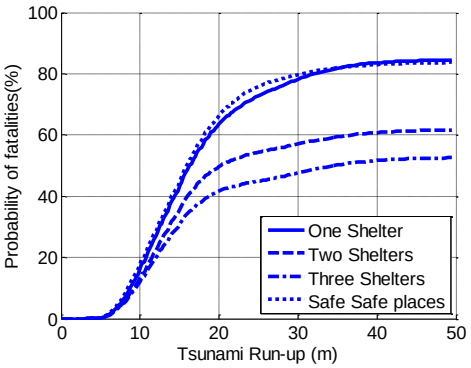
DBE	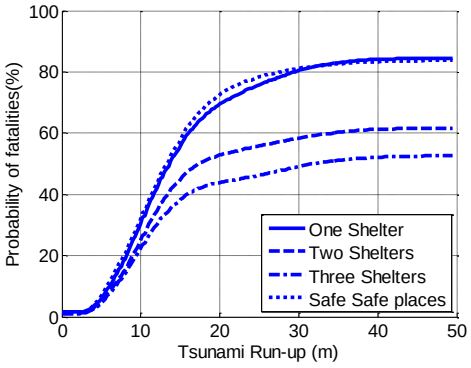	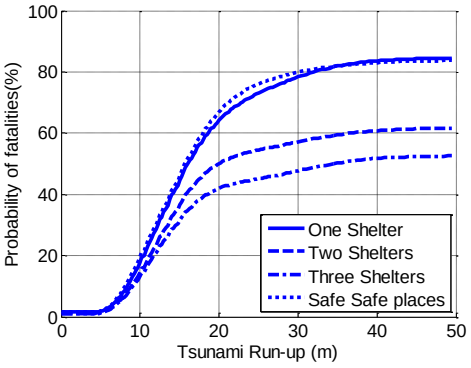
MCE	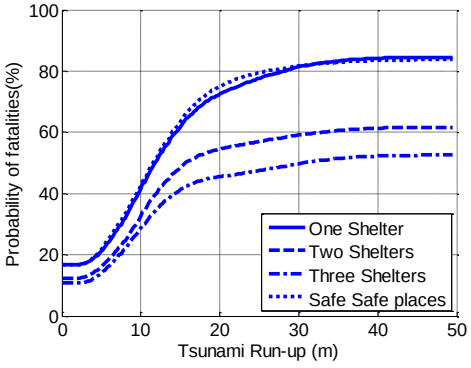	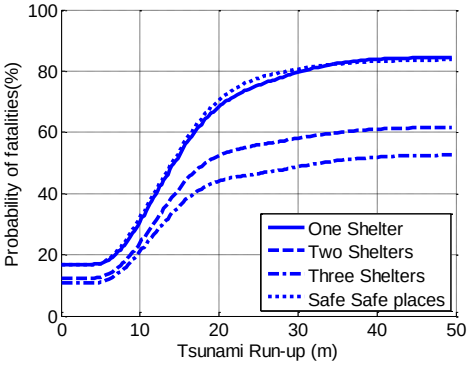

Table G.10: Time to wave arrival: 5 minutes, for a wave COV of 50.0%.

EQ	0.00 meter Elevation	2.44 meter Elevation
NO EQ	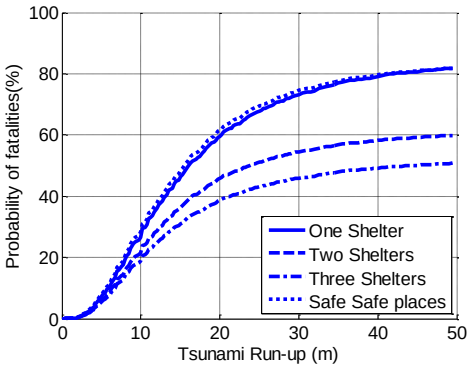	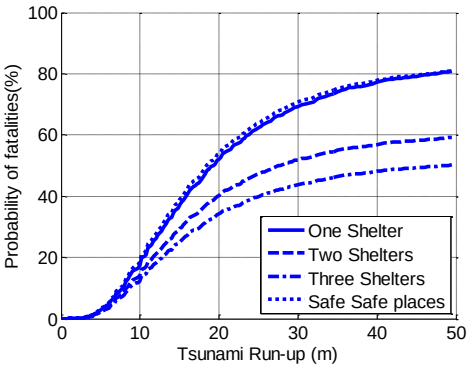
DBE	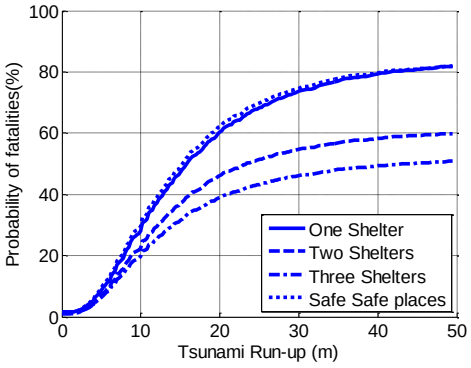	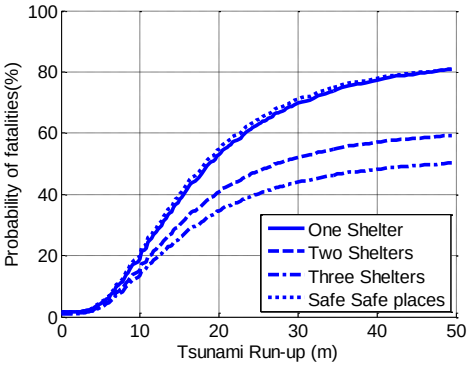
MCE	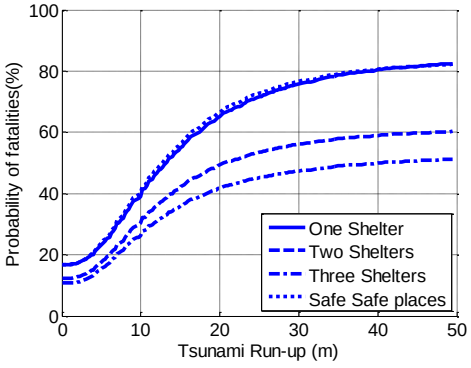	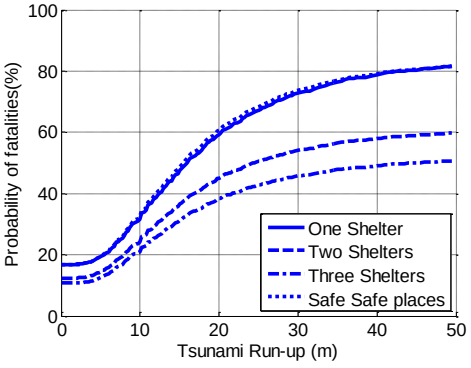

Table G.11: Time to wave arrival: 20 minutes, for a wave COV of 13.6%.

EQ	0.00 meter Elevation	2.44 meter Elevation
NO EQ	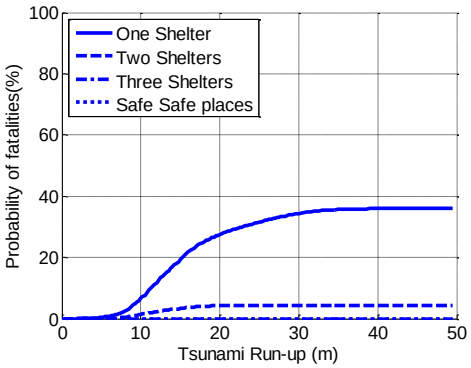	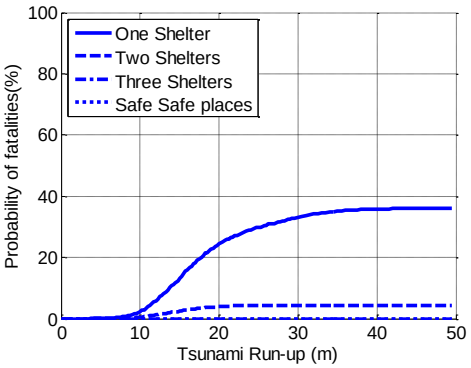
DBE	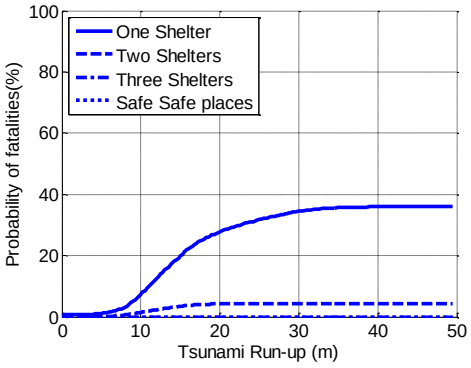	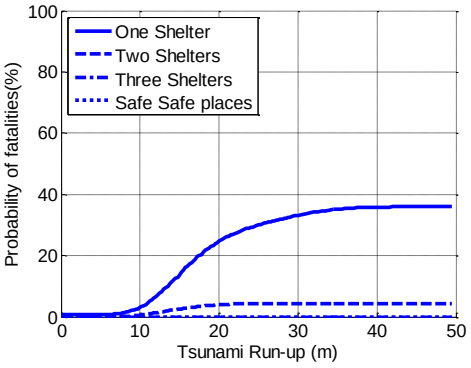
MCE	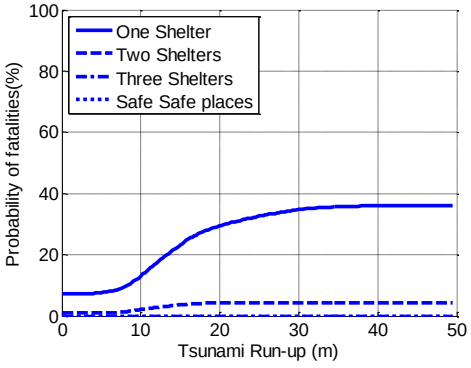	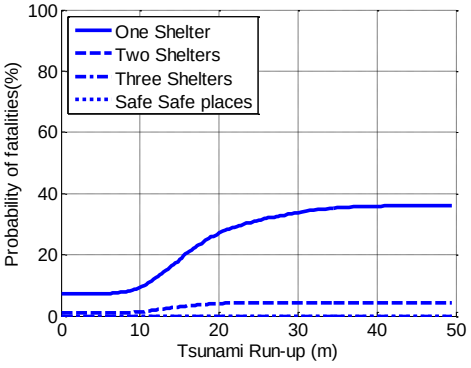

Table G.12: Time to wave arrival: 20 minutes, for a wave COV of 50.0%.

EQ	0.00 meter Elevation	2.44 meter Elevation
NO EQ	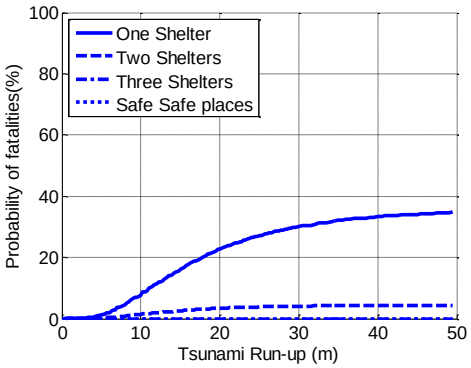	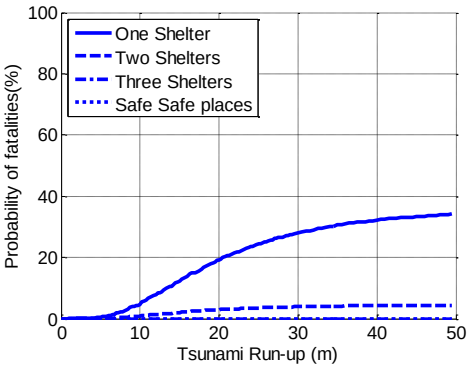
DBE	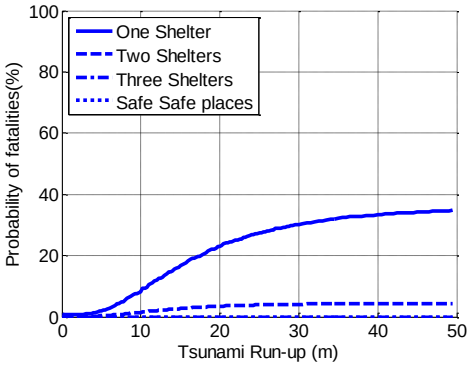	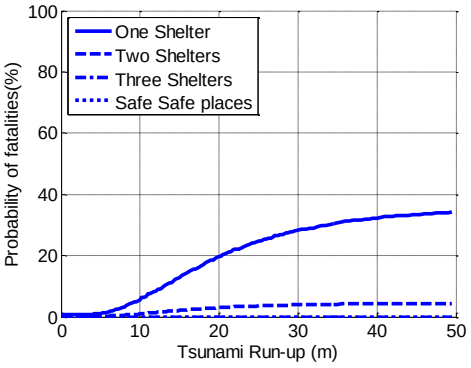
MCE	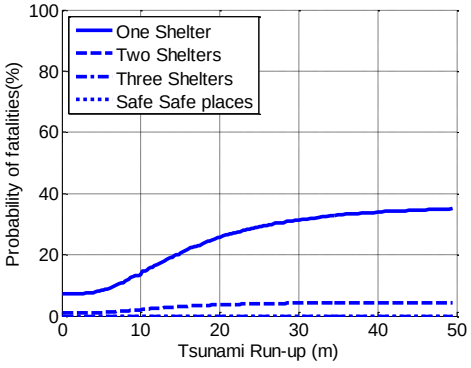	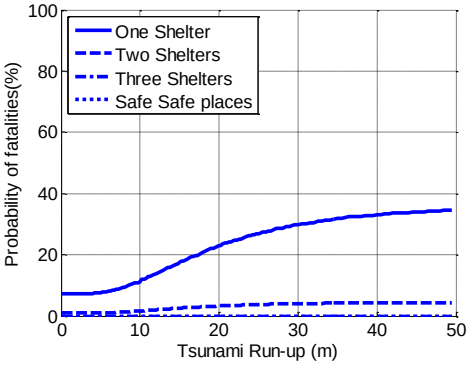

APPENDIX H
HOUSES IN THE CITY OF CANNON BEACH, OREGON

Table H.1: Detailed information of the houses in the City of Cannon Beach, OR

No.	Coordinate		Structure Type
	X (m)	Y (m)	
1	-15.7575	5854.215	6
2	-3.5864	5825.844	6
3	51.617	5988.676	8
4	112.2785	5947.662	8
5	72.4393	5869.751	1
6	87.0219	5896.668	2
7	123.0321	5875.65	8
8	120.6512	5827.367	7
9	266.18	5815.767	2
10	152.1974	5827.07	3
11	68.5704	5803.573	8
12	34.1971	5766.394	8
13	119.7537	5791.787	4
14	112.016	5764.573	3
15	56.0663	5701.517	7
16	110.9744	5738.547	5
17	110.9744	5717.132	5
18	109.9932	5686.42	3
19	110.3586	5670.643	3
20	109.2623	5651.651	7
21	142.7359	5743.175	7
22	139.8124	5702.782	7
23	148.0712	5654.792	1
24	151.6524	5785.394	1
25	187.1724	5787.95	4
26	185.7107	5767.06	7
27	184.6144	5742.663	2
28	185.1991	5702.343	8
29	184.7606	5684.375	2
30	183.5582	5663.341	5
31	185.2784	5647.05	5
32	223.0403	5650.898	5
33	554.2123	5737.864	8
34	747.1004	5502.114	3
35	454.9569	5681.566	6
36	783.9064	5119.598	2
37	760.4394	5098.608	5
38	738.1512	5081.581	2
39	716.7201	5064.125	6
40	812.1788	3807.363	4
41	802.4627	3775.575	4
42	835.9293	3801.221	6
43	863.0847	3809.935	4
44	825.881	3770.679	5
45	877.9495	3792.556	6
46	904.0253	3797.569	8
47	928.6062	3782.713	4
48	941.5611	3757.897	7
49	873.7143	3763.707	4
50	716.9222	3751.141	2
51	736.4374	3741.098	7
52	755.1223	3733.131	3
53	706.3756	3711.054	8
54	729.6279	3713.544	6
55	748.6449	3706.241	1
56	696.4103	3675.366	3
57	716.0087	3663.415	2
58	735.8562	3657.937	1
59	683.7877	3634.948	4
60	676.4798	3605.734	5
61	707.5382	3641.504	3
62	723.8148	3628.889	4

No.	Coordinate		Structure Type
	X (m)	Y (m)	
63	690.0159	3589.633	7
64	712.1056	3583.408	7
65	783.756	3552.196	2
66	677.8751	3559.251	5
67	701.2935	3550.951	4
68	654.789	3522.65	2
69	744.1441	3487.045	8
70	1062.22	3427.487	6
71	1075.715	3419.209	5
72	1089.676	3408.884	4
73	930.5213	3339.771	5
74	199.6381	3457.626	3
75	195.7896	3441.394	2
76	153.7172	3440.612	5
77	156.5872	3423.793	2
78	152.8692	3407.691	1
79	192.0716	3424.575	5
80	190.3756	3407.169	2
81	186.8427	3389.914	3
82	184.1031	3374.464	1
83	147.2489	3375.572	8
84	106.6768	3370.031	6
85	346.905	2438.321	5
86	272.6797	5677.258	8
87	73.4674	5618.624	3
88	75.1057	5581.13	2
89	120.1579	5610.765	3
90	268.6418	5741.429	7
91	271.0538	5697.931	4
92	182.0639	5617.151	5
93	188.0363	5600.239	7
94	265.6786	5601.234	1
95	352.2795	5612.376	8
96	382.341	5595.066	4
97	382.341	5613.212	2
98	382.341	5577.557	4
99	373.9837	5565.329	2
100	224.626	5618.237	4
101	223.6434	5601.419	4
102	223.0292	5585.216	6

No.	Coordinate		Structure Type
	X (m)	Y (m)	
103	304.2179	5613.94	3
104	303.6038	5596.509	5
105	303.3581	5566.311	5
106	223.6434	5568.889	4
107	191.4096	5586.132	6
108	191.4096	5570.924	6
109	263.863	5584.577	4
110	268.5318	5567.641	8
111	268.8777	5551.569	2
112	222.1893	5553.988	7
113	221.1518	5537.57	4
114	220.1143	5522.017	8
115	220.1143	5505.772	7
116	264.5547	5505.081	4
117	264.2089	5488.663	1
118	264.7276	5472.936	6
119	265.2464	5455.482	4
120	301.2137	5534.633	4
121	301.5595	5550.877	7
122	266.0836	5518.635	6
123	217.1199	5483.336	4
124	215.5695	5458.156	3
125	211.112	5443.048	2
126	91.3414	5486.435	7
127	83.2017	5521.493	7
128	177.9466	5443.407	7
129	183.9545	5410.673	7
130	217.0949	5402.732	5
131	266.9025	5406.993	2
132	297.7172	5403.507	8
133	264.1892	5391.498	8
134	345.0053	5405.444	4
135	344.2301	5452.898	5
136	301.7871	5504.613	7
137	343.4549	5470.33	6
138	345.0053	5492.023	7
139	298.6862	5454.834	6
140	298.88	5439.92	5
141	266.5149	5439.727	7
142	299.6553	5485.825	5

No.	Coordinate		Structure Type
	X (m)	Y (m)	
143	300.0429	5469.167	7
144	457.2176	5465.1	7
145	457.6052	5442.632	5
146	429.5036	5434.691	6
147	424.4648	5401.763	1
148	425.24	5385.106	1
149	375.8201	5399.827	5
150	459.737	5482.145	3
151	132.0006	5268.659	6
152	136.2643	5242.317	7
153	190.1417	5268.078	7
154	182.002	5251.614	7
155	189.1727	5233.988	2
156	216.1114	5239.024	3
157	253.5155	5239.412	6
158	285.6869	5244.448	3
159	248.6704	5279.506	3
160	251.7713	5296.357	6
161	175.4126	5302.748	6
162	164.5596	5333.351	7
163	294.2142	5278.731	3
164	293.8266	5293.645	5
165	293.439	5311.852	3
166	293.8266	5326.378	4
167	263.2725	5360.045	2
168	345.3776	5389.568	4
169	344.5088	5372.853	6
170	374.7009	5372.853	5
171	373.0702	5292.992	4
172	294.4018	5375.587	7
173	295.5961	5351.716	4
174	292.0773	5262.724	7
175	259.7934	5263.56	5
176	343.9707	5357.607	4
177	342.6555	5341.952	4
178	342.8946	5324.744	1
179	341.8185	5308.373	3
180	341.938	5293.077	2
181	340.7423	5276.705	1
182	340.6228	5260.931	2
183	339.1879	5244.799	7
184	340.0249	5228.308	4
185	372.0697	5227.352	3
186	371.9501	5244.56	3
187	372.4284	5260.812	2
188	372.4284	5276.586	7
189	373.7437	5308.253	7
190	374.5807	5325.461	7
191	373.8632	5341.355	6
192	374.9394	5357.009	6
193	262.9023	5330.002	1
194	263.261	5345.776	5
195	260.9891	5312.436	7
196	459.3092	5240.614	7
197	418.8945	5225.796	2
198	418.8945	5242.765	5
199	420.5685	5257.105	4
200	420.9272	5274.074	2
201	422.4816	5290.564	5
202	422.0034	5306.577	8
203	421.6446	5323.307	4
204	424.3948	5348.044	6
205	455.0047	5328.565	2
206	454.2801	5361.118	6
207	576.0451	5220.751	2
208	572.4019	5204.045	5
209	570.6874	5186.482	4
210	611.6207	5186.91	3
211	611.8349	5235.316	6
212	615.2639	5267.872	1
213	524.6107	5265.944	3
214	581.1886	5268.086	7
215	581.8315	5251.808	2
216	613.7637	5250.951	3
217	578.6169	5236.387	6
218	613.1208	5219.68	6
219	612.9065	5203.616	4
220	695.9921	5339.184	2
221	696.635	5302.559	7
222	662.9883	5303.416	3

No.	Coordinate		Structure Type
	X (m)	Y (m)	
223	660.8452	5264.434	6
224	738.2112	5306.414	3
225	771.4293	5306.2	3
226	817.9346	5331.474	6
227	851.1527	5318.194	6
228	739.9257	5262.935	7
229	772.2865	5262.935	4
230	737.5683	5246.443	2
231	737.9969	5230.379	3
232	691.4916	5184.758	5
233	660.6309	5202.321	7
234	660.2023	5179.189	3
235	661.9168	5247.514	6
236	665.1314	5233.163	5
237	809.7908	5252.868	6
238	890.4862	5337.664	4
239	368.9799	5183.316	4
240	336.5377	5163.953	6
241	336.5377	5148.492	7
242	336.0872	5132.58	5
243	334.435	5116.519	3
244	333.8342	5100.758	4
245	367.9286	5117.119	4
246	478.136	4907.902	8
247	477.8356	4897.245	1
248	490.1517	4954.436	4
249	488.6497	4936.123	6
250	494.6575	4902.649	4
251	489.1003	4884.936	3
252	487.7485	4870.976	5
253	528.0009	4916.008	7
254	543.3208	4915.858	7
255	534.9099	4901.448	5
256	618.5686	4914.657	5
257	646.8053	4895.293	4
258	263.4592	4606.968	4
259	263.219	4621.131	6
260	275.709	4672.262	4
261	270.9052	4654.498	8
262	267.6247	4638.152	3
263	480.3705	4600.994	5
264	249.1203	4456.238	2
265	232.4299	4429.065	2
266	262.042	4428.796	2
267	248.8511	4404.044	7
268	182.8969	4461.619	4
269	183.1661	4435.253	5
270	182.6277	4405.658	6
271	173.101	4375.355	6
272	173.3728	4359.093	7
273	172.2409	4339.295	2
274	169.4109	4320.628	7
275	168.4676	4296.87	2
276	166.7696	4274.432	2
277	165.6376	4254.823	3
278	304.3565	4332.748	4
279	304.4888	4318.476	7
280	288.8866	4324.423	6
281	272.3589	4320.987	7
282	226.3456	4369.484	5
283	246.4434	4364.727	3
284	262.5744	4364.066	3
285	241.0223	4327.462	6
286	249.6167	4328.255	5
287	262.31	4324.027	6
288	215.239	4322.176	1
289	217.619	4338.827	2
290	209.7131	4374.592	5
291	214.6609	4288.782	4
292	213.4754	4272.194	6
293	204.7322	4252.645	5
294	242.6689	4280.932	4
295	260.1554	4278.859	3
296	274.9745	4279.007	6
297	241.1871	4251.608	7
298	260.0072	4251.46	6
299	242.5208	4235.02	7
300	262.0819	4234.724	3
301	203.3985	4236.501	6
302	220.2922	4235.613	6

No.	Coordinate		Structure Type
	X (m)	Y (m)	
303	173.1676	4210.139	5
304	165.4617	4238.427	4
305	171.5375	4194.292	8
306	168.2773	4177.852	3
307	170.2038	4162.301	2
308	200.8792	4195.477	2
309	224.8861	4199.623	7
310	240.1497	4199.179	7
311	256.4507	4198.291	2
312	271.2697	4198.291	2
313	270.0842	4166.3	6
314	254.376	4167.781	3
315	238.0751	4167.781	5
316	221.9223	4168.966	7
317	206.6587	4168.818	4
318	310.9848	4203.77	1
319	309.5029	4185.998	2
320	299.5741	4161.413	5
321	314.8377	4160.82	6
322	332.7688	4196.217	2
323	348.6252	4195.18	6
324	332.176	4161.709	2
325	345.8096	4162.894	8
326	364.9262	4192.811	1
327	361.9623	4160.82	7
328	378.7079	4159.932	7
329	381.0789	4194.292	6
330	393.8233	4160.376	2
331	411.3098	4159.636	3
332	426.8698	4158.451	6
333	396.7871	4192.811	7
334	413.829	4192.366	1
335	429.9818	4189.552	5
336	175.0771	4136.158	1
337	174.911	4119.559	4
338	170.4266	4103.126	4
339	172.9179	4087.025	1
340	208.7929	4127.195	5
341	232.0451	4125.701	7
342	252.3078	4124.539	2

No.	Coordinate		Structure Type
	X (m)	Y (m)	
343	267.9201	4132.672	4
344	267.754	4115.741	7
345	202.4815	4093.665	7
346	219.7546	4093.665	7
347	236.1973	4091.673	2
348	250.9791	4093.333	2
349	266.9235	4099.806	3
350	266.9235	4084.369	6
351	329.3725	4087.855	2
352	343.3239	4088.353	3
353	330.0369	4120.555	5
354	345.3169	4120.389	4
355	361.5935	4119.393	3
356	376.2092	4119.559	4
357	361.2613	4090.345	4
358	376.5414	4088.353	1
359	391.8215	4089.017	7
360	408.098	4086.859	4
361	423.8764	4087.357	3
362	394.811	4117.401	4
363	409.925	4118.563	4
364	424.7068	4117.567	8
365	163.7813	4062.458	6
366	186.8675	4051.502	5
367	201.4832	4053.328	2
368	217.5937	4051.668	3
369	234.3685	4050.672	7
370	249.4825	4050.838	1
371	264.2643	4049.012	3
372	263.4339	4016.976	6
373	165.4422	4046.191	4
374	166.6047	4030.421	2
375	165.7743	4013.49	2
376	199.8223	4021.624	8
377	215.4345	4020.462	7
378	231.8772	4019.3	4
379	247.4895	4018.138	7
380	300.8036	4056.482	7
381	302.6306	4039.053	4
382	301.8001	4023.782	2

No.	Coordinate		Structure Type
	X (m)	Y (m)	
383	301.4679	4007.183	4
384	326.5472	4047.186	3
385	340.9968	4045.859	2
386	357.4395	4045.195	3
387	324.222	4015.648	3
388	340.3325	4013.656	6
389	355.9447	4012.827	7
390	371.723	4013.324	5
391	386.3387	4012.661	8
392	404.2762	4011.499	2
393	421.0511	4010.337	6
394	413.411	4043.369	2
395	388.9961	4045.029	6
396	373.2178	4046.522	3
397	160.1289	3989.106	6
398	162.4541	3971.346	3
399	159.6306	3956.074	2
400	155.9767	3941.799	4
401	188.0316	3980.973	7
402	208.4604	3981.305	7
403	245.664	3989.77	5
404	244.1693	3968.358	2
405	180.7238	3948.273	7
406	197.0004	3946.613	6
407	215.6022	3946.613	5
408	234.7023	3946.447	6
409	258.1206	3940.969	8
410	292.3347	3982.965	7
411	298.9782	3966.864	5
412	299.1443	3952.423	7
413	298.646	3935.824	1
414	322.2305	3974.997	7
415	321.2339	3943.293	5
416	338.1749	3973.005	7
417	337.1783	3942.629	3
418	353.621	3972.673	3
419	353.1228	3940.637	5
420	370.2298	3972.01	7
421	369.5654	3939.973	5
422	385.3438	3971.346	5
423	384.5133	3939.475	8
424	402.2847	3975.661	3
425	400.956	3944.289	2
426	418.063	3966.864	7
427	436.6649	3971.844	7
428	457.0936	3974.333	6
429	455.5989	3950.763	3
430	454.6023	3924.868	2
431	434.8379	3950.099	4
432	148.6689	3917.067	6
433	152.821	3899.306	4
434	149.1671	3877.727	2
435	171.9211	3875.735	8
436	192.0177	3875.569	6
437	206.4674	3874.241	8
438	216.2665	3873.743	4
439	227.5605	3873.743	5
440	241.844	3872.083	8
441	256.958	3871.254	2
442	257.7885	3904.452	6
443	242.5084	3904.95	4
444	226.3979	3905.447	2
445	177.9003	3913.249	2
446	196.1699	3905.945	6
447	210.9517	3905.447	6
448	294.1616	3909.597	3
449	293.6634	3893.496	7
450	293.8295	3877.561	4
451	287.0199	3860.796	5
452	318.9087	3903.124	7
453	334.8531	3900.966	2
454	350.6315	3899.804	5
455	318.2444	3863.95	3
456	332.0296	3876.067	5
457	348.4723	3860.962	7
458	364.4167	3867.602	3
459	379.5307	3866.274	1
460	402.6169	3863.452	3
461	442.1458	3860.796	7
462	368.4028	3898.476	4

No.	Coordinate		Structure Type
	X (m)	Y (m)	
463	384.0151	3896.152	8
464	452.4432	3900.634	5
465	399.6273	3897.148	7
466	414.4091	3895.156	5
467	433.177	3894.492	2
468	512.7408	3932.487	2
469	529.3495	3932.155	4
470	543.6331	3931.823	6
471	567.8819	3929.167	6
472	600.1029	3927.507	4
473	617.376	3926.677	8
474	632.9883	3926.843	5
475	658.0675	3927.009	7
476	479.025	3893.313	6
477	477.198	3859.451	2
478	494.4712	3858.953	2
479	494.4711	3893.479	4
480	525.8617	3891.985	8
481	542.8027	3890.989	1
482	533.6678	3859.285	2
483	558.7471	3888.665	3
484	575.8541	3885.844	5
485	571.7019	3856.795	5
486	608.9055	3894.807	2
487	607.0786	3879.702	6
488	609.2377	3862.605	3
489	604.7533	3847.168	6
490	637.9709	3885.844	6
491	662.3858	3886.508	5
492	1085.227	3801.055	4
493	1015.802	3768.023	7
494	752.8855	3864.131	4
495	772.9821	3869.111	3
496	793.577	3858.487	4
497	823.3067	3836.245	6
498	741.2594	3830.435	7
499	726.4776	3791.095	6
500	781.1204	3808.192	4
501	760.1934	3811.014	5
502	772.6499	3781.468	4
503	752.3872	3789.768	3
504	805.5966	3495.428	8
505	853.0976	3501.901	6
506	840.8071	3476.339	3
507	883.6578	3475.177	3
508	1081.57	3492.261	2
509	1061.141	3491.431	5
510	1099.175	3469.354	6
511	1035.563	3492.925	1
512	1002.678	3472.508	2
513	1007.827	3492.427	5
514	961.316	3437.976	1
515	967.7934	3423.867	7
516	974.603	3402.122	3
517	990.3813	3402.62	4
518	999.8483	3438.474	3
519	999.6189	3423.876	5
520	1020.222	3431.088	5
521	1034.422	3429.576	6
522	1047.226	3430.158	2
523	892.3613	3406.93	4
524	855.3182	3398.744	2
525	907.9976	3358.002	7
526	890.686	3341.073	6
527	873.0021	3340.329	3
528	854.9459	3340.515	7
529	835.7729	3340.515	2
530	596.6472	3820.279	5
531	596.6473	3802.605	6
532	595.5304	3777.304	4
533	616.0065	3814.884	6
534	612.842	3781.583	2
535	474.5353	3821.953	6
536	490.9162	3820.837	6
537	506.7386	3818.977	4
538	524.4225	3823.069	2
539	564.6301	3777.676	5
540	471.7431	3787.35	4
541	506.9248	3781.025	2
542	489.7993	3785.118	4

No.	Coordinate		Structure Type
	X (m)	Y (m)	
543	540.4311	3815.814	6
544	555.3228	3815.07	5
545	573.0067	3814.698	7
546	538.5696	3782.513	5
547	521.6303	3786.048	7
548	290.9361	3835.534	3
549	291.4945	3817.488	3
550	290.9361	3802.047	7
551	288.33	3786.234	7
552	330.5852	3826.976	3
553	348.083	3825.302	5
554	345.2908	3792.559	4
555	314.3905	3792.001	7
556	315.3212	3827.348	6
557	328.7238	3793.303	6
558	363.347	3792.187	7
559	446.3682	3828.092	7
560	447.2989	3789.955	4
561	428.1259	3793.862	2
562	428.6843	3822.325	3
563	400.7624	3816.558	3
564	401.507	3798.326	7
565	391.0828	3781.211	5
566	411.3727	3781.769	2
567	148.2502	3841.121	7
568	148.2502	3824.378	4
569	174.1245	3831.633	3
570	190.8777	3831.261	6
571	206.8862	3829.959	2
572	222.3364	3829.959	2
573	239.0895	3829.401	3
574	147.1333	3810.797	7
575	145.8303	3793.868	8
576	173.5661	3798.519	1
577	190.6915	3799.821	3
578	206.8862	3799.263	7
579	220.8472	3798.147	2
580	243.9293	3804.286	7
581	144.5272	3767.636	7
582	147.8779	3752.009	8
583	147.1333	3738.987	2
584	146.2026	3723.174	2
585	171.1461	3761.683	2
586	187.3409	3760.567	3
587	202.2326	3761.683	5
588	228.8515	3757.218	2
589	251.0029	3758.707	3
590	170.0293	3729.127	7
591	185.6656	3729.313	3
592	209.8646	3734.708	3
593	207.6308	3719.267	6
594	240.0203	3718.523	5
595	289.5352	3763.358	6
596	289.9075	3745.684	5
597	288.7906	3730.429	2
598	287.8599	3716.476	7
599	312.0589	3752.94	6
600	312.4312	3719.639	7
601	326.9506	3719.081	3
602	342.2146	3718.337	2
603	359.34	3716.848	3
604	374.4179	3716.476	1
605	389.868	3716.476	5
606	406.6212	3716.29	5
607	429.7033	3748.103	7
608	444.9673	3717.034	7
609	426.725	3718.709	5
610	447.2011	3746.8	3
611	472.3308	3747.172	1
612	478.1013	3714.802	6
613	502.6726	3713.314	3
614	493.7376	3745.498	2
615	519.7981	3744.754	3
616	535.9928	3742.894	5
617	518.8674	3712.011	3
618	535.4344	3712.57	5
619	324.5156	3644.6	6
620	405.1169	3680.691	2
621	384.2685	3682.737	7
622	356.5327	3684.039	6

No.	Coordinate		Structure Type
	X (m)	Y (m)	
623	295.4669	3504.405	2
624	294.9085	3486.36	3
625	352.2415	3520.59	6
626	307.1941	3555.751	7
627	339.5836	3560.588	6
628	389.6569	3560.216	7
629	373.6484	3561.146	2
630	356.3368	3561.704	5
631	324.5058	3562.821	2
632	307.9387	3569.89	2
633	306.4496	3526.171	4
634	330.8347	3524.497	4
635	369.1809	3518.172	3
636	387.7955	3518.73	8
637	324.5058	3492.313	6
638	341.2589	3485.243	4
639	358.0121	3483.755	3
640	372.5315	3481.895	5
641	563.7109	3712.143	1
642	551.053	3743.77	6
643	568.7363	3743.487	2
644	595.9136	3739.394	6
645	618.6235	3742.184	7
646	594.6106	3712.419	6
647	595.5414	3668.514	5
648	593.6799	3640.98	6
649	329.7245	3685.443	2
650	424.6591	3675.955	8
651	443.2737	3676.513	4
652	468.9619	3674.467	5
653	483.2952	3674.095	5
654	500.2345	3671.676	1
655	516.6153	3674.095	4
656	533.1824	3671.863	8
657	557.3814	3669.816	3
658	475.6632	3642.655	7
659	442.5291	3641.166	5
660	420.5639	3643.213	4
661	431.1742	3598.378	5
662	430.2435	3579.774	2
663	470.2649	3594.574	3
664	471.7541	3572.622	7
665	493.9055	3591.226	1
666	515.3123	3596.993	1
667	537.836	3589.923	6
668	535.23	3563.32	4
669	546.9572	3538.019	7
670	529.4594	3531.694	8
671	512.8924	3530.391	7
672	491.1133	3529.833	2
673	471.0095	3530.391	1
674	456.1178	3529.461	4
675	438.0616	3533.368	3
676	431.5465	3548.437	1
677	426.3344	3560.902	7
678	455.5531	3505.906	8
679	427.4451	3506.65	5
680	428.7481	3478.931	1
681	457.4146	3486.558	4
682	459.6484	3467.955	2
683	502.6481	3466.28	8
684	507.3018	3504.976	6
685	507.3018	3487.303	3
686	538.3882	3477.629	7
687	523.4298	3428.762	5
688	512.0749	3397.508	4
689	485.8283	3433.413	4
690	448.4129	3437.133	1
691	432.032	3436.575	3
692	417.3264	3428.948	2
693	417.8849	3397.322	7
694	433.1488	3392.299	2
695	257.6129	3461.132	5
696	296.1452	3451.644	5
697	120.6463	3546.937	4
698	121.1681	3532.465	2
699	120.2549	3515.906	2
700	118.559	3498.175	3
701	117.7762	3482.138	7
702	115.2976	3465.58	4

No.	Coordinate		Structure Type
	X (m)	Y (m)	
703	112.297	3449.021	4
704	111.5143	3434.027	7
705	110.9925	3419.555	6
706	108.5138	3403.91	4
707	106.5569	3388.394	5
708	166.6977	3479.791	2
709	200.747	3474.119	5
710	162.2621	3455.997	1
711	152.5324	3390.305	6
712	229.7109	3333.447	5
713	229.9718	3317.149	7
714	256.846	3356.916	8
715	271.4572	3357.698	5
716	254.4978	3324.451	5
717	270.544	3324.19	4
718	286.8511	3323.408	4
719	301.8537	3323.147	5
720	318.8131	3322.234	5
721	335.1202	3322.104	4
722	351.1665	3320.018	7
723	366.169	3320.018	6
724	414.5464	3311.383	3
725	429.8099	3310.08	8
726	446.117	3310.21	1
727	441.551	3270.574	6
728	461.1196	3268.749	5
729	480.0359	3267.185	5
730	419.2422	3238.911	8
731	380.366	3273.07	6
732	378.8005	3240.997	5
733	364.3198	3273.853	2
734	362.8848	3241.127	1
735	346.3167	3242.04	8
736	348.404	3274.374	7
737	331.836	3274.113	3
738	316.703	3274.505	6
739	301.1786	3275.417	8
740	285.0019	3276.591	8
741	268.4338	3277.634	5
742	251.8658	3276.721	6

No.	Coordinate		Structure Type
	X (m)	Y (m)	
743	330.5314	3241.518	2
744	314.4852	3242.431	4
745	298.6999	3242.953	6
746	282.1318	3244.387	7
747	267.3902	3245.43	7
748	250.8221	3244.778	8
749	433.9839	3194.06	2
750	418.329	3165.246	6
751	411.2596	3133.919	7
752	194.6391	3173.821	8
753	377.5399	3192.466	4
754	361.1023	3192.987	4
755	344.4038	3194.421	2
756	329.9231	3194.161	8
757	312.8332	3194.682	5
758	297.0479	3195.204	1
759	281.2626	3195.464	4
760	265.9991	3196.116	6
761	249.9529	3195.986	8
762	232.4716	3197.42	6
763	216.8168	3165.216	1
764	233.1239	3165.347	4
765	247.996	3164.825	3
766	264.4401	3164.288	4
767	280.8077	3164.522	3
768	296.2401	3161.951	5
769	312.3739	3162.652	6
770	328.7416	3161.484	1
771	345.343	3160.082	6
772	360.0739	3160.549	5
773	376.6754	3159.614	2
774	81.345	3244.344	7
775	75.7333	3229.622	4
776	74.0965	3202.514	5
777	73.1612	3166.526	3
778	109.8715	3136.147	6
779	67.5494	3116.05	6
780	66.6141	3091.046	6
781	66.1465	3062.77	3
782	165.9892	3128.903	6

No.	Coordinate		Structure Type
	X (m)	Y (m)	
783	159.4421	3109.974	7
784	153.5965	3092.682	7
785	147.2833	3076.557	2
786	139.5671	3054.357	6
787	176.2774	3043.841	7
788	187.7348	3157.646	1
789	219.5336	3116.835	5
790	253.9057	3114.966	4
791	285.0042	3114.966	1
792	317.5057	3113.564	5
793	351.8778	3111.227	7
794	418.0498	3077.81	7
795	219.066	3083.185	4
796	255.7763	3082.016	7
797	278.2234	3081.549	6
798	293.1881	3080.147	1
799	309.0881	3079.446	7
800	325.4557	3080.848	4
801	341.3557	3079.679	2
802	364.5042	3079.212	1
803	192.8777	3085.989	7
804	128.3424	3019.388	6
805	59.5983	3028.736	5
806	104.9601	3095.57	7
807	63.8071	2993.916	4
808	43.2307	2964.005	4
809	50.4792	2928.952	5
810	125.7704	2964.939	6
811	130.9145	2935.962	6
812	163.6498	3016.818	6
813	196.6189	3037.148	1
814	212.5189	3036.447	6
815	227.016	3035.045	3
816	244.5528	3035.279	4
817	260.4528	3035.045	1
818	274.716	3033.877	6
819	292.2528	3033.643	5
820	307.9189	3032.708	7
821	323.1175	3033.877	5
822	339.9528	3034.11	3
823	356.5542	3032.241	5
824	371.9866	3032.708	4
825	172.5392	2935.09	1
826	172.773	2915.694	3
827	87.1936	2918.498	6
828	43.0009	2904.009	8
829	62.4083	2903.308	3
830	52.3539	2885.081	6
831	86.7259	2885.081	3
832	167.3951	2877.603	2
833	172.0715	2859.142	3
834	200.8318	2863.582	2
835	201.2995	2828.996	4
836	126.4759	2853.416	6
837	55.3936	2868.956	5
838	86.9598	2867.788	1
839	86.0245	2851.664	4
840	58.1994	2851.897	1
841	155.9377	2824.322	5
842	70.1144	2823.907	5
843	74.557	2804.043	6
844	76.1938	2783.012	5
845	78.7659	2754.736	2
846	132.3115	2807.549	4
847	161.0718	2803.576	5
848	154.4538	2786.775	2
849	138.2306	2760.243	5
850	164.1222	2769.251	1
851	160.6809	2755.494	4
852	87.093	2728.35	7
853	92.9924	2711.481	5
854	100.2027	2690.845	5
855	130.191	2647.773	3
856	144.7755	2728.677	6
857	145.9226	2711.972	2
858	171.6503	2717.704	6
859	170.9949	2688.88	3
860	142.4813	2692.319	2
861	203.4483	2613.251	5
862	269.3244	2644.859	6

No.	Coordinate		Structure Type
	X (m)	Y (m)	
863	324.8766	2661.892	5
864	263.2612	2609.156	3
865	331.5953	2558.55	7
866	353.7178	2585.082	3
867	375.3488	2616.69	4
868	173.7877	2534.639	2
869	132.9839	2609.975	3
870	391.8071	2648.206	6
871	396.0678	2587.61	5
872	435.2329	2581.878	8
873	376.2394	2539.788	2
874	414.9129	2541.589	8
875	467.0238	2463.141	4
876	427.2032	2461.831	4
877	371.651	2485.415	5
878	310.1995	2511.455	6
879	333.633	2507.688	3
880	146.1635	2498.408	6
881	171.8912	2495.788	6
882	188.7699	2486.944	4
883	205.9763	2488.254	4
884	220.8886	2487.926	6
885	236.2924	2488.09	5
886	274.1466	2488.745	4
887	156.8151	2478.591	5
888	158.7815	2464.834	4
889	149.7686	2448.129	3
890	166.9751	2448.621	3
891	188.1144	2455.663	7
892	203.6821	2454.025	4
893	218.7583	2454.516	5
894	169.4331	2417.012	6
895	311.1814	2480.229	6
896	310.6898	2456.973	4
897	362.9646	2457.301	4
898	408.3568	2420.615	2
899	436.5426	2435.682	5
900	466.8587	2435.191	5
901	453.5851	2490.219	4
902	169.269	2401.062	5
903	171.8909	2384.685	1
904	158.2897	2367.161	5
905	179.7567	2364.704	2
906	208.2702	2407.613	5
907	232.8509	2412.854	6
908	248.4186	2407.285	8
909	264.478	2406.303	4
910	280.3734	2405.975	4
911	321.8327	2411.38	1
912	309.5424	2375.841	2
913	333.4676	2385.176	4
914	331.3372	2363.558	1
915	280.5373	2372.893	6
916	263.9863	2373.548	3
917	247.927	2374.858	3
918	231.7038	2375.841	4
919	213.0225	2376.168	6
920	481.3085	2378.482	6
921	433.786	2339.012	2
922	479.3421	2294.629	4
923	469.3459	2271.045	5
924	403.9615	2266.624	3
925	373.9731	2292.172	6
926	420.1847	2300.034	1
927	446.5679	2311.334	7
928	438.0466	2256.961	7
929	177.0004	2333.116	3
930	171.2649	2306.912	8
931	169.954	2288.078	5
932	196.501	2304.619	6
933	196.8288	2285.458	7
934	213.3797	2295.448	7
935	222.3926	2328.53	4
936	245.3345	2328.694	1
937	204.5307	2327.384	2
938	229.6029	2292.991	4
939	245.6623	2301.508	5
940	244.5152	2286.113	6
941	261.5578	2290.371	2
942	278.4364	2292.5	4

No.	Coordinate		Structure Type
	X (m)	Y (m)	
943	301.0506	2327.711	4
944	317.6016	2338.848	8
945	333.497	2326.893	7
946	333.2821	2313.038	7
947	333.2821	2282.507	3
948	303.8816	2312.235	6
949	304.5707	2299.609	4
950	305.3746	2290.312	8
951	303.9964	2280.441	2
952	331.1	2298.92	7
953	379.3353	2342.077	2
954	165.8956	2256.85	4
955	198.5874	2254.831	3
956	196.5671	2236.475	6
957	170.8545	2238.495	6
958	165.8956	2223.443	3
959	168.8342	2205.455	4
960	190.8736	2221.424	6
961	211.4437	2212.797	5
962	227.6059	2208.575	5
963	238.442	2251.343	6
964	259.1957	2250.793	5
965	215.1169	2247.122	3
966	275.909	2250.793	4
967	270.3991	2217.753	3
968	250.0126	2232.07	6
969	236.8698	2225.486	6
970	240.6693	2210.082	5
971	301.6342	2246.356	7
972	330.2462	2247.366	4
973	303.3529	2212.203	2
974	328.9318	2203.615	8
975	328.5274	2231.098	5
976	320.9447	2218.771	7
977	335.8068	2218.569	6
978	370.4893	2227.978	4
979	367.9023	2207.133	4
980	366.1238	2186.127	7
981	366.7705	2158.98	1
982	330.3918	2165.282	5
983	306.1392	2165.444	5
984	173.8821	2158.334	7
985	192.4757	2158.98	5
986	212.3628	2174.331	7
987	256.8258	2172.553	2
988	291.7504	2121.486	5
989	314.5478	2121.809	4
990	314.5478	2106.619	2
991	279.4625	2083.674	4
992	296.4392	2084.159	8
993	314.0627	2083.351	4
994	366.6099	2119.223	5
995	363.8613	2078.826	5
996	331.3629	2082.704	5
997	262.4857	2043.277	4
998	278.9774	2039.722	3
999	295.9542	2039.237	1
1000	322.9553	2042.469	7
1001	317.1347	2028.572	7
1002	265.396	2001.425	3
1003	285.4447	2003.364	2
1004	302.2599	2004.011	7
1005	322.7937	2002.88	2
1006	431.825	2109.849	1
1007	461.4131	2068.483	3
1008	439.4241	2052.001	2
1009	403.5304	1998.192	7
1010	437.969	1995.768	6
1011	370.2236	1992.213	1
1012	185.7455	1966.601	4
1013	187.3623	1950.119	4
1014	185.2605	1934.445	8
1015	185.2604	1916.994	4
1016	230.2085	1966.278	1
1017	230.3702	1948.18	4
1018	231.0169	1932.668	3
1019	231.3402	1916.509	7
1020	255.9161	1965.793	3
1021	259.4732	1924.588	6
1022	289.5463	1955.937	4

No.	Coordinate		Structure Type
	X (m)	Y (m)	
1023	312.5054	1963.693	7
1024	314.4456	1932.021	2
1025	314.6073	1914.408	8
1026	291.9716	1924.427	6
1027	276.2883	1924.912	5
1028	369.418	1963.531	1
1029	368.4479	1947.049	8
1030	365.0525	1913.762	4
1031	390.4368	1917.963	3
1032	408.222	1921.195	1
1033	390.9219	1954.482	5
1034	408.3837	1953.19	3
1035	426.3306	1956.26	6
1036	440.5587	1954.482	4
1037	470.6319	1957.068	1
1038	459.314	1924.104	4
1039	456.4037	1876.435	1
1040	362.9506	1881.444	6
1041	364.5675	1865.124	5
1042	361.9805	1834.584	8
1043	400.4612	1878.859	2
1044	432.9596	1875.304	7
1045	431.9895	1920.71	8
1046	186.0689	1888.126	6
1047	188.1708	1870.028	5
1048	186.7156	1854.192	7
1049	184.6137	1838.033	3
1050	232.3104	1886.025	6
1051	233.6038	1869.705	3
1052	233.6038	1851.768	4
1053	231.3402	1835.61	4
1054	273.7013	1876.33	4
1055	289.5463	1877.784	3
1056	317.1942	1881.177	8
1057	315.254	1865.503	3
1058	269.1742	1839.811	4
1059	290.3547	1842.073	5
1060	313.9605	1840.619	5
1061	363.5974	1806.362	7
1062	184.1287	1803.453	6
1063	186.2305	1782.285	7
1064	185.5838	1755.3	8
1065	373.3015	1769.416	7
1066	184.7785	1728.534	4
1067	183.8084	1709.628	2
1068	231.3433	1805.935	6
1069	231.3433	1789.614	6
1070	223.9059	1772.324	7
1071	221.804	1757.943	3
1072	256.566	1798.017	8
1073	255.9192	1765.376	4
1074	272.896	1796.078	6
1075	288.0943	1797.37	2
1076	272.5726	1763.437	5
1077	287.7709	1763.921	7
1078	184.9399	1680.271	7
1079	230.5347	1724.062	7
1080	229.8879	1706.449	5
1081	229.2412	1692.391	1
1082	227.6244	1675.424	8
1083	253.6554	1683.18	6
1084	281.95	1682.857	7
1085	268.2069	1721.638	1
1086	310.083	1677.524	3
1087	357.4562	1704.833	5
1088	359.3964	1688.512	3
1089	358.9745	1666.829	8
1090	376.4887	1633.413	2
1091	406.0329	1651.094	3
1092	350.482	1504.173	5
1093	344.2901	1460.326	3
1094	367.4654	1459.796	6
1095	347.6514	1446.182	1
1096	370.8267	1443	6
1097	389.0486	1448.657	3
1098	344.9977	1414.888	7
1099	385.3334	1396.855	6
1100	389.9331	1424.436	6
1101	182.4353	1395.982	2
1102	207.7336	1395.982	4

No.	Coordinate		Structure Type
	X (m)	Y (m)	
1103	225.2478	1395.805	4
1104	184.3814	1378.125	3
1105	212.5102	1377.064	5
1106	182.4353	1361.329	7
1107	185.089	1345.417	3
1108	211.6257	1354.434	3
1109	184.3814	1335.339	5
1110	185.089	1324.201	5
1111	178.7202	1301.747	5
1112	183.3199	1282.829	1
1113	253.1998	1396.335	4
1114	268.4141	1394.921	7
1115	294.9508	1380.247	5
1116	258.1533	1365.395	2
1117	255.1458	1348.422	8
1118	290.528	1333.041	7
1119	295.1277	1313.416	1
1120	293.5355	1296.443	4
1121	255.3227	1321.549	2
1122	255.6765	1293.614	1
1123	346.9626	1364.865	3
1124	508.8362	1369.285	3
1125	564.7401	1362.566	2
1126	524.0506	1349.837	5
1127	528.8272	1334.278	5
1128	509.7208	1320.841	8
1129	486.3685	1302.985	3
1130	515.7358	1298.918	1
1131	539.4418	1272.928	4
1132	578.1854	1311.648	2
1133	623.9299	1367.807	6
1134	599.9047	1349.71	6
1135	603.266	1305.863	6
1136	638.2944	1305.333	5
1137	493.0504	1272.448	2
1138	488.8045	1232.314	2
1139	537.9858	1248.403	5
1140	569.6529	1258.657	1
1141	637.4098	1265.199	2
1142	661.1159	1231.607	6
1143	658.1084	1203.849	3
1144	595.4819	1205.971	4
1145	535.509	1230.546	5
1146	537.1012	1208.976	8
1147	488.6276	1208.623	7
1148	483.6741	1185.108	3
1149	563.1072	1214.28	1
1150	701.6285	1185.108	3
1151	606.4504	1259.895	6
1152	710.6496	1146.542	4
1153	710.4727	1127.624	3
1154	706.4037	1111.182	7
1155	704.2808	1095.446	3
1156	703.3962	1079.888	5
1157	481.7267	1161.747	5
1158	477.4808	1146.188	3
1159	473.9426	1131.867	8
1160	472.7042	1116.663	5
1161	471.8196	1098.098	2
1162	468.9891	1083.07	2
1163	467.3969	1066.805	8
1164	466.5123	1035.511	7
1165	528.6081	1164.399	4
1166	550.0143	1164.752	7
1167	572.1282	1162.277	5
1168	613.8792	1134.166	5
1169	611.7563	1115.071	5
1170	612.8177	1097.391	4
1171	611.2256	1081.656	6
1172	610.341	1063.976	5
1173	612.4639	1047.357	4
1174	610.6948	1028.969	4
1175	561.8674	1136.818	4
1176	523.6546	1138.409	2
1177	523.4777	1119.491	6
1178	522.0624	1100.22	7
1179	517.1089	1080.065	7
1180	564.6979	1117.016	6
1181	563.9903	1098.452	2
1182	563.1058	1080.595	5

No.	Coordinate		Structure Type
	X (m)	Y (m)	
1183	559.7444	1059.556	3
1184	560.9828	1041.522	5
1185	559.2137	1024.196	6
1186	518.3472	1027.025	4
1187	704.6346	1062.385	6
1188	703.5731	1045.942	2
1189	706.9344	1028.793	4
1190	709.0675	977.0772	7
1191	646.2641	982.2044	2
1192	607.1668	1012.614	4
1193	608.7589	988.2157	4
1194	579.7455	982.558	1
1195	545.7786	984.1492	6
1196	510.7502	985.7404	8
1197	490.2286	985.5636	7
1198	463.8688	1013.852	5
1199	177.1057	1253.179	4
1200	208.9497	1249.997	1
1201	208.4189	1232.316	5
1202	177.6364	1235.145	5
1203	177.4595	1219.94	4
1204	177.2826	1202.437	6
1205	207.0037	1212.161	3
1206	173.9213	1186.348	8
1207	175.1597	1169.552	6
1208	174.2751	1152.579	1
1209	171.2676	1138.435	7
1210	200.458	1135.96	6
1211	255.4773	1249.113	2
1212	290.3288	1246.814	4
1213	343.2252	1241.333	6
1214	341.1022	1224.007	6
1215	342.1637	1208.095	6
1216	339.1562	1192.713	4
1217	340.3946	1164.425	4
1218	340.2177	1147.982	5
1219	338.0947	1130.302	8
1220	340.2177	1112.445	7
1221	374.8922	1160.182	2
1222	374.8922	1137.728	5

No.	Coordinate		Structure Type
	X (m)	Y (m)	
1223	254.7696	1233.731	1
1224	251.7621	1216.581	1
1225	252.6467	1199.608	8
1226	249.2854	1184.227	3
1227	249.4623	1169.022	6
1228	250.8776	1152.756	8
1229	252.4698	1135.253	6
1230	288.3827	1149.75	7
1231	286.4367	1132.424	7
1232	282.8985	1184.227	2
1233	177.451	1104.853	6
1234	197.442	1096.19	7
1235	168.7824	1084.875	5
1236	172.6745	1063.482	1
1237	205.2261	1070.2	7
1238	246.091	1098.485	2
1239	244.1048	1036.702	7
1240	246.8358	1020.326	3
1241	283.4569	1050.969	1
1242	281.3465	1034.345	2
1243	280.6017	1020.326	2
1244	283.0845	1005.191	5
1245	281.9673	987.8219	8
1246	247.7048	1005.067	6
1247	248.0772	989.0625	2
1248	201.3459	1043.892	8
1249	171.9902	1051.205	7
1250	171.032	1038.843	3
1251	168.5058	1025.001	6
1252	170.248	1007.155	4
1253	197.8616	1006.458	5
1254	170.2062	990.4385	7
1255	201.6936	989.0461	3
1256	161.8691	955.561	3
1257	160.8839	940.6695	5
1258	160.2682	924.5473	7
1259	155.5886	908.5482	4
1260	191.3012	956.6686	4
1261	209.7732	955.3149	7
1262	233.91	954.5765	6

No.	Coordinate		Structure Type
	X (m)	Y (m)	
1263	246.1016	953.3458	7
1264	258.4163	953.3458	7
1265	276.8883	952.6073	8
1266	275.0411	936.6082	1
1267	236.9887	937.8389	2
1268	233.048	921.7167	2
1269	233.6637	905.3484	3
1270	279.105	920.7321	5
1271	276.0263	904.3638	5
1272	337.1072	950.3921	7
1273	334.3979	933.4084	1
1274	332.797	917.7784	3
1275	332.6739	901.6563	8
1276	194.1336	943.3771	4
1277	198.0743	933.7776	5
1278	195.365	922.5782	3
1279	194.3799	907.5636	4
1280	151.8908	882.8765	3
1281	151.2751	867.8619	7
1282	149.3047	851.1244	4
1283	149.1816	834.1407	3
1284	146.7187	818.5107	1
1285	142.5317	786.2663	2
1286	182.5544	785.5279	5
1287	184.1553	802.2655	7
1288	184.8942	818.5108	6
1289	185.6331	832.4177	1
1290	188.9581	848.0476	3
1291	188.5886	865.0313	1
1292	191.0516	881.2766	2
1293	271.2202	829.2179	1
1294	227.9956	847.3092	6
1295	226.0253	831.5562	5
1296	229.4734	814.4494	7
1297	239.8177	790.5738	3
1298	272.3285	781.5897	2
1299	324.4197	812.6034	5
1300	324.1734	793.7736	5
1301	273.0674	813.3418	6
1302	273.0674	795.8658	6
1303	220.3605	791.0661	4
1304	138.78	754.7023	6
1305	176.2033	752.9307	6
1306	138.583	737.1833	4
1307	175.1637	736.8713	5
1308	173.7816	721.2631	7
1309	139.367	721.2631	1
1310	135.9117	698.0581	3
1311	131.9036	663.2505	5
1312	318.9652	698.1271	4
1313	318.0998	667.8015	5
1314	312.5287	652.1428	2
1315	305.565	631.2646	2
1316	263.6665	717.1165	2
1317	265.3591	701.4306	6
1318	262.2816	686.3599	3
1319	263.051	670.3665	3
1320	269.2061	653.1429	7
1321	131.9222	635.8174	2
1322	155.9273	634.5872	5
1323	173.7772	632.1266	5
1324	188.8573	632.7418	6
1325	304.5722	574.9667	7
1326	131.4589	599.4181	3
1327	131.4589	583.2709	4
1328	136.5369	549.9001	5
1329	153.9251	586.9617	5
1330	177.0069	555.8976	3
1331	201.0119	555.2825	7
1332	225.1709	553.1296	3
1333	245.1751	587.1155	6
1334	227.9407	589.8836	2
1335	170.544	589.7298	6
1336	187.7784	589.4223	1
1337	203.7817	587.7306	3
1338	125.3037	522.8951	6
1339	125.4576	505.8252	5
1340	124.3805	489.2167	3
1341	126.8425	472.762	1
1342	165.9276	514.1295	2

No.	Coordinate		Structure Type
	X (m)	Y (m)	
1343	163.3117	477.2216	7
1344	180.3922	479.9897	7
1345	223.6321	510.4387	6
1346	238.4044	509.8236	4
1347	227.7868	477.5292	6
1348	267.7952	473.0695	6
1349	182.8543	511.5152	1
1350	198.0882	511.5152	2
1351	197.0111	479.3746	5
1352	115.2989	438.0674	5
1353	136.2264	437.606	4
1354	155.9229	440.3741	5
1355	178.6968	435.2993	7
1356	198.3933	434.3766	3
1357	217.0126	432.3774	2
1358	169.1564	407.157	6
1359	187.9296	407.0033	3
1360	206.8566	404.6965	6
1361	164.0784	379.4762	5
1362	194.8541	377.3232	7
1363	102.5182	400.298	4
1364	110.8276	383.0743	3
1365	101.9027	367.6961	5
1366	128.062	366.9272	2
1367	94.6704	351.3951	3
1368	128.5237	349.0884	7
1369	126.0616	325.7134	4
1370	159.4532	364.0053	2
1371	189.9212	363.2364	1
1372	187.3052	347.7043	6
1373	161.6075	348.0119	1
1374	186.2281	330.3269	6
1375	160.3765	331.2496	7
1376	160.2226	314.4873	4
1377	186.0742	314.0259	2
1378	90.054	325.7134	2
1379	83.2753	293.9009	1
1380	118.6673	285.1353	6
1381	137.7483	287.2883	6
1382	155.2904	287.4421	3
1383	184.6812	289.4412	2
1384	182.0653	271.2949	2
1385	79.5822	265.9125	7
1386	78.9667	247.7661	5
1387	122.8221	229.1584	8
1388	141.4414	240.8459	6
1389	162.0611	245.9208	7
1390	182.373	231.619	4
1391	64.656	205.1683	2
1392	62.5017	188.7136	2
1393	114.6665	259.7612	1
1394	30.4125	9.8722	2
1395	50.8403	46.0291	2
1396	80.1283	67.428	6
1397	50.348	100.8792	3
1398	91.2036	118.0968	3
1399	103.0173	163.6003	8
1400	151.9948	190.1645	5
1401	53.7937	137.528	6
1402	0.9811	6026.523	3
1403	613.9262	3267.416	2
1404	640.3259	3244.663	6
1405	608.84	3219.732	2
1406	680.7731	3237.886	7
1407	663.3348	3218.522	8
1408	732.3615	3212.229	8
1409	788.5517	3193.107	7
1410	811.8028	3180.762	5
1411	789.5205	3121.461	5
1412	756.097	3146.15	7
1413	733.8147	3161.399	2
1414	690.2189	3178.826	2
1415	714.681	3168.902	2
1416	652.4358	3171.081	3
1417	668.9054	3159.462	3
1418	687.7969	3139.856	1
1419	719.0405	3120.25	6
1420	744.9558	3106.454	7
1421	538.8445	3122.913	7
1422	532.7667	3101.184	4